UNIVERSIDAD DE CONCEPCIÓN
FACULTAD DE CIENCIAS QUÍMICAS
DOCTORADO EN CIENCIAS GEOLÓGICAS

FUENTES Y EVOLUCIÓN DEL MAGMATISMO TRIÁSICO DEL MARGEN SUROCCIDENTAL DE GONDWANA: NUEVOS ANTECEDENTES PETROGENÉTICOS DE LA ALTA CORDILLERA (28°S – 30°S), CHILE

JAVIERA CONSTANZA GONZÁLEZ ALARCÓN

Tesis presentada a la Facultad de Ciencias Químicas de la Universidad de Concepción para optar al grado de Doctora en Ciencias Geológicas

Profesora Guía: Dra. Verónica Laura Oliveros Clavijo

Mayo de 2023

Concepción, Chile

© 2023, Javiera Constanza González Alarcón

Se autoriza la reproducción total o parcial, con fines académicos, por cualquier medio o procedimiento, incluyendo la cita bibliográfica del documento.

A mi familia

AGRADECIMIENTOS

Mis primeras palabras de agradecimiento van dirigidas a la Dra. Verónica Oliveros, quién impulsó y mantuvo los ánimos arriba durante este largo periodo de mi desarrollo en el doctorado. Gracias por tu energía inconmensurable y tu claro ejemplo de que las mujeres podemos hacer mucho más de lo que nos han hecho creer. Espero haber estado a la altura como tu tesista. Destaco la importancia de la Dra. Laura Hernández quién me apoyó los últimos años de mi doctorado desde diversas aristas para dar continuidad a mis estudios y por su intensa colaboración y ayuda para llevar a cabo los análisis de química mineral en su atesorada microsonda. Además, le agradezco por sus comentarios y sugerencias, que realizaron en conjunto con el Dr. Osvaldo Rabbia y el Dr. Andrés Tassara para mejorar y conducir el desarrollo de esta tesis doctoral, en las diferentes instancias a lo largo de mi permanencia en el Programa Doctorado en Ciencias Geológicas.

Recalco y agradezco la importante colaboración que recibí por parte del Dr. Christian Creixell, Felipe Coloma, Ismael Murillo y Ricardo Velásquez, geólogos del Servicio Nacional de Geología y Minería, tanto en las campañas de terreno como en sus comentarios para mejorar los manuscritos de las publicaciones que componen esta tesis; y por facilitarme muestras que ellos consiguieron durante la confección de las cartas de geología básica, para su posterior análisis. No puedo dejar de mencionar al Dr. Friedrich Lucassen y a Annete Meixner quiénes trabajaron conmigo intensamente durante tres meses, enseñándome y guiándome en la cromatografía y en el posterior análisis en un espectrómetro de masa por ionización termal, un fantástico desafío. Le agradezco a la Dra. Laura Giambiagi y al Dr. Juan Ottamendi por darme la oportunidad de conocer parte de la geología el otro lado de la Cordillera de Los Andes, con su propio prisma.

Mis sinceros agradecimientos a Don Pedro, Don Luis, Don Carlos y Don Emiliano, por ayudarme con la oportuna confección de los cortes transparentes, por ir a calibrar el microscopio las veces que fuese necesario, con excelente disposición y por resolver mis dudas en la confección de los mapas. También agradezco a Lucy por su buena disposición a facilitarme el material de biblioteca y a María Esperanza por siempre mantener la fe en alto con que culminaría esta etapa y gestionar todo lo necesario de manera oportuna. Hago una mención especial al Dr. Mauricio Espinoza por ser un excelente compañero de doctorado, enseñarme sus habilidades con Illustrator y por su constante preocupación junto a la Dra. Fernanda Álvarez, quienes me han apoyado para concluir esta y otras fases de la vida.

Le doy las gracias a mis padres por esforzarse para que sus hijas e hijos logren estar donde estamos, por su amor incondicional y su paciencia; y a mi hermana por su presencia y compañía en esta fase y a lo largo de mi vida.

Le agradezco a mis hijos por entregarme la motivación y la fuerza para trabajar a cualquier hora y en cualquier circunstancia, por enseñarme a desafiar los límites y lo seguro. Por último, le doy mis sinceros agradecimientos a mi amado Edward por siempre sostenerme y apoyarme en el desarrollo de mi carrera y por escoger ser mi compañero de vida, por ser el que jamás perdió la fe ni en mí ni en mi trabajo y por estar sumamente orgulloso por cada uno de los pasos que doy.

RESUMEN

Desde el surgimiento de la teoría de la tectónica de placas, Los Andes ha sido considerado como un ejemplo de un orógeno formado por subducción. El margen occidental de Sudamérica ha estado periódicamente activo desde el Paleozoico, y en base al registro geológico presente en el norte de Chile y Argentina, se han propuesto dos etapas orogénicas: Ciclo Gondwánico (Carbonífero Temprano – Pérmico Temprano) y Ciclo Andino (Jurásico temprano - Presente), que son marcadamente diferentes en sus estilos de deformación, metamorfismo y magmatismo. Entre ambas etapas, se desarrolló un periodo estacionario respecto al movimiento de las placas, llamado Ciclo Pre-Andino, propuesto como un periodo en el que cesa la subducción y prevalece una tectónica extensional que permite el desarrollo de un rift continental. Sin embargo, recientemente, nuevos antecedentes petrológicos y geoquímicos proveniente de las rocas pre-andinas de la Alta Cordillera Chilena muestran ser compatibles con una subducción activa, tales como extensos afloramientos de rocas ígneas con un amplio espectro composicional, calcoalcalinas y con un enriquecimiento en elementos de gran radio iónico en relación a los elementos de alto potencial iónico, además de anomalías negativas de Nb-Ta, generando algunas inconsistencias con el modelo actual.

De este modo, el problema a abordar en esta investigación es determinar cómo cambiaron las condiciones tectónicas entre las dos etapas orogénicas que se han propuesto para la evolución del margen andino, a través del estudio del magmatismo pre-andino, expuesto en un área específica de la Cordillera Frontal Chilena (28°30’S – 30°30’S) donde extensos volúmenes de rocas volcánicas y plutónicas están excepcionalmente bien expuestas debido a la tectónica mesozoica y cenozoica y a las condiciones climáticas áridas. El magmatismo pre-andino fue caracterizado desde el punto petrográfico y geoquímico, tanto elemental como isotópico, evaluando de esta manera sus fuentes, y comparado con el magmatismo de los ciclos Gondwánico y Andino. Unidades representativas del magmatismo pre-andino fueron estudiadas en detalle, tales como los complejos plutónicos Chollay y Piuquenes, la Formación Pastos

Blancos y los Sienogranitos Colorado, unidades que previamente habían sido catalogadas como parte del magmatismo del Choiyoi.

El amplio espectro composicional en las unidades pre-andinas, junto a la presenta de texturas porfídicas, minerales máficos hidratados, una naturaleza calcoalcalina, enriquecimientos en LILE respecto a los HFSE, depresiones en Nb-Ta, Ti y P, además de enriquecimientos en Pb sugieren que el magmatismo pre-andino se generó en un contexto de subducción activa. La isotopía (Sr-Nd-Pb) arroja razones iniciales que son compatibles con una mezcla de dos fuentes, que corresponden a un manto deprimido y a la litósfera continental. Por otro lado, al comparar la geoquímica de los tres ciclos tectónicos es posible detectar que los cambios geoquímicos son graduales y que la señal de subducción se encuentra presente desde el Carbonífero al Jurásico (18°S - 40°S). Es posible identificar una disminución gradual de las razones vinculadas al espesor cortical (La_N/Yb_N y Sr/Y) a medida que las rocas ígneas son más jóvenes; además de una disminución del $^{87}Sr/^{86}Sr_i$ y un incremento del εNd_i, lo que apunta a una disminución del componente litosférico/continental a la fuente de los magmas. Estos cambios, son explicados mediante modificaciones en la configuración de la zona de subducción, proponiendo que un escenario de *roll-back* del *slab*, sería lo más probable para el Ciclo Pre-Andino, que habría permitido el desarrollo de una tectónica extensional en la corteza y probablemente la pérdida litosférica por erosión termal o delaminación, disminuyendo esta fuente en la génesis del magmatismo pre-andino y aumentando la proporción de una fuente deprimida, de manera progresiva hasta el Jurásico.

ABSTRACT

Since the emergence of the plate tectonics theory, the Andes have been regarded as an example of a subduction orogen. The western margin of South America has been periodically active since the Paleozoic, and in northern Chile and Argentina, two orogenic stages have been proposed: Gondwanan Cycle (Early Carboniferous–Early Permian) and the Andean Cycle (Early Jurassic–Recent), which are markedly different in their styles of deformation, metamorphism, and magmatism type. Between both, a stationary period respect to the movement of the plates was developed, called Pre-Andean Cycle, proposed as a period in which ceases subduction and extensional tectonics prevail, which allows the development of a continental rift. Nevertheless, recently, new petrological and geochemical background from the pre-andean igneous rocks of the Chilean High Andes, show compatibility with the development of this magmatism in a context of active subduction (extensive outcrops of igneous rocks of broad compositional range, calcalkaline nature and enrichment large-ion lithophile elements (LILE) in relation to high field strength elements (HFSE), in addition to negative anomalies of Nb-Ta, generating some inconsistencies with the current model.

Thus, the problem to be addressed in this thesis is to determine how tectonic conditions changed in the transition between both orogenies that have been proposed for the evolution of the Andean margin and aims to be resolved through the study of part of the pre-andean magmatism, in a specific area in the Chilean High Andes (28°30'S and 30°30'S), where vast volumes of pre-andean volcanic and plutonic rocks are exceptionally well exposed due to the Mesozoic and Cenozoic tectonic events and arid climatic conditions. The pre-Andean magmatism was characterized from the petrographic and geochemical perspective, evaluating its sources, and compared with the Gondwanan and Andean magmatism. Representative units oh pre-andean magmatism were studied in detail, such as the Chollay and Piuquenes plutonic complexes, the Pastos Blancos Formation and Colorado Syenogranites, units that had previously been catalogued as part of Choiyoi Group.

The wide compositional spectrum in the pre-andean units, together with the presence of porphyritic texture, hydrated mafic minerals, a calc-alkaline nature, LILE enrichment

with respect to HFSE, Nb-Ta, Ti and P toughs, as well as Pb enrichments, suggest that pre-andean magmatism was generated in an active subduction context. The isotopy (Sr-Nd-Pb) yields initial ratios that are compatible with a mixture of two sources which correspond to a depleted mantle and the continental lithosphere. On the other hand, when comparing the geochemistry of the three tectonic cycles, it is possible to detect that the geochemical changes are gradual, and that the subduction signal is present from the Carboniferous to the Jurassic (18°S - 40°S). It is possible to identify a gradual decrease in the ratios related to crustal thickness (La_N/Yb_N and Sr/Y) as the igneous rocks are younger; in addition to a decrease in $^{87}Sr/^{86}Sr_i$ and an increase in εNd_i, which point to a decrease in the lithospheric/cortical component at the source of magmas. These changes are explained by changes in the configuration of the subduction zone, proposing that a slab roll-back scenario would have allowed the development of extensional tectonics in the crust, and probably the lithospheric loss due to thermal erosion or delamination, decreasing this source in the genesis of pre-andean magmatism and increasing the proportion of a depleted source, progressively until the Jurassic.

TABLA DE CONTENIDO

ÍNDICE DE FIGURAS

ÍNDICE DE TABLAS

CAPÍTULO I: INTRODUCCIÓN

1.1 Formulación del problema científico

1.1.1 Evolución del margen suroccidental de Gondwana

Desde el surgimiento de la tectónica de placas, Los Andes han sido considerados como un orógeno generado en un contexto de subducción. Su evolución tectonoestratigráfica ha estado marcada por diferentes hitos que dan paso a la definición de cuatro etapas desde el Proterozoico tardío hasta el Presente, comenzando con una fase caracterizada por la acreción de sucesivos terrenos alóctonos y/o parautóctonos al margen continental de Sudamérica (Ramos, 1988), siendo Chilenia el último terreno en acrecionarse, durante el Devónico (Álvarez et al., 2011; Ramos et al., 1986). Posteriormente, desde el Carbonífero temprano el margen ha sido definido como periódicamente activo (por ejemplo, Bahlburg et al., 2009; Charrier et al., 2007, 2014; Mpodozis & Ramos, 1989) reconociéndose dos etapas orogénicas, en base a la geología del norte de Chile y Argentina, que contrastan fuertemente en sus estilos de deformación, cambios en la geometría de la zona de subducción, modificaciones en la posición y orientación del arco y de las cuencas, traduciéndose también en cambios en el tipo de metamorfismo y magmatismo. Estas etapas corresponden al Ciclo Gondwánico (Carbonífero temprano – Pérmico temprano) y al Ciclo Andino (Jurásico – Presente) (Charrier et al., 2007).

El reinicio de la subducción a lo largo del margen, durante el Carbonífero temprano (Hyppolito et al., 2014; Willner et al., 2012), marca el inicio del Ciclo Gondwánico, una etapa caracterizada por una acelerada convergencia entre las placas Panthalassa y Sudamericana (Riel et al., 2018; Vilas & Valencio, 1978; Young et al., 2019) que permitió la formación de un prisma de acreción activo desde el Carbonífero tardío hasta el Pérmico Temprano, expuesto actualmente en la Cordillera de la Costa entre los 26°S – 31°S, y la generación de grandes volúmenes de magma cuya fuente mantélica incorpora importantes cantidades de corteza continental (Deckart et al., 2014a; del Rey et al., 2016; Lucassen et al., 1999; Oliveros et al., 2018), que representan el arco magmático expuesto con una orientación preferentemente NNW-SSE, en la Cordillera Frontal y en la Cordillera de Domeyko entre los 22°S – 31”S (del Rey et al., 2016;

Hervé et al., 2014; Mpodozis & Kay, 1992) y en la Cordillera de la Costa entre los 33°S – 38°S (Deckart et al., 2014b). Durante esta etapa también se forman cuencas de antearco y trasarco, con la misma orientación del arco (Charrier et al., 2007). El término del Ciclo Gondwánico está marcado por una fase compresiva conocida como la Fase Orogénica San Rafael (Pérmico Temprano, Sato et al., 2015) cuya deformación se propaga hacia el continente y corresponde a fallas y pliegues con una orientación preferentemente NNW a NW (Kleiman & Japas, 2009). El desarrollo de esta fase compresiva ha sido vinculado a la colisión de un terreno continental (terreno Equis, Mpodozis & Kay, 1992), pero recientemente ha sido atribuido a otros procesos no colisionales tales como una subducción oblicua (Kleiman & Japas, 2009), una disminución en el ángulo de subducción (del Rey et al., 2016, 2019) o incluso el aplanamiento del slab (Martínez, 2004; Ramos & Folguera, 2009).

El Ciclo Andino (Jurásico temprano – Presente), está dividido en dos subetapas diferenciadas principalmente por el contexto tectónico que pasa de uno de tipo extensional – transtensional a una dinámica compresiva - transpresiva en el Cretácico tardío (Coira et al., 1982; Arriagada et al., 2006; Charrier et al., 2014). El arco magmático generado durante la primera subetapa del Ciclo Andino se encuentra expuesto en la actual Cordillera de la Costa y se caracteriza por estar conformado por rocas de composición principalmente andesítica – basáltica y un volumen restringido de magmatismo silíceo (Oliveros et al., 2018). La composición elemental e isotópica de estas rocas indica una fuente mantélica deprimida con una pequeña o inexistente contribución de una corteza continental delgada (Lucassen et al., 2006; Oliveros et al., 2007; Rossel et al., 2013).

Entre ambos ciclos orogénicos que difieren en sus estilos de deformación, tipo y fuentes del magmatismo y espesor cortical (Franzese & Spalletti, 2001; Mpodozis & Ramos, 1989) se desarrolla el Ciclo Pre-Andino (Pérmico Medio – Triásico Tardío) cuya evolución tectónica y magmática se considera aún materia de debate. El Ciclo Pre-Andino abarca el término del amalgamiento de Pangea y el inicio de su desmembramiento, por ende, corresponde a un periodo en el que la velocidad de convergencia entre las placas (Panthalassa y Sudamericana) se ve fuertemente

disminuida e incluso se ha planteado como un periodo en el cuál la subducción a lo largo del margen se pausó como consecuencia del colapso del *slab* (Franzese & Spalletti, 2001; Mpodozis & Kay, 1992, 1990). Estas nuevas condiciones habrían favorecido la acumulación de calor en el manto superior, gatillando la producción de grandes volúmenes de magma silíceo a lo largo de Los Andes (Kay et al., 1989; Kleiman & Japas, 2009; Llambías & Sato, 1995; Martin et al., 1999; Mpodozis & Kay, 1990) y la formación de cuencas extensionales con una orientación NNW-SSE (Mpodozis & Kay, 1990; Mpodozis & Ramos, 1989; Suarez & Bell, 1992).

Una de las unidades más representativas de este gran volumen de magmatismo, corresponde al Grupo Choiyoi que se expone a lo largo de la Codillera Frontal, la Cuenca Neuquina y el Bloque San Rafael, y consiste en depósitos volcánicos de composición frecuentemente riolítica con sus cuerpos intrusivos subvolcánicos asociados (Charrier et al., 2007). Este grupo ha sido dividido en dos miembros (Kleiman & Japas, 2009): el Choiyoi inferior (Pérmico temprano) caracterizado por un magmatismo calcoalcalino relacionado a un arco continental (Ciclo Gondwánico); y el Choiyoi superior (Pérmico tardío – Triásico Inferior) con un magmatismo transicional entre calcoalcalino y uno alcalino bimodal que marca la evolución hacia un ambiente anorogénico de intraplaca. Las unidades chilenas equivalentes al Choiyoi Superior en la Cordillera Frontal entre los 28°S - 31°S corresponden a la Superunidad Ingaguás (Charrier et al., 2007; Mpodozis & Kay, 1992, 1990) y la Formación Pastos Blancos (Charrier et al., 2007; Martin et al., 1999).

El desarrollo de cuencas durante el ciclo Pre-Andino, ha sido dividido en dos etapas: (1) Pérmico Tardío? – Anísico Tardío y (2) Nórico – Sinemuriano. Estos episodios están separados por una extensa secuencia volcánica y volcanoclástica del Triásico Medio – superior (Formación La Totora), que ha sido propuesta como el pulso más joven del magmatismo del Choiyoi (Charrier et al., 2007). Los depósitos de la primera etapa son principalmente marinos y ellos están representados por las formaciones San Félix y Canto del Agua que afloran en la Precordillera y Cordillera de la Costa, respectivamente. Las unidades de la segunda etapa son secuencias volcano-sedimentarias de hasta 2,5 km de espesor con un volcanismo silíceo y basáltico y

características sedimentológicas propias de depósitos *syn-rift* (Suarez & Bell, 1992) y ellos corresponden a la Formación La Ternera, Estratos del Mono, Estratos del Verraco y la Formación Quebrada El Salitre, que afloran en la Precordillera y en la Cordillera Frontal. Ellos corresponden a los equivalentes temporales del Grupo Pre-Cuyo definido en Argentina. Este grupo incluye varios depocentros *syn-rift* que acumulan material volcánico intermedio a ácido y depósitos sedimentarios en hemigrábenes durante el Triásico Tardío – Jurásico Temprano (Franzese & Spalletti, 2001), que constituyen el basamento de la Cuenca Neuquina.

1.1.2 Limitaciones del modelo clásico propuesto para el Ciclo Pre-Andino

El modelo geotectónico propuesto para el Ciclo Pre-Andino, considera la transición hacia un contexto extensional con el desarrollo de un rift continental durante una subducción inactiva. Estas interpretaciones están basadas en datos geoquímicos limitados (principalmente análisis de roca total), análisis isotópicos de los sistemas Rb-Sr y Sm-Nd (siendo el primero fuertemente afectado por la alteración hidrotermal; White, 2013) y datos geocronológicos imprecisos basados en los métodos K-Ar y Rb-Sr. Actualmente, el cese de la subducción ha sido cuestionado por la nueva evidencia geológica, que presenta algunas inconsistencias con el modelo clásico. Una de ellas es una investigación de la evolución P-T-t de las rocas metamórficas que forman parte del antearco en el norte de Chile (31°S – 32°S), en el que se ha determinado que el desarrollo del prisma de acreción tomó lugar entre el Carbonífero y el Triásico Temprano (aproximadamente hasta los 245 Ma), proponiendo que la subducción fue un proceso activo al menos hasta ese momento (Willner et al., 2012). Parada (2013) sugiere que la subducción podría haber sido un proceso continuo entre el Carbonífero - Triásico, basado en un estudio petrográfico y geoquímico en rocas ígneas de esta edad, cuyos afloramientos se encuentran en la Alta Cordillera entre los 29°S – 29°30'S. Algunos autores proponen que las cuencas del Triásico Medio – Jurásico Temprano fueron desarrolladas en durante una subducción activa y que el magmatismo fue continuo desde el Pérmico hasta el Cretácico Tempano (Parada et al., a1999; Suarez & Bell, 1992). Además, recientes estudios llevados a cabo en el marco del FONDECYT 1120715 en rocas triásicas expuestas en la Alta Cordillera entre los 28°S – 30°S

(Coloma et al., 2015; González, 2015; Valin, 2014), han detectado una evidencia petrográfica y geoquímica que es consistente con un magmatismo generado en un margen activo. Oliveros et al. (2015) utilizando la geoquímica de las rocas ígneas Carboníferas - Jurásico Tardío que afloran en la Cordillera de la Costa, Pre-Cordillera y Altos Andes en el Norte de Chile (24°30'S – 30°S) proponen que la subducción fue un proceso continuo desde el Ciclo Gondwánico al Ciclo Andino, basado en la naturaleza calcoalcalina, el amplio espectro composicional y el dominio de composiciones intermedias.

De esta manera surgen las interrogantes que motivan esta investigación: ¿La subducción fue un proceso activo en el margen suroccidental de Gondwana desde el Paleozoico Superior hasta el Presente? ¿Cuáles son las características geoquímicas y petrográficas del magmatismo generado entre el Ciclo Gondwánico y el Ciclo Andino?

1.1.3 El magmatismo como una herramienta para descifrar la evolución andina

Las condiciones tectónicas que prevalecieron durante el Ciclo Pre-Andino, específicamente la pausa o desarrollo continuo de la subducción a lo largo del margen occidental de Gondwana, se pueden rastrear estudiando la evolución del magmatismo, considerando los cambios en sus fuentes y composición. Por un lado, si la subducción fue un proceso continuo, el magmatismo preandino tiene que registrar las características de un magmatismo continental relacionado a un arco, pero si ésta cesó e inició un contexto extensional que permitió el desarrollo de un rift continental, debe registrarse un cambio en las fuentes de los magmas. Por ello, es necesario investigar qué características tienen los magmas generados en zonas de subducción, que permiten distinguirlos de aquellos generados en un rift continental, teniendo en consideración que se podría haber desarrollado un escenario mixto.

Las rocas ígneas de un margen continental activo (MCA), se concentran en un área rectangular de 20 a 30 km de ancho, paralela a la fosa (Ducea et al., 2015; Stern, 2002). Tienen una afinidad principalmente calco-alcalina, con un amplio rango en el contenido de sílice (~45 – 75% SiO_2), típicamente sin brechas composicionales (Ducea et al., 2015), donde las andesitas son las rocas volcánicas más abundantes. Estas

rocas ígneas asociadas al arco tienen cantidades significativas de volátiles (H_2O y CO_2) y patrones distintivos de elementos traza (Pearce & Peate, 1995) con un enriquecimiento en LILE (*Large Ion Lithophile Elements*: K, Ba, Rb, La, Pb y U) en comparación con los HFSE (*High Field Strength Elements*: P, Ti, Nb, Ta, Zr y Hf) y una depresión frecuente en Nb-Ta (Philpotts & Ague, 2009; White, 2013; Wilson, 1989). Esta relación LILE - HFSE se ha atribuido al metasomatismo de la cuña del manto por los fluidos liberados del slab subductado (Stern, 2002; Wilson, 1989).

El magmatismo relacionado a un rift continental (RC) se distribuye en áreas donde la corteza se está adelgazando (en general son algunas decenas de kilómetros de ancho y decenas o cientos de largo; Wilson, 1989). Tiene afinidad principalmente alcalina (Wilson, 1989), con una composición bimodal habitual (ausencia de términos intermedios) (Philpotts & Ague, 2009; Wilson, 1989). Sus rocas ígneas presentan un enriquecimiento en volátiles (CO_2 y halógenos) y sus patrones de elementos traza muestran un enriquecimiento LILE, debido a la participación de la fuente enriquecida en la génesis del magma (litósfera continental, Wilson, 1989) y anomalías positivas en Nb-Ta. Sus patrones de elementos de tierras raras tienen un enriquecimiento LREE (*Light Rare Earth Elements*), y los HREE (*High Rare Earth Elements*) tienen concentraciones de dos a cinco veces la del condrito (Wilson, 1989).

Además de los contrastes en geoquímica elemental, las rocas de estos ambientes geotectónicos tienen diferencias en su composición isotópica y en su mineralogía (por ejemplo, piroxenos y anfíboles cálcicos en MCA, y sódicos en RC; Barbarin, 1999).

1.1.4 Revisión del magmatismo Pre-Andino de los Altos Andes del norte de Chile

En la Cordillera Frontal Chilena, entre los 28°30’S – 30°30’S, se encuentra expuesta una extensa franja de rocas ígneas generadas durante el Ciclo Pre-Andino (Figura 1.1), cuya nomenclatura y estratigrafía han experimentado cambios importantes en los últimos nueve años. Esto se debe a que se ha incrementado el control geocronológico con métodos más confiables (U-Pb, por ejemplo,. Maksaev et al., 2014) y se han confeccionado nuevas cartas geológicas a escala 1:100.000 (trabajo efectuado por el SERNAGEOMIN), que ha entregado nueva información sobre la distribución espacial de las unidades ígneas, sus relaciones de contacto y litologías. Haciendo uso de esta

nueva nomenclatura (Figura 1.2), las unidades que se han seleccionado para llevar a cabo esta investigación, corresponden a los complejos plutónicos Chollay (CPC) y Piuquenes (CPP), que representan la unidad intrusiva pre-andina de mayor extensión y a la Formación Guanaco Sonso, en parte contemporánea a estos complejos, que son representantes del Pérmico Superior – Triásico Medio; y a los Sienogranitos Colorado y la Formación Pastos Blancos como representantes del Cárnico – Nórico.

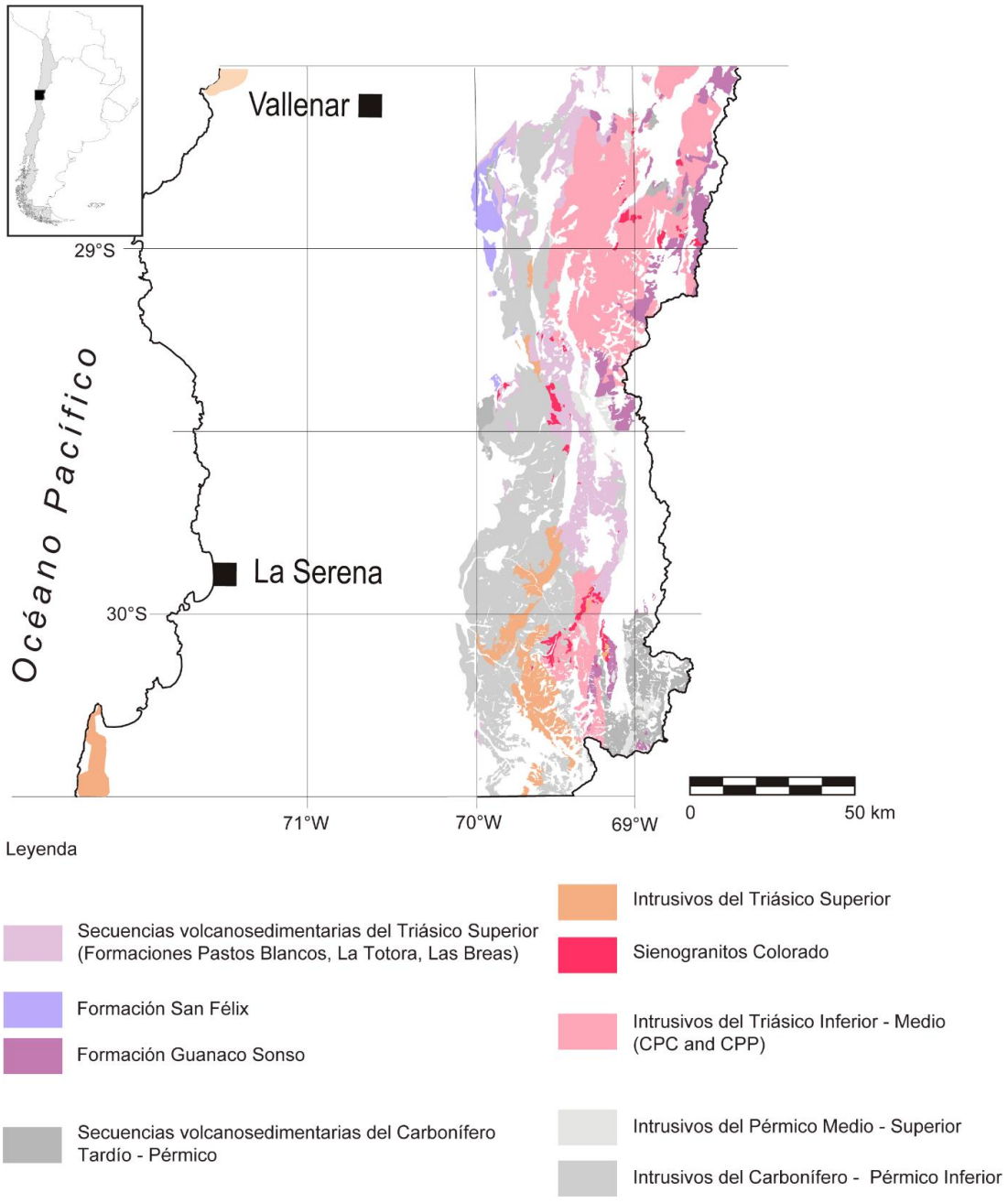

Figura 1.1 Distribución de las rocas ígneas del Carbonífero – Triásico entre los 28°30'S y los 30°30'S. Compilación de las cartas geológicas efectuadas por el SNGM a escala 1:100.000 (Murillo et al., 2017; Ortiz & Merino, 2015; Salazar et al., 2013; Salazar & Coloma, 2016)

A)

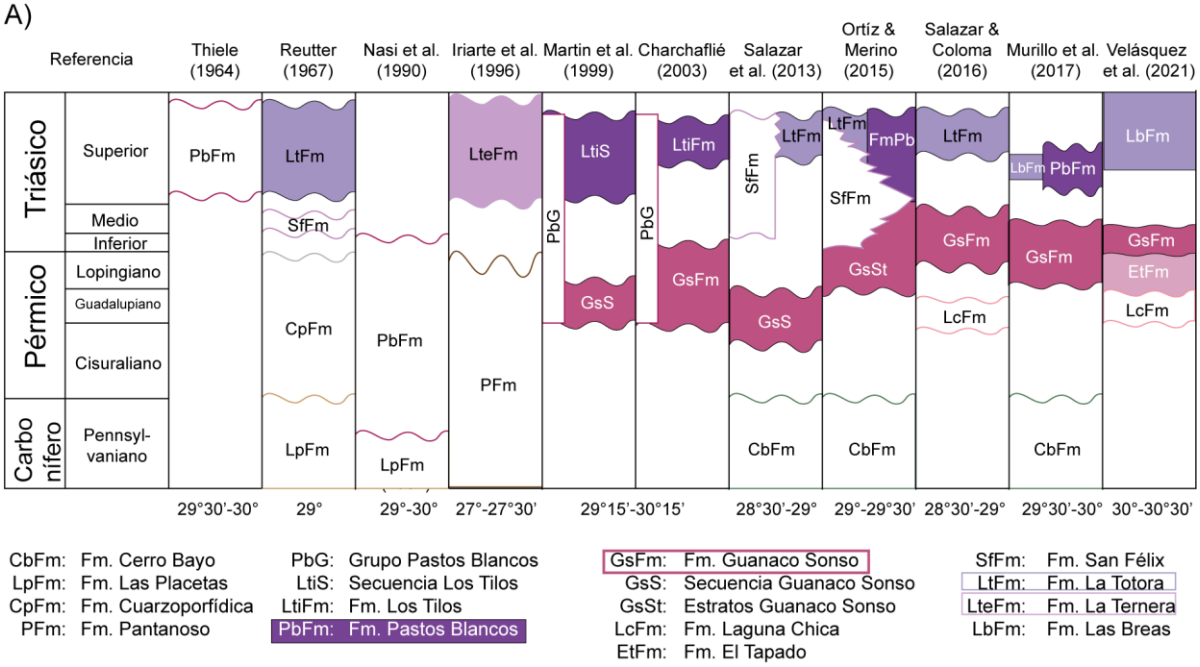

B)

Nasi et al., 1985	Mpodozis & Cornejo, 1988; Nasi et al., 1990; Martin et al., 1999; Moscoso et al., 2010	Salazar et al., 2013; Ortiz & Merino, 2015; Salazar & Coloma, 2016; Murillo et al., 2017; Velásquez et al., 2021
Batolitos Montosa - El Potro Chollay Elqui - Limarí	Superunidad Ingaguás (Pérmico - Triásico): Unidad El Colorado, Unidad El León, Unidad Chollay, Unidad Los Carricitos	Granito Monte Grande(219 - 214 Ma) Complejo Plutónico Los Carricitos (217 Ma) Gabros La Laguna (218 - 215 Ma) Sienogranitos Colorado (227 - 214 Ma) Monzogranitos El León (224 - 220 Ma) Complejo Plutónico Chollay (249 - 233 Ma) Complejo Plutónico Piuquenes (247 - 235 Ma) Monzogranitos y granodioritas La Ortiga (252 Ma)
	Superunidad Elqui (Carbonífero - Pérmico): Unidad El Volcán, Unidad Cochiguás, Unidad Montosa, Unidad Guanta	Tonalitas Quebrada Las Cañas (257 - 256 Ma) Granitos del Pérmico Medio - Triásico Inferior (262 - 248 Ma) Granodiorita Toro Muerto (262 Ma) Tonalita Quebrada El Pintado (275 - 263 Ma) Granodiorita Primero (276 Ma) Complejo Plutónico Chanchoquín (296 - 285 Ma) Complejo Plutónico Guanta (296 - 276 Ma) Intrusivos Plutónicos del Carbonífero Superior (322 - 299 Ma) Granito El Volcán (333 - 331 Ma)

Figura 1.2 Resumen de la actualización en la nomenclatura de las rocas (A) volcánicas y volcano-sedimentarias e (B) intrusivas de edad Carbonífero – Triásico Superior.

El Complejo Plutónico Chollay (249 – 233 Ma) se distribuye en una franja de orientación NE-SW que se extiende desde los 28°30'S hasta los 29°30°S, con un ancho de al menos 50 km. Dentro de ella se reconocen cinco asociaciones litológicas

principales: (1) dioritas-gabros con plagioclasa, ortopiroxeno, clinopiroxeno, anfíbol, apatito y titanita; (2) monzogranitos formados por cuarzo, plagioclasa, ortoclasa y algunos minerales máficos (biotita y anfíbol); (3) granodioritas con cuarzo, plagioclasa, feldespato alcalino, biotita, anfíbol, mica blanca, epidota y titanita; (4) tonalitas, compuestas por cuarzo, plagioclasa, ortoclasa y microclina, con biotita, anfíbol, apatito y circón; y (5) sienogranitos hololeucocráticos, localmente porfídicos, de color rojo ladrillo intenso (Ortiz & Merino, 2015; Salazar et al., 2013; Salazar & Coloma, 2016). El Complejo Plutónico Piuquenes (247 – 235 Ma), se expone entre los 29°50'S y los 30°30'S y está compuesto por cuatro litofacies: (1) monzogranitos y escasos sienogranitos de biotita de grano medio a grueso; (2) granodioritas a tonalitas; (3) sienogranitos porfídicos de color rojizo a marrón; y (4) dioritas, dioritas cuarcíferas de anfíbol y monzodioritas de anfíbol y clinopiroxeno (Velásquez et al., 2021). La unidad Sienogranitos Colorado (227 – 214 Ma), presenta afloramientos mucho más restringidos y corresponden a sienogranitos porfídicos de color rojo anaranjado compuestos por ortoclasa (escasa microclina), cuarzo, plagioclasa y pequeñas cantidades de moscovita y anfíbol. Dentro de esta unidad también se encuentran monzogranitos y granitos alcalinos (Salazar & Coloma, 2016).

Las rocas volcánicas y volcanoclásticas afloran en dos fajas con orientaciones N-S y NNE-SSW. En la franja occidental se encuentra la Formación La Totora (28°30'S – 29°S) que consiste en flujos de lava andesítica y basáltica-andesítica y potentes facies brechosas, con arcosas líticas rojizas intercaladas, cuarzoarenitas, tobas de lapilli y de ceniza, domos riolíticos, lutitas y basaltos negros de orto y clinopiroxeno (Salazar et al., 2013). En la franja oriental aflora la Formación Pastos Blancos, formada por flujos de lava (andesitas basálticas – riolitas), rocas piroclásticas y rocas sedimentarias menores (González, 2015) y la Formación Guanaco Sonso, compuesta por tobas vítricas soldadas, tobas dacíticas y areniscas finas laminadas, intercaladas con lapillitas. Las rocas de la Formación Guanaco Sonso tienen un amplio rango de composición, pero las composiciones ácidas son las más dominantes (Salazar & Coloma, 2016).

La geoquímica de roca total de estas unidades muestra que las rocas presentan una tendencia calcoalcalina y pertenecen a las series de medio a alto potasio. Además, tienen un enriquecimiento LILE y depresiones en Ta, Nb, Ti y P, razones $(La/Yb)_N$ entre 4 y 20 y un amplio rango de SiO_2 (45% - 82%) (Coloma et al., 2015; González, 2015; Oliveros et al., 2015; Salazar et al., 2013; Salazar & Coloma, 2016).

1.1.5 Una nueva perspectiva para el Ciclo Pre-Andino

Las unidades descritas anteriormente son un elemento clave en la comprensión de cómo ocurrieron los cambios para generar condiciones contrastantes entre los ciclos Gondwánico y Andino. En términos petrográficos y geoquímicos elementales, las unidades a estudiar presentan importantes similitudes con aquellos magmas generados en un margen continental activo, por lo que surge la hipótesis de que estas rocas ígneas se formaron en un contexto de subducción, proponiendo que la subducción pudo haber sido un proceso continuo desde el Ciclo Gondwánico hasta el presente. En particular, los complejos plutónicos Chollay y Piuquenes y las unidades volcánicas contemporáneas se proponen como el arco del Triásico en el norte de Chile (28°30’S - 30°30’S).

Según la bibliografía, estas unidades han sido estudiadas en numerosos trabajos, que incluyen la descripción petrográfica de secciones clave y dataciones radiométricas, pero en general se han realizado pocos análisis geoquímicos sistemáticos, por lo que no se han podido determinar con claridad las fuentes magmáticas y por lo tanto existen dudas sobre el contexto tectónico que permitió su formación.

Para testear la hipótesis, se analizará el arco propuesto comparándolo con otros sistemas de arcos magmáticos y con el magmatismo generado durante los ciclos Gondwánico y Andino. Por otro lado, se determinarán las fuentes magmáticas que dan origen a las unidades preandinas, a partir de estudios isotópicos (Sr-Nd-Pb) tomando los resguardos necesarios, considerando la alteración hidrotermal existente en el área de estudio. También se considerará la evaluación de los posibles procesos involucrados en la génesis de los magmas, mediante modelado geoquímico con elementos traza. De esta forma se determinará el entorno tectónico más probable en el que se podrían haber generado.

Hipótesis de trabajo

Las rocas intrusivas y volcánicas triásicas que afloran en la Cordillera Frontal Chilena entre los 28°S y los 30°S se formaron en un ambiente de suprasubducción, específicamente en un ambiente de arco.

1.2 Objetivo principal

Evaluar si la subducción fue un proceso activo durante la formación de los magmas que dieron origen a las rocas ígneas triásicas que afloran en la Alta Cordillera entre los 28°S y 30°S

1.3 Objetivos específicos

Objetivo específico I (O.E.I): Determinar los mecanismos de construcción del Complejo Plutónico Chollay y evaluar la relación entre ese complejo y el volcanismo contemporáneo de la Formación Guanaco Sonso.

Objetivo específico II (O.E.II): Determinar las fuentes de los magmas, con particular atención en la contribución cortical a aquellas fuentes, los procesos que operan durante la evolución de los magmas y el ambiente tectónico más probable que hizo posible su formación.

Objetivo específico III (O.E.III): Comparar el magmatismo triásico en estudio con batolitos cordilleranos generados a lo largo de márgenes de placa activos y contrastar sus características con aquellas del magmatismo gondwánico y andino.

1.4 Metodología

A continuación, se describe la metodología empleada para cumplir con cada uno de los objetivos específicos planteados en este trabajo.

1.4.1 Metodología asociada al O.E.I

Construcción del Complejo Plutónico Chollay: Se efectuará una revisión del mapeo en una sección específica del Complejo Plutónico Chollay en el Valle del Río El Tránsito (aproximadamente a los 29°S), poniendo especial énfasis en los contactos con la roca hospedante y en las relaciones internas de contacto dentro del batolito. Los diferentes

cuerpos que conformen al complejo serán caracterizados petrográfica y geoquímicamente (*X-Ray Fluorescence, XRF* para elementos mayores; *Inductively Coupled Plasma Mass Spectrometry, ICP-MS* para elementos traza). Se utilizarán las dataciones ya efectuadas por el Servicio Nacional de Geología y Minería durante la confección de las cartas El Tránsito – Lagunillas, Cerros de Cantaritos - Laguna Chica y Río Chollay – Matancilla y Cajón del Encierro, y aquellos datos geocronológicos que se encuentren publicados. Se estimarán las profundidades de cristalización mediante química mineral, midiendo el contenido de Al en los cristales de anfíbol (vía *Electron Probe Micro-Analyzer,* EPMA). La información recolectada por medio de estos análisis y las relaciones entre los plutones del Complejo Plutónico Chollay, permitirán determinar el estilo de construcción del complejo.

1.4.2 Metodología asociada al O.E.II

Fuentes del magmatismo triásico: Para determinar las fuentes del magmatismo Pre-Andino, se seleccionarán muestras de las diferentes unidades ígneas triásicas, tras su descripción petrográfica y la medición de la concentración de elementos mayores y traza en roca total. Las muestras seleccionadas, serán sometidas a un análisis geoquímico isotópico de roca total para determinar las razones isotópicas de los sistemas Rb-Sr, Sm-Nd y U-Th-Pb por medio de espectrometría de masa por ionización termal (*Thermal Ionization Mass Spectrometry, TIMS*). Además, algunas muestras de la roca hospedante del magmatismo triásico serán analizadas también para caracterizar parte de la corteza triásica.

Procesos involucrados en la evolución de los magmas: Los procesos involucrados en la evolución de los magmas pueden ser detectados por medio de la descripción petrográfica o mediante diagramas geoquímicos, y evaluados mediante modelación geoquímica. Algunos de los procesos que pueden ser testeados corresponden a la contaminación cortical, fusión parcial y procesos de asimilación y cristalización fraccionada. Para estos modelos, las rocas magmáticas menos evolucionadas serán utilizadas como una fuente mantélica y la corteza será modelada utilizando la composición del basamento en el que el magmatismo triásico se encuentra emplazado

(por ejemplo: Gneisses La Pampa, Complejo Metamórfico El Tránsito, Tonalitas Quebrada El Pintado, Tonalita Quebrada Pinte).

1.4.3 Metodología asociada al O.E.III

Base de datos geoquímicos: Los resultados de elementos mayores, traza e isótopos serán incorporados en una base de datos geoquímicos que contará con todos los resultados de los análisis de rocas ígneas triásicas estudiadas durante el desarrollo del proyecto FONDECYT 1120715, los datos disponibles en la literatura de las unidades triásicas chilenas y finalmente los análisis disponibles de las unidades argentinas equivalentes. La información geoquímica de las rocas volcánicas e intrusivas de los ciclos Gondwánico y Andino, serán también añadidas a esta base de datos para generar comparaciones con el magmatismo del Ciclo Pre-Andino. Para llevar a cabo estas comparaciones, se utilizarán ciertas razones de interés para evaluar cambios en el espesor cortical (por ejemplo, La_N/Yb_N) y la contribución de la corteza a la fuente de los magmas (por ejemplo, εNd, εHf). Por último, se agregará a esta base de datos, la información geoquímica de un batolito cordillerano para contrastarla con el magmatismo Pre-Andino expuesto en el norte de Chile.

1.5 Estructura de la tesis

El cuerpo de la tesis consta de tres publicaciones enfocadas en el magmatismo triásico, que cumplen los objetivos de este trabajo. El primer artículo (Capítulo II, publicado en *Gondwana Research*) abarca el estudio del plutonismo y volcanismo Triásico expuesto entre los 25°S – 30°S, caracterizando las unidades expuestas desde el punto de vista petrográfico y geoquímico, y se contrasta con una gran base de datos geoquímicos de rocas ígneas que afloran entre los 18°S – 40°S del magmatismo Gondwánico, Pre-Andino y Andino, proponiendo un nuevo modelo geotectónico que permite explicar los cambios reconocidos en el registro magmático. El segundo artículo (Capítulo III, enviado a *Contribution to Mineralogy and Petrology*) se enfoca en dos unidades específicas que corresponden a los complejos plutónicos Chollay y Piuquenes, aflorantes en la Cordillera Frontal Chilena, que representan las unidades Pre-Andinas con mayor área expuesta abarcando aproximadamente 2.100 km^2. Estas unidades conforman un batolito del Triásico Inferior – Triásico Medio, dominado por

monzogranitos y granodioritas hololeucocráticas a leucocráticas. En este trabajo, ambos complejos fueron caracterizados incluyendo sus características de campo y relaciones de contacto, su petrografía y geoquímica tanto elemental como isotópica y en base a sus características es posible corroborar que fueron emplazadas en un contexto de subducción. Sus razones La/Yb_N, la baja contribución cortical a la fuente de sus magmas, su emplazamiento contemporáneo con el desarrollo de las cuencas San Félix y Guanaco Sonso, sumado a las nuevas reconstrucciones de la dinámica de placas, permiten proponer que corresponde a un cinturón magmático creado en un margen convergente extensional y en retroceso. Los complejos fueron comparados con un batolito generado en un margen convergente compresivo, que corresponden a los batolitos más comunes y estudiados. El tercer artículo (Capítulo IV, publicado en *Journal of South American Earth Sciences*), está enfocado en las rocas volcánicas del Triásico Superior que forman parte de la Formación Pastos Blancos y un enjambre de diques máficos contemporáneos, correlacionables con enjambre de diques máficos del Valle del Elqui. Se llevó a cabo una descripción de sus afloramientos y relaciones de contacto, un estudio petrográfico y geoquímico, y una posterior comparación con otras unidades triásicas para evaluar los cambios temporales desde el punto de vista geoquímico, proponiendo un contexto geotectónico para el margen suroccidental de Gondwana durante el Triásico Superior.

Se incluye además un capítulo complementario (Capítulo V) que corresponde a un cuarto artículo publicado en *Journal of South American Earth Sciences* en el que se realizó una estimación del volumen y composición de la Provincia Magmática del Choiyoi (ChMP) con la finalidad de compararlo con otras SLIPs (*Silicic Large Igneous Provinces*). El magmatismo de la ChMP se divide en tres grandes regiones: Andino, Corredor Permo-Triásico de La Pampa y Patagonia Norte. La ChMP es comparada con otros SLIPs generado en zonas de rift continental y en márgenes convergentes, y se puede concluir que el ChMP fue parcialmente generado en un contexto de subducción activa.

Por último, en el sexto capítulo se encuentra la discusión y principales conclusiones de la tesis en la que se integran los resultados obtenidos en este trabajo, entregando

una nueva visión del magmatismo triásico expuesto en la Alta Cordillera en el norte de Chile.

CAPÍTULO II: EVOLUCIÓN DEL MAGMATISMO CARBONÍFERO – JURÁSICO EXPUESTO EN EL MARGEN OCCIDENTAL DE GONDWANA (18°S – 40°S)

Manuscript title: Lithospheric evolution of the Pre- and Early Andean convergent margin, Chile.

Authors: Verónica Oliveros[1*], Paulina Vásquez[2], Christian Creixell[2], Friedrich Lucassen[3], Mihai Nicolae Ducea[4,5], Isabella Ciocca[1], Javiera González[1], Mauricio Espinoza[1], Esteban Salazar[2], Felipe Coloma[2], Simone Kasseman[3]

[1] Departamento Ciencias de la Tierra, Universidad de Concepción, Casilla 160-C, Concepción, Chile.

[2] Servicio Nacional de Geología y Minería, Av. Santa María 104, Santiago, Chile.

[3] MARUM Center for Marine Environmental Sciences, University of Bremen, Leobener Strasse, D-28359, Bremen, Germany

[4] Department of Geosciences, University of Arizona, Tucson, AZ 85721, USA

[5] Universitatea Bucuresti, Facultatea de Geologie Geofizica, Strada N. Balcescu Nr 1, Bucuresti, Romania

Published as: Oliveros, V., Vásquez, P., Creixell, C., Lucassen, F., Ducea, M. N., Ciocca, I., González, J., Espinoza, M., Salazar, E., Coloma, F., & Kasemann, S. A. (2020). Lithospheric evolution of the Pre- and Early Andean convergent margin, Chile. In Gondwana Research (Vol. 80, pp. 202–227). Elsevier Inc. https://doi.org/10.1016/j.gr.2019.11.002

Abstract

The proto-Andean and Early Andean evolution of the southwestern Gondwana margin comprises three stages that differ in their magmatic evolution and deformational style: the Gondwana cycle (~330-280 Ma), the Pre-Andean stage (~280-210 Ma) and the Early Andean Cycle (210-100 Ma). These stages have been traditionally interpreted as the upper crustal response to changes in the tectonic setting which include: Cordilleran-style continental arc (Gondwana cycle), orogenic collapse and possibly slab break-off that led to continental rifting and extensive crustal melting (Pre-Andean stage), and subsequent subduction re-initiation in oceanic arc-style context (Early Andean cycle).

The petrological and geochemical characteristics of Carboniferous to Jurassic igneous rocks from this region however do not support the described model. Elemental and Sr-Nd-Pb isotopic data of 86 samples, along with a compilation of ~1230 samples from the literature suggest that subduction was the most likely process by which the magmatic record was generated. Sub-alkaline affinities, LILE enrichment over HFSE, Nb-Ta troughs, porphyritic textures and hornblende- and biotite-bearing lithologies are present in all studied units, whereas isotopes suggest that magma sources are a mixture of depleted mantle and variable contribution from the continental crust. Even though the aforementioned features are common to all igneous rocks, some changes point to a decline in the contribution of crustal/lithospheric sources to the magmatism with time. Thus, SiO_2, La_N/Yb_N and $^{87}Sr/^{86}Sr_{initial}$ exhibit a systematic decrease from ~285 to 150 Ma, whereas the $\varepsilon Nd_{initial}$ parameter increases in the same period.

These changes were accompanied by the shift from dominant compressional (Carboniferous-Early Permian) to transtentional (Middle Permian-Jurassic) stresses in the upper crust, suggesting that the margin went from advancing to retreating due to Pangea reorganization and break-up. Following a potential flat slab event, slab roll-back may have induced extension in the upper crust and lithospheric loss as a consequence of delamination or thermal erosion.

2.1 Introduction

The continental margin of southwestern South America has been periodically active since the Early Paleozoic, as early as the Cambrian (Escayola et al., 2007), but certainly since the Early Carboniferous (e.g. Bahlburg et al., 2009; Charrier et al., 2007; 2014; Mpodozis and Ramos, 1989, Willner et al., 2008). Two orogenic cycles, the Early Carboniferous-Early Permian Gondwana cycle and the Jurassic to recent Andean cycle, both separated by the Pre-Andean stage, from the Middle Permian to Late Triassic (Charrier et al., 2007) have been widely proposed in the southern central Andes of north and central Chile between the Pacific coast and the border region to Argentina (e.g., Coira et al., 1982; Ruiz, 1965; Vicente, 1975). Published research indicates that both cycles differ mostly in their magmatic products and tectonic regime. While the Gondwanan cycle involves, beside the mantle source, relevant amounts of crustal additions to arc magmatism in a compressive tectonic setting (e.g. Hervé et al., 2014; Lucassen et al., 1999; Mpodozis and Ramos, 1989), the Andean Cycle is dominated by mantle additions to magmatism (Lucassen et al., 2006; Oliveros et al., 2007; Rossel et al., 2013) in a variable tectonic setting, from dominantly extensional/transtensional in the Jurassic-early Cretaceous, to compressive and transpressive since the Late Cretaceous (Arriagada et al., 2006; Charrier et al., 2014; Pichowiak et al., 1990; Scheuber et al., 1994). In this region, as often is the case with subduction-related magmatic arcs elsewhere in the geologic archive, the main set of tools used for identifying past tectonics environments comes primarily from the geochemistry of magmatic rocks themselves.

This study focuses on the tectonic and magmatic evolution associated to the period in between the two orogenic cycles, from Middle Permian to Late Triassic times, which is still a subject of debate. The time span of this stage is bracketed in between the initial phases of the Choiyoi magmatism, at ~285 Ma (Sato et al., 2015), and the beginning of the Andean subduction at the Triassic-Jurassic boundary (Charrier et al., 2007). The classic interpretation of the Choiyoi magmatism and its tectonic setting includes orogenic collapse that triggered extensive crustal anatexis followed by continental rifting, possibly slab break-off and the termination of subduction (Kleinman and Japas,

2009; Mpodozis and Ramos, 1989), a model that has also been proposed for northern Chile and Perú (Miskovic et al., 2009; Mpodozis and Kay, 1992). However, many recent studies have highlighted the lack of geochemical and petrological signatures of such tectonic configuration in the Permian and Triassic geological record (e.g. Coloma et al., 2017; Del Rey et al., 2016, 2019; Espinoza et al., 2019; González et al. 2018; Rocher et al., 2016). In addition to that, there is no tectono-magmatic model that accounts for the geodynamics mechanisms by which the subduction would have resumed along the margin in the Early Jurassic, perhaps due to the fact that the lithological units of this time span do not correspond to what would be expected for a subduction initiation setting (e.g., forearc ophiolites with chemical evolution from tholeiitic basalt to high-Mg andesites and boninites, Stern et al., 2012; Whattam and Stern 2009). Thus, whereas the processes of Early Andean subduction are fairly well understood (Lucassen et al., 2006; Oliveros et al., 2007; Pichowiak et al., 1990), the inferred onset of this subduction process is much less clear. On the other hand, recent global reconstructions of plate motion back to the Devonian, suggest that Southwestern Gondwana would have been a convergent margin from the Carboniferous to the Jurassic, and would have maintained this character after supercontinent break-up (Müller et al., 2016; Riel et al. 2018; Young et al., 2019). A reappraisal of the classic model for the Late Paleozoic-Early Mesozoic evolution of the margin seems thus necessary at this point.

The modern forearc region of north-central Chile (22º-30ºS) preserves the geological record from three stages mentioned above (Gondwana cycle, Pre-Andean stage and Andean cycle) (Fig. 2.1). Remarkably large volumes of volcanic, plutonic and sedimentary rocks of Carboniferous to Early Cretaceous ages are exceptionally well exposed due to prevalent arid to semiarid climatic conditions. Consequently, this area is suitable for a large temporal scale study of the magmatic evolution of the continental margin, in order to get a more detailed image of the tectonic regime associated to the transition between the Gondwana and Andean cycles.

In this work, we present newly acquired elemental and Sr-Nd-Pb isotopic data for volcanic and plutonic rocks of mainly Triassic age cropping out in northern Chile between 25º and 30º S, along with a comprehensive compilation of stratigraphic data

and structural relationship of the geological units of this period. The geochemical data are contrasted to a database of ~1050 geological samples from igneous units of Carboniferous to Jurassic age, cropping out between 18º and 40ºS in Chile and western Argentina (Fig. 2.1), in order to unravel the tectonic evolution of the continental lithosphere during this time span.

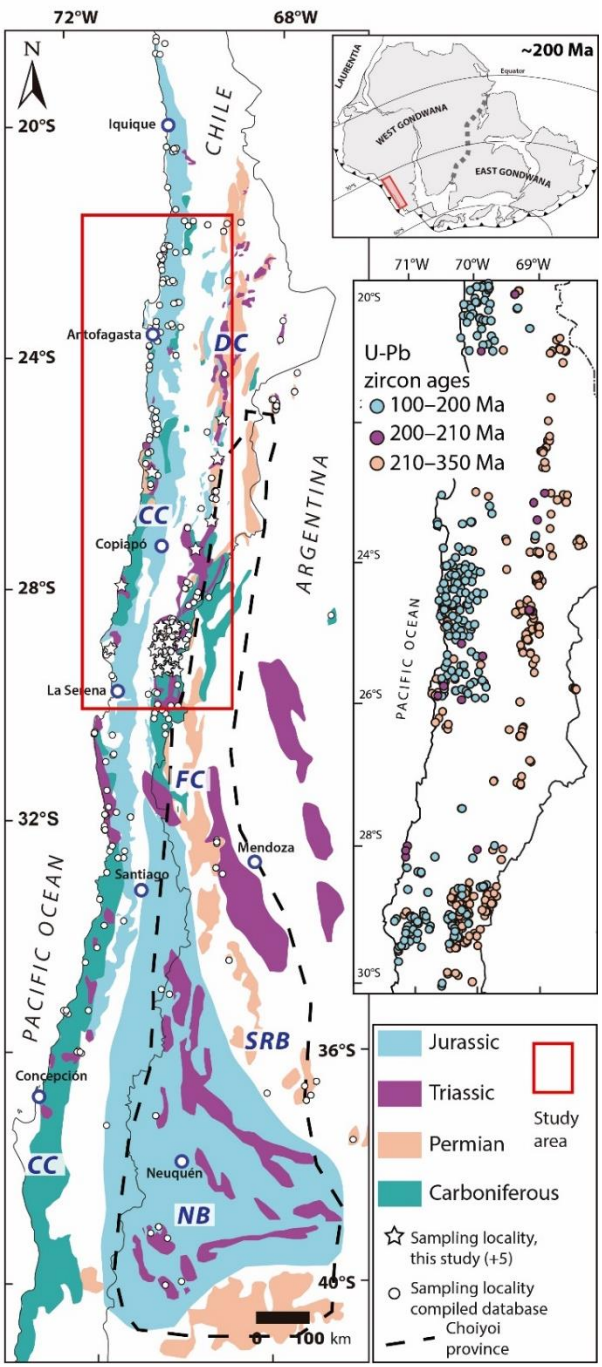

Figure 2.1. Schematic distribution of the Late Paleozoic to Jurassic units cropping out in Chile and Western Argentina between 20º and 40ºS and sample locations. In the case of Jurassic deposits of the Neuquén Basin, they are represented as the proposed full extension of the basin during the Jurassic (Howell et al., 2005). DC: Domeyko Cordillera; FC: Frontal Cordillera; SRB: San Rafael Block and NB: Neuquén Basin. White stars indicate locations with 5 or more samples analyzed for this study (see Tables 2.2 and 2.3 for specific locations). White dots show locations of samples from the compiled database of published works (Supplementary Material). The limits of the Choiyoi province are after Kleiman and Japas (2009) and Limarino and Spalleti (2017), and include only Middle Permian to Early Triassic rocks. Compilation of the U-Pb zircon ages in the study area is from the Chilean National Geological and Mining survey (SERNAGEOMIN) and its program for the updating of the geological cartography in northern Chile.

2.2 Geological Setting

The Andean region in northern Chile, between 22º and 30ºS features three important morphostructural units where Paleozoic and Mesozoic units crop out: the Coastal Cordillera, Frontal Cordillera (27º30'- 30º'00'S) and Domeyko Cordillera (22º00' – 27º30'S) (Figs. 2.2, 2.3). In the Frontal Cordillera, large portions of crystalline Paleozoic to Triassic rocks, mostly fragments of magmatic arcs, are exposed. Their current exposure was controlled by a thick-skinned deformation style which occurred in response to crustal shortening during the Eocene and Miocene compressional events (Cembrano et al., 2002; Fosdick et al., 2015; Lossada et al., 2017) (Fig. 2.2). The cover of these crystalline rocks consists mostly of Triassic to Late Jurassic inverted backarc basins (Oliveros et al., 2012), Neogene, arc-related, volcanic sequences (Bissig et al., 2003; Kay and Mpodozis, 2001) and sedimentary filling of foreland basins in the Argentinian side (Fosdick et al., 2015).

Gondwana Cycle (Late Carboniferous to ~285 Ma). The representative units of this orogenic cycle between 22º and 30ºS are distributed along two parallel N-S oriented belts: 1) voluminous plutonic complexes with minor metamorphic and volcanic rocks in the Frontal and Domeyko Cordilleras to the east, 2) and metamorphic complexes in the Coastal Cordillera to the west (Fig. 2.1). In the eastern belt, restricted patches of Devonian to Early Carboniferous metasedimentary and metavolcanic complexes (Fig. 2.3, Cornejo et al., 2009; Maksaev et al., 2014; Tomlison et al., 1999) are exposed as tectonic slices controlled by Incaic transpressive/reverse structural systems around 26º S, and similar to the south, between 28º and 30º S (Nasi et al., 1990; Ribba et al., 1988; Salazar and Coloma, 2016), or as roof-pendant on Late Paleozoic granitoids (e.g. El Cepo Metamorphic Complex, 30ºS, Murillo et al., 2017; Ortiz and Merino, 2015). These granitoids are in turn the most voluminous constituents of the Frontal and Domeyko Cordilleras. They are represented by dominantly metaluminous and calk-alcaline diorites to granites with ages ranging from the Late Carboniferous (330 Ma) to the Cisuralian (260 Ma) (Hervé et al., 2014; Maksaev et al., 2014; Ortiz and Merino, 2015; Pankhurst et al., 1996; Salazar et al., 2013). Volumetrically minor volcanic sequences of the same age have also been recognized in the study area,

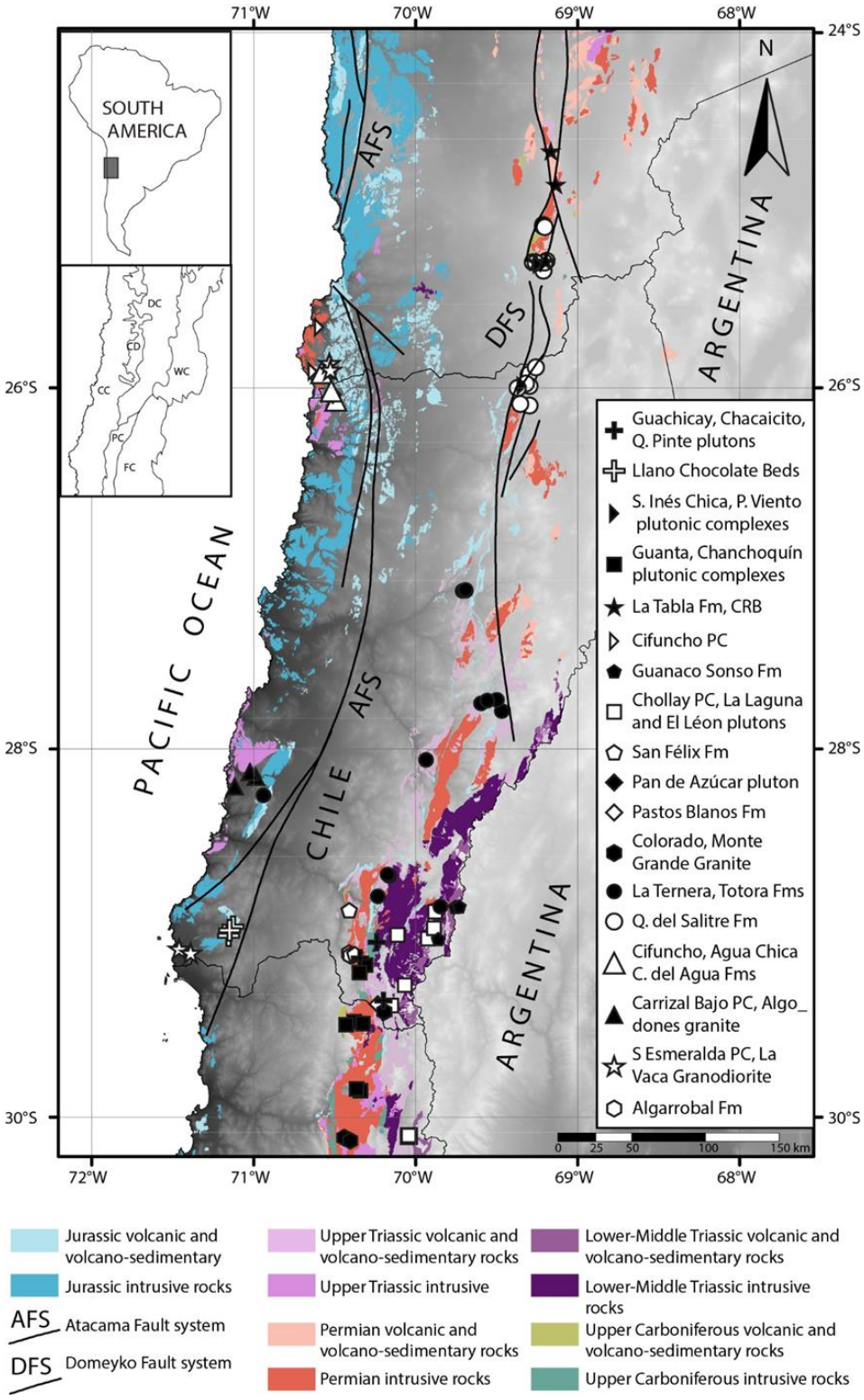

Figure 2.2. Simplified geological map showing the distribution of Upper Carboniferous to Jurassic volcano-sedimentary and intrusive rocks in northern Chile between 22º and 30ºS, and limits of the main morphotectonic units in Chile and Argentina at the same latitudes (inset).. CC: Coastal Cordillera, DC: Domeyko Cordillera, CD: Central Depression, PC: Principal Cordillera, WC: Western Cordillera, FC: Frontal Cordillera, PC: plutonic complex, CRB: Cerro Ratones Beds.

corresponding to the Cerro Bayo Formation and the lower part of the La Tabla Formation (Maksaev et al., 2014; Salazar et al., 2013).

These rocks are partly coeval with Late Paleozoic forearc sedimentary sequences and metamorphic complexes that are currently exposed along the coast south between 26º and 29ºS, (Fig. 2.3)(Bell, 1987; Creixell et al., 2016; Fuentes et al., 2019) and their equivalents around 31ºS (Choapa Metamorphic Complex, Arrayán and Huentelauquén formations; Rebolledo and Charrier, 1994; Thiele and Herve, 1984; Willner et al., 2008). These rocks are representative of an accretionary prism (Bell, 1987) that was active during the Late Carboniferous-Early Permian, when subduction resumed along the western margin of Gondwana after the Devonian (Mpodozis and Ramos, 1989; Pankhurst et al., 2015). In the study area, the Carboniferous to Cisuralian Permian granitoids and volcanic rocks that crop at the Frontal and Domeyko Cordilleras in the study area represent the magmatic arc (Mpodozis and Kay, 1992; Hervé et al. 2014; del Rey et al., 2016). Similarly, the Carboniferous plutons cropping out in the Coastal Cordillera south between 32º and 38ºS, are also interpreted as the Gondwana magmatic arc (Deckart et al., 2014). This cycle ended with the development of the San Rafael orogenic phase, a compressive event that would have propagated deformation inland as fold-and-thrust belts during the Early Permian at least between 35° and 30°S (Rapalini and Astini, 2005; Kleiman and Japas, 2009) but also in northermost Chile at 23°-22°S (Tomlinson et al., 2012). It has been proposed that this orogenic phase may have been due to the collision of a continental terrain (Mpodozis and Kay, 1992) but more recently has been attributed to the processes of non-collisional orogens such as slab shallowing or flat-slab subduction (Martínez, 2004; Kleiman and Japas, 2009; Tomlinson et al., 2012; Del Rey et al., 2016, 2019).

Pre-Andean stage (~285 Ma to Rhaetian). In the Frontal and Domeyko Cordilleras between 24º and 30ºS, Permian pyroclastic and effusive rocks along with plutonic complexes of intermediate to acidic composition are the youngest Paleozoic units cropping out (Fig. 2.2). Among the volcanic units, the La Tabla and Guanaco Sonso formations are the thickest and more widespread sequences. Both units extend beyond the Permian boundaries: the lower sequences of the la Tabla Formation are

Carboniferous in age and the upper strata of the Guanaco Sonso Formation overlap in time with the Early Triassic plutons and sedimentary units (Fig. 2.3). Cisuralian to Lopingian intrusives also crop out in this area and are spatially related to the coeval volcanic rocks (Brown, 1991; Ortiz and Merino, 2015; Salazar and Coloma, 2016).

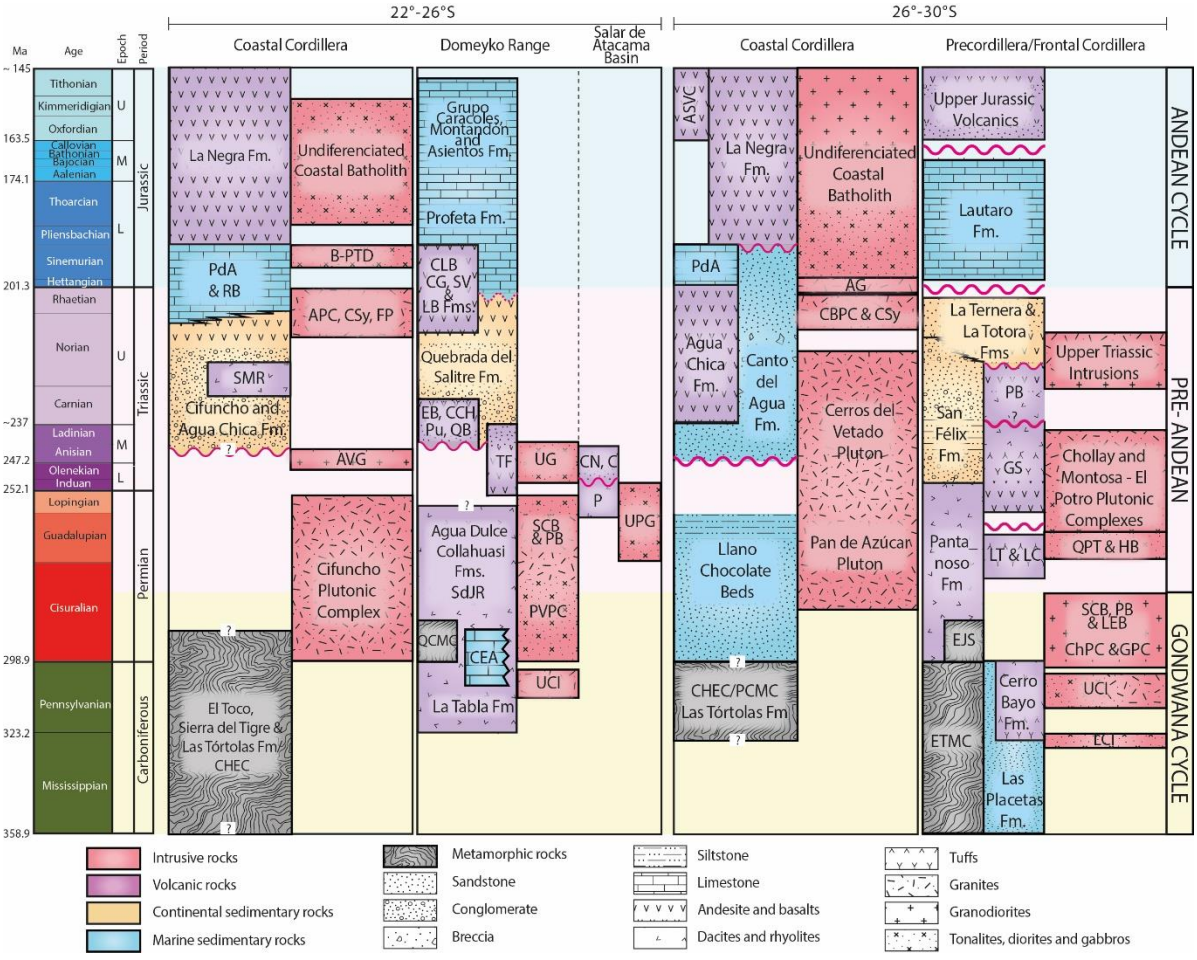

Figure 2.3. Chronostratigraphic scheme of the relevant units in northern Chile between 22º and 30ºS.CHEC: Chañaral Epimetamorphic Complex, QCMC: Quebrada del Carrizo Metamorphic Complex; PCMC: Punta de Choros Metamorphic Complex; CMR: Sierra Miranda Rhyolites; PdA: Pan de Azúcar Fm; RB: Rencoret beds; ACP: Anchuña Plutonic Complex; FP: Flamenco Pluton; CSy: Capitana Syenogranites; B-PTD: Bolfin-Punta Tetas Metadiorites; AVG: Agua Verde Granodiorite; CLB: Cerro La Ballena Fm; CG: Cerro Guanaco Fm; SV: Sierra de Varas Fm; LL: Las Lomas; EB: El Bordo Beds, CCH: Cerros de Chuquicamata; Pu: Pular Fm; TF: Tuina Fm; SdJR: Sierra del Jardín Rhyolites; CA: Cerro El Árbol Fm; UG: Undiferentiated granitoids; SCB: Sierra del Castillo Batholith; PB: Pedernales Batholith; PVPC: Punta del Viento Plutonic Complex; UCI: Upper Carboniferous intrusives; CNB: Cerro Negro Beds; C: Cas FM.; P: Peine Fm; AG: Algodones Granite; CBPC: Carrizal Bajo Plutonic Complex; EJL: El Jardín Schists; ETMC: El Tránsito Metamorphic Complex; PBF: Pastos Blancos Fm; GS; Guanaco Sonso Fm and Paso del Guanaco Sonso Beds; LT: La Tabla Fm; LC: Laguna Chica Fm; QPT: Quegrada del Pintado Tonalites; HB: Hielo Batholith; LEB: La Estancilla Batholith; ChPC: Chanchoquín Plutonic Complex; GPC: Guanta Plutonic Comple. Upper Jurassic Volcanics include the volcano-sedimentary units: Lagunillas, Algarrobal and Sierra Fraga formations, and Quebrada Vicuñita BedsStratigraphic series and their numerical ages are from Cohen et al. (2017).

Triassic magmatic rocks make up most of the volume of the eastern part of the Frontal Cordillera in the Chilean side south of 28º S (Fig. 2.2). Lower-Middle Triassic intrusive rocks ranging from diorite to granites in composition crop out between 28º and 30ºS in the Frontal Cordillera with the most representative unit being the Chollay Plutonic Complex (Fig. 2.3). These plutonic complexes are covered by Permian and Late Triassic, that include pyroclastic, hypabyssal and effusive rocks of ages between 233 and 219 Ma (Maksaev et al., 2014; Ortiz and Merino, 2015). Upper Triassic plutons are also found in the Frontal Codillera, although they are volumetrically much more restricted than the older intrusives. These units are composed of monzo and syenogranite of ca. 225-220 Ma in age (Nasi et al., 1990) and intermediate to acidic, cordierite-bearing, small plutons of ca 217-214 Ma in age (Hervé et al., 2014; Nasi et al., 1990). Lower-Middle Triassic volcanic rocks crop out in the eastern flank of the Domeyko Cordillera, in the vicinity of the Salar de Atacama (~23º40'S, 68ºW) (Breitkreuz et al., 1989). The youngest Late Triassic volcanic units correspond to basic to intermediate lava sequences and related volcanosedimentary rocks of Norian-Rhaetian (Domeyko Cordillera) or Carnian-Norian (Frontal Cordillera) age, which were deposited directly over Late Paleozoic to Early-Middle Triassic plutonic rocks (Martínez et al., 2015; Salazar et al., 2013).

Along the Coastal Cordillera, the record of Cisuralian to Triassic rocks is restricted. Around 25º30'-26ºS there are two plutonic complexes of Permian age (Cifuncho and Pan de Azúcar, Figs. 2.2,2.3), composed of granodiorite to syenogranite intrusives, which are the sole Late Paleozoic plutonic rocks documented so far for the coast of northern Chile (Brown, 1991). Scarce outcrops of Late Triassic plutons are also recognized along the coast, that in some cases were emplaced along associated synplutonic normal faults (Grocott et al., 2009). Volcanic and volcanoclastic sequences are even less common, with some limited outcrops of Cisuralian age at ~28ºS and of Upper Triassic age at ~28ºS and ~25º30'S (Cifuncho and Agua Chica formations; Contreras et al., 2013; Welkner et al., 2006).

The Cisuralian to Lower Triassic igneous rocks, in particular those cropping out in the Frontal and Domeyko Cordilleras, are thought to be the products of an anorogenic

magmatism resulted from extensive crustal melting, (Parada et al. 1982; Mpodozis and Kay, 1992) and have been interpreted as the equivalent to the Choiyoi Group in Argentina based in their similar age range, from 285 Ma to 245 Ma (Maksaev et al., 2014; Sato et al., 2015). The Middle to Late Triassic volcanic sequences are often reported as bimodal basaltic-rhyolite suites (Cornejo and Mpodozis, 1996; Parada et al. 1999; Morata et al., 2000) and have been interpreted as products of continental rift magmatism with mantle sources (Kay and Ramos, 1990) and related to the development of NW-oriented large-scale rift basins in a passive margin (e.g.: Ichigualasto, Cuyo and San Félix basins, Charrier et al., 2007). On the other hand, some authors have interpreted the Guadalupian to Rhaetian magmatism (del Rey et al. 2016; Coloma et al. 2017; González et al. 2018), the Middle-Late Triassic basins in Chile (Espinoza et al. 2019; Salazar et al. 2019), and also the Choiyoi magmatism (Rocher et al. 2016), as subduction-related.

The dominant structural style during the entire Pre-Andean stage would have been extensional, with the development of large volcanic calderas controlled by normal faults and abundant dyke swarms in the Permiam and Triassic magmatism (Giambiagi and Martínez, 2008, González et al., 2018; Llambías and Sato, 1995; Salazar and Coloma, 2016). A major deformational phase (Huárpica) that separates the Choiyoi magmatism from Middle Triassic rocks is interpreted as an extensional event (Sato et al.,2015 and references therein. During the Triassic, the development of NW-oriented rift basins is well documented, both in the continental foreland (Ichigualasto and Cuyo basins) and margin (Profeta, La Ternera, San Félix basins) (Charrier et al., 2007; Giambiagi et al., 2009; Salazar et al., 2019; Espinoza et al., 2019).

Early Andean cycle (Jurassic). The early stage of the Andean subduction system or Andean orogeny is represented in northern Chile by the Coastal Batholith, which is mostly composed by intermediate plutons that span the entire Jurassic period. Whereas the intrusive units constitute the roots of the magmatic arc, the Jurassic La Negra Formation and its equivalents along the Coastal Cordillera represent the penecontemporaneous volcanic products (Kramer et al., 2005; Oliveros et al., 2006). In the Frontal and Domeyko Cordillera, Jurassic marine and volcanic sequences are

interpreted as the back-arc basin and associated back-arc volcanism to the early Andean subduction system, respectively (Ardill et al., 1998; Oliveros et al., 2012; Prinz et al., 1994; Rossel et al., 2013).

Even though the Early Andean arc was emplaced over Paleozoic continental crust, due to the rather primitive nature of its magmatism and its tectonic and palaeogepgraphic configuration (intra-arc and back-arc basins), it has been compared to modern oceanic-type subductions systems or island arcs (Lucassen et al., 2006; Rossel et al., 2013) rather to typical continental arcs. An extensional strucutral setting would have been dominated the margin during the Early Andean cycle, due to the oblique subduction of the Phoenix plate, that induced stress partition on the upper plate developing transtensional sinistral systems (Grocott and Taylor, 2002; Scheuber and González, 1999).

2.3 Samples and methods

86 samples of volcanic and plutonic rocks from units cropping out in the Coastal, Domeyko and Frontal Cordilleras of northern Chile (25ºS-30ºS) and ranging in age from Upper Carboniferous to Upper Jurassic (Table 2.1) were selected for petrographical and geochemical analysis. In total, 65 samples were analyzed for major and trace elements (Table 2.2): 48 by total fusion XRF and ICP-MS, at the Activation Laboratories, Ontario, Canada, and 17 by ICP-MS at the Laboratory of the National Geological and Mining Survey (SERNAGEOMIN), Chile. 69 samples were analyzed for whole rock Sr-Nd-Pb isotopic composition (Table 2.3): 27 at the Geosciences Department, University of Arizona, USA by TIMS (Sr-Nd isotopes) and MC-ICP-MS (Pb isotopes) (following the procedures outlined in Drew et al., 2009 and Otamendi et al., 2009), and 42 at the Isotope Geochemistry laboratory of the MARUM Center, University of Bremen, Germany.

Due to the high alteration degree that affects the vast majority of the Paleozoic and Mesozoic Andean rocks, collecting fresh samples in the field is not a feasible task and it is only possible to remove weathered surfaces and/or to gather relatively fresh rock chips. Therefore, the samples selected for geochemical analyses were crushed to <5 mm fraction and cleansed, small fresh fragments, representative of the entire lithology,

were handpicked under binocular lens in order to avoid altered areas of the rock. The selected fragments were powdered under 50 um for further chemical treatment prior to the elemental and isotopic analyses. Details of geochemical procedures are in the Supplementary Material 2.

A database of 1237 samples from the Andean region of Chile and western Argentine between 18º00' and 40º00'S has been compiled (Supplementary Material 2.3) in order to compare the magmatism represented by the samples analyzed in this work to the Carboniferous-Jurassic magmatism along the entire western Gondwana margin. The amount of information for the samples in the database is variable but at least it includes precise location in UTM coordinates, age or age range and major elements composition. For the majority of the samples (75%) petrography (lithological classification) and trace elements are also reported and Sr, Nd and Pb isotope composition is available for the 23%, 19% and 13% of samples, respectively.

2.4 Petrography

A detailed list of the petrographic results for the analyzed samples can be found in the Supplementary Material 2.1. All collected samples are altered to some extent and exhibit variable proportions of hydrothermal or very low-grade metamorphic minerals such as chlorite(-smectite), sericite, calcite, epidote, clays, Fe-oxihydrates and quartz. Much less common is the occurrence of biotite, actinolite or opaque minerals. These secondary minerals may fill amygdules or veinlets, replace igneous crystals, volcanic glass or small crystal within the groundmass. Details of secondary mineral phases are listed in the Supplementary Material 2.1.

	Unit	Samples	Lithologies	Alteration degree	Age range
Gonwdana cycle	Chacaicito Pluton	RCM-077q	Syenogranite	0.12	329-324 Ma[1]
	Quebrada Pinte Diorite	MCM-168 Bq	Diorite	0.07	324 Ma[1]
	Guachicay Pluton	MCM-159q	Tonalite	0.09	303 Ma[1]
	Llano de Chocolate Beds	CPV-12-12, CPV-12-105, CPV-12-127	Rhyolite, Dacite, Rhyolitic tuff	0.24-0.8	318-285 Ma[2]
	Punta del Viento Plutonic Complex	CPV-15-365	Granite	0.18	295-277 Ma[3]
	Chanchoquín and Guanta Plutonic Complexes	MCM-129q, RCM-133q, O7-13, O7-15, MCM-205q, MCM-280q, RCM-015q	Quartz Monzodiorite, Tonalite, Granodiorite, Syenogranite	0.00-0.16	296-285 Ma[4]
	La Tabla Formation, Cerro Rincones Beds	CPV-14-176, CPV-14-249, CPV-14-263, CPV-15-353	Rhyolitic tuff, Dacite	0.11-0.26	294-289 Ma[3]
Pre-Andean stage	Cifuncho Plutonic Complex	CPV-14-180A, CPV-14-191	Monzogranite	0.08-0.09	284-256 Ma[5]
	Sierra de Doña Inés Chica Plutonic Complex	CPV-15-320	Quartz Monzodiorite	0.28	280-255 Ma[6]
	Guanaco Sonso Formation	SCL-28q, SCL-96q, RCM-150q	Dacitic tuff, Rhyolitic tuff	0.13-0.35	265-240 Ma[4]
	La Laguna Gabbro	O7-10, O7-11	Gabbro	0.01-0.02	255 Ma[7]
	Chollay Plutonic Complex	SCL-02q, SCL-09q, MCM-010q, MCM-022q, MCM-265q, RCM-040q	Granodiorite, Tonalite, Syenogranite, Monzogranite	0.015-0.17	247-237 Ma[4]
	San Felix Formation	CPV-12-38, CPV-12-49b	Lithic tuff	0.5-0.7	254-212 Ma[8]
	Pan de Azúcar Pluton	CPV-14-192	Granite	0.13	230 Ma[9]
	Pastos Blancos Formation	RCM-78q	Andesite	0.33	231-216 Ma[1]
	Colorado Syenogranite	RCM-61q	Syenogranite	0.05-0.09	229-219 Ma[4]
	La Totora Formation	CPV-12-23, CPV-12-24, CPV-12-60, SCL-26q	Basalt, Andesite, Rhyolithic tuff	0.15-0.49	221-210 Ma[4,10]
	Montegrande Granite	O7-06, O7-07	Granite, Granodiorite	0.01	215 Ma[11]
	Canto del Agua Formation	CPV-12-90	Lithic tuff	0.4	212.6 Ma[8]
	La Ternera Formation	CPV-15-271, CPV-15-274, CPV-15-278, CPV-15-279, CPV-15-280, CPV-15-281, CPV-15-284, CPV-15-285, CPV-15-287, CPV-15-410	Basalt, Basaltic Andesite, Andesite, Andesitic Tuff, Dacitic tuff, Lithic tuff	0.28-0.51	220-199 Ma[12,13]
	Quebrada del Salitre Formation	CPV-14-245, CPV-14-247, CPV-14-253, CPV-14-256, CPV-15-303, CPV-15-310, CPV-15-311, CPV-15-312, CPV-15-314, CPV-15-319, CPV-15-322, CPV-15-330, CPV-15-332, CPV-15-337, CPV-15-359, CPV-15-386	Basalt, Basaltic Andesite, Andesite, Dacite, Rhyolite, Andesitic breccia, Lithic tuff	0.17-0.60 mean=0.32	212 Ma[3]
	Cifuncho Formation	CPV-14-184, CPV-14-187, CPV-14-190	Andesite, Dacite	0.16-0.32	212-205 Ma[5]
	Carrizal Bajo Complex	CPV-12-91A, CPV-12-91B, CPV-12-93	Diorite, Tonalite, Granodiorite	0.05-0.23	208-206 Ma[14]
	Agua Chica Formation	CPV-14-194, CPV-14-198	Andesite, Dacitic tuff	0.3-0.4	200 Ma[15]
	Algodones Granite	CPV-12-92	Diorite	0.4	203-199 Ma[14]
Early Andean cycle	Sierra Esmeralda Plutonic Complex	CPV-14-181B, CPV-14-182B	Tonalite, Monzodiorite	0.14-0.32	194 Ma[5]
	La Vaca Granodiorite	CPV-12-01, CPV-12-03	Granodiorite, Dike (andesite)	0.02-0.13	193-191 Ma[16]
	Algarrobal Formation	CPV-12-26B, CPV-12-28x, CPV-12-30x	Basaltic andesite, Andesite	0.2-0.3	152-137 Ma[1]

[1]Ortiz and Merino (2015)
[2]Creixell et al. (2016)
[3]Venegas et al. (2013)
[4]Salazar et al. (2013)
[5]Contreras e al. (2013)
[6]Cornejo et al. (1993)
[7]Hervé et al. (2014)
[8]Vallejos (2012)
[9]Berg and Baumann (1985)
[10]Maksaev et al. (2014)
[11]Coloma et al. (2017)
[12]Espinoza et al. (2015)
[13]Peña et al. (2013)
[14]Arévalo and Welkner (2008)
[15]Espinoza et al. (2015)
[16]Creixell et al. (2012)

Table 2.1. Lithologies, alteration degree and age range for the studied units. Listed lithologies correspond only to analyzed samples and not to the entire petrographic range of each unit, see Petrography section for a more detailed description of all lithological types. Alteration degree was estimated through petrographic analysis of each sample and it is represented by the total volume of alteration minerals in each sample (Supplementary Material 2.1; Coloma et al., 2017; Ortiz and Merino, 2015). Age data from the literature for the studied samples are listed in Supplementary Material 2.2.

Gondwana cycle. The older units are Carboniferous small plutons that crop out in the Frontal Cordillera (29º00'-29º30'): Chacaicito, Quebrada Pinte and Guachicay. Guachicay pluton is a leucocratic, coarse grained, biotite -and minor muscovite-tonalite; Quebrada Pinte diorites correspond to melanocratic, coarse grained amphibole diorites and quartz diorites with penetrative planar fabric and Chacaicito pluton is composed of leucocratic, coarse-grained biotite syenogranites (Ortiz and Merino, 2015). Cisuralian plutons (>285 Ma) are volumetrically more significant in the Frontal and Domeyko Cordilleras, sampled units correspond to: the Punta del Viento Plutonic Complex (25º00'-26º00'), a leucocratic quartz monzonite with scarce clinopyroxene; the Chanchoquín Plutonic Complex (28º30'-29º15'S) and Guanta Unit (29º15-31ºS) are leucocratic, medium to coarse grained quartz monzodiorite, tonalite, granodiorite and syenogranite with biotite and minor amphibole or muscovite; and the Cifuncho Plutonic Complex (27º00'-28º15'S) a leucocratic, medium grained biotite monzogranite with scarce amphibole. The Llano de Chocolate beds (28º45'-29º05'S) crop out in the Coastal Cordillera and are the only volcanic unit assigned to this cycle that was sampled. Rocks are porphyritic ryholites and dacites, with plagioclase, quartz and minor alkali-feldspar phenocrysts, felsitic groundmass and devitrified glass.

Pre-Andean stage. The Guadalupian to Rhaetian intrusives are voluminous in the Frontal Cordillera and much less represented in the Coastal Cordillera. In the former, sampled units from older to younger, correspond to: the La Laguna Gabbro (30º05'S); the Chollay Plutonic Complex (28º30'-29º30'S) leucocratic medium to fine grained biotite-amphibole tonalite and quartz mozodiorite, leucocratic, medium grained biotite-muscovite granodiorite and monzo and syenogranite; the Sierra de Doña Inés Chica Plutonic Complex (26º00'-26º30') a medium to coarse grained, leucocratic, hornblende and biotite granodiorite; the Colorado Syenogranite (28º45'-30º15'S), a leucocratic, coarse to medium to grained, biotite syenogranite; and the Montegrande Granite

(30º05'S), an inequigranular, leucocratic, biotite granite with minor intersticial amphibole and clinopyroxene. In the Coastal Cordillera, samples correspond to the Pan de Azúcar pluton (26º00'-26º20'S), a leucocratic, coarse grained muscovite granite; the Carrizal Bajo Plutonic Complex (28º00'S), medium to fine grained, equigranular biotite tonalites and granodiorites and amphibole tonalite; and Algodones Granite (28º00'), a medium grained quartz diorite, with clinopyroxene and biotite.

Volcanic and volcanosedimentary units crop out mainly in Frontal and Domeyko Cordilleras, with less voluminous sequences in the Coastal Cordillera. In general, these units exhibit variable petrographic compositions, ranging from basalt to rhyolite, but with prevalence of intermediate to acidic rocks particularly in the Permian units. The only exception is the Pastos Blancos Formation that in its base is composed of basaltic andesites whereas the upper part is a sequence of rhyolites and rhyolitic tuffs. The volcanic rocks are all porphyritic but some aphanitic basalts are present in the Quebrada del Salitre and La Ternera formations. Sampled units cropping out in the Frontal and Domeyko Cordillera are, from north to south: Cerro Rincones Beds and the La Tabla, Cerro Guanaco, Quebrada del Salitre, La Ternera, Guanaco Sonso, Pastos Blancos, La Totora and Algarrobal formations.

The collected samples from Permian units (La Tabla Formation, 24º'00-27º00'S; Guanaco Sonso Formation, 27º30'-31º00'S; Cerro Rincones Beds, 24°10'-24°30'S) correspond to rhyolitic tuffs and dacites with plagioclase, quartz and minor alkali feldspar phenocyrsts, felsitic groundmass or glassy matrix, and scarce acidic lithics. Samples from Cerro Guanaco Formation (24º45-25º10'S) are andesites and andesitic tuffs bearing plagioclase amphibole and opaque minerals phenocrysts, with minor clinopyroxene or biotite, and intersestal or intergranular groundmass with plagioclase microliths, altered mafics and devitrified glass.

The Quebrada del Salitre (25º15'-26º15'S) samples comprise: i) apahnitic to fine grained porphyritic basalts with small and scarce clinopyroxene or olivine phenocrysts in a groundmass of slightly oriented plagioclase microliths, altered mafics (clinopryroxene and olivine?) and opaque minerals; ii) porphyritic basaltic andesites with plagioclase and minor clinopyroxene phenocrysts, in an intersestal groundmass of

plagioclase microliths, mafics and devitrified glass; iii) porphyritic andesites with either plagioclase-clinopyroxene or plagioclase-quartz-K-feldspar-amphibole phenocrysts and intersestal groundmass; iv) porphyritic dacites with plagioclase, quartz and undetermined mafic phenocryst in a felsitic or intersestal groundmass; and v) porphyritic (fine grained) rhyolites with scarce plagioclase and quartz phenocysts in a felsitic groundmass. Pyroclastic and epiclastic samples in this unit correspond to lithic and crystalline tuffs with quartz and plagioclase phenocryst and minor pyroxene or undetermined mafic minerals, andesitic to dacitic lithics in a glassy matrix.

Samples from La Ternera Formation (27º00'-28º15'S) correspond to aphanitic to fine grained porphyritic basalts with small clinopyroxene and altered olivine phenocrysts in a hialopilitic groundmass with altered mafics and opaque minerals; porphyritic basaltic andesites and andesites with plagioclase and clinopyroxene phenocrysts, in an intersertal groundmass of plagioclase microliths, variable amounts of quartz, mafics and devitrified glass. Pyroclastic and epiclastic samples in this unit correspond to lithic and crystalline tuffs with quartz, plagioclase and K-feldspar phenocrysts, andesitic to dacitic lithics in a glassy matrix. Samples from la Totora Formation (28º15'-29º15'S) correspond to aphanitic or fine grained porphyritic basaltic andesites with small plagioclase, clinopyroxene or olivine phenocrysts in an intersertal groundmass with plagioclase microliths, altered mafics, opaque minerals and devitrified glass. The only sample from the Pastos Blancos Formation (27º00'-31º00'S) is a porphyritic andesite with plagioclase, scarce biotite and undetermined mafic phenocrysts in and intersertal groundmass with plagioclase microliths, altered mafics, opaque minerals and devitrified glass.

Three volcanic units, the Canto del Agua, Agua Chica and Cifuncho formations, were sampled near the coastline (Fig. 2.2). The single sample of the Canto del Agua Formation (28º15'S) is a lithic tuff with andesitic fragments, plagioclase and minor quartz phenocrysts and an ash (mainly glassy) matrix. The samples from Agua Chica Formation (26º05'S) are one andesitic lava flow and one crystalline tuff with plagioclase and minor biotite and amphibole phenocrysts, instersticial groundmass or glassy matrix. The Cifuncho formation (25º20'-26º00'S) samples are porphyritic and dacitic

lavas or subvolcanic bodies, with plagioclase and quartz as the most abundant phenocrysts, and minor biotite and/or amphibole, the groundmass is intergranular (andesite) of felsitic (dacite) with scarce mafics.

Early Andean cycle. The Jurassic intrusives are very common in the Coastal Cordillera (Coastal Batholith) but absent in the Frontal and Domeyko Cordilleras, the two units sampled for this study are the Lower Jurassic: Sierra Esmeralda Plutonic Complex (25º55'S), medium grained biotite- amphibole monzodiorite and amphibole-muscovite tonalite; and Quebrada la Vaca Granodiorite (29º05'S), a medium grained biotite-clinopyroxene grandiorite with (and one aphanitic equivalent). The Upper Jurassic-Lower Cretaceous volcanic Algarrobal Formation (29º00'-31ºS) was also sampled in the Frontal Cordillera, the collected rocks correspond to porphyritic basaltic andesites.

2.5 Elemental and Sr-Nd-Pb isotope geochemistry

Elemental and Sr-Nd-Pb isotopic compositions of the analyzed samples are listed in Table 2.2 and Table 2.3, respectively. Additional data on elemental composition, concerning samples with isotope results in this work, are Supplementary Material 2.3. The ages used for the calculation of initial isotopic ratios and for εNd initial are given in the Supplementary Material 2.2.

The normalized SiO_2 content (wt% free of volatile phase) of the analyzed samples and published data exhibit a mixed distribution with two pronounced peaks at the 51.0-56.5% (~basaltic andesite) and 62.1-70.0% (~dacite) intervals (Fig. 2.4). In the Carboniferous to Permian and in many Triassic rocks there is a strong dominance of intermediate to silicic compositions although the Triassic suites have a slightly higher proportion of ~basaltic andesite compositions. The Jurassic rocks are different with a large population below 60% SiO_2. According to the TAS classification diagrams volcanic rocks range from basalts to rhyolite and plutonic rocks from gabbro to granite; the samples plot within or close to the subalkaline field (Fig. 2.5). In the case of volcanic rocks, when using the classification diagram for altered rocks, all but three samples plot in the subalkaline field (Fig. 2.5), suggesting that the moderate to strong alteration degree observed in the studied volcanic units (see Table 2.1 and Supplementary Material 2) may have induced a Na-K metasomatism in the rocks. Intrusive rocks are

mostly peraluminous but plot close to the metaluminous field. Carboniferous to Permian rocks and, to a minor extent Triassic rocks, are peraluminous, whereas Jurassic intrusion are mostly metaluminous; only two samples of the late Triassic Montegrande Granite plot in the peralkaline field (Fig. 2.5).

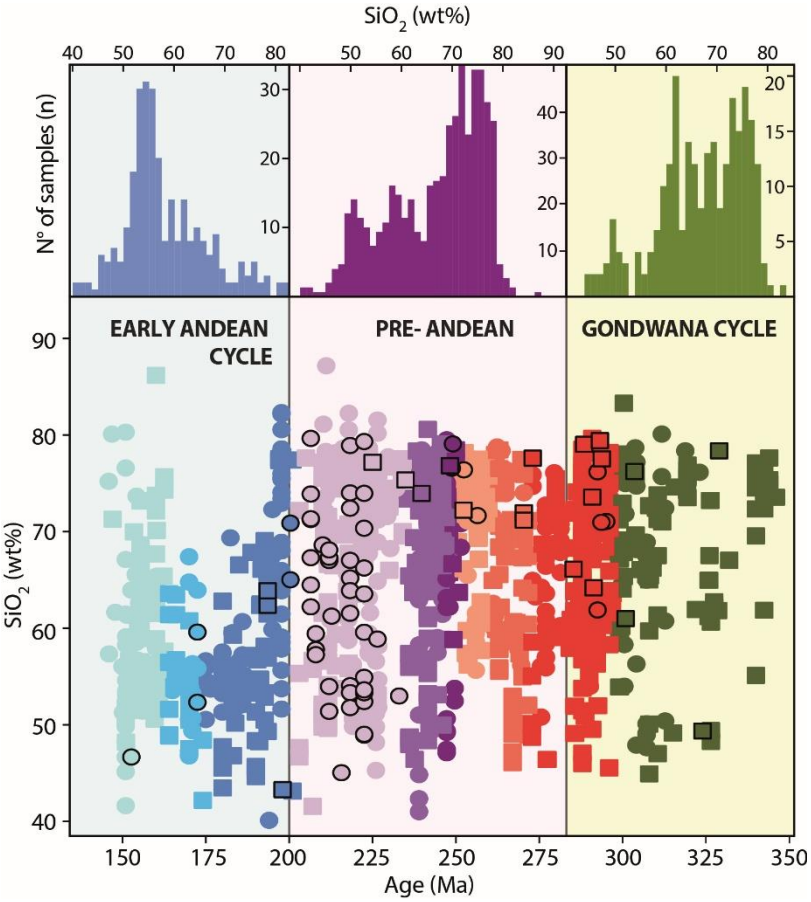

Figure 2.4. SiO_2 content (wet-free basis) of samples from Carboniferous to Jurassic igneous units. Circles correspond to volcanic rocks and squares to plutonic rocks, symbols with black stroke correspond to samples analyzed for this study.

The chondrite normalized REE patterns of the samples are relatively flat, with the exception of some Permian and Triassic samples, the La_N/Yb_N range from 1.08 to 16.50 (with two Permian samples as outliers at 38 and 40). The highest REE contents are for Carboniferous and Permian samples, whereas the lowest are for Upper Triassic and Jurassic rocks (Fig. 2.6). Negative Eu anomalies are observed in the majority of the samples, but much less pronounced for the Jurassic rocks; thus Eu/Eu* ranges from 0.19 to 1.10 in all samples and from 0.67 to 1.03 in the Jurassic samples. The Primitive Mantle-normalized spider diagrams for trace elements show similar patterns for all the studied samples (Fig. 2.6). Although there is a significant dispersion among LILE (large-

ion lithophile elements), these elements are systematically enriched over HFSE (high field strength elements), for which the contents are similar to depleted mantle sources. Marked troughs in Nb, Ta, Ti and Zr, along with prominent peaks in K and Pb are also shared features in all samples (Fig. 2.6).

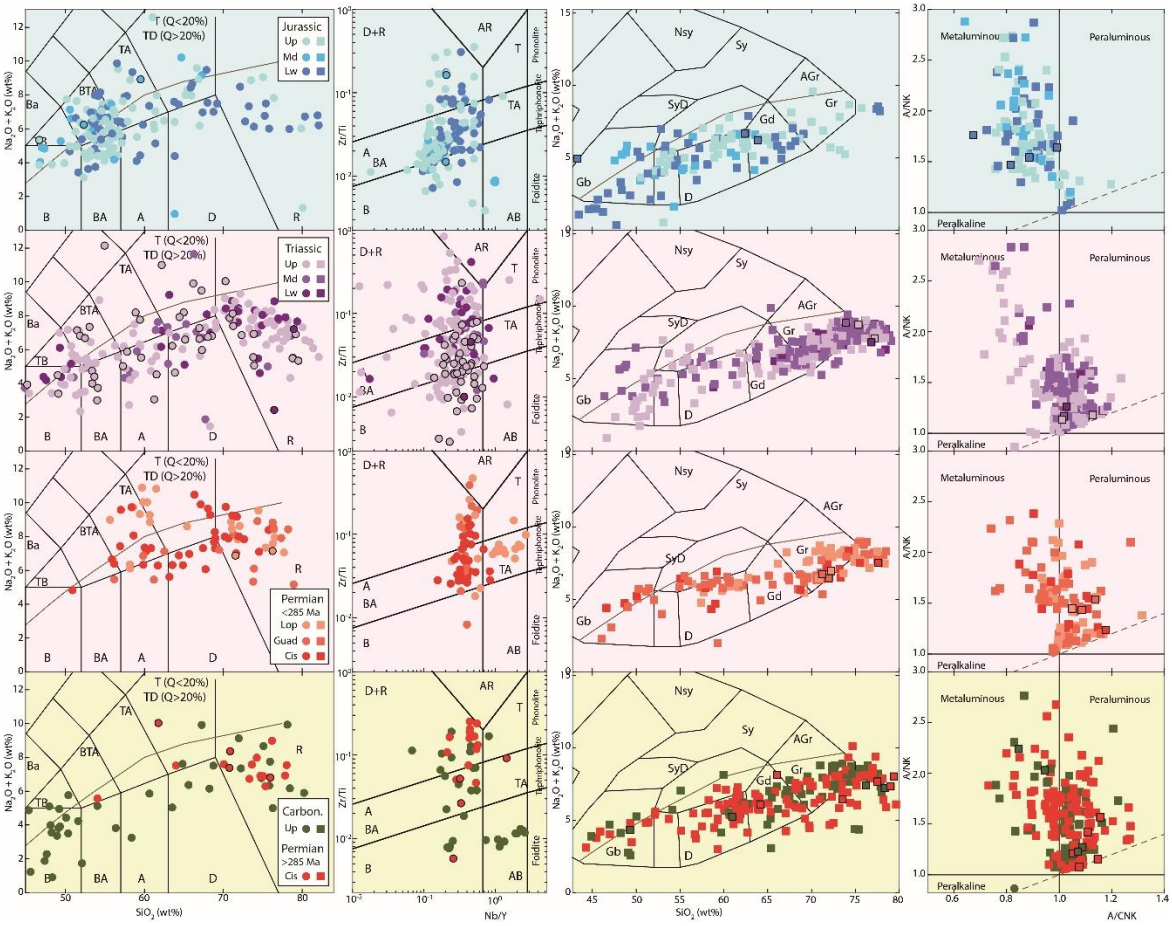

Figure 2.5. Irvine and Baragar (1971) TAS diagram (first column from left to right) for volcanic rocks, Sr/Ti vs Nb/Y diagram (second column) for altered volcanic rocks (Pearce, 1996, after Winchester and Floyd, 1977); TAS (third column) (Cox et al., 1979) and Shand's index diagram (Shand, 1943) (fourth column) for plutonic rocks. Circles correspond to volcanic rocks and squares to plutonic rocks, symbols with black stroke correspond to samples analyzed for this study. Carbon.: Carboniferous; Cis >285 Ma: Cisuralian older than 285 Ma; Cis <285 Ma: Cisuralian younger than 285 Ma; Guad: Guadalupian; Lop: Lopingian; Up: Upper, Md: Middle; Lw: Lower. Series age limits are from (Cohen et al., 2013). Background colors are as in Fig. 2.3 and refer to the Gondwana, Pre-Andean, and Andean cycles. Ba: Basanite; TB: Trachybasalt; B: Basalt; AB: Alkali Basalt; BTA: Basaltic Trachyandesite; TA: Trachyandesite; A: Andesite; T: Trachyte; TD: Trachydacite; D: Dacite; R: Rhyolite; AR: Alkali Rhyolite; Q: Quartz; Gb: Grabbro: SD: Syenodiorite; D: Diorite; GD: Graniodiorite/Quartz-diorite; Sy: Syenite; Gr: Granite; A-Gr: Alkali Granite; NSy: Nepheline syenite.

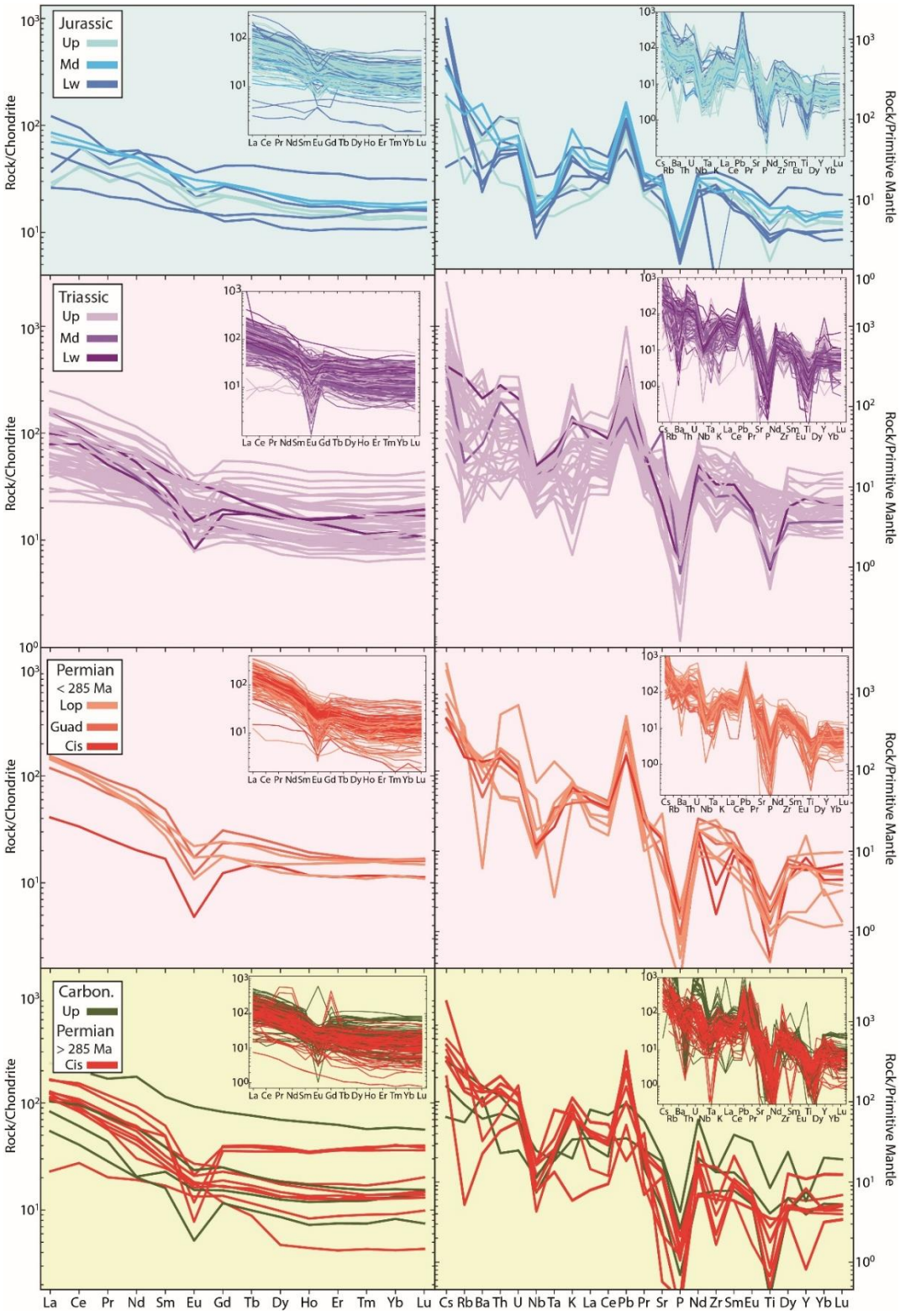

Figure 2.6. Chondrite-normalized REE (left column diagrams) and primitive mantle normalized trace elements composition of analyzed rocks (right column diagrams). Inset in each diagram correspond to published data. Legends are as in Fig. 2.5. Chondrite and primitive mantle composition are from Sun and McDonough (1989). Background colors are as in Fig. 2.3 and refer to the Gondwana, Pre-Andean, and Andean cycles.

The isotopic composition of the samples is moderately variable for Nd and Pb and more scattered for Sr. Most of the analyzed samples plot along or near the mantle array, but units representing the Gondwana cycle plot closer to the continental crust than those representing the Early Andean cycle (Fig. 2.7a). Samples representing the Pre-Andean stage plot roughly in between the other two groups (Fig. 2.7a). The Pb isotopic composition is close to the enriched mantle field for the samples of the Gondwana, Pre-Andean and Early Andean units (Fig. 2.7b).

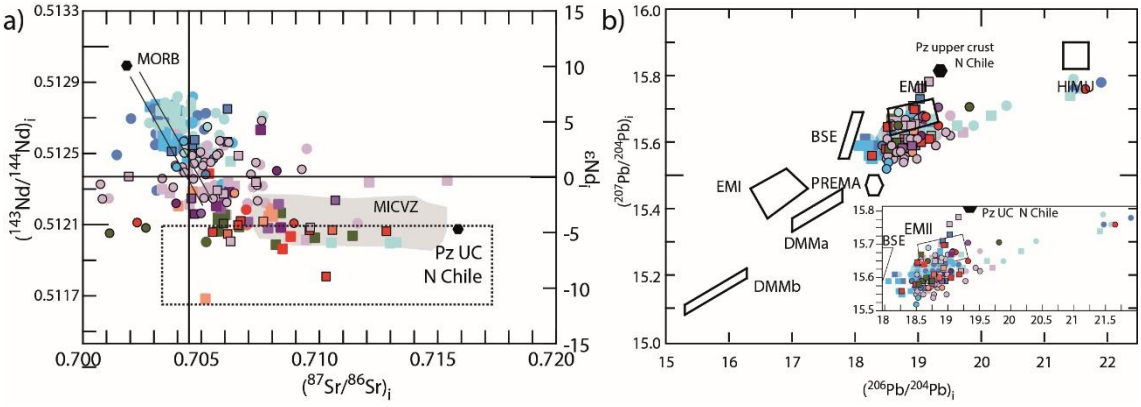

Figure 2.7. Initial a) $^{87}Sr/^{86}Sr$ versus $^{143}Nd/^{144}Nd$ (εNd) and b) $^{206}Pb/^{204}Pb$ versus $^{207}Pb/^{204}Pb$ diagrams for the analyzed samples and published data. Ages for the calculation are in the Supplementary Material 2. Symbols are as in Fig. 2.5. Inset shows the fields where the majority of the samples plot. Average Paleozoic Upper Crust in northern Chile is from Lucassen et al. (2006). Dotted line represents the range of Sr-Nd isotopic values of the continental crust (White, 2015). Bulk Silicate Earth (BSE) and mantle reservoirs (EMI, EMII, PREMA, DMMa, DMMb and HIMU) in b) are from Zindler and Hart (1986), not recalculated. MORB and BSE in a) are recalculated at 200 Ma (compilation of Vásquez et al. 2011), MICVZ: Miocene ignimbrites of the Central Andean Volcanic Zone (compilation of De Silva et al., 2005).

2.6 Discussion

2.6.1 A geochemical perspective for the evolution of the SW Gondwana margin: continuous subduction from Carboniferous to Jurassic?

It has long been proposed that the composition of the igneous rocks of the Gondwana cycle and Pre-Andean stage is highly variable in response to tectonic reorganization that changed the sources and generation conditions of magmatism (Mpodozis and Kay, 1992). The new and compiled data however, do not completely support that idea. The available geochemical data suggest that some patterns of regional magmatism changed from the late Paleozoic to Mesozoic but others remained constant throughout the period.

Whereas rocks of the Gondwana cycle have higher SiO_2 contents than Jurassic rocks (Fig. 2.4) as it would be expected from continental- and oceanic-type arc magmatism, the Pre-Andean units do not exhibit the rhyolite-basalt bimodal distribution that has previously been interpreted as the product of continental rift processes (Parada et al., 1999; Ramos and Kay, 1991). SiO_2 contents akin to rhyolites are the dominant composition, but the volume of ~dacites (SiO_2 60-70%) is very similar to that of basalts and basaltic-andesites (SiO_2 50 to 55%). Moreover, a compilation of reported lithologies of all Triassic igneous outcrops in northern Chile indicate that basaltic andesite and andesites are the dominant petrographic type for volcanic rocks (>50% total area of Triassic volcanic rocks) and diorite-tonalite-granodiorite represent 40% to 55% of the exposed intrusions (Oliveros et al., 2018). Additionally, although the Permian Pre-Andean magmatism (Choiyoi) has been interpreted as the result of extensive crustal melting (Kay et al., 1989; Kleiman and Japas, 2009; Llambías and Sato, 1995) and its composition is strongly dominated by the rhyolite-granite types, the fact is that the most silicic compositions are found in Triassic rocks (Figs. 2.4 and 2.5). Such feature has been observed for continental arcs and attributed to variation in crustal thickness: in arcs emplaced on thinned crust, the thermal lifespan of the magma chambers may equal the time of melt segregation, allowing a rather small volume of very silicic magmas to reach upper crustal levels, whereas arcs on a thick crust allow extensive differentiation that leads to larger volumes of intermediate magmatism (Farner and Lee, 2017). The progressive thinning of the crust after the San Rafael orogeny may have had an influence in the generation of very silicic magmas.

Another way to produce high volumes of intermediate-silicic magmatism in a continental arc setting, such as those observed in the Pre-Andean stage (Permian), is the lithospheric melting of the slab following its vertical detachment due to collision, a phenomenon known as slab failure (Hildebrant et al., 2018). The rocks generated in this context would have a clear subduction signature but with more silicic composition that normal arcs and trace element composition akin to deep magma sources (Hillebrand et al. 2018). According to the tectonic discrimination diagrams of Whalen and Hildebrand (2014), the silicic Permian and Triassic (and also Carboniferous) rocks plot both in the range of typical slab failure magmatism and of normal arc magmatism,

not allowing to distinguish if this process may have taken place during the Pre-Andean stage.

The majority of the volcanic and all the plutonic rocks are sub-alkaline (Fig. 2.5); minor volumes of volcanic alkaline rocks are found in every period, but particularly in the Pre-Andean stage (for example, the Lopingian Choyoi volcanics and partly the Norian Pastos Blancos Fm in the Frontal Cordillera, Fig. 2.5). Although the alteration degree of the rocks is moderate to high, the AFM diagram suggest that the igneous rocks are largely calc-alkaline, with minor tholeiitic volcanism restricted to the Jurassic period (Fig. 2.6a) (Lucassen et al., 2006; Lucassen and Franz, 1994). The Al-Ca-alkalis composition of plutonic rocks varies from mixed but peraluminous dominated in the Gondwana cycle and Pre-Andean stage (with the former slightly more peraluminous), to dominantly metaluminous in the Early Andean cycle. This suggests a continuous shifting from S-type to I-type plutonism with time, typical of Cordilleran arcs (Ducea et al., 2015), but the majority of the intrusions have a transitional character and do not correspond to the S or I end members. Moreover, cordierite- or muscovite-bearing, or ilmenite dominated granitoids are only reported as relatively restricted volume intrusions of Lopingian and Norian ages in the Frontal Cordillera between 28º and 30º30'S (Hervé et al., 2014; Llambías and Sato, 1995; Mpodozis and Cornejo, 1988; Nasi et al., 1990; Parada, 1988), whereas biotite- or hornblende-bearing or magnetite dominated granitoids are the most common plutonic lithology in the three stages (Oliveros et al., 2018 and references therein).

In terms of their trace elements content, the rocks of the three stages exhibit ubiquitous enrichment in LILE over HFSE, with characteristic troughs in Nb-Ta, Ti, and P compared to primitive mantle (Fig. 2.6). In the tectonic discriminations diagrams for basaltic and granitic rocks most of the samples plot either on the arc basalts (Fig. 2.8b) or volcanic arc granites field, with a minor number of samples (Late Permian, Late Triassic and Jurassic) falling on the within plate or syn-collisional fields for granitoids (Fig. 2.8c,d). The involvement of fluids in the source of the Gondwana cycle, Pre-Andean stage and Early Andean Cycle magmas can also be inferred from the Th-Ta-Yb contents of the studied rocks (Fig. 2.9), which indicate that even the most primitive

samples correspond to magmas dominated by a subduction (fluid-induced melting of a depleted mantle) component (Fig. 2.9). The magmas may have been oxidized, implying the involvement of fluids in their sources, because even for strongly fractionated REE compositions and high contents of light REE, the Eu anomalies are not so pronounced (Fig. 2.10a,b).

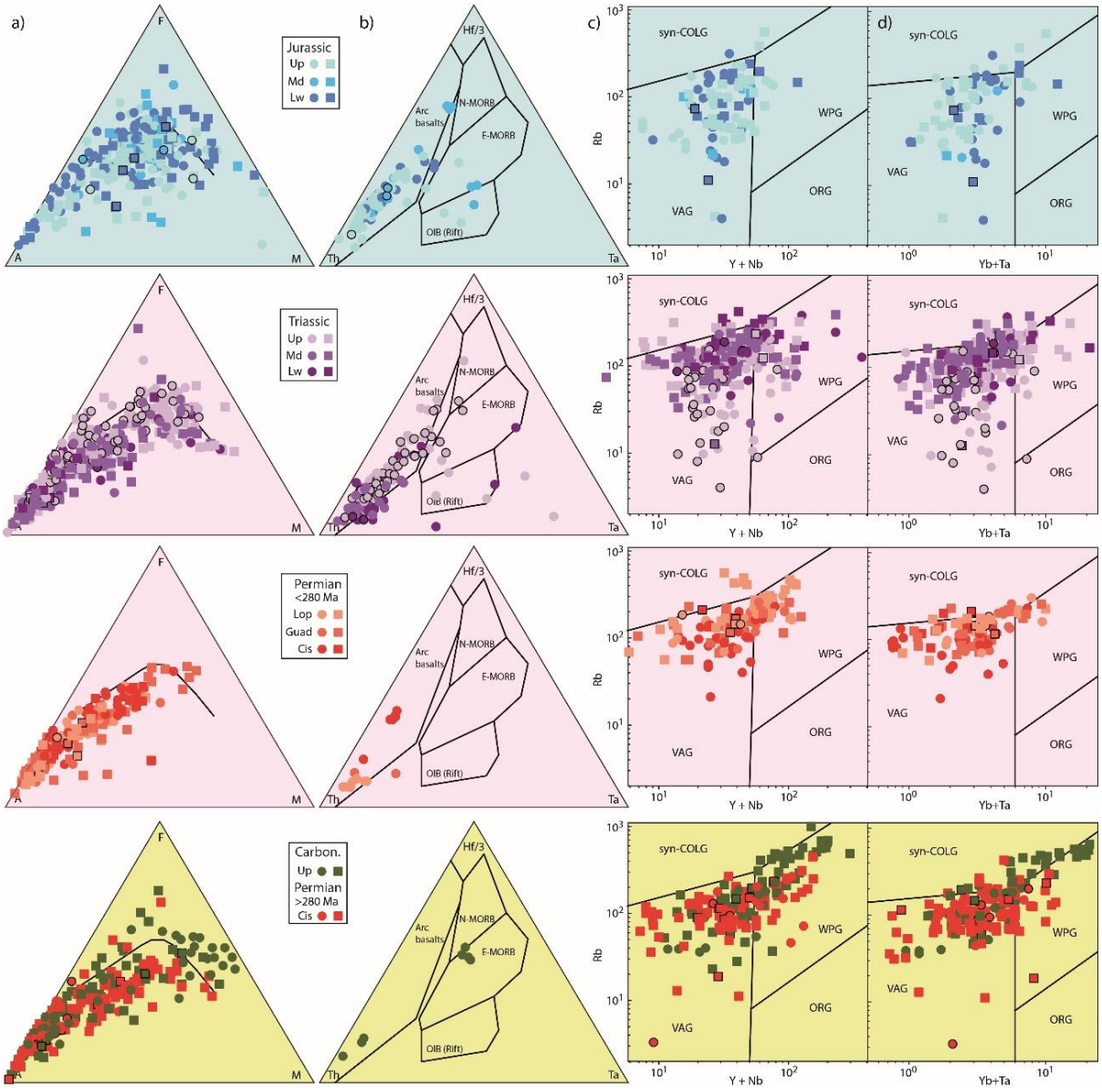

Figure 2.8. a) AFM diagrams (Irvine and Baragar, 1971) and b) basalts Th-Ta-Hf/3 (Wood, 1980) and granites c) Rb-Y-Nb, d) Rb-Yb-Ta (Pearce 1984), tectonic discrimination diagrams for Carboniferous to Jurassic igneous rocks. Legends and symbols are as in Fig. 2.5. Background colors are as in Fig. 2.3 and refer to the Gondwana, Pre-Andean, and Andean cycles.

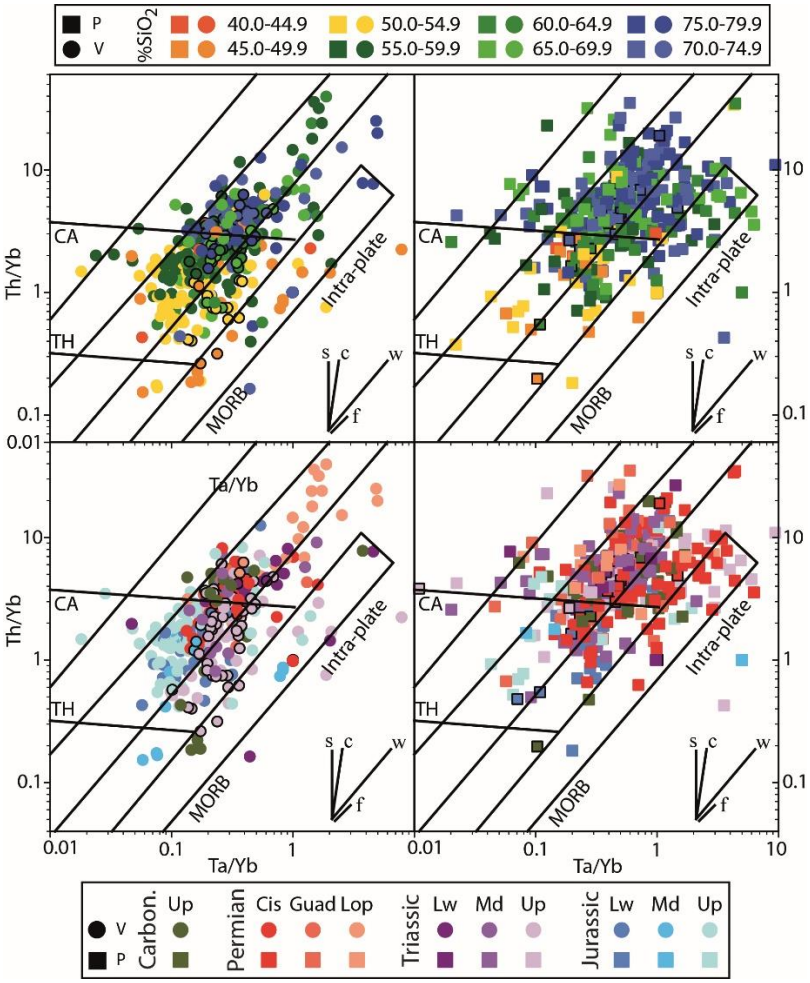

Figure 2.9. Th/Yb vs Ta/Yb diagrams (Pearce, 1982), for Carboniferous to Jurassic igneous rocks. Ranges of SiO_2 content are delimited in the upper plots. Legends and symbols in the lower plots are as in Fig. 2.5.

The isotope composition of Carboniferous and Permian rocks suggest that magmas were evolved (i.e. radiogenic Sr and Pb and unradiogenic Nd) yet less than expected for a magmatism with high degree of continental crust assimilation or for crust-derived melts, as it would be the case for the Gondwana cycle and Pre-Andean stage magmatism, respectively. For example, the Gondwana cycle magmas, thought to represent a continent-ocean subduction setting with a thick continental crust (Mpodozis and Ramos, 1989), have lower $^{87}Sr/^{86}Sr$ and higher $^{206}Pb/^{204}Pb$, εNd and εHf (del Rey et al., 2016) than the rocks of the modern Central Andean Volcanic Zone (εNd: -2 to -5 versus -4 to -9, $^{87}Sr/^{86}Sr_i$: 0.702 to 0.708 versus 0.705 to 0.709, $^{206}Pb/^{204}Pb_i$: 18.20 to 19.20 versus 17.75 to 18.75, Mamani et al., 2010; Scott et al. 2018). In a similar way, the isotope compositions of Pre-Andean Permian intrusions and volcanics, emplaced not only over the Gondwana arc but also on the metasedimentary cover of the margin

(Coloma et al., 2017; González et al., 2018; Hervé et al., 2014; Llambías and Sato, 1995), are far from the average of Paleozoic crust for Nd, Sr and Pb (Fig. 2.7a,b). Hf isotopic composition (initial εHf) for zircons of the Gondwana cycle range from -5 to +2 and for zircons of the Pre-Andean stage from -4 to +7 (Willner et al., 2008; Bahlburg et al., 2009, Deckart et al., 2014, Hervé et al., 2014; del Rey et al., 2016); indicating that the latter are less evolved and the Pre-Andean magmatism would not have had a large input of Carboniferous curst or older.

This suggest that the crust cannot be the sole source of Pre-Andean Permian magmatism but, as much as for Gondwana and Early Andean igneous rocks, the measured isotopic ratios are better explained by the variable mixing of two magmatic sources: a somewhat depleted mantle and the continental crust. A similar conclusion has been advocated for Carboniferous to Triassic batholiths in the High Andes and Coastal Cordillera of central Chile (Parada et al., 1999; Deckart et al., 2014; del Rey et al., 2016; Hervé et al., 2014; Vásquez et al., 2009). Deviations from the mantle array in the Sr isotopic composition of Triassic Pre-Andean and Early Andean rocks with positive εNd (Fig. 2.7a) may be in part due to fluid remobilization by extensive, post-magmatic, seawater or hydrothermal alteration (Rogers and Hawkesworth, 1989; Kramer et al., 2005; Lucassen et al., 2006; Rossel et al. 2013), which is a common feature for the rocks exposed in the modern forearc of northern Chile (Oliveros et al., 2006; 2007).

Thus, the dominant lithological types in the Gondwana, Pre-Andean and Early Andean magmatism, the systematic chemical signature of a source compatible with a flux-melting of the depleted mantle, and the isotope composition that is best explained by mixture of mantle and continental crust sources are independent evidence that point out to subduction-related processes.

2.6.2 Tectonic evolution of the Andean convergent margin between 18° and 40°S

The magmatism that characterizes the Gondwana cycle, represents a period bracketed in between the onset of subduction somewhere after ca. 330 Ma and the ca. 280-270 Ma San Rafael orogenic phase (Astini et al., 2009; Bahlburg et al., 2009; Hervé et al., 2014; Mpodozis and Kay, 1992). This magmatism would have started after the

emplacement of Mississipian plutons interpreted as anorogenic (Fig. 2.8) and the extrusion of minor volumes N/E-MORB type volcanism (Fig. 2.9) interpreted as an ensialic basin to the east and farther inland of what would later be the Gonwana arc (Astini et al., 2009; Dahlquist et al., 2010; Koukharsky et al., 2014; Alasino et al., 2012;2017). The Coastal (south of 31ºS) and the Frontal (north of 31ºS) Cordillera batholiths are composed of plutons emplaced in a progressively thickened crust and have a significant crustal component in their source with protracted lithospheric residence (Fig. 2.11a) (Deckart et al., 2014; Hervé et al., 2014; Martin et al., 1999; Mpodozis and Kay, 1992; Tomezzoli, 2009). The end of this cycle is marked by the San Rafael Orogenic Phase that deformed the 330-280 Ma batholiths and sedimentary units in the Frontal Cordillera (Kleiman and Japas, 2009) and exhumed the arc roots north of the Domeyko Cordillera (Tommlison et al., 2012). This orogenic phase was initially attributed to collision of a continental mass during the Cisuralian (Mpodozis and Kay, 1992) but more recently it has been suggested that it could be related to flat-slab subduction, that resulted in the diachronic deformation advance in fold-and-thrust belts (Rapalini and Astini, 2005) and migration of the magmatism towards the foreland (Kleiman and Japas, 2009). Taking into account the characteristic of its magmatism and the compressive structural setting, it is likely that the margin acted as an advancing orogen (Cawood and Buchman, 2007) during the Gonwdana cycle.

The Pre-Andean Choiyoi Group (ca. 285-248 Ma) comprises several magmatic units that crop out along ca. 2000 km in western Argentina and northeastern Chile (Fig. 2.2), with an estimated volume of 1,260,000 km^3 (Fig. 2.1) and it is interpreted as the gravitational collapse of the previous orogeny (Kleiman and Japas, 2009; Llambías et al., 2003, 1993; Llambías and Sato, 1995; Rocher et al., 2015; Sato et al., 2015; Spalletti and Limarino, 2017). The vast majority of the rocks are acid in composition, having magmatic affinities that define a temporal rend from calk-alkaline to anorogenic (Llambías and Sato, 1995) and they are interpreted as magmatism due to crustal melting or extensive recycling, triggered by basaltic underplating (that provided the heat) in an extensional tectonic regime (Hervé et al., 2014; Llambías and Sato, 1995; Mpodozis and Kay, 1990; Ramos and Kay, 1991; Rapela and Llambías, 1985). The database complied in this work contains most of the reported chemical data for the

Choiyoi magmatism in Argentina and Chile and yet the composition the analyzed samples is largely consistent with a straightforward subduction-related origin (see above) (Fig. 2.11b).

An alternative explanation to the systematic subduction signature is that melting affected only the more mafic and less evolved lower crust, that was in turn generated in a previous subduction setting during the Upper Carboniferous or Ordovician (Alasino et al., 2017, 2012; Coira et al., 2016; Ducea et al., 2015; Martina et al., 2011; Otamendi et al., 2010; Walker et al., 2015). However, no inherited zircons of that age range or lower crustal xenoliths in the plutonic units of the Choiyoi province have been reported, and only local metasedimentary enclaves of the host rocks are found (Llambías and Sato, 1995). Furthermore, there is lack of >280 Ma inherited zircons in the Permian-Triassic (Choiyoi) samples dated by the in-situ U-Pb method (del Rey et al., 2016; Hervé et al., 2014; Sato et al., 2015), even though Mesoproterozoic model ages have been reported for the crustal component in some of them (del Rey et al., 2016). Therefore, even though anorogenic or crustal-derived signatures have been identified in some of the Choiyoi intrusions in Argentina (Llambías and Sato, 1995) and equivalents units in Chile (Mpodozis and Kay, 1992; del Rey el al., 2019), the case for the generation of the Choiyoi magmatism solely through crustal meting or reworking seems rather unlikely.

Continuous subduction during the entire Pre-Andean Permian period is then a plausible scenario for the SW margin of Gondwana, although this process could have had a restricted contribution to crustal growth, implying a significant amount of recycling through assimilation, as it has been observed for southern Perú (Garzione et al., 2017; Mišković and Schaltegger, 2009) or Patagonia (Castillo et al., 2017)

By the end of the magmatic activity of the Choiyoi province another episode of magmatism during the Early-Middle Triassic preceded the rifting of large-scale intracontinental basins, in which restricted volumes of basaltic flows with intraplate signatures extruded (Castro de Machuca et al., 2019; Martínez, 2004; Ramos and Kay, 1991; Sommer et al., 2018), suggesting a passive margin configuration. These large cale basins (Ichigualasto and Cuyo) were located farther inland with respect to position

of the main magmatic axis (Fig. 2.1) that was closer to the margin's edge. On the other hand, the units cropping out in the Frontal and Domeyko Cordilleras that represent marine and continental depocenters, and their related igneous rocks, have been interpreted as subduction-related rifting basins (Suarez and Bell, 1992), located either in forearc (San Felix basin, Salazar et al., 2019), or back-arc (Domeyko basin, Espinoza et al., 2019) positions (Fig. 2.11c). This variety of contradicting interpretations implies there is no consensus regarding the tectonic configuration of the Pre-Andean stage for the Triassic. Furthermore, the volumetrically most significant magmatism at the time was not bimodal, as expected for continental rift settings. This magmatism has an arc-related signature and less crustal contribution than the Permian counterparts (Figs. 2.7, 2.8, 2.9). Thus, the Pre-Andean Triassic record of magmatism and the architecture of the rift basins in the continent margin (northern Chile) suggest that this stage represents a subduction setting, whereas the magmatism and depocenters in the inner part of the continent (northwestern Argentina) may have developed through continental rifting with NW orientation (Castro de Machuca et al., 2009; Giambiagi et al., 2011).

Nonetheless, transitional (calk-alkaline) to alkaline magmatism did occur during the Pre-Andean stage in the Late Triassic (Norian), as it is attested by the chemistry of some of the basaltic lava flows and syenogranites in the Frontal Cordillera (Quebrada del Salitre, La Ternera and Pastos Blancos formations, Colorado granites, Coloma et al., 2017; González et al., 2018). Samples with such signatures do not represent the entire magmatic record of each unit and their volume of rocks is rather restricted compared to the units that bear a clear calc-alkaline subduction-related chemical composition (Ortiz and Merino, 2015; Salazar and Coloma, 2016; Murillo et al., 2017; González et al., 2018). Coloma et al. (2017) have interpreted this transitional magmatism as a potential precursor of the ultimate emplacement of the Andean arc along the present-day Coastal Cordillera. This tectonic setting is likely given that some of the Pre-Andean Norian-Rhaetian volcanic units represent the early stages of the Jurassic back-arc basin (Espinoza et al., 2018) located to the east of the Jurassic Andean arc (Oliveros et al., 2006), as an analogue to the Rhaetian-Hettangian Pre-Cuyo group that preceded the development of the Jurassic Neuquén back-arc basin in the southern Andes (D'Elia et al., 2012). In fact, during the main activity of the Early

Andean arc, alkaline to transitional volcanism occurred in the eastern (inner continent) edge of the back-arc basin and it is interpreted in the context of the extensional tectonic that dominated during the early stages of the Andean arc (Rossel et al., 2015, 2013). Therefore, the presence of alkaline igneous rocks in the Pre-Andean Triassic record cannot be directly attributed to passive margin within plate magmatism (Kay and Mpodozis 1991; Charrier et al. 2007), but rather to back-arc depocenters (Rossel et al. 2013).

Subduction of an oceanic (Panthalassa-related) plate under the SW Gondwana margin might have then persisted throughout the Permian and Triassic periods (Fig. 2.11) but the dynamics of this process must have undergone significant changes. If the Carboniferous to Jurassic magmatism of the SW Gondwana margin is considered as the product of a continental-type margin, the La_N/Yb_N and Sr/Y ratios of the studied and published samples may be related to crustal thickness (Chapman et al., 2015; Profeta et al., 2015), with a maximum at ca. 280 Ma, right after the San Rafael Orogeny (Kleiman and Japas, 2009; Sato et al., 2015) and then a steady decrease until the end of the Jurassic (Fig. 2.10a,c). In a similar way, crustal contribution to magma sources also decreased from ca 280 Ma to 150 Ma (Fig. 2.10d,e). This is in very good agreement with the overall extensional setting proposed for the continental margin at the same time span (del Rey et al., 2016; Grocott and Taylor, 2002; Hervé et al., 2014; Llambías and Sato, 1995; Mpodozis and Kay, 1992; Mpodozis and Ramos, 1989; Sato et al., 2015). Recent models of the plate configuration suggest that the continental margin of SW Gondwana was active and overriding an oceanic plate with spreading centers (Müller et al., 2016; Riel et al., 2018; Torsvik and Cocks, 2013; Young et al., 2019) at least since the Late Carboniferous and until the Late Jurassic. This reinforces the idea that magmatism along the SW Gondwana margin must has been generated by subduction.

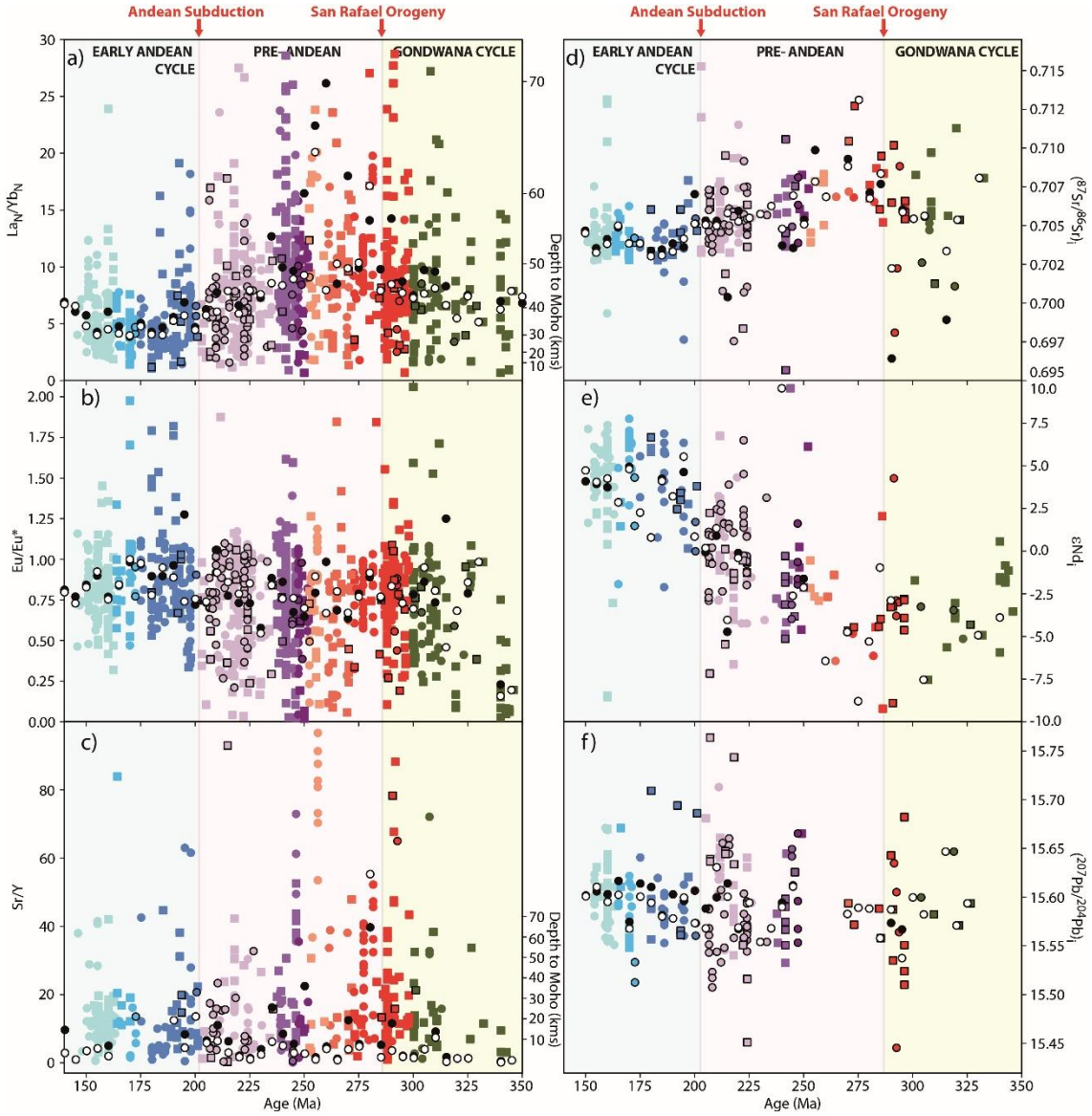

Figure 2.10. Age versus a) chondrite-normalized La/Yb and b) Eu/Eu* (Eu*=Eu/(Sm*Gd)^{½}), and c) Sr/Y for analyzed and published samples with 55 < SiO_2 <70 %wt and MgO <6 wt%. Age versus d) initial $^{87}Sr/^{86}Sr$, e) initial $^{143}Nd/^{144}Nd$ (εNd) and f) initial $^{207}Pb/^{204}Pb$ for all analyzed and published samples. Chondrite values from Sun and McDonough (1989). Ages without errors for each sample were assigned from data in Supplementary Material 2.2 and 2.3, using the following criteria: radiometric age reported in literature for the very same sample, or age reported for the nearest sample of the same unit or sub-unit, or mean value of the age range reported for the entire unit, or mean absolute value for the numerical range of the stratigraphic age assigned to the entire unit (age limits for stratigraphic stages from Cohen et al. 2013). Black and white dots represent mean and median values, excluding outliers, for each 5 Myr interval, respectively. Symbols and legends are as in Fig. 2.5. Background colors are as in Fig. 2.3 and refer to the Gondwana, Pre-Andean, and Andean cycles.

Sr/Y and La_N/Yb_N peaks towards the end of the Lopingian to the Middle Triassic (~255-245 Ma) escape from the more general trend of decreasing ratios (Fig. 2.10 a, c) and are not coupled to $^{87}Sr/^{86}Sr$ positive or εNdi negative peaks (Fig. 2.10 d,e), nor with εHf

negative peaks (del Rey et al. 2019). The model of kinematic evolution of Young et al. (2019) proposes a shift in the absolute motion of the continental plate, from northeastward to southwestward (oceanic plate maintained its northeastward motion), that roughly coincides with the high Sr/Y- La_N/Yb_N magmatism, implying perhaps a period of compression or thickened crust, although now with increased crustal contribution to magmatism. The model also suggests that shortly after, at ~240-225 Ma, the convergence shifted from dextral to sinistral and again the absolute motion of the continental plate change to northeastward, diminishing the convergence with the oceanic plate (Matthews et al. 2016; Young et al., 2019). This time frame coincides with the inception and development of the NW-oriented rift basins, both close to the continental the margin (Cifuncho, Domeyko, La Ternera and San Félix basins, Suárez and Bell, 1992; Espinoza et al., 2019; Salazar et al., 2019) and farther into the foreland (Ichigualasto and Cuyo basins, Giambiagi et al. 2019). Thus, the conditions for plates convergence, and not only the far field stresses related to the Pangea break-up (Charrier et al., 2007), may have played a role in the generation and evolution of the Triassic rift basins.

In contrast to what the geochemistry and geologic evidence suggest for the evolution of the present-day Andean region of Chile and Argentina, extensive alkaline magmatism of the Triassic Mitu Group and continental anatectites have been linked to continental rifting due to Pangea disassembly without penecontemporaneous subduction (Spikings et al., 2016). The margin should have then been significantly segmented if simultaneous passive and active zones were developed along it.

Variation in the geometry and physics of the subducting plate are the most probable control on tectonic segmentation but it is difficult to identify in the geological record at the temporal scales of this study. The continental margin may have been interacting an active ridge in the Panthalassa ocean with during the Pre-Andean stage (Matthews et al. 2016; Young et al. 2019). Although there is no direct evidence of ridge subduction in the Carboniferous to Jurassic record, the passage of this plate boundary could have induced differential deformation and magmatism along the margin and it is a hypothesis that should be tested.

Aside from changes in the geometry and rheology of the subducting oceanic plate which is for example the main factor for modern Andean segmentation (Stern, 2004), the Pre-Andean stage segmentation could have been the result of heterogeneities in the upper South American plate (Ramos, 1994) or differential response to Pangea realm reorganization as proposed by Riel et al. (2018). Given that the distribution of Triassic rift basins would have been controlled by the location of boundary zones of terrains accreted to South America (Giambiagi et al., 2011) it is possible that such heterogeneities would have in part influenced the response of the margin to convergence.

Steepening of the oceanic plate and roll-back would have triggered the dominant extensional tectonics of the margin after the San Rafael phase, and would have been responsible for a more significant mantle signature of the Triassic magmas. The temporal and spatial variation of the subduction angle however, did not affected the locus of magmatism which continued to develop mainly in the present-day High Andes with minor expressions in the Coastal Cordillera (Fig. 2.1). It was not until 210 Ma that a major shift of the magmatic axis took place from south Peru to Central Chile, where more voluminous magmatism was emplaced along the present-day Coastal Cordillera (Figs. 2.1-2.3)(Parada et al., 1999; Boekhout et al., 2012; F. Coloma et al., 2017; Vásquez et al., 2011) and continued throughout the Jurassic with no counterpart in the High Andes until ca. 160 Ma (Rossel et al., 2013). Whatever the reason for this important spatial migration of the magmatic loci, it does not relate to any detectable break in the geochemical evolution of the Pre-Andean rocks analyzed so far (Fig. 2.10). The post-210 Ma magmatism of the Coastal Cordillera is widely known as the first stage of the Andean subduction dominated by the development of the “La Negra” Arc (Fig. 2.11d)(Oliveros et al., 2006; Charrier et al. 2007). The arc produced voluminous magmatism with variable composition but dominantly intermediate and calc-alkaline to tholeiitic affinities (Fig.2.5), over a thinned crust that underwent sinistral transtention due to the stress partitioning of an oblique subduction of the Phoenix (or Panthalassa) plate (Scheuber and González, 1999; Grocott and Taylor, 2002; Lucassen et al., 2006). The overall extensional setting and the development of a marine back-arc region is

consistent with a model of retreating orogen (Cawood and Buchman, 2007) for the Early Andean cycle.

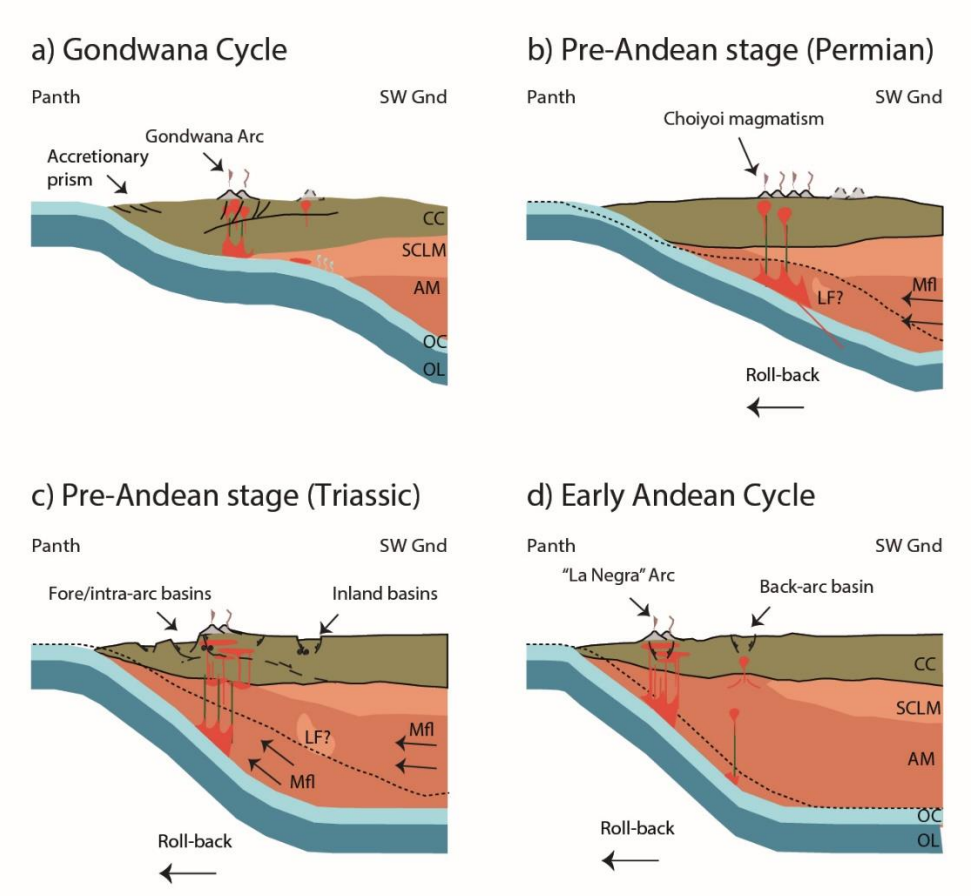

Figure 11. Proposed tectonic and paleogeographic configuration for the Proto- and Early-Andean margin of SW Gondwana at a) the end of the Gondwana cycle, during the Latest Carboniferous and Early Permian, where the San Rafael Orogeny took place, likely due to flat slab subduction, inducing hydroweakening of the lithospheric mantle; b) the Permian Pre-Andean stage where slab roll-back induced lithospheric loss (either through foundering of the lithospheric roots or thermal erosion due to asthenospheric mantle flow) c) the Triassic Pre-Andean stage where increased roll-back and mantle flow caused generalized extension in the upper crust and the development of fore-arc, intra-arc and inland basins; and d) during the Early Andean cycle, where the arc was emplaced westward of the former magmatic fronts. Panth: Panthalassa Ocean (and oceanic plate), SW Gnd: Southwestern Gondwana continental interior; Mfl: asthenospheric mantle flow; LF: lithospheric foundering. OC: Oceanic crust, OL: Oceanic lithospheric mantle; CC: Continental Crust; SCLM: Sub-continental lithospheric mantle; AM: Asthenospheric mantle.Dotted line represent the upper limit of the slab from the previous stage.

2.6.3 Lithospheric evolution of the Early Andes

The chemistry of Late Carboniferous to the Late Jurassic igneous rocks strongly suggest that magmatism was dominantly of subduction-related nature. Although it is possible to explain the geological and tectonic changes that took place along the

margin during this period in the context of continuous plate convergence, an evolutionary model that accounts for the systematic increase in the sub-arc mantle component of magmas is still needed. The formation of prevailing magmatic crust in longstanding immobile arcs may induce the increase of the sub-arc mantle component, but this process would not explain the extension that occurred in the Pre-Andean stage. Another process that may account for the geochemical evolution in magmatism is the foundering of subcontinental lithospheric mantle (Fig. 2.11b,c). Most long-lived Phanerozoic arcs have a cyclic geochemical and isotopic behavior that is partly related to lithospheric delamination. (DeCelles et al. 2009; Ducea and Barton, 2007). Loss of the lithospheric roots of Cordilleran-type arcs through delamination or foundering has been well documented in the Andes and the North American Mesozoic arc (e.g. Ducea and Saleeby, 1998; Ducea et al., 2013; Kay and Kay, 1993; Zandt et al., 2004). It is a process that results both in magmatism with an asthenospheric mantle source in regions of thick crust and asthenosphere upwelling-driven exhumation of the crust and development of plain elevated areas such as the Puna in northwestern Argentina (Ducea et al., 2013; Kay and Kay, 1993).

The spatial and temporal scales in which delamination has been reported vary between 20-100 km and ca. 5 to 40 Myr (Ducea, 2011; Gutiérrez-Alonso et al., 2011). Although increasing mantle signature and exhumation are characteristics of the Pre-Andean stage magmatism and tectonic evolution, they are observed along ca. 2000 km of the margin and from ca. 270 to 200 Ma, which is far in excess of what can be a single delamination process. Multiple-stages delamination has been suggested in some tectonic models (DeCelles et al., 2009) but it is a process unlikely to have taken place wholesale at the thousand-kms-long scale needed for explaining the observed features of the pre-Andean margin.

Another process that may result in loss of lithosphere and its replacement by fertile asthenospheric mantle is “decratonization” (Kusky et al., 2014; Spencer et al., 2017), which would have taken place in North China craton during the Cretaceous in response to slab roll-back. Mesozoic magmastim in this area transitioned from calc-alkaline, adakitic rocks mainly derived from thickened ancient lower continental crust (negative

εNd) to extensive magmatism including A-type granites, alkaline to calc-alkaline composition and increased contribution of a depleted mantle source (less ngetive to positive εNd), during the peak of decratonization (Zhang et al., 2014). This change in the petrography of the magmatism would be similar to the changes in the magmatic chemistry from the Gondwana cycle to the Pre-Andean stage, although the subduction component is much more intense in the latter. The thermal erosion of the cratonic lithosphere due to asthenospheric upwelling in the space left by a stagnant lid that triggers slab roll-back induces both more juvenile magmatism and extensional tectonics and exhumation on the upper continental plate. As much as lithospheric foundering, decratonization is intrinsically associated to continent-oceanic subduction, but it has been documented in much larger spatial and temporal scales (Spencer et al., 2017) and could take place along an entire margin without the need of shortening/compression events and phase changes in the lower crust to induce delamination.

In the case of the Pre-Andean stage, the San Rafael orogenic phase would have provided the fluids from a dehydrating flat slab, when slab roll-back started to act after the orogenic collapse (del Rey et al. 2016), the space left by the retreating slab may have been filled by asthenospheric mantle, which melted in the presence of those fluids. The melted asthenosphere could have thermochemically eroded the continental lithosphere, and at the same time generated the extension that prevailed during the Permian and Triassic along the margin (Fig. 2.11). The persistent signal of evolution from lithospheric-dominated to asthenosphere-dominated sources of magmatism, coupled to protracted extensional regime and the large spatio-temporal scales of such evolution suggest that decratonization might have occurred along the proto-Andean margin, prior to the establishment of the Andean arc in the very edge of the continental plate.

2.7 Conclusions

The elemental and isotopic composition of 86 samples of volcanic and plutonic rocks spanning ca. 330 to 150 Ma analyzed for this study, along with 1054 geochemical data of Carboniferous to Jurassic igneous rocks, representing the Gondwana cycle, Pre-

Andean stage and Early Andean cycle magmatism, from the Chilean and Argentinean Andes provide a first order record of magmatic evolution along the South American margin during Pangea's life and break-off. In spite of previous tectonic models that proposed arrested subduction during the supercontinent disassembly, the magmatism along the proto-Andean margin is consistently of subduction-related nature throughout the period. Typical features of arc magmatism are found in most of the analyzed and reported samples: calc-alkaline affinities, LILE enrichment over HFSE, Nb-Ta troughs and moderate to small Eu negative anomalies. SiO_2 content of the Pre-Andean rocks is higher than expected for arc rocks and the compositional bimodality that had been attributed to Triassic magmatism is not observed in the compiled record. Sr-Nd-Pb isotope composition of the samples analyzed for this study and published data suggests that magma sources included depleted mantle reservoir and continental crust. Although the Pre-Andean magmatism had been previously interpreted as the result of crustal melting, this seems unlikely given the less evolved isotopic signatures of volcanic and plutonic rocks compared to the Paleozoic basement.

The temporal evolution of the magmatism from the Gondwana to Early Andean cycle suggests an increase of the sub-arc mantle component in the latter. This shift in the magmatic composition was accompanied by prevailing extensional tectonics both in the continental margin and foreland. Loss of the lithospheric roots of the arc or thermal erosion of the lithosphere after a flat subduction event are proposed as the most likely scenarios for the geodynamic evolution of the Pre-Andean margin.

Acknowledgements

This research was funded through the Fondecyt grant 1120715, the "Plan Nacional de Geología" of the National Geological and Mining Survey (SERNAGEOMIN), the ENLACE 218.040.025-1.0 (Universidad de Concepción) and the Conicyt doctoral grants 21140774 (ME) and 21150502 (JG). M.N.D. acknowledges support from US National Science Foundation grant EAR 1725002 and the Romanian Executive Agency for Higher Education, Research, Development and Innovation Funding projects PN-III-P4-ID-PCE-2016-0127 and PN-III-P4-ID-PCCF-2016-0014. Natalia Astudillo, Rodolfo Ferrando, Rodrigo González, Diego Montecino, Miguel Ortiz, Roberto Merino, Ismael

Murillo and Ricardo Velásquez are thanked for the fruitful discussions on the updated geological mapping in northern Chile. Florencia Bechis, Amancay Martínez, Laura Giambiagi are thanked for collaborations in the field work.

2.8 References

Alasino, P.H., Dahlquist, J. a., Pankhurst, R.J., Galindo, C., Casquet, C., Rapela, C.W., Larrovere, M. a., Fanning, C.M., 2012. Early Carboniferous sub- to mid-alkaline magmatism in the Eastern Sierras Pampeanas, NW Argentina: A record of crustal growth by the incorporation of mantle-derived material in an extensional setting. Gondwana Res. 22, 992–1008. doi:10.1016/j.gr.2011.12.011

Alasino, P.H., Larrovere, M.A., Rocher, S., Dahlquist, J.A., Basei, M.A.S., Memeti, V., Paterson, S., Galindo, C., Macchioli, M., Campos, C., 2017. Incremental growth of an upper crustal , A-type pluton , Argentina : Evidence of a re-used magma pathway. Lithos 284–285, 347–366. doi:10.1016/j.lithos.2017.04.013

Ardill, J., Flint, S., Chong, G., Wilke, H., 1998. Sequence stratigraphy of the Mesozoic Domeyko Basin, northern Chile. J. Geol. Soc. London. 155, 71–88.

Arriagada, C., Roperch, P., Mpodozis, C., Fernandez, R., 2006. Paleomagnetism and tectonics of the southern Atacama Desert (25-28°S), northern Chile. Tectonics 25, 1–26. doi:10.1029/2005TC001923

Astini, R., Martina, F., Ezpeleta, M., Dávila, F.M., Cawood, P., 2009. Chronology from rifting to foreland basin in the Paganzo Basin (Argentina), and a reapprisal on the “Eo- and Neohercynian” tectonics along Western Gondwana. XII Congr. Geológico Chil. 1–4.

Bahlburg, H., Vervoort, J. D., Du Frane, S. A., Bock, B., Augustsson, C., Reimann, C. 2009. Timing of crust formation and recycling in accretionary orogens: Insights learned from the western margin of South America. Earth-Sci Rev. 9, 215-241.doi: 10.1016/j.earscirev.2009.10.006

Bell, C.M., 1987 The origin of the Upper Palaeozoic Chanaral mélange of N Chile. J Geol Soc London 144, 599–610.

Bissig, T., Clark, A.H., Lee, J.K.W., von Quadt, A., 2003. Petrogenetic and metallogenetic responses to Miocene slab flattening: new constraints from the El Indio-Pascua Au–Ag–Cu belt, Chile/Argentina. Miner. Depos. 38, 844–862. doi:10.1007/s00126-003-0375-y

Boekhout, F., Spikings, R., Sempere, T., Chiaradia, M., Ulianov, A., Schaltegger, U., 2012. Mesozoic arc magmatism along the southern Peruvian margin during Gondwana breakup and dispersal. Lithos 146–147, 48–64. doi:10.1016/j.lithos.2012.04.015

Breitkreuz, C., Bahlburg, H., Delakowitz, B., Pichowiak, S., 1989. Paleozoic volcanic events in the Central Andes. J South Am. Earth Sci. 2, 171–189. doi: 10.1016/0895-9811(89)90045-X

Brown, M., 1991. Comparative geochemical interpretation of Permian–Triassic plutonic complexes of the Coastal Range and Altiplano (25º30' to 26º30' S), northern Chile. Geol. Soc. Am. Spec. Pap. 265, 157–171. doi: 10.1130/SPE265-p157

Castillo, P., Fanning, C.M., Pankhurst, R.J., Hervé, F., Rapela, C.W., 2017. Zircon O- and Hf-isotope constraints on the genesis and tectonic significance of Permian magmatism in Patagonia. J. Geol. Soc. London. 174, jgs2016-152. doi:10.1144/jgs2016-152

Cawood, P. A., Buchan, C., 2007). Linking accretionary orogenesis with supercontinent assembly. Earth-Sci Reviews, 82(3-4), 217-256. Doi: 10.1016/j.earscirev.2007.03.003

Cembrano, J., Lavenu, A., Reynolds, P., Arancibia, G., López, G., Sanhueza, A., 2002. Late Cenozoic transpressional ductile deformation north of the Nazca – South America – Antarctica triple junction. Tectonophysics 354, 289–314. doi:10.1016/S0040-1951(02)00388-8

Chapman, J.B., Ducea, M.N., Decelles, P.G., Profeta, L., 2015. Tracking changes in crustal thickness during orogenic evolution with Sr / Y : An example from the North American Cordillera Tracking changes in crustal thickness during orogenic

evolution with Sr / Y ; an example from the North American Cordillera. doi:10.1130/G36996.1

Charrier, R., Pinto, L., Rodríguez, M.P., 2007. Tectonostratigraphic evolution of the Andean Orogen in Chile, in: Moreno, T., Gibbons, W. (Eds.), The Geology of Chile. The Geological Society, London, pp. 21–114. doi:10.1144/GOCH.3

Charrier, R., Ramos, V. a., Tapia, F., Sagripanti, L., 2014. Tectono-stratigraphic evolution of the Andean Orogen between 31 and 37 S (Chile and Western Argentina). Geol. Soc. London, Spec. Publ. 399, 13–61. doi:10.1144/SP399.20

Cohen, K.M., Finney, S.C., Gibbard, P.L., Fan, J.-X., 2013 (updated). The ICS International Chronostratigraphic Chart. Episodes 36, 199-204. doi:10.1111/j.1502-3931.1980.tb01026.x

Coira, B., Cisterna, C.E., Ulbrich, H.H., Cordani, U.G., 2016. Extensional Carboniferous magmatism at the western margin of Gondwana: Las Lozas valley, Catamarca, Argentina. Andean Geol. 43, 105–126. doi:10.5027/andgeoV43n1-a06

Coloma, F., Valin, X., Oliveros, V., Vásquez, P., Creixell, C., Salazar, E., Ducea, M.N., 2017. Geochemistry of permian to triassic igneous rocks from northern Chile (28°-30°15‘S): Implications on the dynamics of the proto-Andean margin. Andean Geol. 44, 147–148. doi:10.5027/andgeoV44n2-a03

Cornejo, P., Mpodozis, C., Rivera, O., Matthews, S.J., 2009. CARTA EXPLORADORA, REGIONES DE ANTOFAGASTA Y ATACAMA. Servicio Nacional de Geología y Minería, Santiago.

Cox, K.J., Bell, J.D., Pankhurst, R.J., 1979. The Interpretation of Igneous Rocks, First. ed. Springer, Dordrecht.

Creixell, C., Oliveros, V., Vásquez, P., Navarro, J., Vallejos, D., Valin, X., Godoy, E., N. Ducea, M., 2016. Geodynamics of Late Carboniferous–Early Permian forearc in north Chile (28°30′–29°30′S). J. Geol. Soc. London. 173, jgs2016-010. doi:10.1144/jgs2016-010

Dahlquist, J. A., Alasino, P. H., Eby, G. N., Galindo, C., Casquet, C., 2010. Fault controlled Carboniferous A-type magmatism in the proto-Andean foreland (Sierras Pampeanas, Argentina): Geochemical constraints and petrogenesis. Lithos, 115, 65–81.

De Silva, S., Zandt, G., Trumbull, R., Viramonte, J. G., Salas, G., & Jiménez, N. (2006). Large ignimbrite eruptions and volcano-tectonic depressions in the Central Andes: a thermomechanical perspective. Geol. Soc. London. Spe. Pub. 269, 47-63.

D'Elia, L., Muravchik, M., Franzese, J.R., Bilmes, A., 2012. Volcanismo de sin-rift de la Cuenca Neuquina, Argentina: Relación con la evolución Triásico Tardía-Jurásico Temprano del margen Andino. Andean Geol. 39, 106–132.

Deckart, K., Hervé, F., Fanning, C.M., Ramírez, V., Calderón, M., Godoy, E., 2014. U-Pb Geochronology and Hf-O Isotopes of zircons from the Pennsylvanian Coastal Batholith, South-Central Chile. Andean Geol. 41, 49–82. doi:10.5027/andgeoV41n1-a03

del Rey, A., Deckart, K., Planavsky, N., Arriagada, C., Martínez, F., 2019. Tectonic evolution of the southwestern margin of Pangea and its global implications: Evidence from the mid Permian–Triassic magmatism along the Chilean-Argentine border. Gondwana Res. 76, 303–321. doi: 10.1016/j.gr.2019.05.007

del Rey, A., Deckart, K., Arriagada, C., Martínez, F., 2016. Resolving the paradigm of the late Paleozoic-Triassic Chilean magmatism: Isotopic approach. Gondwana Res. 37, 172–181. doi:10.1016/j.gr.2016.06.008

Ducea, M., Saleeby, J., 1998. A case for delamination of the deep batholithic crust beneath the sierra nevada, california. Int. Geol. Rev. 40, 78–93. doi:10.1080/00206819809465199

Ducea, M.N., 2011. Fingerprinting orogenic delamination. Geology 39, 191–192. doi:10.1130/focus022011.1

Ducea, M.N., Otamendi, J.E., Bergantz, G.W., Jianu, D., Petrescu, L., 2015. The Ordovician Famatinian-Puna arc. GSA Mem. 212, 125–138. doi:10.1130/2015.1212(07).

Ducea, M.N., Seclaman, A.C., Murray, K.E., Jianu, D., Schoenbohm, L.M., 2013. Mantle-drip magmatism beneath the Altiplano-Puna plateau, central Andes. Geology 41, 915–918. doi:10.1130/G34509.1

Espinoza, M., Montecino, D., Oliveros, V., Astudillo, N., Vásquez, P., Reyes, R., Celis, C., González, R., Contreras, J., Creixell, C., Martínez, A. 2019. The synrift phase of the early Domeyko Basin (Triassic, northern Chile): Sedimentary, volcanic and tectonic interplay in the evolution of an ancient subduction-related rift basin. Basin Research, 31, 4-32. DOI: 10.1111/bre.12305

Espinoza, M., Oliveros, V., Vásquez, P., Bechis, F., 2015. U-Pb geochronology and kinematic preliminary analyses of Late Triassic-Early Jurassic basins in northern Chile (24.5° -26°S). XIV Congreso Geológico Chileno, La Serena, Chile.Escayola, M.P., Pimentel, M.M., and Armstrong, R, 2007. Neoproterozoic backarc basin: Sensitive high-resolution ion microprobe U-Pb and Sm-Nd isotopic evidence from the Eastern Pampean Ranges, Argentina. Geology, 35, 495–498. doi: 10.1130/G23549A.1

Farner, M.J., Lee, C.-T.A., 2017. Effects of crustal thickness on magmatic differentiation in subduction zone volcanism: A global study. Earth Planet. Sci. Lett. 470, 96–107. doi:10.1016/j.epsl.2017.04.025

Fosdick, J.C., Carrapa, B., Ortíz, G., 2015. Faulting and erosion in the Argentine Precordillera during changes in subduction regime: Reconciling bedrock cooling and detrital records. Earth Planet. Sci. Lett. 432, 73–83. doi:10.1016/j.epsl.2015.09.041

Fuentes, P., Fernández, C., Díaz-Alvarado, J.,Díaz-Azpiroz, M., 2019. Using 3D kinematic models in subduction channels. The case of the Chañaral tectonic mélange, Coastal Cordillera, northern Chile. Gondwana Res. 74, 251–270 Doi: 10.1016/j.gr.2018.12.009

Giambiagi, L., Martinez, A.N., 2008. Permo-Triassic oblique extension in thePotrerillos-Uspallata area, western Argentina. J. South Am. Earth Sci. 26,252–260. Doi: 10.1016/j.jsames.2008.08.008

Giambiagi, L., Mescua, J., Bechis, F., Martinez, a., Folguera, a., 2011. Pre-Andean deformation of the Precordillera southern sector, southern Central Andes. Geosphere 7, 219–239. doi:10.1130/GES00572.1

González, J., Oliveros, V., Creixell, C., Velásquez, R., Vásquez, P., Lucassen, F., 2018. The Triassic magmatism and its relation with the Pre-Andean tectonic evolution: Geochemical and petrographic constrains from the High Andes of north central Chile (29°30' - 30°S). J. South Am. Earth Sci.87, 95–112. doi:10.1016/j.jsames.2017.12.009

Grocott, J., Arévalo, C., Welkner, D., Cruden, A., Sciences, E., Kt, K., Valley, M., Limited, E., Street, W.G., Survey, G., Mar, S., Nacional, S., Street, R., Arevalo, C., 2009. Fault-assisted vertical pluton growth: Coastal Cordillera, north Chilean Andes. J. Geol. Soc. London. 166, 295–301. doi:10.1144/0016-76492007-165

Grocott, J., Taylor, G.K., 2002. Magmatic arc fault systems, deformation partitioning and emplacement of granitic complexes in the Coastal Cordillera, north Chilean Andes (25°30'S to 27°00'S). J. Geol. Soc. London. 159, 425–442. doi:10.1144/0016-764901-124

Gutiérrez-Alonso, G., Murphy, J.B., Fernández-Suárez, J., Weil, A.B., Franco, M.P., Gonzalo, J.C., 2011. Lithospheric delamination in the core of Pangea: Sm-Nd insights from the Iberian mantle. Geology 39, 155–158. doi:10.1130/G31468.1

Hervé, F., Fanning, C.M., Calderón, M., Mpodozis, C., 2014. Early Permian to Late Triassic batholiths of the Chilean Frontal Cordillera (28°-31°S): SHRIMP U-Pb zircon ages and Lu-Hf and O isotope systematics. Lithos 184–187, 436–446. doi:10.1016/j.lithos.2013.10.018

Howell, J.A., Schwarz, E., Spalletti, L.A., Veiga, G.D., 2005. The Neuquén Basin: an overview. Geol. Soc. London, Spec. Publ. 252, 1–14. doi:10.1144/GSL.SP.2005.252.01.01

Irvine, T.N., Baragar, W.R. a., 1971. A Guide to the Chemical Classification of the Common Volcanic Rocks. Can. J. Earth Sci. 8, 523–548. doi:10.1139/e71-055

Kay, R.W., Kay, S.M., 1993. Delamination and delamination magmatism. Tectonophysics 219, 177–189. doi:10.1016/0040-1951(93)90295-U

Kay, S.M., Mpodozis, C., 2001. Central Andean Ore deposits linked to evolving shallow subduction systems and thickening crust. GSA Today 11, 4–9. doi:10.1017/CBO9781107415324.004

Kay, S.M., Ramos, V.A., Mpodozis, C., Sruoga, P., 1989. Late Paleozoic to Jurassic silicic magmatism at the Gondwana margin: analogy to the Middle Proterozoic in North America? Geology. doi:10.1130/0091-7613(1989)017<0324:LPTJSM>2.3.CO;2

Kleiman, L.E., Japas, M.S., 2009. The Choiyoi volcanic province at 34°S-36°S (San Rafael, Mendoza, Argentina): Implications for the Late Palaeozoic evolution of the southwestern margin of Gondwana. Tectonophysics 473, 283–299. doi:10.1016/j.tecto.2009.02.046

Kusky, T.M., Windley, B.F., Wang, L., Wang, Z., Li, X., Zhu, P., 2014. Flat slab subduction, trench suction, and craton destruction: Comparison of the North China, Wyoming, and Brazilian cratons. Tectonophysics 630, 208–221. doi:10.1016/j.tecto.2014.05.028

Llambías, E.J., Kleiman, L.E., Salvarredi, J.A., 1993. El Magmatismo Gondwanico. Ramos, V.A., (Ed.), Geol. y Recur. Nat. Mendoza, Relat. XII Congr. Geológico Argentino y II Congr. Explor. Hidrocarburos.

Llambías, E.J., Quenardelle, S., Montenegro, T., 2003. The Choiyoi Group from central Argentina: A subalkaline transitionalto alkaline association in the craton adjacent to the active marginof the Gondwana continent. J. South Am. Earth Sci. 16, 243–257. doi:10.1016/S0895-9811(03)00070-1

Llambías, E.J., Sato, A.M., 1995. El batolito Colanguil transicion entre orogenesis y anorogenesis 50, 111–131.

Lossada, A.C., Giambiagi, L., Hoke, G.D., Fitzgerald, P.G., Creixell, C., Murillo, I., Mardonez, D., Velásquez, R., Suriano, J., 2017. Thermochronologic Evidence for Late Eocene Andean Mountain Building at 30°S. Tectonics 36, 2693–2713. doi:10.1002/2017TC004674

Lucassen, F., Franz, G., 1994. Arc related Jurassic igneous and meta-igneous rocks in the Coastal Cordillera of northern Chile/Region Antofagasta. Lithos 32, 273–298. doi:10.1016/0024-4937(94)90044-2

Lucassen, F., Franz, G., Thirlwall, M.F., Mezger, K., 1999. Crustal Recycling of Metamorphic Basement: Late Palaeozoic Granitoids of Northern Chile (22 S). Implications for the Composition of the Andean Crust. J. Petrol. 40, 1527–1551. doi:10.1093/petroj/40.10.1527

Lucassen, F., Kramer, W., Bartsch, V., Wilke, H.G., Franz, G., Romer, R.L., Dulski, P., 2006. Nd, Pb, and Sr isotope composition of juvenile magmatism in the Mesozoic large magmatic province of northern Chile (18-27??S): Indications for a uniform subarc mantle. Contrib. to Mineral. Petrol. 152, 571–589. doi:10.1007/s00410-006-0119-y

Maksaev, V., Munizaga, F., Tassinari, C., 2014. Temporalidad del magmatismo del borde paleo-Pacífico de Gondwana: Geocronología U-Pb de rocas ígneas del Paleozoico tardío a Mesozoico temprano de los Andes del norte de Chile entre los 20° y 31°S. Andean Geol. 41, 447–506. doi:10.5027/andgeoV41n3-a01

Mamani, M., Wörner, G., Sempere, T., 2010. Geochemical variations in igneous rocks of the Central Andean orocline (13°S to 18°S): Tracing crustal thickening and magma generation through time and space. Bull. Geol. Soc. Am. 122, 162–182. doi:10.1130/B26538.1

Martin, M.W., Kato, T.T., Rodriguez, C., Godoy, E., Duhart, P., McDonough, M., Campos, A., 1999. Evolution of the late Paleozoic accretionary complex and overlying forearc-magmatic arc, south central Chile (38°–41°S): Constraints for the tectonic setting along the southwestern margin of Gondwana. Tectonics 18, 582. doi:10.1029/1999TC900021

Martina, F., Viramonte, J.M., Astini, R.A., Pimentel, M.M., Dantas, E., 2011. Mississippian volcanism in the south-central Andes: New U-Pb SHRIMP zircon geochronology and whole-rock geochemistry. Gondwana Res. 19, 524–534. doi:10.1016/j.gr.2010.07.004

Martínez, A.N., 2004. Secuencias volcánicas permo-triásicas de los cordones del Portillo y del Plata, Cordillera Frontal, Mendoza: su interpretación tectónica. Universida de Buenos Aires.

Martínez, F., Peña, M., Arriagada, C., 2015. Geología de las áreas Iglesia Colorada - Cerro del Potro y Cerro Mondaquita, Región de Atacama. Servicio Nacional de Geología y Minería, Carta Geológica de Chile, Serie Geología Básica 179-180. Servicio Nacional de Geología y Minería, Santiago.

Mišković, A., Schaltegger, U., 2009. Crustal growth along a non-collisional cratonic margin: A Lu-Hf isotopic survey of the Eastern Cordilleran granitoids of Peru. Earth Planet. Sci. Lett. 279, 303–315. doi:10.1016/j.epsl.2009.01.002

Mpodozis, C., Cornejo, P., 1988. Hoja Pisco Elqui. IV Región de Coquimbo., Servicio Nacional de Geología y Minería. Carta Geológica de Chile 68. map scale 1:250.000.

Mpodozis, C., Kay, S.M., 1992. Late Paleozoic to Triassic evolution of the Gondwana margin: Evidence from Chilean Frontal Cordilleran batholiths (28°S to 31°S). Geol. Soc. Am. Bull. 104, 999–1014. doi:10.1130/0016-7606(1992)104<0999:LPTTEO>2.3.CO;2

Mpodozis, C., Kay, S.M., 1990. Provincias magmáticas ácidas y evolución tectónica de Gondwana: Andes Chilenos (28-31oS). Rev. Geológica Chile 17, 153–180.

Mpodozis, C., Ramos, V.A., 1989. The Andes of Chile and Argentina, in: Geology of the Andes and its Relation to Hydrocarbon and Mineral Resources 11, 59–90.

Müller, R.D., Seton, M., Zahirovic, S., Williams, S.E., Matthews, K.J., Wright, N.M., Shephard, G.E., Maloney, K.T., Barnett-moore, N., Bower, D.J., Cannon, J., 2016. Ocean basin evolution and global-scale reorganization events since

Pangea breakup. Annu. Rev. Earth Planet. Sci. Lett. 107–138. doi:10.1146/annurev-earth-060115-012211

Murillo, I., Velásquez, R., Creixell, C., 2017. Geología de la Áreas Guanta - Los Cuartitos y Paso de Vacas Heladas, Regiones de Atacama y Coquimbo. Servicio Nacional de Geología y Minería, Carta Geológica de Chile, Serie Geología Básica 192–193.

Nasi, C., Moscoso, R., Maksaev, V.J., 1990. Hoja Guanta, Región de Coquimbo. Servicio Nacional de Geología y Minería, Carta Geológica de Chile, Serie Geología Básica, 67.

Oliveros, V., Féraud, G., Aguirre, L., Fornari, M., Morata, D., 2006. The Early Andean Magmatic Province (EAMP): 40Ar/39Ar dating on Mesozoic volcanic and plutonic rocks from the Coastal Cordillera, northern Chile. J. Volcanol. Geotherm. Res. 157, 311–330.

Oliveros, V., González, J., Espinoza, M., Vásquez, P., Rossel, P., Creixell, C., Sepúlveda, F., Bastías, F., 2017. The early stages of the volcanic arc in the Southern Central Andes, in: Folguera, A., Contreras-Reyes, E., Heredia, N., Encinas, A., Iannelli, S., Oliveros, V., Dávila, F.M., Collo, G., Giambiagi, L.B., Maksymowicz, A., Iglesia Llanos, M.P., Turienzo, M.M., Naipauer, M., Orts, D., Litvak, V.D., Alvarez, O., Arriagada, C. (Eds.), The Evolution of the Chilean-Argentinean Andes. Springer International Publishing, Berlin Heidelberg, pp. 185–212. doi:10.1007/978-3-319-67774-3

Oliveros, V., Labbé, M., Rossel, P., Charrier, R., Encinas, A., 2012. Late Jurassic paleogeographic evolution of the Andean back-arc basin: New constrains from the Lagunillas Formation, northern Chile (27°30'–28°30'S). J. South Am. Earth Sci. 37, 25–40.

Oliveros, V., Morata, D., Aguire, L., Féraud, G., Fornari, M., 2007. Jurassic to Early Cretaceous subduction-related magmatism in the Coastal Cordillera of northern Chile (18º30–24ºS): Geochemistry and petrogenesis. Rev. Geol. Chile 34.

Ortiz, M., Merino, R.N., 2015. Geología de las áreas Río-Chollay y Matancillas y Cajón del Encierro, Regiones de Atacama y Coquimbo. Servicio Nacional de Geología y Minería, Carta Geológica de Cile, Serie Geología Básica 175–176.

Otamendi, J.E., Pinotti, L.P., Basei, M.A.S., Tibaldi, A.M., 2010. Evaluation of petrogenetic models for intermediate and silicic plutonic rocks from the Sierra de Valle Fértil-La Huerta, Argentina: Petrologic constraints on the origin of igneous rocks in the Ordovician Famatinian-Puna paleoarc. J. South Am. Earth Sci. 30, 29–45. doi:10.1016/j.jsames.2010.07.004

Pankhurst, R., Millar, I., Hervé, F., 1996. A Permo-Carboniferous U-Pb age for part of the Guanta Unit of the Elqui-Limari Batholith at Rio del Transito, Northern Chile. Rev. Geol. Chile 23, 35–42 ST–A Permo–Carboniferous U–Pb age for par.

Parada, M.A., 1988. Pre-Andean peraluminous and metaluminous leucogranitoid suites in the High Andes of central Chile. J. South Am. Earth Sci. 1, 211–221. doi:10.1016/0895-9811(88)90039-9

Parada, M.A., Nyström, J.O., Levi, B., 1999. Multiple sources for the Coastal Batholith of central Chile (31-34°S): Geochemical and Sr-Nd isotopic evidence and tectonic implications. Lithos 46, 505–521. doi:10.1016/S0024-4937(98)00080-2

Pearce, J.A., 1982. Trace element characteristics of lavas from destructive plate boundaries. In: Thorps, R.S. (Ed.), Andesites. John Wiley and Sons, New York, pp. 525–548

Pearce, J.A., 1996. Pearce_1996_A users guide to basalt discrimination diagrams.pdf.

Peña, M., Becerra, J., Martínez, F., Arriagada, C., 2013. Geología del Área Yerbas Buenas-Tres Morros, Región de Atacama. Servicio Nacional de Geología y Minería, Carta Geológica de Chile, Serie Geología Básica 155. Servicio Nacional de Geología y Minería, Santiago.

Prinz, P., H. G. Wilke, A. v., H., 1994. Sediment accumulation and subsidence history in the Mesozoic marginal basin of northern Chile. Tectonics South. Cent. Andes Struct. Evol. an Act. Cont. Margin 219–232.

Profeta, L., Ducea, M.N., Chapman, J.B., Paterson, S.R., Gonzales, S.M.H., Kirsch, M., Petrescu, L., DeCelles, P.G., 2015. Quantifying crustal thickness over time in magmatic arcs. Sci. Rep. 5, 17786. doi:10.1038/srep17786

Ramos, V.A., 1994. Terranes of Southern Gondwanaland and Their Control in the Andean Structure (30°-33° S Latitude). Tectonics South. Cent. Andes 249–261. doi:10.1007/978-3-642-77353-2_18

Ramos, V.A, Folguera, A., 2009. Andean flat-slab subduction through time. Geol. Soc. London. Spe. Pub. 327, 31-54.

Ramos, V.A., Kay, S.M., 1991. Triassic rifting and associated basalts in the Cuyo basin, central Argentina. Andean Magmat. its Tecton. setting 79–92. doi:10.1130/SPE265-p79

Rapalini, A.E., Astini, R.A., 2005. La remagnetización sanrafaélica de la Precordillera en el Pérmico: nuevas evidencias. Rev. Asoc. Geol. Argen. 60, 290–300.

Rapela, C.W., Llambías, E.J., 1985. Evolución magmática y relaciones regionales de los complejos eruptivos de La Esperanza, provincia de Río Negro. Rev. la Asoc. Geol. Argentina 40, 4–25.

Rebolledo, S., Charrier, R., 1994. Evolución del basamento paleozoico en el área de Punta Claditas, Región de Coquimbo, Chile (31-32°S). Rev. Geol. Chile 21, 55–69. doi:10.5027/andgeoV21n1-a03

Ribba, L., Mpodozis, C., Hervé, F., Nasi, C., Moscoso, R., 1988. El Basamento del Valle del Tránsito, Cordillera de Vallenar: Eventos magmáticos y metamórficos y su relación con la evolución de los Andes Chileno-Argentinos. Rev. Geológica Chile 15, 129–149. doi:10.5027/andgeoV15n2-a03

Riel, N., Jaillard, E., Martelat, J., Braun, J., 2018. Journal of South American Earth Sciences Permian-Triassic Tethyan realm reorganization : Implications for the outward Pangea margin 81, 78–86. doi:10.1016/j.jsames.2017.11.007

Rocher, S., Vallecillo, G., Castro, B., Machuca, D., Alasino, P., 2015. El Grupo Choiyoi (Pérmico temprano-medio) en la Cordillera Frontal de Calingasta , San Juan , Argentina : volcanismo de arco asociado a extensión 32, 415–432.

Rossel, P., Oliveros, V., Ducea, M.N., Charrier, R., Scaillet, S., Retamal, L., Figueroa, O., 2013. The Early Andean subduction system as an analog to island arcs: Evidence from across-arc geochemical variations in northern Chile. Lithos 179, 211–230.

Rossel, P., Oliveros, V., Ducea, M.N., Hernandez, L., 2015. Across and along arc geochemical variations in altered volcanic rocks: Evidence from mineral chemistry of Jurassic lavas in northern Chile, and tectonic implications. Lithos 239. doi:10.1016/j.lithos.2015.10.002

Salazar, E., Coloma, F., 2016. Geología del área Cerros de Cantaritos-Laguna Chica, Región de Atacama. Servicio Nacional de Geología y Minería, Carta Geológica de Chile, Serie Geología Básica 181. doi:10.13140/RG.2.2.30000.56327

Salazar, E., Coloma, F., Creixell, C., 2013. Geología del Área El Tránsito-Lagunillas, Servicio Nacional de Geología y Minería-Gobierno Regional de Atacama. 1 Mapa escala 1:100.000. Santiago 1–113.

Salazar, E., Vásquez, P., Vallejos, D., Creixell, C., Oliveros, V., Ducea, M.N. 2019. Stratigraphic and provenance analysis of Triassic units between 28-29°S, northern Chile: implications on the tectonic and paleogeographic evolution of the southwestern margin of Gondwana. Andean Geology, in press

Sato, A.M., Llambias, E.J., Basei, M.A.S., Castro, C.E., 2015. Three stages in the Late Paleozoic to Triassic magmatism of southwestern Gondwana, and the relationships with the volcanogenic events in coeval basins. J. South Am. Earth Sci. 63, 48–69. doi:10.1016/j.jsames.2015.07.005

Scheuber, E., Bogdanic, T., Jensen, a., Reutter, K., 1994. Tectonic development of the north Chilean Andes in relation to plate convergence and magmatism since the Jurassic. Tectonics South. Cent. Andes 121–139. doi:10.1007/978-3-642-77353-2_9

Seton, M., Müller, R.D., Zahirovic, S., Gaina, C., Torsvik, T., Shephard, G., Talsma, A., Gurnis, M., Turner, M., Maus, S., Chandler, M., 2012. Global continental and ocean basin reconstructions since 200Ma. Earth-Science Rev. 113, 212–270. doi:10.1016/j.earscirev.2012.03.002

Shand, S.., 1943. Eruptive Rocks: their genesis, composition, and classification, with a chapter on meteorites. John Wiley Sons, Inc. 444 p.

Sommer, C.A., Barreto, C.J.S., Lafon, J. M., Fernandes de Lima, E., Alexandre, F.M., Chemale Jr., F., Koester, E., 2018. Pb isotope geochemistry and reappraisal of Sr-Nd isotopes of the Cerro Morado basic magmatism (Ischigualasto-Villa Union Triassic basin, NW Argentina): Implications for the mantle sources. Braz. J. of Geol. 48, 115-126.

Spalletti, L.A., Limarino, C.O., 2017. The Choiyoi magmatism in south western Gondwana : implications for the end-permian mass extinction - a review 44, 328–338. doi:10.5027/andgeoV44n3-a05

Spencer, C.J., Roberts, N.M.W., Santosh, M., 2017. Growth, destruction, and preservation of Earth's continental crust. Earth-Science Rev. 172, 87–106. doi:10.1016/j.earscirev.2017.07.013

Spikings, R., Reitsma, M.J., Boekhout, F., Miskovic, A., Ulianov, A., Chiaradia, M., Gerdes, A., Schaltegger, U., 2016. Characterisation of Triassic rifting in Peru and implications for the early disassembly of western Pangaea. Gondwana Res. 35, 124–143. doi:10.1016/j.gr.2016.02.008

Stern, C.R., 2004. Active Andean volcanism, its geologic and tectonic setting.pdf. Rev. Geológica Chile 31, 161–206.

Stern, R.J., Reagan, M., Ishizuka, O., Ohara, Y., Whattam, S., 2012. To understand subduction initiation, study forearc crust: To understand forearc crust, study ophiolites. Lithosphere 4,469–483. doi:10.1130/L183.1

Suarez, M., Bell, C.M., 1992. Triassic rift-related sedimentary basins in northern Chile (24°-29°S). J. South Am. Earth Sci. 6, 109–121. doi:10.1016/0895-9811(92)90001-F

Sun, S. -s., McDonough, W.F., 1989. Chemical and isotopic systematics of oceanic basalts: implications for mantle composition and processes. Geol. Soc. London, Spec. Publ. 42, 313–345. doi:10.1144/GSL.SP.1989.042.01.19

Thiele, R., Hervé, F., 1984. Tectonica de ante arco en los terrenos preandinos del norte chico, chile. Rev. Geol. Chile 61–75. doi:10.5027/andgeoV11n2-a06

Tomezzoli, R.N., 2009. The Apparent Polar Wander Path for South America during the Permian-Triassic. Gondwana Res. 15, 209–215. doi:10.1016/j.gr.2008.10.005

Tomlinson, A.J., Blanco, N., García, M., Baeza, L., Alcota, H., Ladino, M., Pérez de Arce, C., Fanning, C.M., Martin, M.W., 2012. Permian exhumation of metamorphic complexes in the Calama area: Evidence for flat-slab subduction in northern Chile during the San Rafael tectonic phase and origin of the Central Andean Gravity High. XIII Congreso Geologico Chileno, Antofagasta, Abstracts, 1, 209-211.

Tomlison, A.J., Cornejo, P., Mpodozis, C., 1999. Hoja Potrerillos, Región de Atacama. Servicio Nacional de Geología y Minería, Mapas Geológicos, 14.

Torsvik, T.H., Cocks, L.R.M., 2013. Gondwana from top to base in space and time. Gondwana Res. 24, 999–1030. doi:10.1016/j.gr.2013.06.012

Vásquez, P., Glodny, J., Franz, G., Frei, D., Romer, R.L., 2011. Early Mesozoic Plutonism of the Cordillera de la Costa (34°–37°S), Chile: Constraints on the Onset of the Andean Orogeny. J. Geol. 119, 159–184. doi:10.1086/658296

Vásquez, P., Glodny, J., Franz, G., Romer, R.L., Gerdes, A., 2009. Origin of fayalite granitoids: New insights from the Cobquecura Pluton, Chile, and its metapelitic xenoliths. Lithos 110, 181–198. doi:10.1016/j.lithos.2009.01.001

Walker, B.A., Bergantz, G.W., Otamendi, J.E., Ducea, M.N., Cristofolini, E.A., 2015. A MASH zone revealed: The mafic complex of the Sierra Valle Fértil. J. Petrol. 56, 1863–1896. doi:10.1093/petrology/egv057

Welkner, D., Arévalo, C., Godoy, E., 2006. Geología de la Carta Freirina-El Morado, Región de Atacama. Servicio Nacional de Geología y Minería, Carta Geológica de Chile, Serie Geología Básica, 100.

Willner, A.P., Gerdes, A., Massonne, H.J., 2008. History of crustal growth and recycling at the Pacific convergent margin of South America at latitudes 29°-36° S revealed by a U-Pb and Lu-Hf isotope study of detrital zircon from late Paleozoic accretionary systems. Chem. Geol. 253, 114–129. doi:10.1016/j.chemgeo.2008.04.016

Winchester, J.A., Floyd, P.A., 1977. Geochemical discrimination of different magma series and their differentiation products using immobile elements. Chem. Geol. 20, 325–343. doi:10.1016/0009-2541(77)90057-2

Whattam, S.A., and Stern, R.J., 2011, The 'subduction-initiation rule': A key for linking ophiolites, intra-oceanic forearcs and subduction initiation: Contrib. to Mineral. Petrol. 162, p. 1031–1045, doi:10.1007/s00410-011-0638-z.

White, W. 2015. Isotope Geochemistry. John Wiley & Sons, 478 p.

Wood, D.A., 1980. The application of a Th-Hf-Ta diagram to problems of tectonomagmatic classification and to establishing the nature of crustal contamination of basaltic lavas of the British Tertiary Volcanic Province. Earth Planet. Sci. Lett. 50, 11–30. doi:10.1016/0012-821X(80)90116-8

Young, A., Flament, N., Maloney, K., Williams, S., Matthews, K., Zahirovi, K., Müller, R.D., In press. Global kinematics of tectonic plates and subduction zones since the late Paleozoic Era. Geosci. Front. doi:10.1016/j.gsf.2018.05.011

Zandt, G., Gilbert, H., Owens, T.J., Ducea, M., Saleeby, J., Jones, C.H., 2004. Active foundering of a continental arc root beneath the southern Sierra Nevada in California. Nature 431, 41–46. doi:10.1038/nature02847

Zindler, A., Hart, S., 1986, Chemical geodynamics. Annu. Rev. Earth Planet. Sci 14, 493–571.

Zhang, S. H., Zhao, Y., Davis, G. A., Ye, H., Wu, F., 2014. Temporal and spatial variations of Mesozoic magmatism and deformation in the North China Craton: Implications for lithospheric thinning and decratonization. Earth-Sci Rev. 131, 49–87. doi: 10.1016/j.earscirev.2013.12.004

CAPÍTULO III: MAGMATISMO DEL TRIÁSICO INFERIOR - MEDIO

Manuscript title: The Triassic magmatism in southwestern Gondwana: an example of arc batholith construction in a retreating margin

Authors: Javiera González[1], Verónica Oliveros[1*], Friedrich Lucassen[2], Christian Creixell[3], Felipe Coloma[3], Ricardo Velásquez[3], Laura Hernández[4], Simone Kasemann[2]

[1] Departamento Ciencias de la Tierra, Universidad de Concepción, Casilla 160-C, Concepción, Chile.

[2] MARUM Center for Marine Environmental Sciences, University of Bremen, Leobener Strasse, D-28359, Bremen, Germany.

[3] Servicio Nacional de Geología y Minería, Avenida Santa María 0104, Santiago, Chile.

[4] Instituto de Geología Económica Aplicada, Universidad de Concepción, Casilla 160-C, Concepción, Chile.

Sent as: González, J.; Oliveros, V.; Lucassen, F.; Creixell, C.; Coloma, F.; Velásquez, R.; Hernández, L.; Kasemann, S. The Triassic magmatism in southwestern Gondwana: an example of arc batholith construction in a retreating margin to Contributions to Mineralogy and Petrology

Abstract

The Chollay and Piuquenes plutonic complexes represent important part of the magmatism generated during the Lower - Middle Triassic in the western margin of Gondwana. They are exposed in the Chilean Frontal Cordillera (28°30'S – 30°30'S) and were previously interpreted as an anorogenic, post-collisional magmatism, generated by crustal anatexis during a stage in which subduction along the margin western Gondwana would have ceased (Pre-Andean Cycle, Middle Permian – Upper Triassic). In this work a field geology, petrography, whole-rock geochemistry, and mineral chemistry characterization of both complexes is carried out to establish a geotectonic context for this magmatism. These complexes are composed of rocks with a wide compositional spectrum, ranging from diorites to syenogranites, with a predominance of monzogranites and granodiorites. They correspond to subalkaline, meta to peraluminous, calc-alkaline to alkaline-calcic rocks, with a ubiquitous enrichment in LILE respect to HFSE, depressions in Nb-Ta, Ti, Sr and P, and enrichments in Pb, characteristic of subduction-related magmatism. These rocks present relatively flat REE patterns (La_N/Yb_N: 3.40 – 13.78) and the crystallization pressures calculated by Al-in-Hbl barometer from samples of the Chollay Plutonic Complex (1.7 – 1.8 ± 0.6 kbar) suggest an epizonal emplacement. The isotopic composition (Sr-Nd-Pb) shows that the source of this magmatism requires the participation of a depleted mantle and not only the continental crust, discarding cortical anatexis as the main magma-generating process. This background allows us to propose that the southwestern margin of Gondwana was active, at least in this segment. These plutonic complexes were emplaced in an extensional context evidenced by the development of contemporaneous forearc and backarc basins, and the geochemical signals that allow us to evaluate a cortical decrease from the Carboniferous to the Jurassic. Therefore, this work allows us to characterize a silicic plutonism of exceptional volume generated in a retreating convergent margin and contrast it with the magmatism generated in advancing convergent margins.

Keywords: arc-magmatism; geochemistry; petrology; SW-Gondwana; Triassic

3.1 Introduction

Cordilleran-type batholiths are large composite intrusive bodies, made up of hundreds or even thousands of individual plutons that are commonly exposed in mountain ranges along plate margins (Schwartz et al., 2014). The study of exposed batholiths allows unravelling the magmatic processes that operate through the Earth's crust such as the generation, segregation, ascent, and emplacement of granitic magmas (eg. Petford et al., 2000), in addition to knowing their time scales and therefore understanding how the continental crust is being created. The batholiths exposed in the western margin of North and South America have been the focus of numerous studies (eg. Sierra Nevada Batholith, Coastal Batholith of Perú, Coast Range Batholith of Northern Chile, Patagonian Batholith) aiming to explain the origin of supra-subduction zone magmatism. Most of the batholiths that are well characterized by their calc-alkaline nature and the predominance of intermediate to felsic composition have been generated in advancing orogens, where the upper plate underwent extensive shortening and uplift (Cawood et al., 2009). In the case of the batholiths generated in retreating margins, where the velocity of plates convergence results in the ocean-ward retreat of the trench and subsequent extension or rifting of the upper plate, is scarce and limited (eg. Parada et al., 1991, 1999).

The geology of the Chilean Frontal Cordillera is dominated by a series of Lower Carboniferous – Upper Triassic, compositionally heterogeneous, batholiths (Montosa – El Potro, Chollay and Elqui-Limarí, Hervé et al., 2014) that crop out between 28°S and 31°S with a N-S to NNE-SSW orientation. These large magmatic bodies represent protracted magmatism developed along the southwestern margin of Gondwana during Pangea amalgamation (Hervé et al., 2014; Maksaev et al., 2014; Mpodozis and Kay, 1992; Nasi et al., 1985). According to the proposed tectonomagmatic evolution of the western margin of South America, these batholiths would have been generated in two stages: the Gondwanan Cycle (Carboniferous – Lower Permian) and the Pre-Andean Cycle (Middle Permian – Upper Triassic) (Oliveros et al., 2020), separated by the San Rafael Orogenic phase (~285 Ma, Sato et al., 2015). Gondwanan plutons have characteristics that are typical of arc magmatism created over an advancing margin

(del Rey et al., 2016; Mpodozis and Kay, 1992; Oliveros et al., 2020; Parada et al., 1999). On the other hand, the Pre-Andean plutons correspond to highly evolved and quite homogeneous calc-alkaline granites (Mpodozis and Kay, 1992) with local presence of A-type granites (Gana, 1991; Molina et al., 2020; Parada et al., 1991). The Pre-Andean magmatism has been interpreted, based on its elemental and isotopic geochemistry and petrography, as the result of an extensive crustal melting induced by stagnation of basaltic magmas at the base of the crust after subduction termination (Mpodozis and Kay, 1992).

Recent geotectonic models, however, suggest continuous subduction from the Carboniferous to the Jurassic as the most likely process to generate the Pre-Andean magmatic record (eg. Coloma et al., 2017; Espinoza et al., 2019; González et al., 2018; Oliveros et al., 2020) with changes in the deformation style of the upper crust from dominantly compressive in the Carboniferous – Early Permian to transtensional from the Middle Permian to the Jurassic, marking a transition from an advancing to retreating margin (Oliveros et al., 2020; Vásquez et al., 2011).

This work focuses on two plutonic complexes emplaced during the Lower - Middle Triassic, exposed in the Chilean Frontal Cordillera between 28°30'S and 30°20'S and which together define an extensive magmatic belt of more than 200 km long. The first of them corresponds to the Chollay Plutonic Complex (CPC), a set of Lower Triassic – Middle Triassic incrementally emplaced plutons, whose outcrops cover an area of ca. 2.100 km^2 and corresponds to the largest pre-Andean magmatic unit exposed in the north of Chile and Argentina. The CPC intrudes into Palaeozoic plutonic and metasedimentary units and presents a wide compositional variety, ranging from gabbros to granites, with monzogranites and granodiorites as the dominant lithologies (Coloma et al., 2017; Ortiz and Merino, 2015; Salazar et al., 2013; Salazar and Coloma, 2016). The second, corresponds to the Piuquenes Plutonic Complex (PPC) emplaced during the Middle Triassic, which outcrops to the south of CPC covering 310 km2 (29°50'S – 30°20'S). The PPC intrudes into Palaeozoic metamorphic and plutonic units and is mainly composed of monzogranites, but also granodiorites, tonalites, syenogranites and diorites are recognized (Murillo et al., 2017; Velásquez et al., 2021).

Both plutonic complexes were previously considered to be part of the proposed anorogenic pre-Andean magmatism (Mpodozis and Kay, 1992; Nasi et al., 1990; Parada, 1990).

We present new field and petrographic, mineral chemistry and whole-rock geochemical and isotopic (Sr, Nd and Pb) data of Pre-Andean magmatism to determine the sources of this magmatism and the petrogenetic processes that allowed the genesis of these large and high evolved plutonic complexes created in an extensional geotectonic context, at a particular moment in the history of Gondwana, since Pangea had completed its amalgamation and the supercontinent was in a quasi-static reference mode (Charrier et al., 2007; Vilas & Valencio, 1978) allowing us to characterize a batholith generated in a retreating margin. This work is based on the new cartography of the Chilean High Andes (28°30'S – 30°30'S) developed by the Chilean Geological and Mining Survey (SERNAGEOMIN) (Murillo et al., 2017; Ortiz and Merino, 2015; Salazar et al., 2013; Salazar and Coloma, 2016; Velásquez et al., 2021).

3.2 Geological setting

During Paleozoic times western margin of Gondwana recorded a collisional history characterized by the progressive accretion of large allochthonous terrains (Ramos et al., 1986). The last of these, Chilenia, accreted to the supercontinent in Devonian times (Willner et al., 2011) was followed by a passive tectonic regime (Charrier et al., 2007). Recently, Dahlquist et al. (2021) propose that calc-alkaline arc magmatism was reactivated from the Devonian onwards, at least between 34-35°. From Carboniferous to Late Triassic, magmatism produced by the subduction process was established in the belt that nowadays are Frontal Cordillera and Domeyko Cordillera (eg. Hervé et al., 2014; Mpodozis & Kay, 1992; Nasi et al., 1985) in a metasedimentary protocrust whose relicts could be founded in the phyllites and mica schists of El Cepo Metamorphic Complex.

The first major magmatic event in the Frontal Cordillera is El Volcán Granite (30°30'S, 333-330 Ma; Velásquez et al., 2021), which would mark the beginning of the subduction of the Gondwanian Tectonic Cycle. It precedes a period with extensive magmatism

during Upper Carboniferous-Lower Permian, represented in the Frontal Cordillera, mainly, by the Chanchoquín and Guanta Plutonic Complexes (Murillo et al., 2017; Ortiz and Merino, 2015; Salazar et al., 2013; Velásquez et al., 2021). They correspond to batholitic dimensions plutons with tonalitic and granodioritic compositions, emplaced in deep cortical levels under high stress conditions (Nasi et al., 1985), which has been recently ratified through geothermobarometric studies (Uribe et al., 2020) (Fig. 3.1). These complexes are generally exposed in the western sector of Frontal Cordillera and were tectonically deformed by the San Rafael Orogenic Phase, well recognized in Argentina (Kleiman and Japas, 2009; Sato et al., 2015) as well as in northern Chile (Tomlinson et al., 2012). Particularly, in the Frontal Cordillera, this compression is responsible for the deformation of the Cerro Agua Negra Formation, which is subsequently covered by the Choiyoi Group (Heredia et al., 2002).

After this compressional stage, a subsiding tectonic event developed regionally related to progressive crustal thinning during Middle-Upper Permian, deforming Lower-Middle Permian volcanic rocks (Laguna Chica Formation, e.g., Salazar & Coloma, 2016) and probably controlling the deposition of Middle-Upper Permian volcanosedimentary El Tapado Formation (30° - 30°30'S, Velásquez et al., 2021). This unit is considered as the Chilean Choiyoi upper section. The extensional system continues and contributes to the development of an intra-arc basin, located in the border with Argentina, whose fill is represented by the Guanaco Sonso Formation (Lopingian – Middle Triassic), and fore-arc basins in the Cordillera de la Costa represented by San Félix and Canto del Agua formations (Salazar et al., 2020). In addition, the presence of back-arc basins in Argentina (Cuyo-Ischigualasto) constitutes another solid evidence of the tectonic system prevailing at that time. Contemporaneous with the formation of these extensional systems, the Chollay Plutonic Complex (248-237 Ma; Ortiz & Merino, 2015; Salazar et al., 2013; Salazar & Coloma, 2016) was emplaced to the east of Carboniferous-Permian complexes, bounded to the west by a sinistral shear zone recorded in the El Portillo Mylonites (Murillo et al., 2013), whose formation is contemporaneous with the emplacement of the Chollay Plutonic Complex.

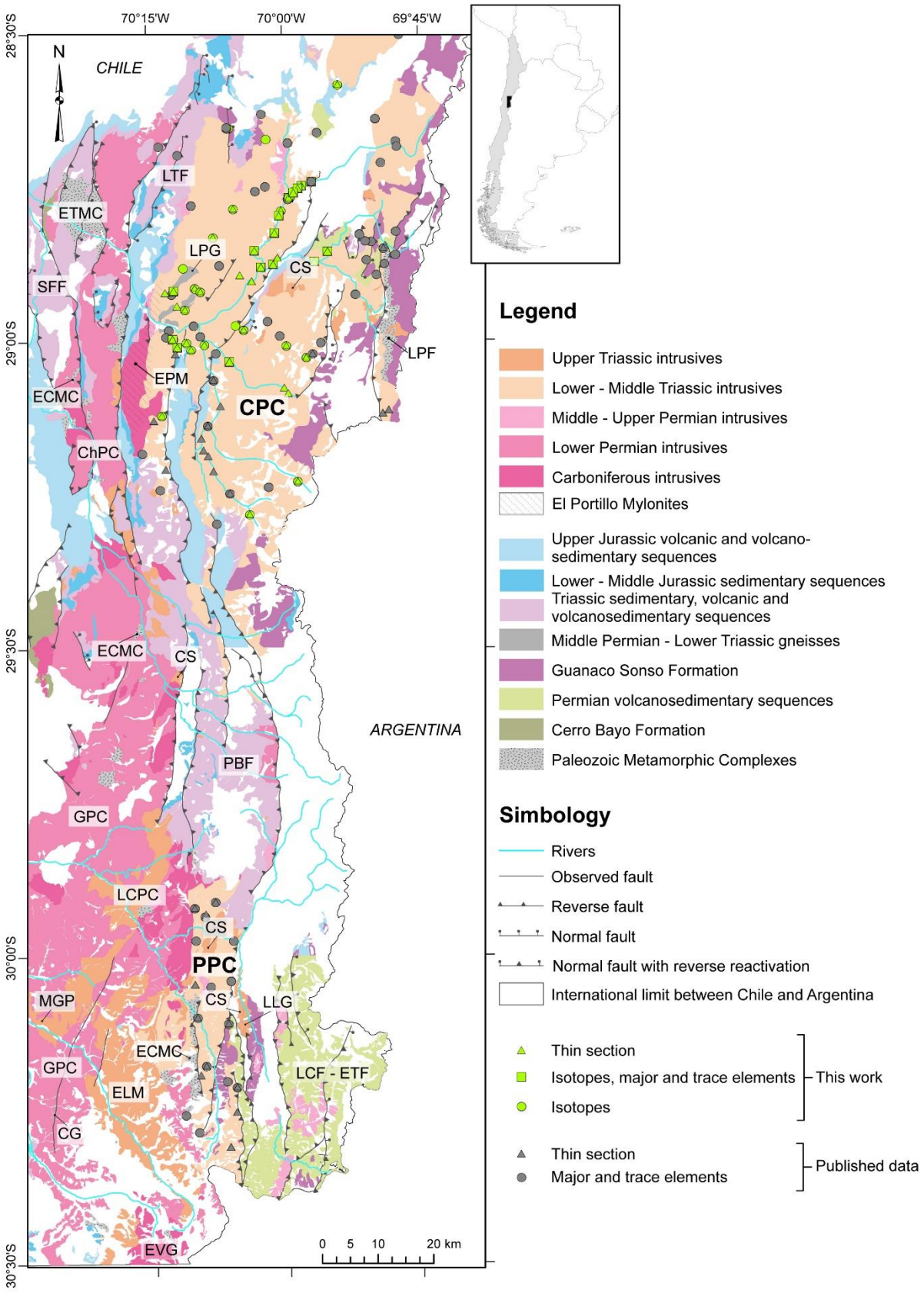
70°15'W
70°00'W
69°45'W
28°30'S
29°00'S
29°30'S
30°00'S
30°30'S
N
CHILE
ARGENTINA
LTF
ETMC
LPG
CS
SFF
LPF
EPM
ECMC
CPC
ChPC
ECMC
CS
PBF
GPC
LCPC
CS
PPC
CS
LLG
MGP
ECMC
GPC
LCF - ETF
ELM
CG
EVG
0 5 10 20 km
Legend
Upper Triassic intrusives
Lower - Middle Triassic intrusives
Middle - Upper Permian intrusives
Lower Permian intrusives
Carboniferous intrusives
El Portillo Mylonites
Upper Jurassic volcanic and volcano-sedimentary sequences
Lower - Middle Jurassic sedimentary sequences
Triassic sedimentary, volcanic and volcanosedimentary sequences
Middle Permian - Lower Triassic gneisses
Guanaco Sonso Formation
Permian volcanosedimentary sequences
Cerro Bayo Formation
Paleozoic Metamorphic Complexes
Simbology
Rivers
Observed fault
Reverse fault
Normal fault
Normal fault with reverse reactivation
International limit between Chile and Argentina
Thin section
Isotopes, major and trace elements
Isotopes
This work
Thin section
Major and trace elements
Published data

Figure 3.1. Simplified geological map showing the pre-Cretaceous units exposed at Chilean Frontal Cordillera between 28°30'S and 30°30'S. Based on updated geological cartography carried out by the Chilean Geology and Mining Survey (Murillo et al., 2017; Ortiz and Merino, 2015; Salazar et al., 2013; Salazar and Coloma, 2016; Velásquez et al., 2021). ETMC: El Transito Metamorphic Complex; ECMC: El Cepo Metamorphic Complex; LPF: Las Placetas Formation; EVG: El Volcán Granite; LCF: Laguna Chica Formation; ETF: El Tapado Formation; GPC: Guanta Plutonic Complex; ChPC: Chancoquín Plutonic Complex; ELM: El León Monzogranites; LPG: La Pampa Gneisses; **CPC**: Chollay Plutonic Complex; CG: Chacayal Gneisses; **PPC**: Piuquenes Plutonic Complex; LCPC: Los Carricitos Plutonic Complex; MGG: Monte Grande Granite; CS: Colorado Syenogranites; LLG: La Laguna Gabbros; SFF: San Félix Formation; PBF: Pastos Blancos Formation; LTF: La Totora Formation.

Moreover, this complex contains Permian gneisses megaxenoliths (Ribba, 1985; Salazar et al., 2013), with a metamorphism peak at ca. 268 Ma (Álvarez et al., 2013). South of 29°50'S, outcrops the Piuquenes Plutonic Complex (247-235 Ma; Velásquez et al., 2021), which together with the Chollay Plutonic Complex constitute a magmatic belt more than 200 km long, dominated by granites, which would be related to a more horizontal position of the slab and high heat flows in the asthenospheric wedge, resulting from changes in the convergence velocity between South America and Panthalassa, which produced crustal melting and granitic magmatism at the western edge of Gondwana (Riel et al., 2018). However, isotopic studies suggest that the Upper Permian-Triassic magmas were originated from mantle sources (Hervé et al., 2014), consistent with extensional tectonic conditions.

During Carnian-Norian subduction processes develops a magmatism, consistent with a crust of normal thickness (González et al., 2018). The volcanic part corresponds to the Pastos Blancos Formation, while its hypabyssal equivalents are the Colorado Syenogranites. At the same time, El León Monzogranite (224-220 Ma), Los Carricitos Plutonic Complex (ca. 217 Ma), La Laguna Gabbros (ca. 218 – 215 Ma) and Monte Grande Granite (219-214 Ma) were emplaced (Velásquez et al., 2021). The latter was emplaced in shallow crustal levels and show characteristics of hypersolvus peralkaline granites, consistent to A-type granites (Molina et al., 2020). Younger Triassic volcanic rocks are represented by basalts and andesites of the La Totora Formation (Norian) and by pyroclastic rocks intercalated in fossiliferous sediments of the Las Breas Formation (Upper Triassic-Lower Jurassic). After Norian (ca. 212 Ma), magmatism migrated at least 50 kms trenchward, settling in the present-day Coastal Cordillera, where relicts remain in Altos de Talinay Plutonic Complex (Coloma et al., 2020).

3.3 Sampling and analytical methods

We collected samples from Chollay and Piuquenes Plutonic Complexes for petrographic studies. The samples from CPC were also analyzed for whole-rock Sr-Nd-Pb isotopes as well as major and trace elements, and mineral chemistry. The details of each of the analyzes can be found in Supplementary materials (Appendix 3.A).

3.4 Results

Within the Chollay Plutonic Complex four strips with NNE-SSW orientation are recognized, distinguishable from each other in terms of their field characteristics, lithologies and radiometric ages (Fig. 3.2.a). The first strip (242-238 Ma), located on the western edge of the complex is bounded on the west by contemporaneous mylonites (El Portillo) and by the east by La Plata Fault, and is characterized by having elongated xenoliths with NE-SW direction up to 5 km long. These xenoliths correspond to large bodies of Permian mica-rich gneisses (La Pampa Gneiss) that show extensive evidence of migmatization attributed to high-grade thermal metamorphism (Álvarez et al. 2013) and are in gradational or net contact with tonalites and granodiorites of the CPC (Fig. 3.3.a). The xenoliths present a subvertical geometry and are intercalated with subvertical plutons of the complex, defining an incremental antitaxial growth for this area (sensu Bartley et al., 2006). In compositional terms this strip includes monzogranites, granodiorites, tonalites and quartziferous diorites. Locally foliated tonalites are observed, rich in dioritic enclaves (Fig. 3.3.b). The second strip, defined by the older ages of the complex (249-244 Ma), is located between the La Plata and Valeriano faults and is characterized by presenting bodies of different lithologies (diorites, granodiorites, tonalites and monzogranites) in subvertical contacts (Fig. 3.3.c). This geometry allows defining an incremental syntaxial growth for this strip of the complex. In this strip, areas rich in dioritic enclaves are also recognized within the monzogranites (Fig. 3.3.d) and areas in which mafic dikes with straight walls and dioritic compositions are recognized, cutting out granodiorites and monzogranites (Fig. 3.3.e). Mingling zones are also observed between monzogranites and tonalites in this strip (Fig. 3.3.f). The third strip, located between the Valeriano Fault and La Coipa-El Potro Fault, is characterized by being a compositionally homogeneous section dominated by

monzogranites with subordinated granodioritic, tonalitic and quartziferous monzodioritic bodies (241-233 Ma). In the western sector of this strip, mafic dikes are recognized cutting monzogranites (Fig. 3.3.g) and in some areas of this strip, it is possible to recognize the intrusion relationship of the plutons with the volcanosedimentary sequences of Laguna Chica Formation, where a low angle tabular geometry is observed suggesting the plutonic ceiling (Fig. 3.3.h). The last strip (245-241 Ma) dominated by monzogranites and tonalites, borders to the east with Guanaco Sonso Formation and presents a geometry like that observed in the third strip. Locally, a normal fault contact with contemporary volcanic rocks of the Guanaco Sonso Formation is observed and the intrusion of the complex in the Las Placetas Formation is also recognized, as a plutonic ceiling, evidencing that towards the east the complex presents shallower emplacement levels.

Within the Piuquenes Plutonic Complex it is possible to recognize two domains with different field characteristics, separated by the Ingaguás Fault (Fig. 3.2.b). The western domain is composed mainly of coarse-grained monzogranites that present abundant megaxenoliths of Carboniferous intrusives as well as metasedimentary rocks of the Lower Ordovician – Carboniferous (El Cepo Metamorphic Complex) (Fig. 3.3.i). This domain is intruded by several Upper Triassic stocks (Colorado Syenogranites). To the east, the Ingaguás Fault rides the El Cepo Metamorphic Complex over the eastern domain of the Piuquenes Plutonic Complex. This second domain is composed of monzogranites, granodioritic plutons of subhorizontal floors, syenogranites of similar geometry and small dioritic stocks of irregular shapes interpreted as part of the same system emplaced during the Middle Triassic (Velásquez et al., 2021). This domain is intruded, in turn, by the Elqui Dike Swarm (Creixell et al., 2009). In the southernmost zone of this domain, the contact of this complex with contemporaneous volcanic rocks of the Guanaco Sonso Formation, is observed. This unit are also in tectonic contact through the southern extension of the Baños del Toro Fault System (Velásquez et al., 2021) (Fig. 3.3.j).

3.4.1 Petrography

A total of seventy-eight thin sections were described to carry out the petrographic characterization of the Chollay and Piuquenes plutonic complexes. Detailed results of this one, can be found in the Table 3.1.

The predominant lithologies within the Chollay Plutonic Complex correspond to monzogranites and granodiorites, although there are also tonalitic, monzodioritic and dioritic bodies (Fig. 3.4.h). Monzogranites and granodiorites are present in all strips; while the tonalites are found in the first, second and third strips, the monzodiorites are found in the third strip and the diorites are exposed only in the first and second ones.

The monzogranites are hololeucocratic to leucocratic, coarse to medium grained rocks and are mainly composed of anhedral quartz, euhedral to subhedral occasionally zoned plagioclase, anhedral crystals of orthoclase with perthitic texture and subhedral to euhedral biotite (0.1 – 6.1%) (Fig. 3.4.a). Some described monzogranites also present amphibole (0.8 – 2.8%) and others, muscovite (0.1 – 2.5%). Accessory minerals correspond to Fe-Ti oxides, and locally to titanite and apatite. The granodiorites are hololeucocratic to leucocratic and medium grained, composed of anhedral quartz, subhedral to euhedral plagioclase, anhedral orthoclase with perthitic texture or microcline and euhedral biotite (1.5 – 11%) (Fig. 3.4.b). Some granodiorites also contain amphibole (1.2 – 10.6%) or muscovite (0.2 – 3.4%). Fe-Ti oxides, apatite, titanite and zircon has been recognized as accessory phases. The tonalites are hololeucocratic to leucocratic and medium grained rocks, with anhedral quartz, subhedral to euhedral plagioclase, euhedral to subhedral biotite (6.9 – 19.6%) and little or no anhedral orthoclase with perthitic texture. Amphibole (0.4 – 15.1%) is present in most of tonalites (Fig. 3.4.c) and the accessory minerals corresponds to Fe-Ti oxides, zircon, titanite and apatite. The diorites and quartz diorites are leucocratic to mesocratic, medium grained rocks with euhedral plagioclase (42.2 – 90.9%), anhedral quartz (0 -11.3%), amphibole (0 – 31.8%), biotite (0 -16.5%) and Fe-Ti oxide as accessory mineral. Some diorites have clinopyroxene (3.5 – 14.2%) and orthopyroxene (3.6 – 26,2%) (Fig. 3.4.d) with or without biotite. In addition, a monzonite has been described, which corresponds to a hololeucocratic, fine to coarse grained rock, with

subhedral plagioclase, anhedral microcline, minor anhedral quartz, subhedral muscovite and Fe-Ti oxides. The quartz monzodiorites are hololeucocratic to leucocratic medium to coarse grained rocks, with anhedral quartz, euhedral to subhedral plagioclase occasionally zoned, anhedral orthoclase with perthitic texture, euhedral clinopyroxene, subhedral amphibole, subhedral to euhedral biotite, and apatite, subhedral titanite and Fe-Ti oxides as accessory minerals.

Two mafic dikes and one enclave were petrographically classified as diorites and quartz-diorite, respectively. The dikes are fine to medium grained and are composed by euhedral plagioclase, clinopyroxene and indeterminate mafic mineral, Fe-Ti oxides and anhedral titanite. The enclave is fine to medium grained and have poikilitic texture where plagioclase, amphibole and biotite crystals are included in large orthoclase and quartz ones (Fig. 3.4.e). The accessory minerals correspond to Fe-Ti oxides and anhedral titanite.

As in the Chollay Plutonic Complex, in the Piuquenes Plutonic Complex the monzogranites correspond to the dominant lithology, although granodiorites, syenogranite, tonalite and quartz syenite are also recognized. The monzogranites are hololeucocratic to leucocratic and mainly medium to coarse grained rocks composed by anhedral quartz, orthoclase with pertitic texture, subhedral plagioclase, subhedral to euhedral biotite (<1 - 8%), accompanied by titanite, sphene and apatite as accessory phases. The granodiorites are hololeucocratic to leucocratic and medium-grained rocks. They are composed of euhedral of plagioclase, anhedral orthoclase, and quartz, scant or absent subhedral biotite and opaque minerals (0.5 – 2.4%). The syenogranite is hololeucocratic and fine to medium grained rock with anhedral quartz and orthoclase, anhedral to subhedral plagioclase and euhedral to subhedral biotite (1.6%). The tonalite is medium-grained rock, leucocratic, with euhedral plagioclase, anhedral quartz and orthoclase, and euhedral biotite. The quartz syenite is hololeucocratic and medium to coarse grained rock, with anhedral orthoclase and quartz, subhedral plagioclase, and subhedral biotite (4,7%).

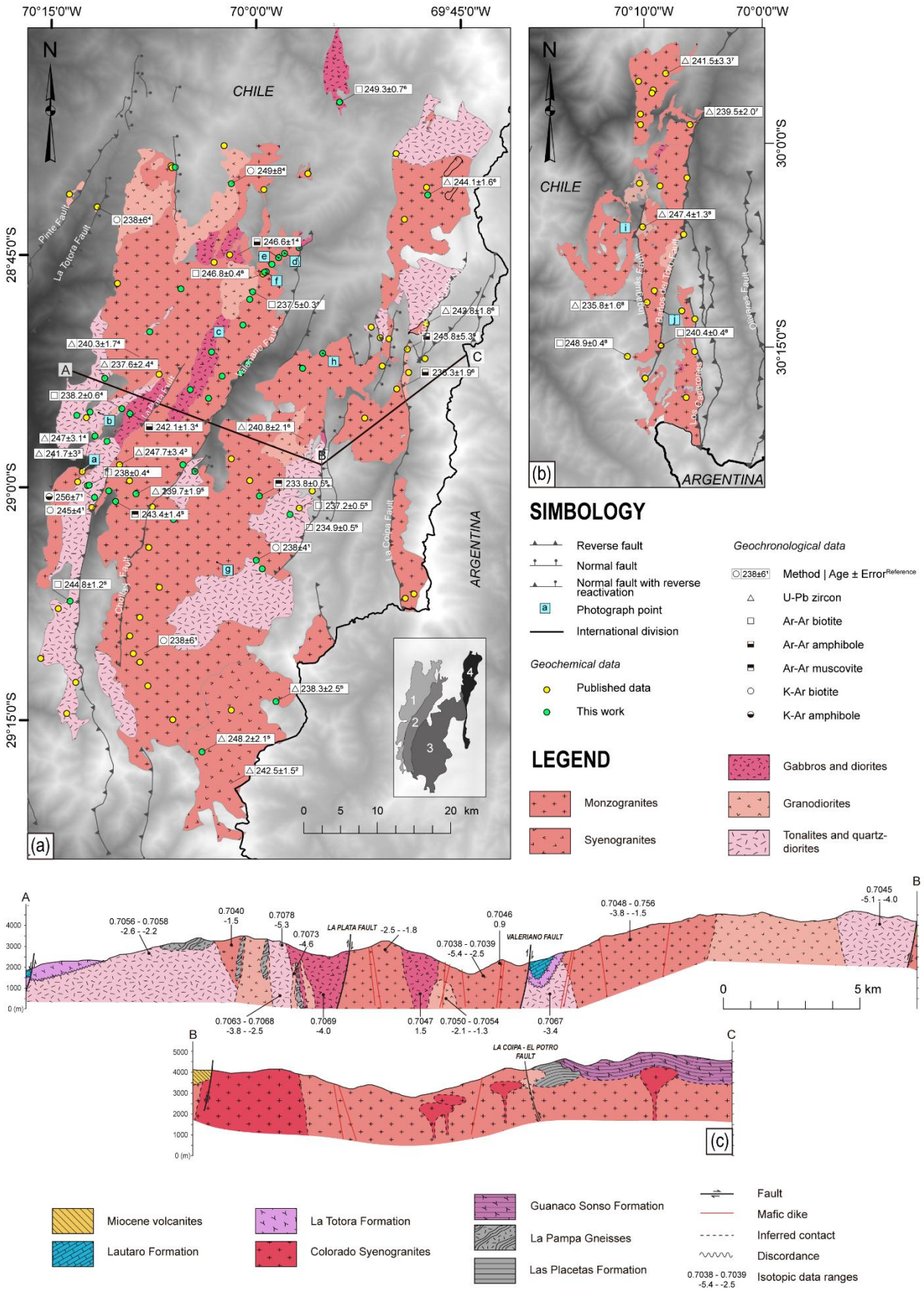
70°15'0"W
70°0'0"W
69°45'0"W
28°45'0"S
29°0'0"S
29°15'0"S
N
CHILE
ARGENTINA
Pinte Fault
La Totora Fault
Culqui Fault
La Coipa Fault
Talacaspio Fault
249.3±0.7⁶
249±8⁴
238±6⁴
244.1±1.6⁶
246.6±1⁴
246.8±0.4⁶
237.5±0.3⁷
243.8±1.6⁶
243.8±5.3⁶
240.3±1.7⁴
237.6±2.4⁴
238.3±1.9⁶
238.2±0.6⁴
242.1±1.3⁴
240.8±2.1⁶
247±3.1⁴
241.7±3³
247.7±3.4³
238±0.4⁴
239.7±1.9⁵
233.8±0.5⁵
256±7¹
245±4¹
243.4±1.4⁵
237.2±0.5⁵
234.9±0.5⁵
238±4¹
244.8±1.2⁵
238±6¹
238.3±2.5⁵
248.2±2.1⁵
242.5±1.5²
0 5 10 20 km
(a)
70°10'0"W
70°0'0"W
30°0'0"S
30°15'0"S
241.5±3.3⁷
239.5±2.0⁷
247.4±1.3⁸
235.8±1.6⁸
248.9±0.4⁸
240.4±0.4⁸
Infiernillos Fault
Portillos del Tigre Fault
La Cortadera Fault
Olivares Fault
(b)
ARGENTINA
SIMBOLOGY
Reverse fault
Normal fault
Normal fault with reverse reactivation
Photograph point
International division
Geochemical data
Published data
This work
Geochronological data
Method | Age ± Error Reference
U-Pb zircon
Ar-Ar biotite
Ar-Ar amphibole
Ar-Ar muscovite
K-Ar biotite
K-Ar amphibole
LEGEND
Monzogranites
Syenogranites
Gabbros and diorites
Granodiorites
Tonalites and quartz-diorites
A
B
C
0.7056 - 0.7058
-2.6 - -2.2
0.7040
-1.5
0.7078
-5.3
0.7073
-4.6
LA PLATA FAULT
-2.5 - -1.8
0.7046
0.9
VALERIANO FAULT
0.7038 - 0.7039
-5.4 - -2.5
0.7048 - 0.756
-3.8 - -1.5
0.7045
-5.1 - -4.0
0.7063 - 0.7068
-3.8 - -2.5
0.7069
-4.0
0.7047
1.5
0.7050 - 0.7054
-2.1 - -1.3
0.7067
-3.4
0 5 km
LA COIPA - EL POTRO FAULT
(c)
Miocene volcanites
Lautaro Formation
La Totora Formation
Colorado Syenogranites
Guanaco Sonso Formation
La Pampa Gneisses
Las Placetas Formation
Fault
Mafic dike
Inferred contact
Discordance
Isotopic data ranges

Figure 3.2. (a) Distribution map of the lithological associations present in the Chollay Plutonic Complex (Ortiz & Merino, 2015; Salazar et al., 2013; Salazar & Coloma, 2016). The samples of this work, used for geochemical analysis, are indicated with green circles and samples with published geochemical data, by yellow circles. The location of the photographs that make up figure 3.3 is also indicated. (b) Distribution map of the lithological associations present in the Piuquenes Plutonic Complex (Murillo et al., 2017; Velásquez et al., 2021). (c) Schematic profile showing the internal relationships between the different lithological associations present in the Chollay Plutonic Complex. Representative $^{87}Sr/^{86}Sr_{initial}$ ratios and the $\varepsilon Nd_{initial}$ values are included for the different bodies. See profile location in (a). The geochronological data reported for the Chollay and Piuquenes plutonic complexes are included (1: Nasi et al., 1985; 2: Martin et al., 1999; 3: Álvarez et al., 2013; 4: Salazar et al., 2013; 5: Ortiz & Merino, 2015; 6: Salazar & Coloma, 2016; 7: Murillo et al., 2017; 8: Velásquez et al., 2021).


La Pampa Gneisses
Chollay Plutonic Complex
(a)
(b)
SSE
NNW
Monzogranites
Chollay Plutonic Complex
Diorites
Chollay Plutonic Complex
(c)
(d)
(e)
(f)
SSE
NNW
(g)
NW
SE
(h)
SE
NW
Carboniferous Intrusives
Piuquenes Plutonic Complex
Colorado Syenogranites (Upper Triassic)
El Cepo Metamorphic Complex
(i)
S
N
Piuquenes Plutonic Complex
Guanaco Sonso Formation
Baños del Toro Fault
(j)

Figure 3.3. Field characteristics of Chollay and Piuquenes Plutonic Complexes. (a) Gneisses xenolith present in granodiorites of CPC, on the south bank of the El Tránsito River. These xenoliths, up to five km long, are exposed within the CPC only west of the La Plata Fault and in the vicinity of the El Tránsito River. (b) Amphibole and biotite tonalite of CPC with magmatic foliation and abundant dioritic enclaves that follow the foliation in Sierra El Dadín. (c) Subvertical contact between diorites and monzogranites of CPC. (d) Dioritic enclaves with amphibole and biotite, present in granodiorites of the CPC. They are scarce, from centimeter to decimeter sizes, and their edges are generally net. (e) Straight-walled subvertical mafic dikes with aphanitic edges and porphyry centres that intrude monzogranites from the CPC. (f) Mingling zone recognized in the Valeriano River between monzogranites and tonalites of CPC. (g) Swarm of mafic subvertical dikes and net contacts, intruding monzogranites of the CPC in the Pachuy River. (h) Monzogranite of CPC intruding to tuff of the Laguna Chica Formation (Artinskian-Wordian) in the Laguna Chica River. The same relationship is observed with Guanaco Sonso Formation to the east. (i) Megaxenoliths of Carboniferous Intrusives and Lower Ordovician – Carboniferous metamorphic rocks in Piuquenes Plutonic Complex. (j) Tectonic contact between Piuquenes Plutonic Complex and Guanaco Sonso Formation through Baños del Toro Fault.

The alteration degree of the samples is very variable and can reach up to 69% of the total volume of the rock, but most of them (~85%) contain up to 25% of alteration minerals (for specific proportions see Table 3.1). Among the most common alteration minerals within the samples studied is sericite replacing plagioclase to different degrees and occasionally as a replacement for orthoclase; clays replace feldspars with different intensities; chlorite is found replacing the biotite, amphibole and pyroxene, and in some samples filling veinlets and spaces; epidote is part of the alteration of biotite and plagioclase, in most cases locally; calcite is a less frequent alteration mineral than the previous ones and is replacing locally plagioclase, amphibole and filling veinlets and amygdales; Fe-Ti oxides are associated in some samples to biotite alteration.

3.4.2 Whole-rock geochemistry

Nineteen samples of Chollay Plutonic Complex were analysed for major and trace elements. They correspond to diorites, tonalites, granodiorites and monzogranites, microdioritic and tonalitic enclaves and microdioritic dikes. Results are listed in Table 3.2 and in Fig. 3.5, 3.6, 3.7 and 3.8. In these figures, the previously published geochemical data of the Chollay and Piuquenes plutonic complexes (Murillo et al., 2017; Ortiz and Merino, 2015; Salazar et al., 2013; Salazar and Coloma, 2016; Velásquez et al., 2021) have been added. These samples and sixteen samples provided by the (SERNAGEOMIN), which already had analysis of major elements and trace, were analyzed by TIMS to obtain whole-rock Sr, Nd and Pb isotope ratios.

3.4.2.1 Major elements

Most of the analysed samples have low loss on ignition (LOI) values, ranging from 0.38 to 2.55 wt. % and only a few, which correspond to mafic dikes have slightly higher values (4.08 – 6.56 wt. %). The major-element oxide concentrations have been recalculated to 100% on an anhydrous basis and the Fe_2O_3 and FeO abundances are expressed as $Fe_2O_{3(T)}$.

The SiO_2 content of the analysed samples varies continuously between 49.45 wt. % and 77.92 wt. % and have total alkali contents between 3.04 wt. % and 8.78 wt. % (Fig. 3.5). The TiO_2 (0.09 – 1.80 wt. %), Al_2O_3 (12.35 – 21.07 wt. %), Fe_2O_3 (0.60 – 11.60 wt. %), MnO (0.02 – 0.20 wt. %), CaO (0.29 – 10.15 wt. %) contents decrease with SiO_2 increasing, associated with the crystallization of ferromagnesian minerals. The P_2O_5 (0.01 – 0.54 wt. %) concentrations also decrease as the rocks are more differentiated, but this is evident from SiO_2 contents of ca. 65 wt. %, probably controlled by the initiation of apatite crystallization. On the contrary, the K_2O (0.21 – 4.91 wt. %) and Na_2O (2.83 – 5.24 wt. %) contents increase as the concentration of SiO_2 is higher, although it is less evident in the case of Na_2O which shows a greater dispersion. The variations observed in the analyzed samples generally coincide with the behavior of the published samples.

When comparing the data of both plutonic complexes, no great differences are observed in most of major elements, except for the Fe and Mg content, which is slightly higher in the PPC compared to the CPC.

The samples CPV-16-435 and CPV-16-436 (enclaves) are outside the trend lines described above for MgO, P_2O_5 and Na_2O. Although these samples are spatially and temporally related to the Chollay Plutonic Complex, their major elements suggest that the magmas that give rise to these enclaves would not have been generated from the same magma as the rest of the complex.

In the total alkali vs. silica diagram (Fig. 3.6.a), the studied samples follow a trend of subalkaline evolution in agreement with the already published samples of Chollay and

Piuquenes plutonic complexes, except for the microdioritic enclaves (CPV-16-435 and CPV-16-436) and mafic dikes (CPV-16-475 and CPV-16-444), which are found in the alkaline field. Most of the subalkaline samples fall in the calc-alkaline field of the AFM diagram, except for the diorite CPV-16-450 (Fig. 3.6.b). The analyzed samples of the Plutonic Chollay Complex are found preferentially in the calcic and calc-alkalic fields in the Na_2O+K_2O-CaO vs SiO_2 diagram and published samples of this complex and Piuquenes Plutonic Complex are found in the calc-alkalic and alkali-calcic fields (Fig. 3.6.c). The analysed rocks of the Chollay Plutonic Complex are mainly metaluminous and to a lesser extent peraluminous (Fig. 3.6.d) contrary to the published samples of the complex, which are mainly peraluminous. The peraluminous samples correspond to those with higher SiO_2 (> 64 wt. %). In the case of Piuquenes Plutonic Complex, the published samples correspond only to peraluminous rocks. Following to Frost & Frost (2008), the analyzed samples are mainly magnesian (Fig. 3.6.e) and have #Mg between 0.08 and 0.43, and the range of the published samples of Chollay Plutonic Complex corresponds to 0 – 0,52. In the case of Piuquenes Plutonic Complex, the #Mg is in the range between 0 and 0,62, but the values are preferably less than 0,24.

Table 3.1. Mineralogy and classification of the studied samples as determined through petrographic analysis with modal count. Their mineralogy is expressed as volume percentage of the total rock (Qz: quartz; Pl: plagioclase; Or: orthoclase; Mi: microcline; Opx: orthopyroxene; Cpx: clynopiroxene; Amp: amphibole; Bt: biotite; Ms: muscovite; Ap: apatite; Zrn: zircon; Tit: titanite; Op: opaque minerals; Ind: indeterminate minerals). The alteration minerals observed in the thin sections are also listed (Ser: sericite; Cly: clays; Chl: chlorite; Ep: epidote; Ms: muscovite; Op: opaque minerals; Bt: biotite; Id: iddingsite; Amp: amphibole; Srp: serpentinite). F: fine; M: medium and C: coarse.

Unit	Sample	Petrographic classification	Grain size	Location (m)		Mineralogy																	
				East	North	Qz	Pl	Or	Mi	Opx	Cpx	Amp	Bt	Ms	Ser	Zrn	Tit	Op	Ind	Total	Q	A	P
Chollay Plutonic Complex	CCL-3	Quartz monzodiorite	F-M	412200	6837700	9,3	51,8	11,5	0,0	0,0	19,3	0,2	6,7	0,0	0,0	0,0	0,0	1,2	0,0	100	13	16	71
	CCL-54	Monzogranite	C	403452	6817371	37,1	26,7	30,8	0,0	0,0	0,0	0,0	4,9	0,0	0,1	0,0	0,0	0,4	0,0	100	39	33	28
	CCL-56	Quartz diorite	F-M	403680	6817427	6,7	51,7	0,0	0,0	0,0	0,0	31,8	9,7	0,0	0,0	0,0	0,1	<0.1	0,0	100	11	0	89
	CCL-65	Granodiorite	M-C	420520	6808320	31,0	42,3	17,4	0,0	0,0	0,0	2,6	5,6	0,0	0,1	0,0	0,2	0,6	0,0	99,8	34	19	47
	CPV-16-430	Tonalite	M	382619	6791765	26,5	60,0	0,0	0,0	0,0	0,0	0,0	12,8	0,0	0,0	0,1	0,0	0,6	0,0	100	31	0	69
	CPV-16-431	Granodiorite	M	383436	6790344	34,5	43,2	14,4	0,0	0,0	0,0	0,0	4,5	3,4	0,0	0,0	0,0	<0.1	0,0	100	37	16	47
	CPV-16-434	Tonalite	C	401711	6814136	28,0	57,0	0,0	0,0	0,0	0,0	0,4	13,4	0,0	0,0	0,0	0,0	1,2	0,0	100	33	0	67
	CPV-16-438	Tonalite	M	403468	6817376	23,2	62,7	2,8	0,0	0,0	0,0	0,0	10,3	0,0	0,1	0,0	0,0	0,9	0,0	100	26	3	71
	CPV-16-440	Granodiorite	M	405755	6819577	24,8	56,0	9,1	0,0	0,0	0,0	1,2	7,5	0,0	0,0	0,0	0,0	1,4	0,0	100	28	10	62
	CPV-16-441	Quartz diorite	F-M	405755	6819577	12,4	64,0	6,1	0,0	0,0	0,0	10,4	3,7	0,0	0,0	0,0	0,1	3,3	0,0	100	15	7	78
	CPV-16-442	Quartz diorite	M	407524	6820292	5,5	66,1	0,0	0,0	0,0	0,0	16,8	10,1	0,0	0,0	0,0	0,0	1,5	0,0	100	8	0	92
	CPV-16-443	Diorite	F	405089	6819087	6,0	50,0	0,0	0,0	0,0	0,0	42,0	0,0	0,0	0,0	0,0	1,0	1,0	0,0	100	11	0	89
	CPV-16-444	Diorite	F-M	404308	6818317	0,0	52,1	0,0	0,0	0,0	18,8	0,0	0,0	0,0	0,0	0,0	0,0	11,2	17,9	100	0	0	100
	CPV-16-449	Monzogranite	C	400921	6811025	41,7	25,7	30,7	0,0	0,0	0,0	0,0	1,1	0,1	0,0	0,0	0,0	0,7	0,0	100	43	31	26
	CPV-16-450	Diorite	M	397259	6807776	0,0	73,7	0,0	0,0	7,9	14,2	0,0	0,0	0,0	0,0	0,0	0,0	4,2	0,0	100	0	0	100
	CPV-16-456	Monzogranite	F-M	381227	6800191	47,0	25,0	23,5	0,0	0,0	0,0	0,0	4,0	0,1	0,0	0,0	0,0	0,4	0,0	100	49	25	26
	CPV-16-457	Tonalite	M	382776	6800498	13,5	51,4	0,0	0,0	0,0	0,0	15,1	19,6	0,0	0,2	0,0	0,0	0,2	0,0	100	21	0	79
	CPV-16-460	Granodiorite	M	383387	6797771	47,1	37,3	8,4	0,0	0,0	0,0	0,0	3,8	3,4	0,0	0,0	0,0	0,0		100	51	9	40
	CPV-16-474	Granodiorite	M-C	398494	6804836	29,9	47,2	18,6	0,0	0,0	0,0	0,0	3,1	0,0	0,0	0,0	<0.1	1,2	0,0	100	31	19	49
	CPV-16-475	Diorite	F	398494	6804836	0,0	48,7	0,0	0,0	0,0	0,0	0,0	0,0	0,0	0,0	0,0	6,3	0,0	45,0	100	0	0	100
	CPV-18-502	Monzogranite	C	400693	6805332	40,8	32,4	24,0	0,0	0,0	0,0	0,0	0,1	2,5	0,0	0,0	0,0	0,2	0,0	100	42	25	33
	CPV-18-503	Monzogranite	C-M	401500	6806550	27,9	29,0	40,6	0,0	0,0	0,0	0,0	0,0	0,0	0,0	0,0	0,0	0,9	1,6	100	29	42	30
	CPV-18-504	Monzogranite	C-M	408084	6805916	40,5	30,6	26,2	0,0	0,0	0,0	0,0	2,7	0,0	0,0	0,0	0,0	0,0	0,0	100	42	27	31
	CPV-18-505	Granodiorite	M	410431	6807739	35,3	39,6	17,7	0,0	0,0	0,0	1,5	4,2	0,2	0,0	0,1	0,0	1,3	0,0	99,9	38	19	43
	CPV-18-507	Diorite	M	394712	6803396	0,3	60,1	0,0	0,0	26,2	12,1	0,0	1,2	0,0	0,0	0,0	0,0	0,1	0,0	100	0	0	100
	CPV-18-508	Diorite	M	394712	6803396	0,0	90,9	0,0	0,0	3,6	3,5	0,0	1,3	0,0	0,0	0,0	0,0	0,7	0,0	100	0	0	100
	CPV-18-509	Tonalite	F	394712	6803396	19,3	67,0	0,0	0,0	0,0	0,0	0,0	13,7	0,0	0,0	0,0	0,0	0,0	0,0	100	22	0	78

	CPV-18-510	Monzogranite	M-C	396871	6802316	30,1	36,0	24,5	0,0	0,0	0,0	1,8	5,7	0,0	0,0	0,0	0,9	1,0	0,0	100	33	27	40
	CPV-18-514	Quartz monzodiorite	M	403470	6782185	18,3	61,1	15,0	0,0	0,0	0,4	0,0	4,4	0,0	0,0	0,0	0,1	0,7	0,0	100	19	16	65
	CPV-18-515	Granodiorite	M	402752	6783120	42,3	38,8	16,8	0,0	0,0	0,0	0,0	1,5	0,0	0,0	0,0	0,0	0,6	0,0	100	43	17	40
	CPV-18-516	Granodiorite	M-C	392827	6787785	30,1	49,7	16,6	0,0	0,0	0,0	0,0	2,7	0,0	0,0	0,0	0,0	0,9	0,0	100	31	17	52
	CT-154	Tonalite	M-C	402037	6814985	31,7	57,0	0,7	0,0	0,0	0,0	0,0	9,2	0,0	0,3	0,1	0,1	0,9	0,0	100	35	1	64
	CT-161	Monzogranite	M-C	393442	6815293	39,6	33,7	21,2	0,0	0,0	0,0	0,0	3,1	1,8	0,0	0,0	0,0	0,6	0,0	100	42	22	36
	CT-164	Quartz diorite	M	389794	6810101	11,3	57,0	0,0	0,0	0,0	0,0	21,9	7,6	0,0	0,0	0,0	0,0	2,2	0,0	100	17	0	83
	CT-191	Tonalite	F-M	386550	6800942	28,5	47,3	0,0	0,0	0,0	0,0	0,9	23,3	0,0	0,0	0,0	0,0	<0.1	0,0	100	38	0	62
	CT-193	Quartz diorite	M-C	387560	6800338	10,0	42,2	0,0	0,0	0,0	0,0	30,1	16,5	0,0	0,0	0,0	0,0	0,0	0,0	98,8	19	0	81
	CT-250	Granodiorite	F-M	384825	6797022	38,5	47,0	5,6	0,0	0,0	0,0	0,0	6,9	2,0	0,0	0,0	0,0	0,0	0,0	100	42	6	52
	CT-300	Granodiorite	M	395358	6793507	18,2	49,4	8,6	0,0	0,0	0,0	10,6	11,0	0,0	0,3	0,2	0,0	1,7	0,0	100	24	11	65
	MCM-007	Monzogranite	F-C	392973	6763993	32,4	35,6	30,5	0,0	0,0	0,0	0,0	1,0	0,0	0,0	0,0	0,0	0,2	0,3	100	33	31	36
	MCM-008	Monzogranite	M	389019	6770826	33,6	29,2	36,0	0,0	0,0	0,0	0,0	1,0	0,0	0,0	0,0	0,0	0,2	0,0	100	34	36	30
	MCM-013	Monzogranite	M	391224	6779786	38,4	24,9	34,4	0,0	0,0	0,0	0,0	2,2	0,0	0,0	0,0	0,0	0,1	0,0	100	39	35	25
	MCM-015	Granodiorite	M-C	388913	6776146	31,3	43,7	18,8	0,0	0,0	0,0	0,0	5,1	0,0	0,0	0,0	0,1	1,0	0,0	100	33	20	47
	MCM-016	Granodiorite	M-C	387797	6773940	32,4	41,5	19,5	0,0	0,0	0,0	0,0	5,2	0,0	0,0	0,0	0,0	0,8	0,6	100	35	21	44
	MCM-017	Monzogranite	M-C	388200	6771834	44,3	32,5	22,6	0,0	0,0	0,0	0,0	0,2	0,0	0,0	0,0	0,0	0,1	0,3	100	45	23	33
	MCM-018	Monzogranite	M-C	389978	6768002	29,4	32,1	35,7	0,0	0,0	0,0	0,0	2,6	0,0	0,0	0,0	0,0	0,2	0,0	100	30	37	33
	MCM-022	Granodiorite	F-C	396485	6760228	31,7	42,6	20,7	0,0	0,0	0,0	0,0	4,6	0,0	0,0	0,0	0,0	0,4	0,0	100	33	22	45
	MCM-027	Monzogranite	M	405192	6766258	41,1	10,8	47,2	0,0	0,0	0,0	0,0	0,7	0,1	0,0	0,0	0,0	0,1	0,0	100	41	48	11
	MCM-179	Quartz monzodiorite	C	389932	6784402	5,7	62,5	31,8	0,0	0,0	0,0	0,0	0,0	0,0	0,0	0,0	0,0	0,0	0,0	100	6	32	63
	MCM-253	Monzonite	F-C	385924	6789866	2,6	54,1	0,0	40,1	0,0	0,0	0,0	0,0	2,9	0,0	0,0	0,0	0,3	0,0	100	3	41	56
	MCM-265	Monzogranite	M-C	388323	6790790	33,8	29,8	32,8	0,0	0,0	0,0	0,0	3,2	0,0	0,0	0,0	0,2	0,2	0,0	100	35	34	31
	RCM-039	Monzogranite	M	403058	6790695	32,6	37,7	26,8	0,0	0,0	0,0	0,0	2,1	0,4	0,0	0,0	0,0	0,4	0,0	100	34	28	39
	RCM-040	Monzogranite	F-M	406713	6788541	42,9	32,7	18,3	0,0	0,0	0,0	0,0	6,1	0,0	0,0	0,0	0,0	0,0	0,0	100	46	19	35
	RCM-052	Tonalite	M	407797	6789227	27,6	59,5	1,4	0,0	0,0	0,0	1,9	6,9	0,0	0,1	0,1	0,9	1,6	0,0	100	31	2	67
	RCM-115	Granodiorite	F-M	380639	6777958	27,2	54,8	8,8	0,0	0,0	0,0	0,0	8,7	0,0	0,0	0,0	0,0	0,5	0,0	100	30	10	60
	RCM-117	Granodiorite	M-F	385052	6791122	38,8	42,2	0,0	17,6	0,0	0,0	0,0	0,0	0,2	0,0	0,0	0,0	0,4	0,8	100	39	18	43
	RCM-118	Tonalite	M-C	383105	6789164	19,9	65,1	0,0	0,0	0,0	0,0	1,4	11,3	0,0	0,0	0,1	0,7	1,5	0,0	100	23	0	77
	RCM-120	Tonalite	M	379244	6777118	25,4	64,5	0,0	0,0	0,0	0,0	0,0	9,2	0,0	0,0	0,1	0,1	0,7	0,0	100	28	0	72
	RCM-202	Monzogranite	M-F	381418	6768307	22,5	48,5	25,5	0,0	0,0	0,0	0,8	1,9	0,0	0,0	0,0	0,0	0,8	0,0	100	23	26	50
	RCM-258	Monzogranite	M	420485	6778681	26,4	34,9	30,1	0,0	0,0	0,0	2,8	5,4	0,0	0,0	0,0	0,0	0,4	0,0	100	29	33	38
	SCL-75	Granodiorite	F-M	422822	6826703	31,8	44,8	19,3	0,0	0,0	0,0	0,0	3,9	0,0	0,0	0,0	0,0	0,2	0,0	100	33	20	47
Piuquenes Pluton	GUR-141	Monzogranite	F-M	388634	6688212	35,6	29,1	31,4	0,0	0,0	0,0	0,0	2,2	1,5	0,0	0,0	0,0	0,2	0,0	100	37	33	30
	GUR-142	Monzogranite	F	388478	6687704	42,5	19,4	28,7	0,0	0,0	0,0	0,0	8,0	0,0	0,0	0,0	0,0	0,9	0,5	100	47	32	21
	GUR-143	Monzogranite	M	386586	6689225	26,6	28,0	39,6	0,0	0,0	0,0	0,0	5,2	0,0	0,0	0,0	0,0	0,1	0,4	100	28	42	30
	GUM-19	Monzogranite	C	393633	6683439	54,2	21,6	17,4	0,0	0,0	0,0	0,0	3,5	0,0	0,0	0,0	0,1	0,0	3,2	100	58	19	23
	PRV-043	Monzogranite	M-C	387789	6659249	35,5	27,2	31,3	0,0	0,0	0,0	0,0	4,5	0,0	0,0	0,0	0,0	0,2	1,4	100	38	33	29
	PRV-044	Monzogranite	M-C	388773	6660831	32,0	23,1	39,8	0,0	0,0	0,0	0,0	3,7	0,0	0,0	0,0	0,1	0,3	1,0	100	34	42	24

	PRV-046	Tonalite	M	387204	6669527	39,0	52,5	1,0	0,0	0,0	0,0	0,0	7,2	0,0	0,0	0,0	0,0	0,3	0,0	100	42	1	57
	PRV-049	Monzogranite	M-C	389580	6675115	41,9	24,8	29,1	0,0	0,0	0,0	0,0	1,5	0,0	0,0	0,0	0,0	0,5	2,2	100	44	30	26
	PRV-050	Monzogranite	M	386728	6675553	31,2	26,5	35,3	0,0	0,0	0,0	0,0	4,2	0,0	0,0	0,0	0,0	0,4	2,5	100	34	38	28
	PRV-079	Monzogranite	M-C	388832	6645395	37,2	28,8	27,8	0,0	0,0	0,0	0,0	5,0	0,0	0,0	0,0	0,0	1,1	0,1	100	40	30	31
	PRV-081	Granodiorite	F-M	387539	6648878	39,5	40,7	13,7	0,0	0,0	0,0	0,0	0,0	3,0	0,0	0,0	0,0	0,5	2,6	100	42	15	43
	PRV-085	Syenogranite	F-M	389721	6653326	48,8	10,0	33,1	0,0	0,0	0,0	0,0	1,6	0,0	0,0	0,0	0,0	0,6	5,9	100	53	36	11
	PFC-069	Monzogranite	F-M	392743	6668453	46,5	31,6	21,0	0,0	0,0	0,0	0,0	0,0	0,0	0,0	0,0	0,0	0,2	0,7	100	47	21	32
	PFC-073	Granodiorite	M	394289	6652612	32,0	43,0	21,0	0,0	0,0	0,0	0,0	3,3	0,0	0,0	0,0	0,1	0,7	0,0	100	33	22	45
	PFC-125	Quartz syenite	M-C	393171	6676178	17,7	23,5	53,7	0,0	0,0	0,0	0,0	4,7	0,0	0,0	0,0	0,0	0,4	0,0	100	19	57	25
	PFC-136	Monzogranite	M	394148	6654723	33,7	24,4	35,6	0,0	0,0	0,0	0,0	1,6	0,0	0,0	0,0	0,0	0,7	4,1	100	36	38	26
	PIM-43	Monzogranite	M	394302	6656987	31,1	36,8	27,5	0,0	0,0	0,0	0,0	3,7	0,0	0,0	0,0	0,0	0,8	0,0	100	33	29	39
	PIM-54	Granodiorite	M	393160	6646344	36,7	45,0	15,2	0,0	0,0	0,0	0,0	0,0	0,0	0,0	0,0	0,0	2,4	0,7	100	38	16	46

Table 3.1 continued.

Unit	Sample	Alteration Minerals													
		Ser	Cly	Chl	Ep	Ms	Op	Bt	Ind	Cc	Id	Qz	Amp	Srp	Total
Chollay Plutonic Complex	CCL-3	0,3	0,0	2,0	0,0	0,0	0,0	0,0	0,0	0,0	0,6	0,0	0,5	0,0	3,4
	CCL-54	2,5	7,0	1,5	0,0	0,0	0,0	0,0	0,0	0,0	0,0	0,0	0,0	0,0	11,0
	CCL-56	10,3	2,5	14,4	0,2	0,0	0,0	0,0	0,0	0,0	0,0	0,0	0,0	0,0	27,4
	CCL-65	0,0	0,0	0,0	0,0	0,0	0,0	0,0	0,0	0,0	0,0	0,0	0,0	0,0	0,0
	CPV-16-430	3,0	1,2	0,3	0,0	0,1	0,0	0,0	0,1	0,0	0,0	0,0	0,0	0,0	4,7
	CPV-16-431	0,0	5,7	0,2	0,0	0,0	0,0	0,0	0,0	0,0	0,0	0,0	0,0	0,0	5,9
	CPV-16-434	1,7	4,6	0,3	0,1	0,0	0,0	0,0	0,0	0,0	0,0	0,0	0,0	0,0	6,7
	CPV-16-438	3,1	0,1	2,0	0,1	0,0	0,0	0,0	0,0	0,0	0,0	0,0	0,0	0,0	5,3
	CPV-16-440	2,8	15,7	0,7	0,1	0,0	0,0	0,1	0,0	0,0	0,0	0,0	0,0	0,0	19,4
	CPV-16-441	3,2	6,4	4,7	0,2	0,0	0,0	0,0	0,0	0,0	0,0	0,0	0,0	0,0	14,5
	CPV-16-442	3,3	0,0	10,5	0,2	0,0	0,3	1,6	0,0	0,3	0,0	0,0	0,0	0,0	16,2
	CPV-16-443	0,0	0,0	0,0	0,0	0,0	0,0	0,0	0,0	0,0	0,0	0,0	0,0	0,0	0,0
	CPV-16-444	10,4	0,0	17,0	0,0	0,0	0,0	0,0	0,2	0,9	0,0	0,0	0,0	0,0	28,5
	CPV-16-449	0,5	24,0	0,0	0,0	0,1	0,0	0,0	0,0	0,0	0,0	0,0	0,0	0,0	24,6
	CPV-16-450	1,5	0,0	1,0	0,0	0,0	0,0	0,0	0,0	0,0	0,0	0,0	0,0	0,0	2,5
	CPV-16-456	1,3	0,7	0,0	0,0	0,0	0,0	0,0	0,0	0,0	0,0	0,0	0,0	0,0	2,0
	CPV-16-457	7,7	0,0	1,9	0,2	0,2	0,0	0,0	0,0	0,0	0,0	0,0	0,0	0,0	10,0
	CPV-16-460	9,3	3,4	1,5	0,0	0,0	0,0	0,0	0,0	0,0	0,0	0,0	0,0	0,0	14,2
	CPV-16-474	4,7	22,1	1,5	0,5	0,0	0,0	0,0	0,0	0,0	0,0	0,0	0,0	0,0	28,8
	CPV-16-475	0,0	18,4	45,0	0,0	0,0	0,0	0,0	0,0	5,6	0,0	0,0	0,0	0,0	69,0
	CPV-18-502	2,6	11,3	0,0	0,0	0,1	0,0	0,0	0,0	6,0	0,0	0,0	0,0	0,0	20,0
	CPV-18-503	1,5	31,9	0,0	0,3	0,0	0,0	0,0	0,0	0,0	0,0	0,0	0,0	0,0	33,7
	CPV-18-504	1,5	22,3	0,9	0,1	0,1	0,1	0,0	0,0	0,0	0,0	0,0	0,0	0,0	25,0
	CPV-18-505	0,0	0,0	0,0	0,0	0,0	0,0	0,0	0,0	0,0	0,0	0,0	0,0	0,0	0,0
	CPV-18-507	0,0	0,0	10,0	0,0	0,0	3,0	0,0	0,0	0,0	0,0	0,0	0,0	10,5	23,5
	CPV-18-508	7,3	0,0	0,0	0,0	0,0	0,0	0,0	0,0	0,0	0,0	0,0	0,0	3,6	10,9
	CPV-18-509	0,4	20,1	8,2	0,0	0,0	0,0	0,0	0,0	0,0	0,0	0,0	0,0	0,0	28,7
	CPV-18-510	0,0	0,0	0,0	0,0	0,0	0,0	0,0	0,0	0,0	0,0	0,0	0,0	0,0	0,0
	CPV-18-514	1,2	6,9	0,0	0,0	0,0	0,0	0,0	0,0	0,0	0,0	0,0	0,0	0,0	8,1
	CPV-18-515	0,4	13,1	1,3	0,0	0,0	0,1	0,0	0,0	0,0	0,0	0,0	0,0	0,0	14,9
	CPV-18-516	7,5	5,0	1,4	0,1	0,3	0,0	0,0	0,0	0,0	0,0	0,0	0,0	0,0	14,3
	CT-154	0,0	2,9	0,5	0,0	0,0	0,0	0,0	0,0	0,0	0,0	0,0	0,0	0,0	3,4
	CT-161	1,7	10,9	1,5	0,3	0,0	0,0	0,0	0,0	0,0	0,0	0,0	0,0	0,0	14,4
	CT-164	22,0	0,0	11,9	0,9	0,0	0,0	0,0	0,0	0,0	0,0	0,0	0,0	0,0	34,8
	CT-191	11,8	0,0	1,4	0,5	0,0	0,0	0,0	0,0	0,0	0,0	0,0	0,0	0,0	13,7

	CT-193	0,0	0,0	0,0	0,0	0,0	0,0	0,0	0,0	0,0	0,0	0,0	0,0	0,0	0,0
	CT-250	0,0	11,7	2,0	0,5	0,0	0,0	0,0	0,0	0,0	0,0	0,0	0,0	0,0	14,2
	CT-300	2,5	0,4	3,8	0,0	0,0	0,0	0,0	0,0	0,0	0,0	0,0	0,0	0,0	6,7
	MCM-007	3,1	9,9	0,8	0,0	0,9	0,0	0,0	0,0	0,0	0,0	0,0	0,0	0,0	14,7
	MCM-008	3,3	1,5	0,4	0,0	1,0	0,0	0,0	0,1	0,0	0,0	0,0	0,0	0,0	6,3
	MCM-013	2,0	1,7	0,6	0,5	0,0	0,0	0,0	0,0	0,0	0,0	0,0	0,0	0,0	4,8
	MCM-015	4,4	0,9	1,0	0,0	0,0	0,0	0,0	0,0	0,0	0,0	0,0	0,0	0,0	6,3
	MCM-016	5,0	3,6	5,0	0,5	0,0	0,0	0,0	0,0	0,0	0,0	0,0	0,0	0,0	14,1
	MCM-017	0,0	5,0	<0.1	1,0	0,0	0,0	0,0	0,0	0,0	0,0	0,0	0,0	0,0	6,0
	MCM-018	1,6	5,3	1,3	0,1	0,5	0,1	0,0	0,0	0,0	0,0	0,0	0,0	0,0	8,9
	MCM-022	12,8	7,4	3,7	0,2	0,0	0,2	0,0	0,0	0,0	0,0	0,0	0,0	0,0	24,3
	MCM-027	1,0	17,5	0,0	0,2	0,1	<0.1	0,0	0,0	0,0	0,0	0,0	0,0	0,0	18,8
	MCM-179	2,5	8,9	6,6	12,4	0,0	1,0	0,0	0,0	0,0	0,0	0,0	0,0	0,0	31,4
	MCM-253	2,6	2,6	0,0	0,0	0,0	0,0	0,0	0,0	16,9	0,0	0,0	0,0	0,0	22,1
	MCM-265	8,9	4,0	1,3	0,2	0,0	0,0	0,0	0,0	0,3	0,0	0,0	0,0	0,0	14,7
	RCM-039	3,8	4,6	1,9	0,1	0,0	0,0	0,0	0,0	0,0	0,0	0,0	0,0	0,0	10,4
	RCM-040	1,6	2,5	0,6	<0.1	0,0	0,0	6,0	0,0	0,0	0,0	0,0	0,0	0,0	10,7
	RCM-052	5,9	2,9	3,2	0,0	0,0	0,0	0,0	0,0	0,0	0,0	0,0	0,0	0,0	6,1
	RCM-115	16,4	0,4	0,9	0,2	0,1	0,0	0,0	0,0	0,0	0,0	0,0	0,0	0,0	18,0
	RCM-117	1,8	3,0	0,0	0,0	0,0	0,4	0,0	0,0	0,4	0,0	0,0	0,0	0,0	5,6
	RCM-118	1,3	5,3	7,6	0,6	0,0	0,0	0,0	0,0	0,0	0,0	0,0	0,0	0,0	14,8
	RCM-120	12,4	0,0	0,5	0,1	0,0	0,0	0,0	0,0	0,0	0,0	0,0	0,0	0,0	13,0
	RCM-202	4,8	27,0	2,4	0,2	0,0	0,0	0,0	0,0	0,0	0,0	0,0	0,0	0,0	34,4
	RCM-258	12,2	16,7	3,5	0,5	0,0	0,0	0,0	0,0	0,0	0,0	0,0	0,0	0,0	32,9
	SCL-75	13,4	18,0	3,1	0,6	0,0	0,0	0,0	0,0	0,0	0,0	0,0	0,0	0,0	35,1
Piuquenes Plutonic Complex	GUR-141	3,5	6,3	0,6	0,0	2,0	0,0	0,0	0,0	0,0	0,0	0,0	0,0	0,0	12,4
	GUR-142	2,3	6,6	3,2	3,0	2,0	0,0	0,0	0,0	0,0	0,0	0,0	0,0	0,0	17,1
	GUR-143	2,8	11,5	5,0	3,4	0,0	0,0	0,0	0,0	0,0	0,0	0,0	0,0	0,0	22,7
	GUM-19	3,2	3,0	6,4	3,0	0,0	0,0	0,0	0,0	0,0	0,0	13,0	0,0	0,0	28,6
	PRV-043	2,7	12,7	3,3	0,5	0,0	0,0	0,0	0,0	0,0	0,0	0,0	0,0	0,0	19,2
	PRV-044	2,3	10,9	0,6	0,5	0,5	0,0	0,0	0,0	0,0	0,0	0,0	0,0	0,0	14,8
	PRV-046	3,5	2,6	0,5	0,5	0,0	0,0	0,0	0,0	0,0	0,0	0,0	0,0	0,0	7,1
	PRV-049	2,5	11,7	0,7	0,0	0,5	0,0	0,0	0,0	1,0	0,0	0,0	0,0	0,0	16,4
	PRV-050	2,1	2,4	1,3	0,5	0,5	0,0	0,0	0,0	0,0	0,0	0,0	0,0	0,0	6,8
	PRV-079	2,3	9,9	2,5	2,9	0,0	0,0	0,0	0,0	0,0	0,0	0,0	0,0	0,0	17,6
	PRV-081	6,1	11,5	0,0	0,0	2,0	0,0	0,0	0,0	0,0	0,0	0,0	0,0	0,0	19,6
	PRV-085	0,9	5,5	0,0	0,0	0,0	0,0	0,0	0,0	0,0	0,0	0,0	0,0	0,0	6,4
	PFC-069	0,0	4,0	0,0	0,0	0,0	0,0	0,0	0,0	0,0	0,0	0,0	0,0	0,0	4,0
	PFC-073	4,3	6,6	2,7	0,0	0,0	0,0	0,0	0,0	0,0	0,0	0,0	0,0	0,0	13,6
	PFC-125	2,1	5,1	1,4	0,0	0,0	0,0	5,0	0,0	0,0	0,0	0,0	0,0	0,0	13,6

	PFC-136	1,9	5,8	1,6	1,0	0,0	0,0	0,0	0,0	0,0	0,0	5,0	0,0	0,0	15,3
	PIM-43	3,7	13,3	1,6	0,0	0,0	0,0	0,0	0,0	0,0	0,0	0,0	0,0	0,0	18,6
	PIM-54	5,3	10,5	4,6	2,3	0,0	0,0	0,0	0,0	1,0	0,0	0,0	0,0	0,0	23,7

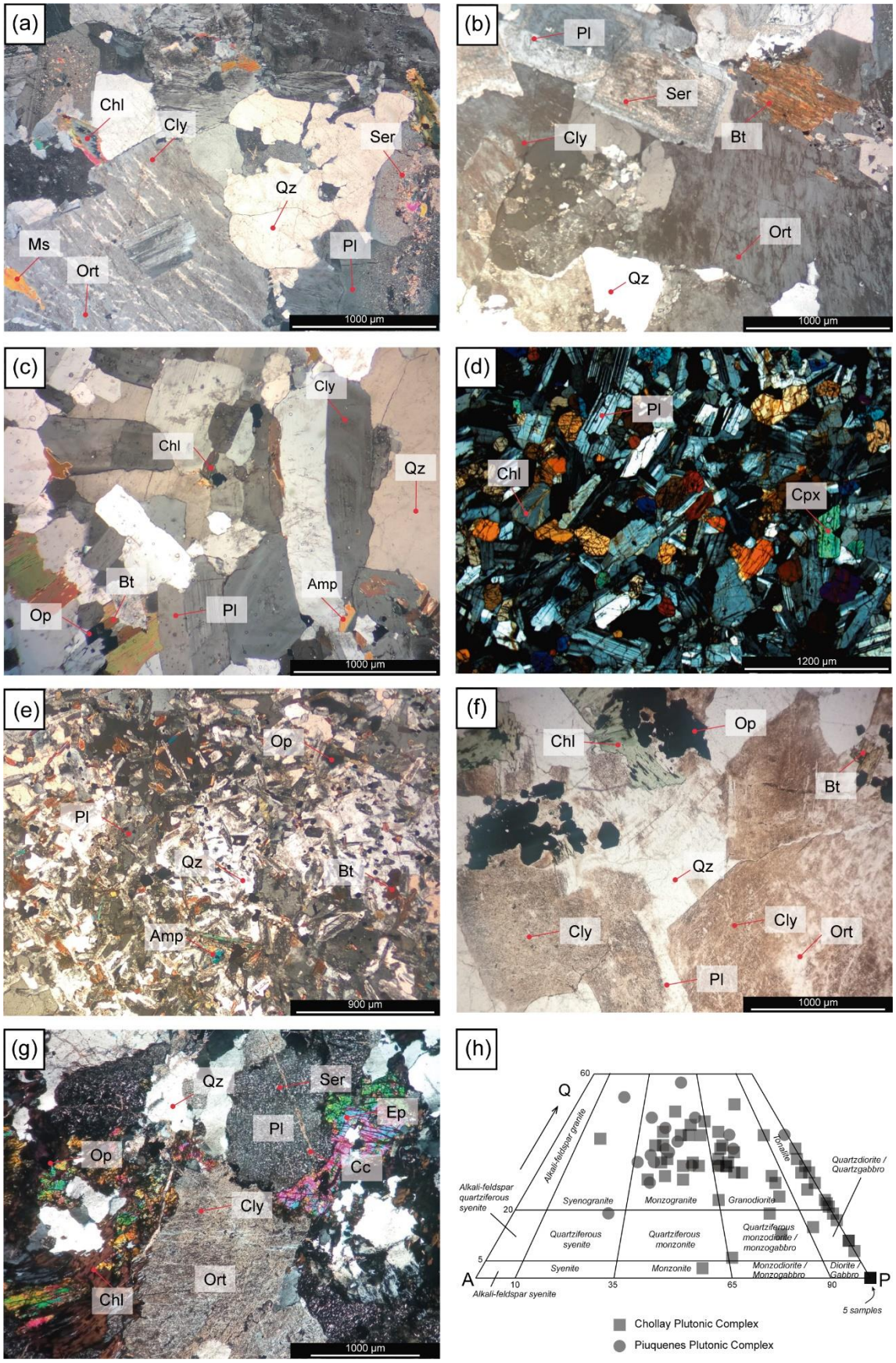
(a)
Chl
Cly
Ser
Qz
Ms
Ort
Pl
1000 µm
(b)
Pl
Ser
Cly
Bt
Ort
Qz
1000 µm
(c)
Cly
Chl
Qz
Bt
Op
Pl
Amp
1000 µm
(d)
Pl
Chl
Cpx
1200 µm
(e)
Op
Pl
Qz
Bt
Amp
900 µm
(f)
Chl
Op
Bt
Qz
Cly
Cly
Ort
Pl
1000 µm
(g)
Qz
Ser
Ep
Pl
Op
Cc
Cly
Ort
Chl
1000 µm
(h)
Q
60
20
5
A
10
35
65
90
P
Alkali-feldspar granite
Alkali-feldspar quartziferous syenite
Syenogranite
Monzogranite
Granodiorite
Tonalite
Quartzdiorite / Quartzgabbro
Quartziferous syenite
Quartziferous monzonite
Quartziferous monzodiorite / monzogabbro
Syenite
Monzonite
Monzodiorite / Monzogabbro
Diorite / Gabbro
Alkali-feldspar syenite
5 samples
Chollay Plutonic Complex
Piuquenes Plutonic Complex

Figure 3.4. Microphotographs of the Chollay Plutonic Complex (a – e) and Piuquenes Plutonic Complex (f - g) samples. (a) Inequigranular, hololeucocratic monzogranite with local perthitic texture (MCM-007). (b) Medium to coarse-grained hololeucocratic granodiorite with scarce biotite (~3%) partially replaced by chlorite, and moderate alteration of feldspars to clays (CPV-18-516). (c) Medium-grained biotite tonalite, with scarce amphibole (~2%) and low alteration degree (RCM-052). (d) Medium-grained pyroxene-bearing diorite (CPV-16-450). (e) Quartz microdiorite of poikilitic texture, with amphibole (10%) and biotite (4%), (CPV-16-441). (f) Inequigranular, hololeucocratic monzogranite with local perthitic texture. The feldspars show an incipient to moderate alteration to clays (PRV-049). (g) Inequigranular medium-grained granodiorite with a local perthitic texture. It is common to recognize epidote and chlorite as secondary mineralogy and small calcite-filled fractures (PIM-054) (h) Modal composition of CPC and PPC rocks in the QAP diagram (Streckeisen, 1976). Amp: amphibole; Bt: biotite; Chl: chlorite; Cly: clays; Cpx: clinopyroxene; Ms: muscovite; Op: opaque mineral; Ort: orthoclase; Pl: plagioclase; Qz: quartz; Ser: sericite; Ep: epidote; Cc: calcite.

3.4.2.2 Trace elements

The analyzed samples from Chollay Plutonic Complex show an enrichment in large ion lithophile elements (LILE) respect to high field strength elements (HFSE) compared to the primitive mantle (Fig. 3.7.a).

The Nb and Ta troughs are present in most of the samples, as well as the Pb enrichment and the depletions in Zr, P, and Ti are common. These patterns are the same as those recognized in the published samples of both plutonic complexes and are typical patterns of magmas generated in subduction zones (Stern, 2002; Wilson, 1989). The diorites (CPV-16-450 and CPV-16-442) have lower contents of LILE and HFSE compared to the tonalites, granodiorites and granites of the complex (Fig. 3.7.b). The mafic dikes (CPV-16-443, CPV-16-444 and CPV-16-475) present homogeneous patterns, with a slight enrichment in LILE with respect to HFSE, strong depressions in Nb-Ta and a notable enrichment in Pb (Fig. 3.7.c). The enclaves (CPV-16-429, CPV-16-441, CPV-16-435 and CPV-16-436) have a composition very similar to the mafic dikes, in terms of their trace elements, but the concentrations of Th, U and Zr are lower (Fig. 3.7.c).

Light rare earth elements (LREE) are enriched respect to the heavy rare earth elements (HREE) in the analyzed samples of Chollay Plutonic Complex (mean La_N/Yb_N = 6.97; La_N/Yb_N: 3.40 – 13.78), and present chondrite-normalized patterns characterized by a slight slope between La and Sm, flat patterns between Sm and Yb and poorly pronounced negative Eu anomalies in most of them (mean Eu/Eu*: 0.87; Eu/Eu*: 0.27 – 0.94). These patterns are also recognized in the already published samples of the

Chollay and Piuquenes plutonic complexes (Fig. 3.7.d). The tonalites, diorites and mafic dikes have slightly positive Eu anomalies with values of Eu/Eu* between 1.02 and 1.77 (Fig. 3.7.e and 3.7.f).

3.4.2.3 Sr, Nd and Pb isotopes

The initial isotopic ratios were calculated using the isotopic ratios measured with TIMS, the concentrations of Rb, Sr, Sm, Nd, U, Th and Pb determined by ICP-MS and the published ages of the Chollay Plutonic Complex. Only 11 of the 35 samples analyzed for isotopes have geochronological data; for the rest, the average of all the dating carried out within the complex was entered as age (Table 3.3). The initial $^{87}Sr/^{86}Sr$ ratios of most samples range between 0.7038 and 0.7078, and only six samples are found outside this range, some with low values, associated with high Rb/Sr ratios (CPV-16-502, CPV-16-504, CT-303, RCM-039 and MCM-027) or low Rb/Sr ratios (MCM-253) (Fig. 3.8.a). The initial $^{143}Nd/^{144}Nd$ ratios are between 0.512054 - 0.512419 and the calculated εNd_i, between -5.3 and +1.8, although most of them correspond to weakly negative values (Fig 3.8.a).

The initial $^{87}Sr/^{86}Sr$ ratios have a slight increase as the samples are more evolved, up to ca. 68% SiO_2 (Fig. 3.8.c). Then the data become more scattered, and even with a slight drop in values as the SiO_2 increases. The dikes and enclaves are overlap to the values obtained in the rock samples from the CPC. As for the initial εNd, the values show a high dispersion when contrasted with SiO_2 (Fig. 3.8.d). However, the samples with higher εNdi values have lower SiO_2 contents. Likewise, the lowest εNdi values, correspond to samples with high SiO_2. The initial ratios of $^{206}Pb/^{204}Pb$, $^{207}Pb/^{204}Pb$ and $^{208}Pb/^{204}Pb$ range between 17.84 – 19.01, 15.53 – 15.68 and 37.26 – 38.99, respectively (Fig. 3.8.b). The Pb isotopes ratios do not show a correlation with the SiO_2 content.

Table 3.2. ICP-MS and ICP-OES geochemical results for analysed samples of CPC, its enclaves and mafic dikes that intrude it. Values below the detection limit (d.l.) are denoted with < d.l.; N.D: no data.

Sample	CPV-16-450	CPV-16-442	CPV-16-457	CPV-16-438	CPV-16-440	CPV-16-474	CPV-18-505	CPV-18-516	CPV-18-502	CPV-16- 431	CPV-16- 449	CPV-18-504	CPV-16-443	CPV-16-444	CPV-16-475	CPV-16- 429	CPV-16- 435	CPV-16- 436	CPV-16-441
East (m)	397259	407524	382776	403468	405755	398494	410431	392827	400693	383436	400921	408084	405089	404308	398494	382619	401711	401711	405755
North (m)	6807776	6820292	6800498	6817376	6819577	6804836	6807739	6787785	6805332	6790344	6811025	6805916	6819087	6818317	6804836	6791765	6814136	6814136	6819577
Petrography	Diorite	Quartz diorite	Tonalite	Tonalite	Granodiorite	Granodiorite	Granodiorite	Granodiorite	Monzo granite	Monzo granite	Monzo granite	Monzo granite	Dike	Dike	Dike	Enclave	Enclave	Enclave	Quartz diorite (enclave)
Major elements (wt. %)																			
SiO_2	49,21	56,36	56,46	66,26	70,3	72,39	73,65	74,64	72,82	73,6	76,37	76,46	56,94	48,2	48,3	56,85	51,1	51,99	61,86
Al_2O_3	18,44	17,33	18,03	16,16	14,87	14,29	13,76	13,24	13,48	14,05	13,12	12,12	15,64	17,45	15,75	17,79	21,04	19,5	16,09
$Fe_2O_{3(T)}$	10,31	6,13	6,95	3,36	2,54	1,99	2,04	1,21	1,44	1,4	0,61	0,59	6,38	11,18	9,57	6,57	9,43	8,6	5,92
MnO	0,183	0,107	0,108	0,116	0,071	0,046	0,081	0,034	0,033	0,044	0,059	0,024	0,162	0,17	0,145	0,094	0,187	0,183	0,196
MgO	6,2	4,09	3,48	1,04	0,85	0,46	0,49	0,38	0,12	0,34	0,09	0,11	4,87	5,33	4,46	3,36	3,21	3,02	1,87
CaO	10,1	6,87	7,05	3,53	2,77	1,21	1,35	1,27	1,91	1,45	0,4	0,28	6,45	6,84	6,03	6,24	7,08	7,57	4,91
Na_2O	2,82	3,67	3,03	4,67	4,3	3,65	4,24	3,94	3,38	3,64	3,9	3,58	3,57	3,89	4,82	2,99	4,97	5,1	4,44
K_2O	0,21	1,48	1,91	1,87	2,64	4,76	3,29	3,47	4,24	4	4,83	4,82	1,2	1,44	1,05	2,15	1,2	0,83	1,6
TiO_2	1,788	0,715	0,934	0,514	0,387	0,29	0,25	0,179	0,307	0,168	0,093	0,102	0,726	1,594	1,516	0,871	1,123	1,133	0,917
P_2O_5	0,25	0,23	0,32	0,18	0,12	0,05	0,07	0,06	0,01	0,09	< 0.01	0,02	0,16	0,32	0,32	0,3	0,54	0,51	0,22
LOI	0,38	1,82	1,34	0,97	0,77	1,14	1,03	0,77	2,55	0,8	0,51	0,58	4,25	4,08	6,56	1,88	0,83	0,93	0,92
Total	99,9	98,81	99,61	98,67	99,61	100,3	100,2	99,19	100,3	99,58	99,99	98,7	100,3	100,5	98,52	99,11	100,7	99,38	98,93
Trace elements (ppm)																			
Y	9,9	13,4	12,2	9,8	12,4	22,4	21,9	14,7	29,9	11,1	15,9	24,2	14,8	27,6	24,6	8,9	29,4	24	19
La	6,3	22,5	20,8	30,7	27,7	37,9	29,6	20,9	36	18,5	20,6	20,9	13,9	15,4	18,2	10,4	30,3	32,3	22,3
Ce	14	49	44,6	59,1	56,7	80,2	59,9	41,4	77,3	37	46	48,2	31,3	35,5	40,5	24,9	71,3	78,3	48,5
Pr	1,97	5,98	5,48	6,44	6,27	9,03	6,37	4,37	8,32	4,07	4,99	5,31	3,78	4,71	5,16	3,51	9,39	10,6	6,01
Nd	9,4	24,1	21,7	23,1	21,9	31,1	21,4	14,2	30,1	14,5	16,9	18,2	15,6	21,7	22	15,8	39,2	45	24,6
Sm	2,41	4,86	4,26	3,91	4,11	6,08	4,05	2,69	5,66	2,9	3,85	4,01	3,34	5,3	4,9	3,84	8,38	9,99	5,59
Eu	1,49	1,5	1,29	1,27	0,986	0,802	0,785	0,49	0,773	0,721	0,339	0,341	1,08	1,86	1,63	1,15	2,02	2,31	1,4
Gd	2,78	3,86	3,55	3,2	3,33	5,15	3,28	2,07	5,09	2,52	3,88	3,62	3,07	5,29	4,57	3,68	7,65	9,12	5,34
Tb	0,43	0,56	0,54	0,45	0,55	0,88	0,55	0,34	0,79	0,49	0,77	0,63	0,49	0,85	0,72	0,56	1,15	1,43	0,88
Dy	2,58	3,08	2,88	2,57	3,17	5,29	3,45	2,15	4,97	3,15	4,8	3,97	2,76	5,23	4,18	3,08	6,57	8,11	4,93
Ho	0,49	0,58	0,54	0,5	0,62	1,05	0,69	0,46	0,99	0,62	1,03	0,83	0,53	1,01	0,82	0,64	1,32	1,6	0,94
Er	1,36	1,59	1,48	1,46	1,87	3,13	2,13	1,43	3,06	1,92	3,34	2,44	1,56	2,84	2,34	1,78	3,73	4,58	2,75
Tm	0,191	0,216	0,203	0,206	0,277	0,473	0,338	0,227	0,486	0,294	0,535	0,373	0,231	0,396	0,332	0,251	0,555	0,661	0,415
Yb	1,23	1,39	1,34	1,49	1,86	3,29	2,41	1,63	3,2	2,01	3,76	2,76	1,46	2,64	2,16	1,61	3,44	4,07	2,59
Lu	0,192	0,222	0,214	0,234	0,289	0,533	0,366	0,28	0,519	0,325	0,622	0,438	0,224	0,421	0,342	0,259	0,55	0,626	0,375
Li	6,8	27,3	32,2	26,9	32,8	15	N.D.	N.D.	N.D.	22,9	49,9	N.D.	N.D.	N.D.	N.D.	41,6	13,8	12,5	23,8

Rb	3,1	36,9	62,1	59,8	64,7	185	111	126	189	109	196	161	61	105	45	42,8	32,3	12,1	48,6
Cs	0,3	4,5	2,6	1,2	1,7	2,7	1,8	1,9	4,4	5,8	5	1,8	2,7	12,6	0,6	2,9	0,6	0,4	1,5
Be	< 1	1	1	2	2	2	2	2	2	1	3	2	1	1	1	1	1	1	2
Sr	489	622	495	278	172	92	136	155	59	148	25	57	419	406	204	393	393	329	220
Ba	126	433	466	713	708	676	784	804	669	677	209	339	268	280	190	305	596	457	511
Zr	26,4	14,9	63,7	9,2	21,6	100	124	71	149	17,5	47,2	40	106	149	135	23,5	29,5	11,5	38,9
Hf	0,8	0,8	1,8	0,3	0,9	3,4	3,9	2,5	4,8	0,7	2,5	1,6	2,8	4,2	3,7	0,7	0,5	0,4	1,4
Nb	1,8	1,4	1,5	0,8	2,4	1,3	7,2	5,4	6,1	4,7	1,7	7,1	3,5	4,5	4,8	3,5	1	0,2	2,2
Ta	0,23	0,43	0,48	0,73	0,87	1,47	1	0,95	1,38	1,14	1,82	1,55	0,29	0,29	0,28	0,5	0,44	0,41	0,92
Mo	0,1	0,1	< 0.1	< 0.1	< 0.1	0,6	< 2	< 2	3	< 0.1	< 0.1	< 2	< 2	< 2	< 2	0,1	< 0.1	< 0.1	< 0.1
W	> 200	30,8	17,1	98	> 200	37,4	731	827	482	> 200	72,6	530	112	53,5	34,2	> 200	135	16	93,3
Sc	22	15	17	4	4	4	4	4	5	3	3	3	19	25	26	8	19	15	10
V	183	68	134	11	16	22	16	12	27	11	< 4	< 5	146	244	234	130	86	56	31
Cr	94	70	21	7	7	7	< 20	< 20	< 20	5	7	< 20	190	40	50	10	6	5	7
Co	45,9	40,5	40,4	63,8	40,4	49,6	34	43	22	40,3	65,7	26	28	42	32	48,5	54,9	43,3	47,4
Ni	66,3	35,5	24,5	< 0.1	< 0.1	< 0.1	< 20	< 20	< 20	< 0.1	< 0.1	< 20	70	80	30	6,4	1	0,6	1,8
Cu	29,6	23	17,9	0,6	5,3	3,7	< 10	< 10	< 10	0,7	0,5	30	< 10	30	40	11,9	15,4	15,8	12,6
Zn	75	72	82	57	45	26	30	< 30	< 30	27	10	< 30	130	110	100	75	111	108	78
Ag	< 0.1	< 0.1	< 0.1	0,2	< 0.1	< 0.1	< 0.5	< 0.5	< 0.5	< 0.1	< 0.1	< 0.5	< 0.5	< 0.5	< 0.5	< 0.1	< 0.1	< 0.1	< 0.1
Au	< 100	< 100	< 100	< 100	< 100	< 100	N.D.	N.D.	N.D.	< 100	< 100	N.D.	N.D.	N.D.	N.D.	< 100	300	< 100	< 100
Cd	< 0.1	< 0.1	< 0.1	< 0.1	< 0.1	< 0.1	N.D.	N.D.	N.D.	< 0.1	0,1	N.D.	N.D.	N.D.	N.D.	< 0.1	0,1	0,3	< 0.1
Ga	19	20	21	20	17	16	16	14	15	15	15	11	17	22	21	21	24	24	20
In	< 0.1	< 0.1	< 0.1	< 0.1	< 0.1	< 0.1	< 0.1	< 0.1	< 0.1	< 0.1	< 0.1	< 0.1	< 0.1	< 0.1	< 0.1	< 0.1	< 0.1	< 0.1	< 0.1
Tl	< 0.05	0,15	0,29	0,3	0,29	0,93	0,52	0,58	0,52	0,64	0,98	0,96	0,36	0,38	0,23	0,4	0,06	< 0.05	0,21
Ge	1,2	1,2	1,1	1,2	1,4	1,3	1,6	1,7	0,9	1,6	1,9	1,4	1,5	1,9	1,3	1,3	1,2	1,2	1,5
Sn	1,3	1,2	1,4	1,4	1	2,2	1	1	1	5,3	3,2	1	1	1	1	3	0,6	0,6	1
Pb	2	9,1	10,8	18,4	11,5	15,7	18	16	10	26,7	20,6	39	7	5	< 5	9,2	6,8	5,6	9,1
Bi	< 0.1	0,1	< 0.1	0,1	< 0.1	< 0.1	< 0.1	< 0.1	< 0.1	< 0.1	< 0.1	< 0.1	< 0.1	< 0.1	< 0.1	< 0.1	< 0.1	< 0.1	< 0.1
Th	0,23	3,17	2,7	5,16	7,01	18,1	9,94	9,39	18,4	6,94	13,8	15,5	2,91	1,05	1,95	1,51	0,86	0,72	5,79
U	0,08	0,71	0,95	0,45	1,3	3,1	1,76	1,58	2,73	1,27	3,73	4,68	0,8	0,35	0,94	1,04	0,33	0,28	1,79
As	< 1	< 1	< 1	< 1	< 1	< 1	< 5	< 5	< 5	< 1	< 1	< 5	< 5	< 5	< 5	< 1	< 1	< 1	< 1
Sb	< 0.1	0,1	< 0.1	< 0.1	< 0.1	< 0.1	< 0.2	0,7	< 0.2	< 0.1	0,2	0,7	< 0.2	0,4	< 0.2	0,1	< 0.1	< 0.1	0,1
S	< 1	< 1	< 1	< 1	< 1	< 1	N.D.	N.D.	N.D.	< 1	< 1	N.D.	N.D.	N.D.	N.D.	< 1	< 1	< 1	< 1

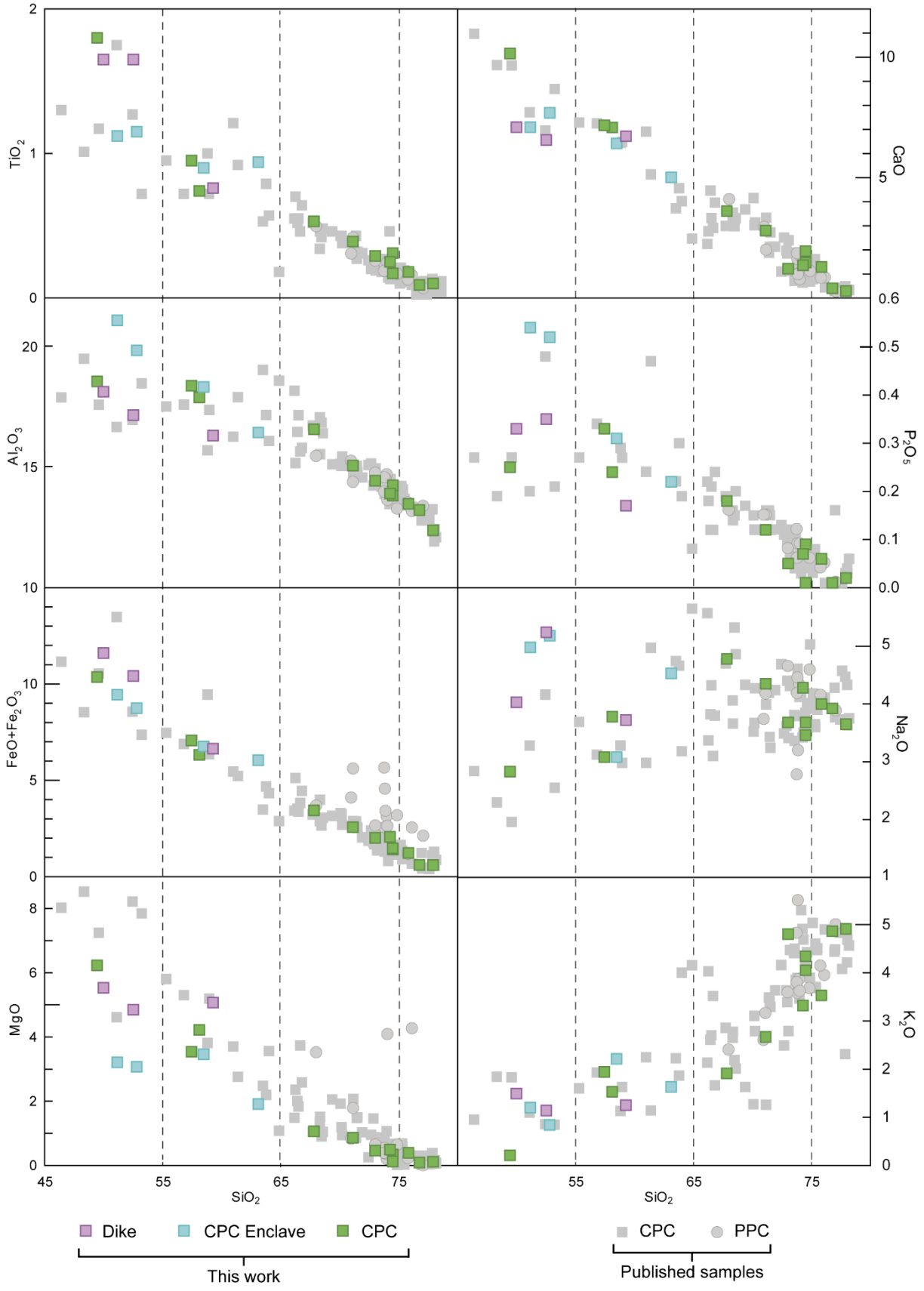
TiO2
CaO
Al2O3
P2O5
FeO+Fe2O3
Na2O
MgO
K2O
SiO2
SiO2
Dike
CPC Enclave
CPC
This work
CPC
PPC
Published samples

Fig. 3.5. Harker diagrams of the analysed samples and previously published data for Chollay and Piuquenes plutonic complexes (Mpodozis and Kay, 1992; Murillo et al., 2017; Oliveros et al., 2020; Ortiz and Merino, 2015; Salazar et al., 2013; Salazar and Coloma, 2016; Velásquez et al., 2021).

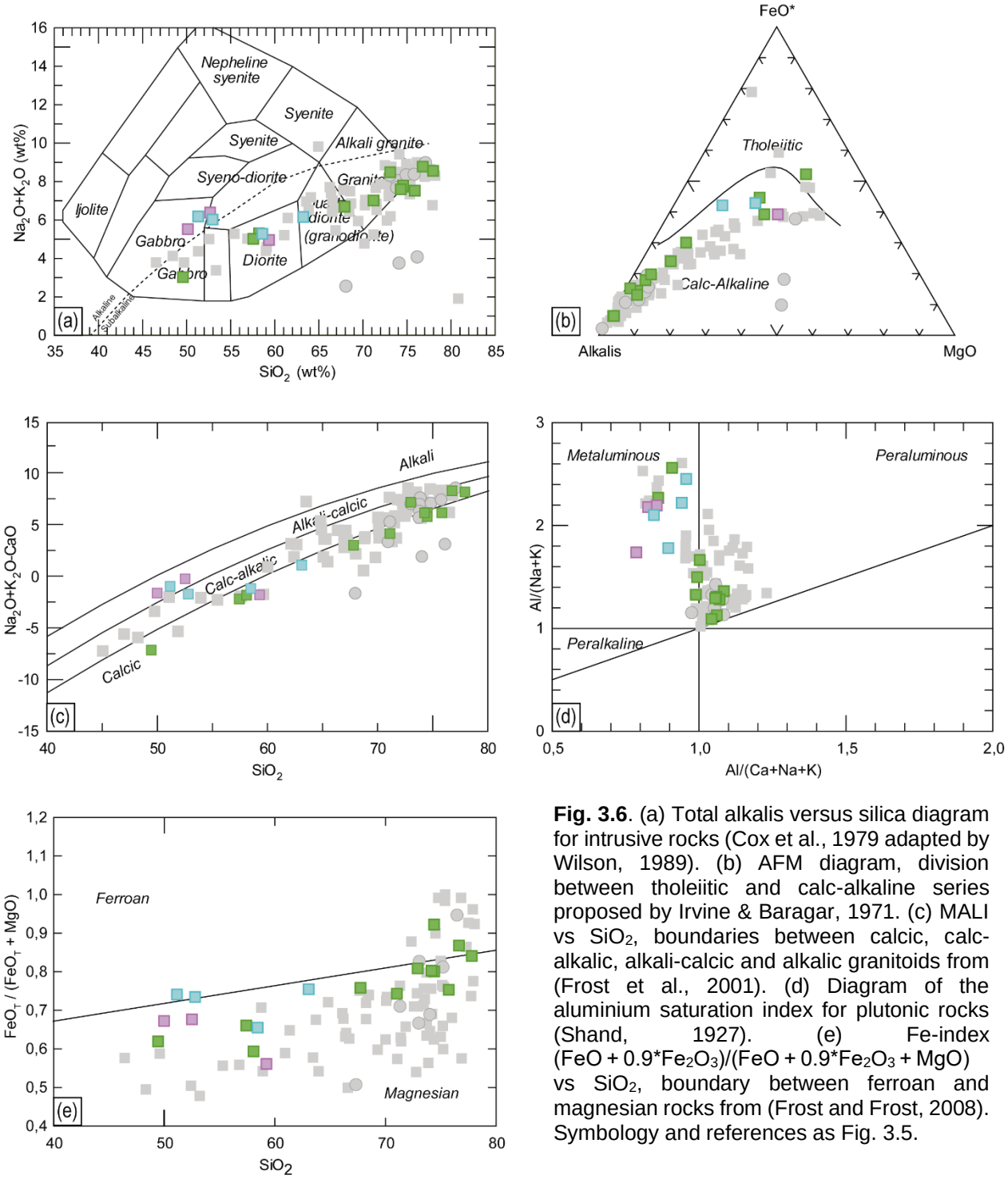

Fig. 3.6. (a) Total alkalis versus silica diagram for intrusive rocks (Cox et al., 1979 adapted by Wilson, 1989). (b) AFM diagram, division between tholeiitic and calc-alkaline series proposed by Irvine & Baragar, 1971. (c) MALI vs SiO_2, boundaries between calcic, calc-alkalic, alkali-calcic and alkalic granitoids from (Frost et al., 2001). (d) Diagram of the aluminium saturation index for plutonic rocks (Shand, 1927). (e) Fe-index $(FeO + 0.9*Fe_2O_3)/(FeO + 0.9*Fe_2O_3 + MgO)$ vs SiO_2, boundary between ferroan and magnesian rocks from (Frost and Frost, 2008). Symbology and references as Fig. 3.5.

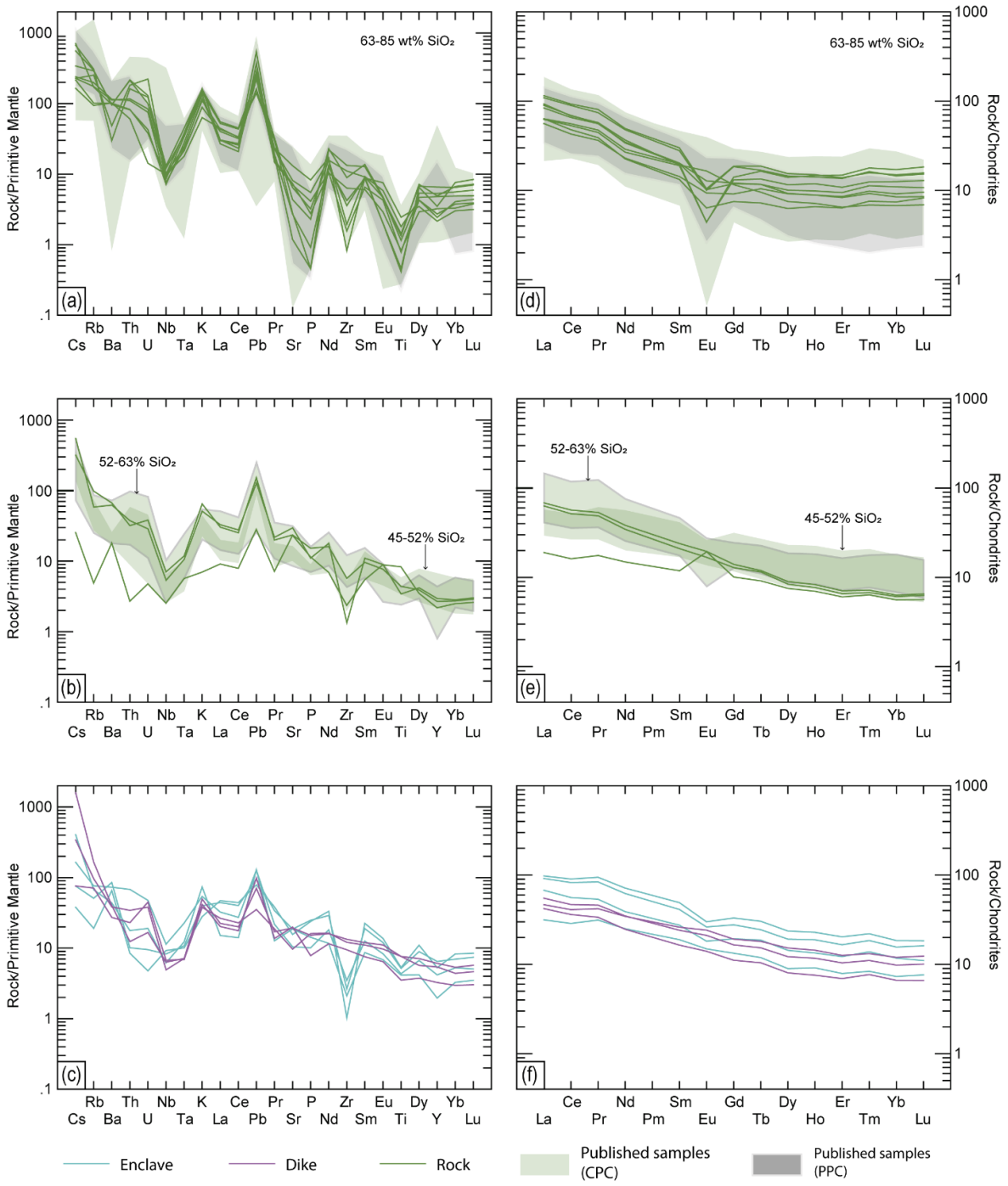

Figure 3.7. (a) Multi-element diagrams normalized to the primitive mantle (Sun and McDonough, 1989) for CPC samples with a SiO_2 greater than 63%. (b) Multi-element diagrams normalized to the primitive mantle (Sun and McDonough, 1989) for CPC samples with a SiO_2 less than 63%. (c) Multi-element diagrams normalized to the primitive mantle (Sun and McDonough, 1989) for CPC enclaves and mafic dikes. (d) Rare Earth Elements diagrams normalized to chondrite (Nakamura, 1974) for CPC samples with a SiO_2 greater than 63%. (e) Rare Earth Elements diagrams normalized to chondrite (Nakamura, 1974) for CPC samples with a SiO_2 less than 63%. (f) Rare Earth Elements diagrams normalized to chondrite (Nakamura, 1974) for CPC enclaves and mafic dikes. The lines represent the analyzed samples, the green areas represent published data of CPC and the grey areas those of the PPC.

3.4.3 Mineral chemistry

The atomic proportions of the elements in plagioclase crystals were calculated based on eight oxygen atoms per formula unit (a.p.f.u.) (Appendix 3.B, Table S1). Plagioclase crystals classify as oligoclase (CCL-65 and CPV-18-510) and labradorite (CT-193). The Fe^{2+} and Fe^{3+} contents of the amphibole analysed points were determined using the procedure described by Holland & Blundy (1994). Amphibole crystals were classified using the nomenclature by Hawthorne et al. (2012). All amphiboles analysed belong to the group of calcium amphiboles and corresponds to magnesio-ferri-hornblendes (Appendix 3.B, Table S2).

Of these samples, two presented the mineralogical association to perform thermobarometric calculations based on Al-in-hornblende (hornblende, plagioclase, biotite, quartz, potassium feldspar, titanite and Fe-Ti oxides, Anderson & Smith, 1995; Holland & Blundy, 1994; Mutch et al., 2016; Schmidt, 1992). However, some pairs of plagioclase-amphibole were discarded because their $Fe^{3+}/(Fe^{2+}+Fe^{3+})$ ratios were less than 2.5 and even less than 2.0. The pressures were calculated using the calibration proposed by Mutch et al. (2016) and the temperature, was estimated based on the edenite – tremolite reaction (Holland & Blundy, 1994). The pressures obtained were 1,7 ± 0,6 kbar and 1,8 ± 0,6 kbar for samples CCL-65 y CPV-18-510, respectively and their temperatures were 706,4 ± 40°C and 703 ± 40 °C, reflecting epizonal emplacement conditions. However, these calculations must be interpreted with caution because the values of $Fe_{Tot}/(Fe_{Tot}+Mg)$ are outside the range between 0.40 - 0.65, preventing the validation of thermobarometric results according to the criteria defined by Anderson & Smith (1995).

Table 3.3. Initial Sr, Nd and Pb isotope ratios, calculated from the measurements of the current isotope ratios (TIMS), the Rb, Sr, Sm, Nd, U, Th and Pb concentrations in ppm (ICP-MS) and the average ages of the CPC. * Instrumental mass-fractionation of Pb was corrected using 0.1% per atomic mass unit. This factor was derived from repeated analyses of NIST 981 and comparison of analyzed and certified Pb isotope ratios. The overall error including the correction for mass-fractionation is better than 0.1% of the respective isotope ratio. N.M: Not measured; N.C: Not calculated.

Sample	East (m)	North (m)	Age (Ma)	Rb (ppm)	Sr (ppm)	$^{87}Sr/^{86}Sr$	Standard error	$^{87}Sr/^{86}Sr$ initial	Sm (ppm)	Nd (ppm)	$^{143}Nd/^{144}Nd$	Standard error	$^{143}Nd/^{144}Nd$ initial	εNd initial
CPV-16-429	382619	6791765	238	42,8	393	0,707355	1,50E-06	0,7063	3,84	15,8	0,512368	1,3,E-05	0,5121	-3,8
CPV-16-431	383436	6790344	241,6	109	148	0,713996	2,20E-06	0,7067	2,9	14,5	0,512390	4,4,E-06	0,5122	-2,5
CPV-16-435	401711	6814136	237,5	32,3	393	0,706089	7,70E-06	0,7053	8,38	39,2	0,512451	4,3,E-06	0,5122	-1,6
CPV-16-438	403468	6817376	241,6	59,8	278	0,707125	2,00E-06	0,7050	3,91	23,1	0,512397	3,9,E-06	0,5122	-1,8
CPV-16-440	405755	6819577	241,6	64,7	172	0,708918	1,20E-05	0,7052	4,11	21,9	0,512389	6,3,E-05	0,5122	-2,3
CPV-16-441	405755	6819577	241,6	48,6	220	0,707767	1,80E-06	0,7056	5,59	24,6	0,512412	3,6,E-06	0,5122	-2,6
CPV-16-442	407524	6820292	241,6	36,9	622	0,705359	2,60E-06	0,7048	4,86	24,1	0,512520	2,8,E-06	0,5123	0
CPV-16-449	400921	6811025	241,6	196	25	0,782401	5,70E-06	0,7039	3,85	16,9	0,512415	5,0,E-06	0,5122	-2,5
CPV-16-450	397259	6807776	241,6	3,1	489	0,704776	2,20E-06	0,7047	2,41	9,38	0,512651	5,1,E-06	0,5124	1,5
CPV-16-457	382776	6800498	241,6	62,1	495	0,706818	2,10E-06	0,7056	4,26	21,7	0,512402	3,5,E-06	0,5122	-2,2
CPV-16-474	398494	6804836	241,6	185	92	0,723799	1,80E-05	0,7038	6,08	31,1	0,512251	4,5,E-06	0,5121	-5,1
CCL-03q	412200	6837700	249,3	74,4	247	0,709263	1,50E-06	0,7062	7,47	33,12	0,512421	2,5,E-06	0,5122	-2,3
CCL-54	403452	6817371	241,6	130	133,4	0,715779	4,40E-06	0,7061	3,79	20,59	0,512403	3,8,E-06	0,5122	-2
CCL-56	403680	6817427	241,6	53	909,3	0,705008	2,40E-06	0,7044	9,35	47,33	0,512608	2,7,E-06	0,5124	1,8
CT-154q	402037	6814985	237,5	48,2	282,1	0,706714	1,80E-06	0,7050	3,49	28,43	0,512382	3,2,E-06	0,5123	-1,3
CT-161q	393442	6815293	241,6	128,4	99,4	0,716826	2,00E-06	0,7040	3,62	20,88	0,512417	5,7,E-06	0,5123	-1,5
CT-164q	389794	6810101	241,6	47,1	416,4	0,706588	1,60E-06	0,7055	3,84	18,42	0,512413	4,0,E-06	0,5122	-2,2
CT-191q	386550	6800942	238,2	109	283,6	0,711048	2,10E-06	0,7073	5,84	30,39	0,512277	3,0,E-06	0,5121	-4,6
CT-250q	384825	6797022	241,6	98,1	450,8	0,70997	2,00E-06	0,7078	3,25	17,72	0,512230	2,5,E-06	0,5121	-5,3
CT-289q	392624	6829798	241,6	202	86	0,729842	4,30E-06	0,7064	7,96	41,14	0,512400	2,3,E-06	0,5122	-2,2
CT-300q	395358	6793507	241,6	75	381	0,708631	2,20E-06	0,7067	6,57	31,6	0,512352	2,3,E-06	0,5122	-3,4
CT-303q	393899	6794283	241,6	175	241	0,707511	2,20E-06	0,7003	4,53	25,05	0,512570	2,5,E-06	0,5124	1,4
MCM-027q	405192	6766258	238,3	187,6	2,5	0,745044	6,40E-06	0,0066	7,73	37,39	0,512414	2,0,E-06	0,5122	-2,2
MCM-253q	385924	6789866	243,4	42	455	0,782789	3,00E-06	0,7819	3,18	12,93	0,512434	4,2,E-06	0,5122	-2,5
RCM-039q	403058	6790695	233,8	150	72,4	0,718558	2,80E-06	0,6986	3,53	13,81	0,512378	3,1,E-06	0,5121	-3,8
SCL-75	422822	6826703	244,1	109,9	236,7	0,710002	1,90E-06	0,7053	4,58	16,61	0,512468	2,9,E-06	0,5122	-2,4
RCM-115q	380639	6777958	244,8	108,6	364,1	0,709962	2,60E-06	0,7070	3,2	15,69	0,512349	2,9,E-06	0,5122	-3,3
CPV-16-436	401711	6814136	237,5	12,1	329	0,705718	2,80E-06	0,7054	9,99	45	0,512435	5,0,E-06	0,5122	-2,1
CPV-16-443	405089	6819087	241,6	61	419	0,706013	8,00E-06	0,7046	3,34	15,6	0,512522	4,0,E-06	0,5123	-0,2
CPV-16-444	404308	6818317	241,6	105	406	0,707249	6,00E-06	0,7047	5,3	21,7	0,512611	4,0,E-06	0,5124	1
CPV-16-475	398494	6804836	241,6	45	204	0,706797	5,00E-06	0,7046	4,9	22	0,512587	4,0,E-06	0,5124	0,9
CPV-18-502	400693	6805332	241,6	189	59	0,727825	6,00E-06	0,6959	5,66	30,1	0,512440	5,0,E-06	0,5123	-1,3
CPV-18-504	408084	6805916	241,6	161	57	0,729347	7,00E-06	0,7012	4,01	18,2	0,512431	3,0,E-06	0,5122	-2,1
CPV-18-505	410431	6807739	241,6	111	136	0,712966	7,00E-06	0,7048	4,05	21,4	0,512433	6,0,E-06	0,5123	-1,5

CPV-18-516	392827	6787785	241,6	126	155	0,713688	6,00E-06	0,7056	2,69	14,2	0,512394	5,0,E-06	0,5122	-2,2

Sample	U (ppm)	Pb (ppm)	Th (ppm)	206Pb/204Pb *	206Pb/204Pb initial	207Pb/204Pb *	207Pb/204Pb initial	208Pb/204Pb *	208Pb/204Pb initial
	0,4	9,2	1,5	18,69	18,59	15,61	15,61	38,37	38,24
CPV-16-429	0,9	26,7	6,9	18,74	18,66	15,59	15,59	38,4	38,2
CPV-16-431	0,2	6,8	0,9	18,52	18,45	15,59	15,58	38,31	38,21
CPV-16-435	0,3	18,4	5,2	18,49	18,45	15,56	15,56	38,57	38,35
CPV-16-438	0,8	11,5	7	18,77	18,6	15,59	15,59	38,72	38,23
CPV-16-440	1	9,1	5,8	N.M.	N.C.	N.M.	N.C.	N.M.	N.C.
CPV-16-441	0,6	9,1	3,2	18,6	18,44	15,61	15,6	38,51	38,24
CPV-16-442	2,6	20,6	13,8	19,06	18,75	15,61	15,59	38,81	38,27
CPV-16-449	0,1	2	0,2	N.M.	N.C.	N.M.	N.C.	N.M.	N.C.
CPV-16-450	0,8	10,8	2,7	18,71	18,52	15,67	15,66	38,69	38,49
CPV-16-457	2,1	15,7	18,1	19,07	18,74	15,63	15,62	39,1	38,18
CPV-16-474	2,4	11	10,3	18,91	18,37	15,59	15,56	38,59	37,82
CCL-03q	1,4	40,3	14,3	18,81	18,72	15,58	15,58	38,83	38,55
CCL-54	1,6	12,4	11,1	19,34	19,02	15,64	15,62	39,72	38,99
CCL-56	0,6	14,3	7,8	18,57	18,47	15,57	15,56	38,84	38,42
CT-154q	1,2	19,2	11,5	18,77	18,62	15,58	15,57	38,7	38,22
CT-161q	0,3	10,6	2,2	18,54	18,46	15,57	15,56	38,4	38,23
CT-164q	1,7	20,3	14	18,7	18,5	15,6	15,59	38,91	38,37
CT-191q	0,7	19,5	3,9	18,53	18,45	15,58	15,58	38,36	38,21
CT-250q	4,3	24	21,4	18,81	18,37	15,61	15,58	38,74	38,03
CT-289q	1,7	18	7,9	18,65	18,43	15,58	15,57	38,51	38,16
CT-300q	3,7	24	30,3	18,58	18,21	15,56	15,54	38,39	37,4
CT-303q	4	12,9	21,8	18,69	17,95	15,58	15,54	38,59	37,27
MCM-027q	1,8	0,3	13,4	18,65	1,36	15,59	14,7	38,6	-4,12
MCM-253q	2,1	12,2	9,5	18,82	18,41	15,59	15,57	38,54	37,94
RCM-039q	2,8	26,2	13,8	18,76	18,5	15,56	15,55	38,61	38,18
SCL-75	0,5	13,9	1,3	18,56	18,47	15,57	15,57	38,23	38,16
RCM-115q	0,1	5,6	0,7	18,43	18,38	15,55	15,55	38,21	38,11
CPV-16-436	2,7	10	18,4	18,78	18,11	15,72	15,69	38,95	37,48
CPV-16-443	4,7	39	15,5	18,67	18,38	15,68	15,67	38,81	38,49
CPV-16-444	1,8	18	9,9	18,83	18,59	15,61	15,59	38,85	38,41
CPV-16-475	2,4	288	11	18,95	18,93	15,64	15,64	38,93	38,9
CPV-18-502	1,6	16	9,4	18,76	18,51	15,63	15,62	38,61	38,14
CPV-18-504	0,8	7	2,9	18,76	18,48	15,61	15,6	38,65	38,32
CPV-18-505	0,9	2,5	2	18,76	17,84	15,62	15,57	38,74	38,12

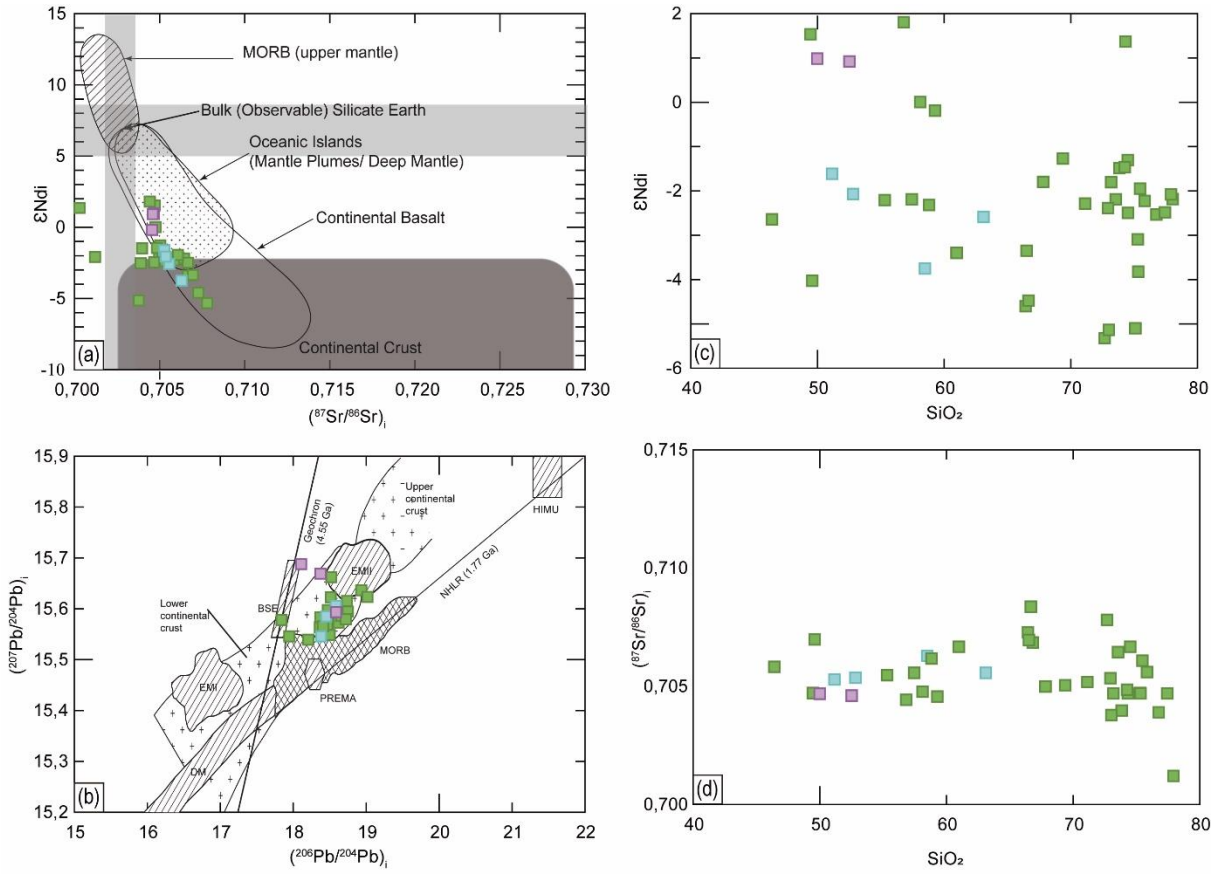

Figure 3.8. Initial isotopic composition for samples of Chollay Plutonic Complex, some enclaves and mafic dikes compared to different reservoirs. (a) εNd_i versus $^{87}Sr/^{86}Sr_i$ diagram including the isotopic composition of mid-ocean ridge basalt (MORB) and the Bulk Silicate Earth, mantle plumes, continental basalt and continental crust (White, 2013; Workman and Hart, 2005). (b) $^{207}Pb/^{204}Pb_i$ versus $^{206}Pb/^{204}Pb_i$ with the isotopic composition of the mantle reservoirs proposed by (Zindler and Hart, 1986): depleted mantle (DM), bulk silicate earth (BSE), mantle with high U/Pb ratio (HIMU), enriched mantle I (EMI), enriched mantle II (EMII) and observed prevalent mantle composition (PREMA). (c) εNd_i versus SiO_2 diagram. (d) $^{87}Sr/^{86}Sr_i$ versus SiO_2 diagram.

3.5 Discussion

3.5.1 Framing the Lower – Middle Triassic magmatism of the Chilean Frontal Cordillera

The petrogenesis of the Upper Paleozoic – Triassic granitoids cropping out in the Andean Frontal Cordillera (28°S – 31°S) was first assessed in the 1980s and early 1990s (Mpodozis & Kay, 1992; Nasi et al., 1985) from regional geology, geochronology, and whole-rock geochemistry. The intrusives were classified as epizonal, hypersiliceous, leucocratic granites with few xenoliths and lack of deformation. The reported dominant lithology was high-SiO_2 (69 – 78 wt%), coarse-grained leucocratic monzogranite, bearing scarce biotite/amphibole, moderately metaluminous to peraluminous, with relatively flat REE patterns, moderate to large negative Eu anomalies, and $^{87}Sr/^{86}Sr_i$ ratios between 0,704 – 0,706 (Mpodozis & Kay, 1992).

The interpretation given to the Triassic granitoids in these early works was one of the foundations of the tectonic model proposed for the SW Gondwana margin during Pangea amalgamation and initial breakup. In this model, after a period of oblique convergence (Carboniferous – Early Permian) a terrain collision would have thickened the crust, shortening, and deforming the back-arc sedimentary deposits and exhuming intrusive rocks. Slab break-off would have prompted lithospheric delamination and asthenosphere upwelling (Gianni and Navarrete, 2022) that resulted in the emplacement of large amounts of basaltic melts at the base of the crust, inducing crust partial melting to produce the Permian – Upper Triassic granitoids grouped in the Ingaguás Complex and considered part of the Choiyoi Magmatic Province (Mpodozis and Kay, 1992). The Choiyoi Magmatic Province, which precedes the magmatism described in this work, has been classified as a silicic large igneous province (SLIP) based on its areal extension and its time span (Bastías-Mercado et al., 2020; Rocher et al., 2015) and its origin has been recently attributed to a large-scale slab loss, based on plate-kinematic reconstructions and confirmed by a slab break-off geochemical signature (Gianni and Navarrete, 2022). This signature has not been recognized in magmatic products in Chile that are contemporary to the Choiyoi province, whose elemental and isotopic geochemistry is interpreted as subduction-related (Oliveros et al., 2020).

The recent updating of the regional geology of the Chilean Frontal Cordillera (28°30'S – 30°30´S) carried out by the SERNAGEOMIN (Murillo et al., 2017; Ortiz and Merino, 2015; Salazar et al., 2013; Salazar and Coloma, 2016; Velásquez et al., 2021), which included extensive high precision U-Pb and Ar^{40}-Ar^{39} dating of Permian – Triassic units (Fig. 3.9), led to the interpretation that the igneous activity represented by the Ingaguás Complex was mostly Triassic and equivalent to the post-Choiyoi magmatism (247 – 200 Ma, Sato et al., 2015). The largest units of the former Ingaguás Complex correspond to the Lower - Middle Triassic Chollay and Piuquenes plutonic complexes which together define a magmatic belt characterized by a wide compositional range from diorites to syenogranites, with predominance of monzogranites and granodiorites. The most common mafic minerals in theses rocks, correspond to biotite and magnesium-ferri-hornblendes.

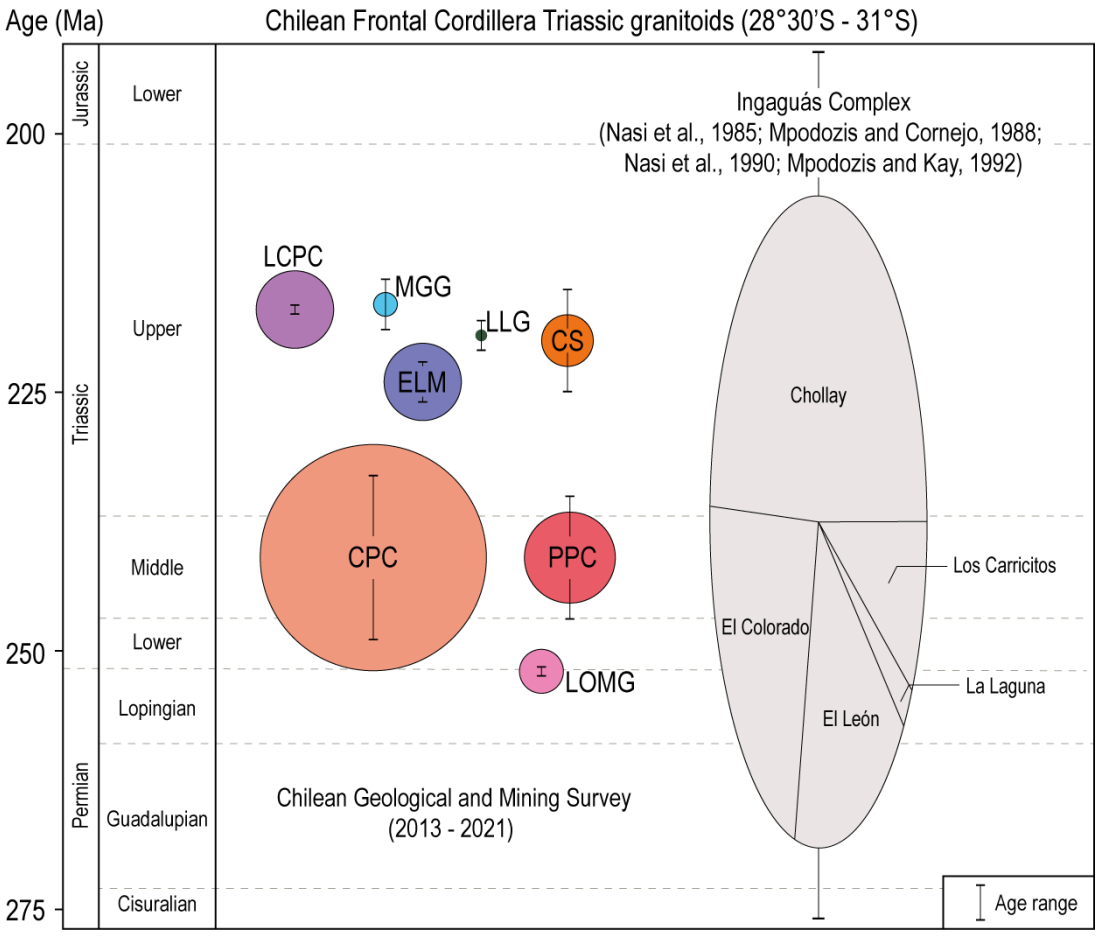

Figure 3.9. Changes in the nomenclature of exposed Triassic intrusive rocks in the Chilean Frontal Cordillera, between 28°30'S and 31°S. On the left is the current nomenclature, defined by the Chilean Geological and Mining Survey. The areas occupied by the circles of each unit allow us to compare the exposed area if each of them. The maximum and minimum age of each unit is also indicated. To the right is the old nomenclature in which these units were grouped in the Ingaguás Complex, divided into five units, indicated in the figure. The size ratio shown between those units in the figure represents the areal comparison of their outcrops. LCPC: Los Carricitos Plutonic Complex; MGG: Monte Grande Granites; LLG La Laguna Gabbros; CS: Colorado Syenogranites; ELM: El León Monzogranites; CPC: Chollay Plutonic Complex; PPC: Piuquenes Plutonic Complex; LOMG: La Ortiga Monzogranites and Granodiorites.

The geochemistry of the complexes shows typical characteristics of arc magmatism, such as a calc-alkaline differentiation trend, meta to peraluminous rocks, with LILE enrichment in relation to HFSE, depressions in Nb-Ta and Zr, as well as Pb enrichment relative to the primitive mantle (Stern, 2002; Wilson, 1989). Regarding to REE chondrite normalized patterns, it is possible to recognize an enrichment in LREE in relation to the HREE, with La_N/Yb_N ratios (3,40 – 13,78) and practically flat HREE patterns (Sm_N/Yb_N: 1,11 – 3,79). When calculating the crustal thickness, using the La_N/Yb_N and Sr/Y proxies defined by (Profeta et al., 2015), a thickness of approximately 40 km is obtained. This thickness is less than obtained in the Carboniferous – Permian rocks exposed in northern Chile (45 – 70 km, Oliveros et al., 2020), supporting crustal thinning from Carboniferous to Lower – Middle Triassic probably related to the extensional context that prevailed during the emplacement of CPC and PPC (del Rey et al., 2019, 2016; Oliveros et al., 2020; Poma et al., 2014; Vásquez et al., 2011, Hervé et al., 2014). Furthermore, when contrasting the crystallization pressures obtained at CPC with those calculated in other Carboniferous, Permian-Triassic and Upper Triassic plutons exposed in northern Chile, between 29°40'S – 29°55'S (Uribe et al., 2020), it is possible to recognize a decreasing trend in pressure as the rocks get younger (Fig. 3.10), which could be linked to the change from a compressional to an extensional regime. Finally, the initial $^{87}Sr/^{86}Sr$ range between 0,704 and 0,708 and εNd_i values between -5,3 and +1,8, suggest a mixture between a depleted mantle and continental crust for the magmatic sources.

The above characteristics suggest that the plutonic rocks studied, most probably represent an arc magmatism generated in an extensional convergent margin with a

crust of normal thickness, as has been previously proposed in previous works (Coloma et al., 2017; del Rey et al., 2016; Espinoza et al., 2019; González et al., 2018; Salazar et al., 2020, Molina et al., 2020).

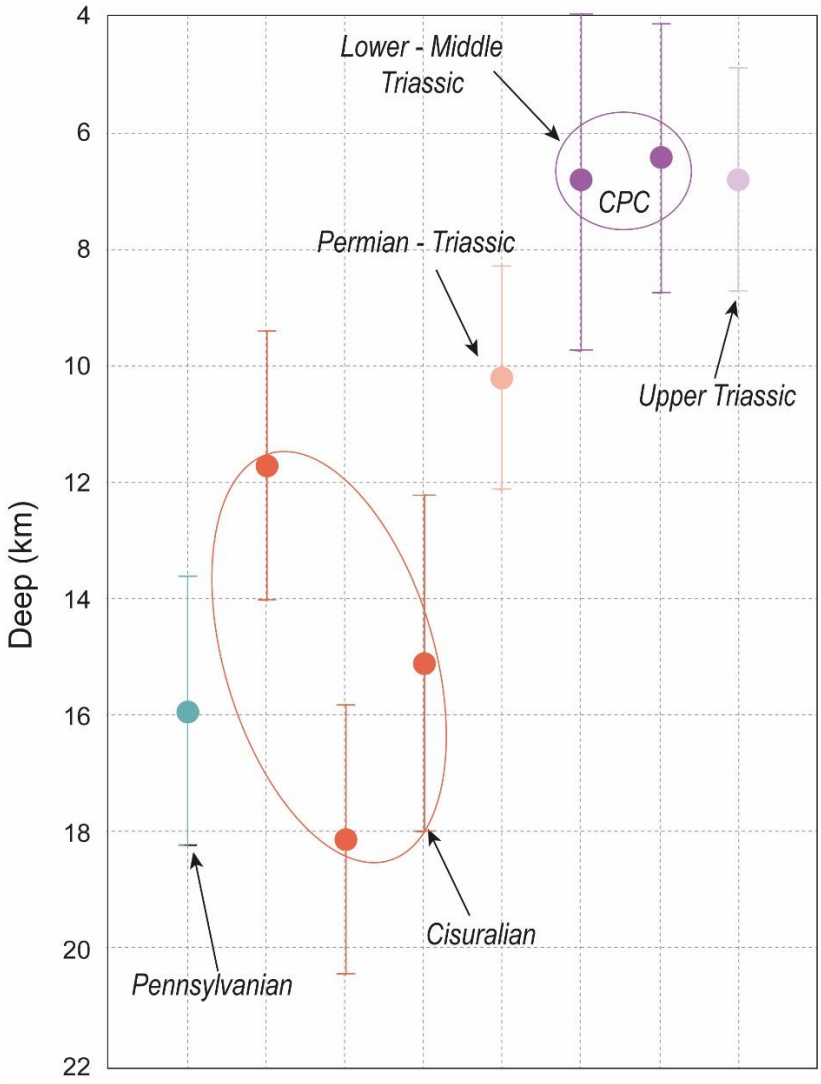

Figure 3.10. Crystallization pressures obtained by Al-in-Hornblende geobarometer. The CPC data are from this work and the rest correspond to already published data (Uribe et al., 2020) belonging to the units: Upper Carboniferous Plutonic Intrusives (*Pennsyllvanian*), Guanta Plutonic Complex (*Cisuralian*), Quebrada Balala Diorite (*Permian – Triassic*) and Los Carricitos Plutonic Complex (*Upper Triassic*).

3.5.2 Comparison of the Lower – Middle Triassic magmatism to advancing margin batholiths

To compare the Lower - Middle Triassic magmatic belt in the frontal Cordillera of northern Chile to magmatism generated in an advancing convergent margin, we have

selected petrographical and geochemical data representative of the Toulumne Intrusive Suite (TIS), which is part of one of the most studied Cordilleran-type plutonic units: the Sierra Nevada Batholith. In general, this batholith was emplaced during three main magmatic episodes: 225 – 195 Ma; 180 – 165 Ma and 102 – 85 Ma (Saleeby et al., 2008 and references there in). Its outcrops cover more than 40.000 km^2, extending approximately 600 km along the western edge of North America (Bateman, 1992) and present a great compositional variability ranging from gabbros to leucogranites with tonalites and granodiorites, being the granites the most abundant lithology (Bateman, 1992).

The TIS correspond to one of the zoned plutonic bodies emplaced along the eastern axis of the Sierra Nevada Batholith and was emplaced in a period of 8 Ma (93 – 85 Ma, Coleman et al., 2004; Matzel et al., 2005). It is a suite that present a concentring zoning and is made up of five units: Kuna Crest granodiorite, equigranular Half Dome Granodiorite, porphyritic Half Dome Granodiorite, Cathedral Peak Granodiorite and Johnson Granite Porphyry, from the margin to the centre (Bateman, 1992). The contacts between the different units are highly variable, being abrupt in some cases to wide and transitional in others (Bateman & Chappell, 1979; Žák et al., 2007). In the Chollay and Piuquenes plutonic complexes, no zonation is recognized and the contacts between the different identified lithofacies are also highly variable, from transitional to abrupt. In mineralogical terms, the granitoids that make up the TIS are composed of plagioclase (andesine – oligoclase), potassium feldspar (microcline), quartz, hornblende (magnesium-hornblendes and actinolites according to the classification of Leake, 1978) (Gray et al., 2008) and biotite, with titanite, magnetite, zircon, apatite and allanite as accessory minerals (Bateman & Chappell, 1979); the colour index decreases from the margins towards the centre of the TIS from 20% to 1% (Gray et al., 2008). In the Chollay and Piuquenes complexes it is recognized: plagioclase (oligoclase - labradorite, in the samples that were subjected to mineral chemistry), potassium feldspar (orthoclase and microcline), quartz, orthopyroxene, clinopyroxene, amphibole (magnesium-ferri-hornblende and actinolite in the samples that were subjected to mineral chemistry) and biotite as main phases; in addition to muscovite, apatite, zircon, titanite and opaque minerals, as accessory minerals. The colour index

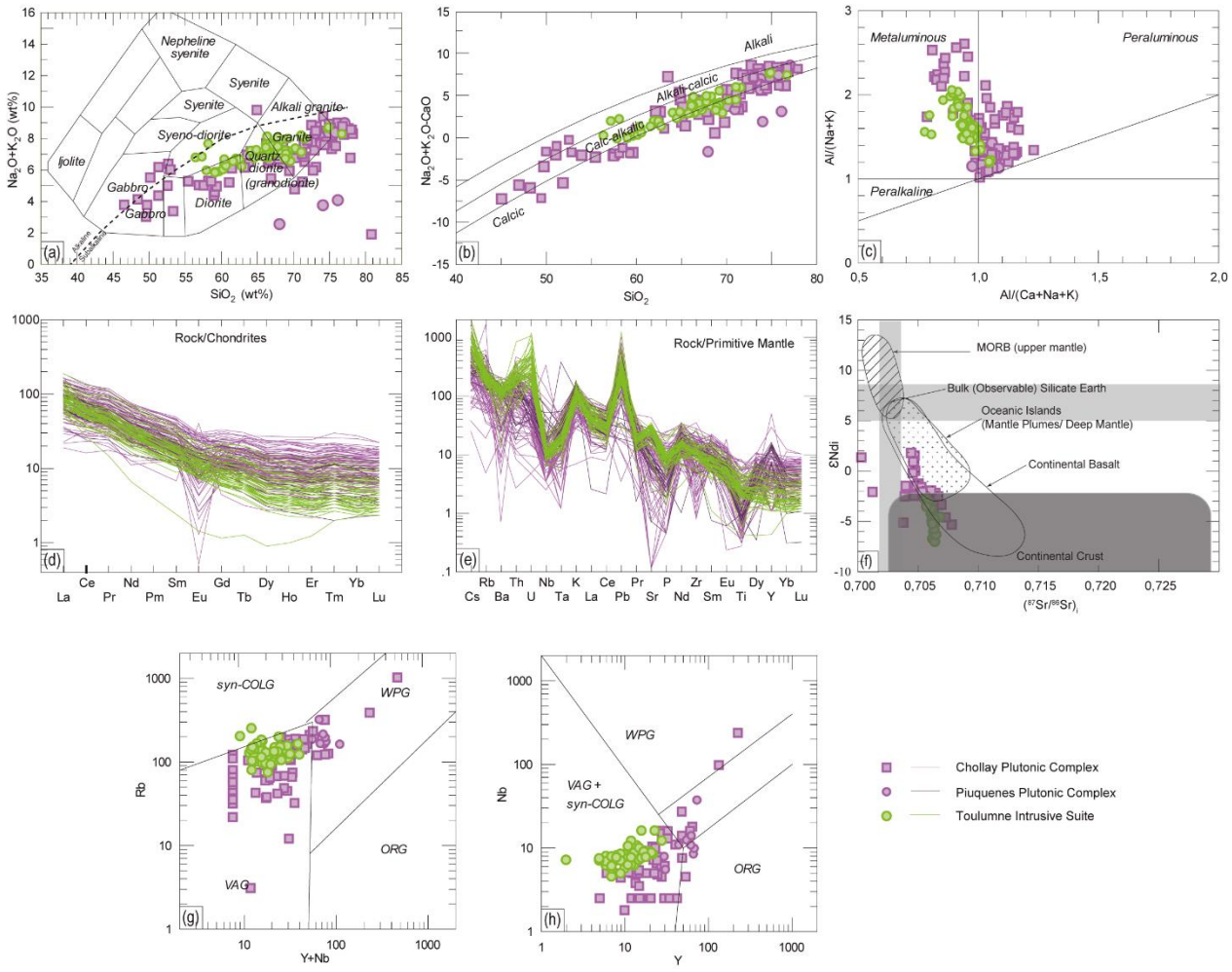

Figure 3.11. Geochemical comparison between Chollay and Piuquenes plutonic complexes with Toulumne Intrusive Suite. (a) Total alkalis versus silica diagram for intrusive rocks (Cox et al., 1979 adapted by Wilson, 1989). (b) MALI vs SiO_2, boundaries between calcic, calc-alkalic, alkali-calcic and alkalic granitoids from (Frost et al., 2001). (c) Diagram of the aluminium saturation index for plutonic rocks (Shand, 1927). (d) Rare Earth Elements diagrams normalized to chondrite (Nakamura, 1974). (e) Multi-element diagrams normalized to the primitive mantle (Sun and McDonough, 1989). (f) εNd_i versus $^{87}Sr/^{86}Sr_i$ diagram including the isotopic composition of mid-ocean ridge basalt (MORB) and the Bulk Silicate Earth, mantle plumes, continental basalt and continental crust (White, 2013; Workman and Hart, 2005). (g) Rb versus Yb + Ta tectonic discrimination diagram for granitic rocks (Pearce et al., 1984), the fields correspond to: ocean ridge granites (ORG), volcanic arc granites (VAG), within plate granites (WPG) and syn-collision granites (syn-COLG). (h) Nb versus Y tectonic discrimination diagram for granitic rocks (Pearce et al., 1984). The geochemical data from CPC and PPC are from this work and from (Mpodozis and Kay, 1992; Murillo et al., 2017; Oliveros et al., 2020; Ortiz and Merino, 2015; Salazar et al., 2013; Salazar and Coloma, 2016; Velásquez et al., 2021); and geochemical data from TIS are those published by Gray et al. (2008).

of the samples described varies between 0 - 46%, without following a defined spatial distribution.

The TIS whole-rock geochemistry indicates that the granitoids cover a wide compositional range from diorites to granites with a predominance of granodiorites, all subalkaline (Fig. 3.11a), which follow a calc-alkaline trend (Fig. 3.11b) and are mainly metaluminous and slightly peraluminous (Fig. 3.11c). In the case of the Chollay and Piuquenes complexes, the compositions range from gabbros to granites, with a predominance of granites, almost all subalkaline, which also follow a calc-alkaline differentiation trend and are mainly peraluminous and to a lesser extent metaluminous. As in the Chollay and Piuquenes plutonic complexes, in the TIS it is possible to identify an enrichment in the LREE in relation to the HREE. However, in the TIS the ratios $(La/Yb)_N$ reach higher values, and the Eu anomalies present at most of the samples of the Chollay and Piuquenes Plutonic Complexes, are not identified (Fig. 3.11d). Within the TIS samples, an enrichment of LILE is also recognized in relation to HFSE, depressions in Nb-Ta and an enrichment in Pb, as in the Chollay and Piuquenes plutonic complexes; but the depressions in Sr, P and Ti, despite being present in the TIS samples, are less pronounced than in those of the CPC and PPC (Fig. 3.11e).

The initial $^{87}Sr/^{86}Sr$ ratios calculated for the TIS are between 0.7056 – 0.7068 (Gray et al., 2008), presenting a narrower range than the CPC (0.7037 - 0.7083). The εNd_i values within the TIS are in the range between -7.13 and -2.92, while in the case of the CPC they are between -5.32 and 1.80 (Fig. 3.11f). On the other hand, TIS shows an increase in the $^{87}Sr/^{86}Sr_i$ ratio and a decrease in εNd_i from the margins of the suite towards its centre (Gray et al., 2008), which is not observed within the Chollay Plutonic Complex (Fig. 3.2.c).

The geochemical signals shared by the TIS rocks and those of the Chollay and Piuquenes plutonic complexes are typical of the magmas generated in convergent margins. Their differences are found mainly in the patterns linked to crustal thickness (eg. La_N/Yb_N) indicating a greater crustal thickness for the rocks that make up the TIS and a lesser thickness for those that form part of the Lower – Middle Triassic magmatic belt of the Frontal Cordillera. This is also evidenced in the proportion of the most

evolved component (crust) in the genesis of the magmas, being more abundant in the rocks that make up the TIS. In the tectonic discrimination diagrams, it is possible to recognize that the samples that make up the TIS are located almost exclusively in the VAG field, while the rocks of the Chollay and Piuquenes plutonic complexes are preferably in the VAG field, but some of them go to the field of the WPG (Fig. 3.11g, h).

3.5.3 The Lower - Middle Triassic belt as an example of a magmatism created on a retreating margin

The southwestern margin of Pangea or South America was a probably active margin from the Carboniferous to the Present (del Rey et al., 2016, 2019; Oliveros et al., 2020; Vásquez et al., 2011). Between the Carboniferous and the Jurassic there have been important geotectonic changes, associated with modifications in the geometry of the subduction zone, that allow defining the three evolution phases of the margin where The Andes are subsequently built: Gondwanan (Carboniferous – Early Permian), Pre-Andean (Middle Permian to Late Triassic) and Andean (Jurassic – Present) cycles (Hervé et al., 2014; Oliveros et al., 2020; Rossel et al., 2013). These changes are reflected in the geochemistry and isotopy of Carboniferous-Jurassic igneous rocks exposed along the margin (del Rey et al., 2019, 2016; Hervé et al., 2014; Maksaev et al., 2014). Specifically, between 18 - 40°S in Chile and Argentina, a continuous record of igneous rocks is recognized that has been extensively studied and in which common characteristics are observed that confirm that subduction was an active process (such as subalkaline affinities, the enrichment in LILE vs HFSE, depressions in Nb-Ta, lithologies rich in hornblende and biotite, porphyritic textures, among others, Oliveros et al., 2020). In turn, it is possible to detect variations that roughly suggest that crustal thickness increases from the Carboniferous to the Lower Permian (ca. 275 Ma, San Rafael Orogeny) and then decreases, generally until the Jurassic (decrease in the La_N/Yb_N and Sr/Y ratios, Oliveros et al., 2020). In addition, and consequently, it has been possible to visualize that the contribution of the crustal source decreases as time progresses and the component of a depressed mantle increases (decrease in the initial ratios of $^{87}Sr/^{86}Sr_i$ and increase in εNd_i, Oliveros et al., 2020; decreases $d^{18}O$, Deckart et al., 2014; del Rey et al., 2016, 2019; Hervé et al., 2014). Recent plate configuration

models reaffirm that the southwestern margin of Pangea was an active margin at least from the Late Carboniferous to the Late Jurassic (Riel et al., 2018; Young et al., 2019).

During the Gondwanan Cycle a compressive tectonic is developed in the upper crust, that changes to a transtensional style towards the Pre-Andean Cycle, after the San Rafael orogeny (ca. 285 Ma, Sato et al., 2015) a change triggered by a possible steepening and roll-back of the slab (del Rey et al., 2019, 2016; Oliveros et al., 2020). During Permian Pre-Andean Cycle the magmatism of Choiyoi Magmatic Province was generated, which has been traditionally interpreted as the result of extensive crustal melting associated with a continental rift process (Kleiman & Japas, 2009; Llambías & Sato, 1995; Mpodozis & Kay, 1992). However, it has now been recognized that this magmatism does not present a bimodal compositional distribution (basalt-rhyolite), but rather a predominance of rhyolites, followed by dacites whose volume is like that of basalts and basaltic andesites (Oliveros et al., 2020). In addition, it displays geochemical signatures typical of a magmatism generated in a process of active subduction (Bastías-Mercado et al., 2020; Oliveros et al., 2020). According to new plate reconstruction models, during the Lower Triassic – Middle Triassic (ca. 250-230 Ma;), occurred a change in the tectonic configuration where South America begins to move towards the SW (before it did towards the NE) meanwhile Panthalassa remains practically static with a slight displacement to the E (Young et al., 2019), generating a retreat of the trench in a context of active subduction, that is, a retreating margin. It is in this time span, in which important basins related to subduction located in the forearc (San Félix basin, Salazar et al. (2020)) or in the back-arc (Domeyko basin, Espinoza et al. (2019)) develop, contemporaneous to the emplacement of the Chollay and Piuquenes Plutonic Complexes.

According to the data presented in this work, the rocks that make up the Chollay and Piuquenes plutonic complexes corresponds to rocks whose compositions range from diorites to granites, with hololeucocratic to leucocratic monzogranites and granodiorites representing approximately 65% of analysed samples. The recognized mafic minerals correspond mainly to calcic amphiboles and biotite, although few clinopyroxenes and orthopyroxenes were also observed in some diorites and quartz monzodiorites of CPC.

In the case of PPC, only biotite was recognized as mafic mineral. The whole-rock chemistry of analysed samples shows that they are mainly subalkaline, and preferably calcoalkaline to alkaline calcic, metaluminous to slightly peraluminous and are located mainly in the field of volcanic arc granites with a small percentage of samples in the field of within plate granites. Trace elements show an enrichment in LILE with respect to HFSE present in all the samples, suggesting fluid participation during the magma genesis, and ubiquitous drops in Nb-Ta, which are typical of a magmatism generated on subduction zones (Stern, 2002; Wilson, 1989). The negative Eu anomalies suggest an important role of plagioclase fractionation in magma evolution, and the REE patterns with mean La_N/Yb_N values of 9.4 and 13.3 for the Chollay and Piuquenes plutonic complexes, respectively, suggest a free garnet source. These interpretations, that suggest a thinned continental crust for the magma emplacement agree with the pressures and temperatures calculated from the hornblende and plagioclase pairs of the Chollay Plutonic Complex samples, which show an epizonal emplacement.

The geochronology indicates that the studied plutonic complexes were built incrementally between 249 – 233 Ma (Hervé et al., 2014; Maksaev et al., 2014; Ortiz and Merino, 2015; Salazar et al., 2013; Salazar and Coloma, 2016). Specifically, within the Chollay Plutonic Complex, it has been possible to identify that there is both an antitaxial growth, where xenoliths of the La Pampa Gneisses, with subvertical geometry are intercalated with subvertical plutons of the complex, as a syntaxial growth where subvertical bodies of different lithologies of CPC are intercalated without the presence of host rock, defined in the first and second strip described in the results section (Fig. 3.2.c). Despite these geometric differences, it is no possible to identify contrasts in the petrography and whole-rock elemental geochemistry of analysed samples. The whole-rock isotopy of CPC exhibits ratios of $^{87}Sr/^{86}Sr_i$ that are between 0.7038 – 0.7078 and values of εNd_i between -5.3 and +1.8, which represent a less evolved magmatism compared to the Carboniferous or Permian plutonism exposed in the Chilean Frontal Cordillera (0.705 - 0.710; Oliveros et al., 2020) for which it is inferred that the magmatism of CPC cannot derive solely from the melting of the preceding intrusive rocks, as had been proposed in the previous geotectonic model (Mpodozis and Kay, 1992), but rather requires the participation of a less evolved source, which in this case

would correspond to the depleted mantle, present in the wedge of subduction zone. Although the amount of data presented is not big enough, the isotopic composition does show a variation in spatial terms and in the area located to the W of the La Plata Fault (first strip), it has values that are more radiogenic than those found between the La Plata Fault and the Valeriano Fault (second strip), which in turn they are more radiogenic than those found east of the Valeriano Fault (Fig. 3.2c). This indicates that during the emplacement of plutons that present antitaxial growth, the crustal contribution (eg, Gneisses de La Pampa, with $^{87}Sr/^{86}Sr_i$ between 0.710 - 0.714 and εNd_i between -5.9 and -5.6, unpublished data Oliveros et al., 2022) is slightly larger compared to the areas where the emplacement is syntaxial.

The Chollay and Piuquenes plutonic complexes are representatives of a magmatism created in a convergent margin, of the retreating type, corresponding to one of the few examples currently described. The extension developed in the continental crust during this stage of the Pre-Andean Cycle, allowed the formation of important basins, such as the San Félix basin to the west of the Chollay Plutonic Complex and the basin where the volcanoclastic rocks of the Guanaco Sonso Formation were deposited, east of Chollay and Piuquenes, semi-contemporaneously with the emplacement of these complexes. CPC and PPC share similarities with the magmatism generated in converging margins of the advancing margin type, such as the predominance of subalkaline rocks with a calc-alkaline evolution trend, a broad compositional spectrum, LILE enrichment with respect to HFSE, depressions in Nb-Ta, Sr, Ti and P, Pb enrichments, the classification in the Volcanic Arc Granite fields and the presence of hydrated mafic minerals, such as biotite and amphibole (in addition to their calcic composition). However, they differ as expected in some signals that are linked to the thickness and participation of the continental crust in the genesis of magmatism, such as the inclination of the REE patterns and less evolved isotopic ratios. In general, contemporaneous intrusive and extrusive rock outcrops are unlikely to be observed simultaneously within convergent margins. However, as occurs in the case of the Chollay and Piuquenes plutonic complexes, in a retreating margin context, observing this relationship becomes more likely and this is what happens when observing

outcrops of the volcanic rocks of the Guanaco Sonso Formation exposed mainly to the east of the complexes.

3.6 Conclusions

The Lower - Middle Triassic magmatic belt, composed of the Chollay Plutonic Complex and the Piuquenes Plutonic Complex, represents an important volume of magmatism generated during the Pre-Andean Cycle exposed in the Chilean Frontal Cordillera, and is one of the few examples of a magmatism created in a convergent margin of the retreating margin type, where the continental crust was subjected to a transtensional stress that has recently been attributed to the possible steepening of the subducting plate in the Triassic of the Pre-Andean Cycle. Based on the petrographic and elemental geochemical characterization carried out in this work, it is possible to detect that this magmatism presents a subduction-related signature reflected in the broad compositional spectrum, calc-alkaline affinities, enrichment in LILE with respect to HFSE, depressions in Nb- Ta, Pb enrichments, and classification in tectonic discrimination diagrams, preferably in the field of volcanic arc granites. The shallow REE patterns, the Eu anomalies and the thermobarometric calculations suggest that the emplacement of the plutons that make up these complexes occurred in a thinned crust, which is consistent with the proposed geotectonic context. Even though there is a predominance of the most differentiated compositions, the isotopic ratios of Sr-Nd-Pb indicate that this magmatism requires the participation of a depressed mantle and a continental crust, so the melting of the continental crust is ruled out as the petrogenetic process at least for the Chollay Plutonic Complex, given that the isotopic compositions of the Paleozoic basement in which it is emplaced present more evolved isotopic ratios.

Aknowledgments

This work was supported by the FONDECYT 1120715 and the Doctoral fellowship of the National Commission for Scientific and Technological Research (Comisión Nacional de Investigación Científica y Tecnológica, CONICYT), now called the National Research and Development Agency (Agencia Nacional de Investigación y Desarrollo,

ANID), grant no. 21150502. The authors acknowledge the collaboration of Anette Meixner in preparing the samples for subsequent analysis in TIMS.

3.7 References

Álvarez, J., Mpodozis, C., Blanco-Quintero, I., García-Casco, A., Arriagada, C., Morata, D., 2013. U-Pb ages and metamorphic evolution of the La Pampa Gneisses: Implications for the evolution of the Chilenia Terrane and Permo-Triassic tectonics of north Central Chile. J South Am Earth Sci 47, 100–115. https://doi.org/10.1016/j.jsames.2013.07.001

Anderson, J.L., Smith, D.R., 1995. The effects of temperature and fO2 on the Al-in-hornblende barometer. American Mineralogist 80, 549–559.

Bartley, J.M., Coleman, D.S., Glazner, A.F., 2006. Incremental pluton emplacement by magmatic crack-seal. Trans R Soc Edinb Earth Sci 97, 383–396. https://doi.org/10.1017/S0263593300001528

Bastías-Mercado, F., González, J., Oliveros, V., 2020. Volumetric and compositional estimation of the Choiyoi Magmatic Province and its comparison with other Silicic Large Igneous Provinces. J South Am Earth Sci. https://doi.org/10.1016/j.jsames.2020.102749

Bateman, P., 1992. Plutonism in the Central Part of the Sierra Nevada Batholith, California. U.S. Geological Survey Proffesional Paper 1–194.

Bateman, P.C., Chappell, B.W., 1979. Crystallization, fractionation, and solidification of the Tuolumne Intrusive Series, Yosemite National Park, California. Geological Society of America Bulletin, Part I 90, 465–482.

Cawood, P.A., Kröner, A., Collins, W.J., Kusky, T.M., Mooney, W.D., Windley, B.F., 2009. Accretionary orogens through Earth history. Geol Soc Spec Publ 318, 1–36. https://doi.org/10.1144/SP318.1

Charrier, R., Pinto, L., Rodríguez, M.P., 2007. Tectonostratigraphic evolution of the Andean Orogen in Chile, in: Moreno, T., Gibbons, W. (Eds.), The Geology of Chile. The Geological Society, London, pp. 21–114.

Coleman, D.S., Gray, W., Glazner, A.F., 2004. Rethinking the emplacement and evolution of zoned plutons: Geochronologic evidence for incremental assembly of the Tuolumne Intrusive Suite, California. Geology 32, 433–436. https://doi.org/10.1130/G20220.1

Coloma, F., Álvarez, J., Creixell, C., Emparán, C., Salazar, E., Calderón, M., 2020. Geología de las áreas Ovalle y Peña Blanca, Región de Coquimbo. Servicio Nacional de Geología y Minería. Carta Geológica de Chile. Serie Geología Básica N°208-209. Escala 1:100.000.

Coloma, F., Valin, X., Oliveros, V., Vásquez, P., Creixell, C., Salazar, E., Ducea, M.N., 2017. Geoquímica de rocas ígneas Permo-Triásicas del norte de Chile (28°-30°15‘S): Implicancias en la dinámica del margen pre-Andino. Andean Geology 44, 147–178. https://doi.org/10.5027/andgeoV44n2-a03

Cox, K.G., Bell, J.D., Pankhurst, R.J., 1979. The Interpretation of Igneous Rocks. Springer, Netherlands.

Creixell, C., Parada, M.Á., Morata, D., Roperch, P., Arriagada, C., 2009. The genetic relationship between mafic dike swarms and plutonic reservoirs in the mesozoic of central chile (30°-33°45′S): Insights from AMS and geochemistry. International Journal of Earth Sciences 98, 177–201. https://doi.org/10.1007/s00531-007-0240-9

Dahlquist, J.A., Morales Cámera, M.M., Alasino, P.H., Pankhurst, R.J., Basei, M.A.S., Rapela, C.W., Moreno, J.A., Baldo, E.G., Galindo, C., 2021. A review of Devonian–Carboniferous magmatism in the central region of Argentina, pre-Andean margin of SW Gondwana. Earth Sci Rev. https://doi.org/10.1016/j.earscirev.2021.103781

Deckart, K., Hervé, F., Fanning, C.M., Ramírez, V., Calderón, M., Godoy, E., 2014. Geocronología U-Pb e isótopos de Hf-O en circones del batolito de la Costa Pensilvaniana, Chile. Andean Geology 41, 49–82. https://doi.org/10.5027/andgeoV41n1-a03

del Rey, A., Deckart, K., Arriagada, C., Martínez, F., 2016. Resolving the paradigm of the late Paleozoic–Triassic Chilean magmatism: Isotopic approach. Gondwana Research 37, 172–181. https://doi.org/10.1016/j.gr.2016.06.008

del Rey, A., Deckart, K., Planavsky, N., Arriagada, C., Martínez, F., 2019. Tectonic evolution of the southwestern margin of Pangea and its global implications: Evidence from the mid Permian–Triassic magmatism along the Chilean-Argentine border. Gondwana Research 76, 303–321. https://doi.org/10.1016/j.gr.2019.05.007

Espinoza, M., Montecino, D., Oliveros, V., Astudillo, N., Vásquez, P., Reyes, R., Celis, C., González, R., Contreras, J., Creixell, C., Martínez, A., 2019. The synrift phase of the early Domeyko Basin (Triassic, northern Chile): Sedimentary, volcanic, and tectonic interplay in the evolution of an ancient subduction-related rift basin. Basin Research 31, 4–32. https://doi.org/10.1111/bre.12305

Frost, B.R., Barnes, C.G., Collins, W.J., Arculus, R.J., Ellis, D.J., Frost, C.D., 2001. A Geochemical Classification for Granitic Rocks. Journal of Petrology 42, 2033–2048.

Frost, B.R., Frost, C.D., 2008. A Geochemical Classification for Feldspathic Igneous Rocks. Journal of Petrology 49, 1955–1969. https://doi.org/10.1093/petrology/egn054

Gana, P., 1991. Magmatismo bimodal del Triásico Superior - Jurásico Inferior en la Cordillera de la Costa, Provincias de Elqui y Limarí, Chile. Revista Geológica de Chile 18, 55–67.

Gianni, G.M., Navarrete, C.R., 2022. Catastrophic slab loss in southwestern Pangea preserved in the mantle and igneous record. Nat Commun 13. https://doi.org/10.1038/s41467-022-28290-z

González, J., Oliveros, V., Creixell, C., Velásquez, R., Vásquez, P., Lucassen, F., 2018. The Triassic magmatism and its relation with the Pre-Andean tectonic evolution: Geochemical and petrographic constrains from the High Andes of north central Chile (29°30′ – 30°S). J South Am Earth Sci 87, 95–112. https://doi.org/10.1016/j.jsames.2017.12.009

Gray, W., Glazner, A.F., Coleman, D.S., Bartley, J.M., 2008. Long-term geochemical variability of the Late Cretaceous Tuolumne Intrusive Suite, central Sierra Nevada, California. Geol Soc Spec Publ 304, 183–201. https://doi.org/10.1144/SP304.10

Hawthorne, F.C., Oberti, R., Harlow, G.E., Maresch, W. v., Martin, R.F., Schumacher, J.C., Welch, M.D., 2012. IMA Report: Nomenclature of the amphibole supergroup. American Mineralogist 97, 2031–2048. https://doi.org/10.2138/am.2012.4276

Heredia, N., Rodríguez Fernández, L.R., Gallastegui, G., Busquets, P., Colombo, F., 2002. Geological setting of the Argentine Frontal Cordillera in the flat-slab segment (30°00'S - 31°30'S latitude). J South Am Earth Sci 15, 79–99.

Hervé, F., Fanning, C.M., Calderón, M., Mpodozis, C., 2014. Early Permian to Late Triassic batholiths of the Chilean Frontal Cordillera (28°-31°S): SHRIMP U-Pb zircon ages and Lu-Hf and O isotope systematics. Lithos 184–187, 436–446. https://doi.org/10.1016/j.lithos.2013.10.018

Holland, T., Blundy, J., 1994. Non-ideal interactions in calcic amphiboles and their bearing on amphibole-plagioclase thermometry. Contributions to Mineralogy and Petrology 116, 433–447. https://doi.org/10.1007/BF00310910

Irvine, T.N., Baragar, W.R.A., 1971. A Guide to the Chemical Classification of the Common Volcanic Rocks. Can J Earth Sci 8, 523–548.

Kleiman, L.E., Japas, M.S., 2009. The Choiyoi volcanic province at 34°S-36°S (San Rafael, Mendoza, Argentina): Implications for the Late Palaeozoic evolution of the southwestern margin of Gondwana. Tectonophysics 473, 283–299. https://doi.org/10.1016/j.tecto.2009.02.046

Leake, B., 1978. Nomenclature of amphiboles. American Mineralogist 63, 1023–1052.

Llambías, E.J., Sato, A.M., 1995. El batolito de Colangüil: transición entre orogénesis y anorogénesis. Revista de la Asociación Geológica Argentina 50, 111–131.

Maksaev, V., Munizaga, F., Tassinari, C., 2014. Timing of the magmatism of the paleo-pacific border of Gondwana: U-Pb geochronology of Late Paleozoic to Early Mesozoic igneous rocks of the north Chilean Andes between 20° and 31°S. Andean Geology 41, 447–506. https://doi.org/10.5027/andgeoV41n3-a01

Martin, M.W., Clavero, J.R., Mpodozis, C.M., 1999. Late Paleozoic to Early Jurassic tectonic development of the high Andean Principal Cordillera, El Indio Region, Chile (29-30°S). J South Am Earth Sci 12, 33–49.

Matzel, J., Mundil, R., Paterson, S., Renne, P., Nomade, S., 2005. Evaluating Pluton Growth Models using High Resolution Geochronology: Tuolumne Intrusive Suite, Sierra Nevada, California. Geological Society of America Abstracts with Programs, 37, 1–131.

Molina, P.G., Parada, M.A., Ma, C., 2020. Zircon inheritance from long-lived sources of Late Triassic post-orogenic plutons, High Andes, Central Chile (~30°S): Magmatic feedbacks and petrogenetic implications. Lithos 370–371, 1–19. https://doi.org/10.1016/j.lithos.2020.105662

Mpodozis, C., Kay, S., 1992. Late Paleozoic to Triassic evolution of the Gondwana margin: Evidence from Chilean Frontal Cordilleran batholiths (28°S to 31°S). Geol Soc Am Bull 104, 999–1014.

Murillo I, Álvarez J, Montecinos P, Creixell C, Salazar E, Arriagada C, 2013. Geochronology and kinematics of the El Portillo Mylonites: relation with San Rafael Orogeny and Middle Triassic extension in North-Central Chile, in: GeoSur2013. p. 83.

Murillo, I., Velásquez, R., Creixell, C., 2017. Geología de las áreas Guanta - Los Cuartitos y Paso de Vacas Heladas, Regiones de Atacama y Coquimbo. Servicio Nacional de Geología y Minería. Carta Geológica de Chile. Serie Geología Básica N°192-193. Escala 1:100.000.

Mutch, E.J.F., Blundy, J.D., Tattitch, B.C., Cooper, F.J., Brooker, R.A., 2016. An experimental study of amphibole stability in low-pressure granitic magmas and a revised Al-in-hornblende geobarometer. Contributions to Mineralogy and Petrology 171. https://doi.org/10.1007/s00410-016-1298-9

Nakamura, R., 1974. Determination of REE, Ba, Fe, Mg, Na and K in carbonaceous and ordinary chondrites. Geochim Cosmochim Acta 88, 757–775.

Nasi, C., Moscoso, R., Maksaev, V., 1990. Hoja Guanta, Región de Coquimbo. Servicio Nacional de Geología y Minería. Carta Geológica de Chile N°67. Escala 1:250.000.

Nasi, C., Mpodozis, C., Cornejo, P., Moscoso, R., Maksaev, V., 1985. El Batolito Elqui-Limarí (Paleozoico Superior – triásico): características petrográficas, geoquímicas y significado tectónico. Revista Geológica de Chile 77–111.

Oliveros, V., Vásquez, P., Creixell, C., Lucassen, F., Ducea, M.N., Ciocca, I., González, J., Espinoza, M., Salazar, E., Coloma, F., Kasemann, S.A., 2020. Lithospheric evolution of the Pre- and Early Andean convergent margin, Chile. Gondwana Research. https://doi.org/10.1016/j.gr.2019.11.002

Ortiz, M., Merino, R., 2015. Geología de las áreas Río Chollay - Matancilla y Cajón del Encierro, Regiones de Atacama y Coquimbo. Servicio Nacional de Geología y

Minería. Carta Geológica de Chile. Serie Geología Básica N°175-176. Escala 1:100.000.

Parada, M.A., 1990. Granitoid plutonism in central Chile and its geodynamic implications; A review, in: Kay, S., Rapela, C. (Eds.), Plutonism from Antarctica to Alaska. Geological Society of America, Colorado, pp. 51–66.

Parada, M.A., Levi, B., Nystrom, J.O., 1991. Geochemistry of the Triassic to Jurassic plutonism of central Chile (30 to 33°S); Petrogenetic implications and a tectonic discussion, in: Harmon, R., Rapela, C. (Eds.), Andean Magmatism and Its Tectonic Setting. Geological Society of America, Colorado, pp. 99–112.

Parada, M.A., Nystrom, J.O., Levi, B., 1999. Multiple sources for the Coastal Batholith of central Chile (31-34°S): geochemical and Sr-Nd isotopic evidence and tectonic implications. Lithos 46, 505–521.

Pearce, J.A., Harris, N.B.W., Tindle, A.G., 1984. Trace Element Discrimination Diagrams for the Tectonic Interpretation of Granitic Rocks. Journal of Petrology 25, 956–983.

Petford, N., Cruden, A.R., McCaffrey, K.J.W., Vigneresse, J.-L., 2000. Granite magma formation, transport and emplacement in the Earth's crust. Nature 408, 669–673.

Poma, S., Zappettini, E.O., Quenardelle, S., Santos, J.O., Koukharsky, M., Belousova, E., McNaughton, N., 2014. Geoquímica, dataciones U-Pb SHRIMP sobre circón e isótopos de Hf del magmatismo gondwánico en el NW de Argentina: Petrogénesis e implicancias geodinámicas. Andean Geology 41, 267–292. https://doi.org/10.5027/andgeoV41n2-a01

Profeta, L., Ducea, M.N., Chapman, J.B., Paterson, S.R., Gonzales, S.M.H., Kirsch, M., Petrescu, L., DeCelles, P.G., 2015. Quantifying crustal thickness over time in magmatic arcs, Scientific Reports. Nature Publishing Group. https://doi.org/10.1038/srep17786

Ramos, V.A., Jordan, T.E., Allmendinger, R.W., Mpodozis, C., Kay, S.M., Cortes, J.M., Palma, M., 1986. Paleozoic terranes of the Central Argentine-Chilean Andes. Tectonics 5, 855–880.

Ribba, L., 1985. Geología regional del Cuadrángulo El Tránsito, Región de Atacama, Chile (Memoria de Título). Universidad de Chile, Santiago.

Riel, N., Jaillard, E., Martelat, J.E., Guillot, S., Braun, J., 2018. Permian-Triassic Tethyan realm reorganization: Implications for the outward Pangea margin. J South Am Earth Sci 81, 78–86. https://doi.org/10.1016/j.jsames.2017.11.007

Rocher, S., Vallecillo, G., Castro de Machuca, B., Alasino, P., 2015. El Grupo Choiyoi (Pérmico temprano-medio) en la Cordillera Frontal de Calingasta, San Juan, Argentina: volcanismo de arco asociado a extensión. Revista Mexicana de Ciencias Geológicas 32, 415–432.

Rossel, P., Oliveros, V., Ducea, M.N., Charrier, R., Scaillet, S., Retamal, L., Figueroa, O., 2013. The Early Andean subduction system as an analog to island arcs: Evidence from across-arc geochemical variations in northern Chile. Lithos 179, 211–230. https://doi.org/10.1016/j.lithos.2013.08.014

Salazar, E., Coloma, F., 2016. Geología del área Cerros de Cantaritos-Laguna Chica, Región de Atacama. Servicio Nacional de Geología y Minería. Carta Geológica de Chile. Serie Geología Básica N°181. Escala 1:100.000.

Salazar, E., Coloma, F., Creixell, C., 2013. Geología del área El Tránsito-Lagunillas, Región de Atacama. Servicio Nacional de Geología y Minería. Carta Geológica de Chile. Serie Geología Básica N°149. Escala 1:100.000.

Salazar, E., Vásquez, P., Vallejos, D., Creixell, C., Oliveros, V., Ducea, M.N., 2020. Stratigraphic and provenance analysis of triassic rock units between 28-29° S, Northern Chile: Implications on the tectonic and paleogeographic evolution of the southwestern margin of Gondwana. Andean Geology 47, 207–255. https://doi.org/10.5027/andgeov47n2-3118

Saleeby, J.B., Ducea, M.N., Busby, C.J., Nadin, E.S., Wetmore, P.H., 2008. Chronology of pluton emplacement and regional deformation in the southern Sierra Nevada batholith, California. Special Paper of the Geological Society of America 438, 397–427. https://doi.org/10.1130/2008.2438(14)

Sato, A.M., Llambías, E.J., Basei, M.A.S., Castro, C.E., 2015. Three stages in the Late Paleozoic to Triassic magmatism of southwestern Gondwana, and the relationships with the volcanogenic events in coeval basins. J South Am Earth Sci. https://doi.org/10.1016/j.jsames.2015.07.005

Schmidt, M.W., 1992. Contributions to Mineralogy and Petrology Amphibole composition in tonalite as a function of pressure: an experimental calibration of the Al-in-hornblende barometer. Contributions to Mineralogy and Petrology 110, 304–310.

Schwartz, J.J., Johnson, K., Mueller, P., Valley, J., Strickland, A., Wooden, J.L., 2014. Time scales and processes of Cordilleran batholith construction and high-Sr/Y magmatic pulses: Evidence from the Bald Mountain batholith, northeastern Oregon. Geosphere 10, 1456–1481. https://doi.org/10.1130/GES01033.1

Shand, S., 1927. On the Relations between Silica, Alumina, and the Bases in Eruptive Rocks, considered as a Means of Classification. Geol Mag 64, 446–449. https://doi.org/https://doi.org/10.1017/S0016756800103760

Stern, R.J., 2002. Subduction zones. Reviews of Geophysics 40, 3-1-3–38. https://doi.org/10.1029/2001RG000108

Streckeisen, A., 1976. To each plutonic rock its proper name. Earth Sci Rev 12, 1–33.

Sun, S.S., McDonough, W.F., 1989. Chemical and isotopic systematics of oceanic basalts: Implications for mantle composition and processes. Geol Soc Spec Publ 42, 313–345. https://doi.org/10.1144/GSL.SP.1989.042.01.19

Tomlinson, A.J., Blanco, N., García, M., Baeza, L., Alcota, H., Ladino, M., Pérez De Arce, C., Fanning, C.M., Martin, M.W., 2012. Permian Exhumation of

Metamorphic Complexes in the Calama Area: Evidence for Flat-Slab Subduction in Northern Chile During the San Rafael Tectonic Phase and origin of the Central Andean Gravity High, in: XIII Congreso Geológico Chileno. pp. 209–211.

Uribe, Y., Ortiz, M., Velásquez, R., 2020. Termobarometría de las unidades plutónicas del Carbonífero - Triásico de la Cordillera Frontal del Norte Chico, Chile: Aplicación al Complejo Plutónico Guanta (29°45'S). Servicio Nacional de Geología y Minería, Informe Registrado IR-20-81: 75p. Santiago.

Vásquez, P., Glodny, J., Franz, G., Frei, D., Romer, R.L., 2011. Early Mesozoic plutonism of the Cordillera de la Costa (34°-37°S), Chile: Constraints on the onset of the Andean Orogeny. Journal of Geology 119, 159–184. https://doi.org/10.1086/658296

Velásquez, R., Coloma, F., Murillo, I., Merino, R., Ortiz, M., 2021. Geología de las áreas Pisco Elqui y Paso del Agua Negra. Servicio Nacional de Geología y Minería. Carta Geológica de Chile. Serie Geología Básica N°211-212. Escala 1:100.000.

Vilas, J.F.A., Valencio, D.A., 1978. Palaeomagnetism of South American and African rocks and the age of the South Atlantic. Revista Brasileira de Geociências 8, 3–10.

White, W., 2013. Geochemistry. Wiley-Blackwell.

Willner, A.P., Gerdes, A., Massonne, H.J., Schmidt, A., Sudo, M., Thomson, S.N., Vujovich, G., 2011. The geodynamics of collision of a microplate (Chilenia) in Devonian times deduced by the pressure-temperature-time evolution within part of a collisional belt (Guarguaraz Complex, W-Argentina). Contributions to Mineralogy and Petrology 162, 303–327. https://doi.org/10.1007/s00410-010-0598-8

Wilson, M., 1989. Igneous Petrogenesis A global tectonic approach. Springer, Dordrecht.

Workman, R., Hart, S., 2005. Major and trace element composition of the depleted MORB mantle (DMM). Earth Planet Sci Lett 231, 53–72. https://doi.org/10.1016/j.epsl.2004.12.005

Young, A., Flament, N., Maloney, K., Williams, S., Matthews, K., Zahirovic, S., Müller, R.D., 2019. Global kinematics of tectonic plates and subduction zones since the late Paleozoic Era. Geoscience Frontiers 10, 989–1013. https://doi.org/10.1016/j.gsf.2018.05.011

Žák, J., Paterson, S.R., Memeti, V., 2007. Four magmatic fabrics in the Tuolumne batholith, central Sierra Nevada, California (USA): Implications for interpreting fabric patterns in plutons and evolution of magma chambers in the upper crust. Bulletin of the Geological Society of America 119, 184–201. https://doi.org/10.1130/B25773.1

Zindler, A., Hart, S., 1986. Chemical Geodynamics. Ann. Rev. Earth Planet. Sci 14, 493–571.

CAPÍTULO IV: MAGMATISMO DEL TRIÁSICO SUPERIOR

Manuscript title: The Triassic magmatism and its relation with the Pre-Andean tectonic evolution: Geochemical and petrographic constrains from the High Andes of north central Chile (29°30′ – 30°S).

Authors: Javiera González[1], Verónica Oliveros[1], Christian Creixell[2], Ricardo Velásquez[2], Paulina Vásquez[2]; Friedrich Lucassen[3]

[1] Departamento Ciencias de la Tierra, Universidad de Concepción, Casilla 160-C, Concepción, Chile.

[2] Servicio Nacional de Geología y Minería, Av. Santa María 104, Santiago, Chile.

[3] MARUM Center for Marine Environmental Sciences, University of Bremen, Leobener Strasse, D-28359, Bremen, Germany

Published as: González, J.; Oliveros, V.; Creixell, C.; Velásquez, R.; Vásquez, P.; Lucassen, F. (2018). The Triassic magmatism and its relation with the Pre-Andean tectonic evolution: Geochemical and petrographic constrains from the High Andes of north central Chile (29°30′ – 30°S), Journal of South American Earth Sciences ,87: 95-112.

Abstract

The western border of South America has been an intermittently active convergent margin since the late Paleozoic, with the recognition of two major orogenic stages: Gondwanian (Early Carboniferous –Early Permian) and Andean (Early Jurassic–Recent), which differ in dominant tectonic regime, magmatism affinities and composition, and inferred crustal thickness. The time span between these stages, known as the Pre-Andean cycle, coincides with the period when the continental drift of Gondwana declined. Arrested subduction and the development of a continental rift along the southwestern margin of Gondwana has been suggested for this stage. However, new petrographic and geochemical data from the Upper Triassic (Carnian – Norian) magmatism exposed between 29°30′ – 30°S in the Chilean High Andes do not support this geotectonic scenario. The Upper Triassic rocks show features that are typical of a magmatism generated by the melting of an asthenospheric mantle triggered by fluids derived from dehydration of the subducted slab, including a broad and continuous compositional range, calc-alkaline differentiation trends, enrichment of LILE in relation to HFSE, and negative anomalies of Nb-Ta, and Ti. The less evolved isotopic composition of the Upper Triassic magmatism compared to the Paleozoic crust, suggests that the studied magmatism could not have been generated exclusively by crustal anatexis, as has been interpreted previously, and that requires a mixture with a more depleted source, hydrated and with a high LILE content. Subduction-related magmatism with similar characteristics is described for the Late Permian to Middle Triassic period in the studied area, which argues against the hypothesis of arrested subduction during the Pre-Andean cycle. Our data indicate that subduction was an active process at least in this segment of the southwestern margin of Gondwana during the Pre-Andean cycle.

Keywords: Subduction; Sr-Nd-Pb isotopes; Pre-Andean cycle; SW-Gondwana

4.1 Introduction

The Lopingian – late Early Jurassic period in SW Gondwana, known as the Pre-Andean cycle (Charrier et al., 2014), is a controversial stage concerning its geotectonic setting within the evolution of the proto-Andean margin. This stage was developed between the final Gondwana assembly and the beginning of its breakup, during which the supercontinent was in quasi-static reference mode (Vilas and Valencio, 1978, Charrier et al., 2014). The Pre-Andean cycle is defined as the transition between two orogenic stages recognized in northern Chile and Argentina: The Gondwanian and Andean cycles, which differ in terms of dominant tectonic regime, magmatic composition and affinities and inferred crustal thickness (Mpodozis and Ramos, 1989, Franzese and Spalletti, 2001, Charrier et al., 2014). The Gondwanian Cycle (Early Carboniferous - Early Permian; 360–260 Ma) developed during a period of high convergence rates at the active southwestern margin of the supercontinent (Vilas and Valencio, 1978), which resulted in a magmatic arc now exposed in the Chilean and Argentinian Frontal Cordillera, between 21°S and 31°S and in the Coastal Cordillera to the south (33°S–38°S). The Gondwanian arc is represented by mainly intermediate to acidic rocks with subduction-related chemical signatures and an inferred source in the depleted mantle source that assimilated ancient radiogenic crust (Mpodozis and Kay, 1992, Hervé et al., 2014, Oliveros et al., 2016). The Andean Cycle (late Early Jurassic – Present) started with an early stage of oblique convergence and extensional/transtensional tectonic setting that produced homogeneous basaltic-andesitic arc magmatism in the current Coastal Cordillera, sourced in a similarly depleted mantle but with small to negligible contributions from a thin continental crust (Kramer et al., 2005, Lucassen et al., 2006, Oliveros et al., 2007, Oliveros et al., 2017). Towards the end of the Mesozoic the style changed to a compressive tectonic deformation along the overriding plate, and the arc progressively migrated eastward to its current position (Coira et al., 1982, Arriagada et al., 2006).

The Permian – Triassic magmatism is exceptionally well exposed along the Chilean Frontal Cordillera (28°S - 31°S). The Pre-Andean cycle has been traditionally considered as a stage during which the subduction along the Andean margin was

interrupted or at least diminished, as has been inferred from field, petrological, geochemical, geochronological and isotopic data from batholiths exposed in this zone (Kay et al., 1989, Mpodozis and Kay, 1992). The Pre-Andean cycle started after the San Rafael Orogeny, a strong deformation stage developed during the Early Permian (Sato et al., 2015) which has been attributed to the accretion of an allochthonous crustal block (Mpodozis and Kay, 1992). This accretion would have triggered the detachment of the subducted slab and the collapse of the collisional orogen, allowing the upper mantle ascent. Mafic magma ponding and heat accumulation at the base of the crust, led to extensive crustal melting which resulted in: a huge volume of silicic magmatism widely distributed along the Andes (Kay et al., 1989, Mpodozis and Kay, 1990) and the development of continental rift extensional basins (Mpodozis and Ramos, 1989, Mpodozis and Kay, 1990, Suárez and Bell, 1992). This voluminous magmatism is locally known as the “Choiyoi Province” (Nasi et al., 1985, Mpodozis and Cornejo, 1988, Charrier et al., 2007) and represented by several lithological units of silicic volcanic rocks and associated subvolcanic-intrusive bodies (Kay et al., 1989, Kleiman and Japas, 2009, Sato et al., 2015). The Choiyoi magmatism in Chile and Argentina exhibits a transition from calc-alkaline affinities and intermediate to rhyolitic compositions, to calc-alkaline – alkaline affinities and bimodal basaltic – rhyolitic compositions, which has been interpreted as evolution from subduction-related to intraplate anorogenic tectonic setting (Kay et al., 1989, Mpodozis and Kay, 1992, Llambías and Sato, 1995, Kleiman and Japas, 2009).

The interruption of plate convergence during the Pre-Andean cycle has been recently questioned by studies concerning the origin of the Carboniferous to Jurassic magmatism exposed in the Coastal, Domeyko, Frontal and Principal Cordilleras of northern Chile. On the one hand, new geochronological data (e.g. zircon U-Pb ages) have shown that the magmatism is continuous since Carboniferous, without a magmatic lull during the Pre-Andean cycle (Maksaev et al., 2014, Hervé et al., 2014). On the other hand, the petrography, geochemistry and isotopic composition of this magmatism show progressive changes over time, but with dominant subduction-related features, thus suggesting continuous plate convergence along the western margin of South America from Late Paleozoic to Present, with dominance of extensional tectonics

during Late Permian – Jurassic times (Vásquez et al., 2011, Poma et al., 2014, del Rey et al., 2016, Coloma et al., 2017, Oliveros et al., 2017).

In this work we present new field, petrographic, geochemical and isotopic data from Upper Triassic magmatic rocks that crop out in the Chilean Frontal Cordillera between 29°30′S and 30°S in order to determine the magma sources and assess the most likely geotectonic setting for this Andean segment. Our study relies on the new geological cartography of northern Chile developed by the National Geological and Mining Survey (SERNAGEOMIN) and focuses on the Upper Triassic volcanic and volcanosedimentary Pastos Blancos Formation, the penecontemporaneous syenogranites and monzogranitic dikes of the Colorado Syenogranites (229–214 Ma), and a coetaneous mafic dike swarm (Elqui Dike Swarm) (Thiele, 1964, Nasi et al., 1990, Martin et al., 1999, Creixell et al., 2009, Ortiz and Merino, 2015). These units are spatially and temporally related (Martin et al., 1999, Hervé et al., 2014, Ortiz and Merino, 2015), and have been proposed as equivalents of the Choiyoi Group (Nasi et al., 1985, Mpodozis and Cornejo, 1988, Charrier et al., 2007). The Upper Triassic magmatism is compared to the Lopingian – Upper Triassic igneous units cropping out at 28°30′S – 29°30′S in the High Andes (Salazar et al., 2013, Ortiz and Merino, 2015, Salazar and Coloma, 2016, Coloma et al., 2017) with the aim of evaluating changes in the composition, nature and sources of the Triassic magmatism.

4.2 Geological setting

In the Chilean Frontal Cordillera between 28°30′S and 30°S, large volumes of igneous rocks of Late Paleozoic to Early Mesozoic age are exposed, distributed in two broadly N-S parallel belts where the oldest igneous rocks are concentrated in the western belt and the youngest in the eastern belt. (Fig. 4.1).

The western belt is mainly composed of the Permian Plutonic Complexes and minor Carboniferous intrusions and volcanic rocks (Salazar et al., 2013, Ortiz and Merino, 2015). The Permian plutons intrude to Silurian – Carboniferous metamorphic units, as well as the Pennsylvanian silicic lavas of the Cerro Bayo Formation and Carboniferous plutonic bodies (Ribba et al., 1988, Salazar et al., 2013, Ortiz and Merino, 2015, Murillo et al., 2017). These Permian plutons (296–279 Ma) are coarse to medium grained

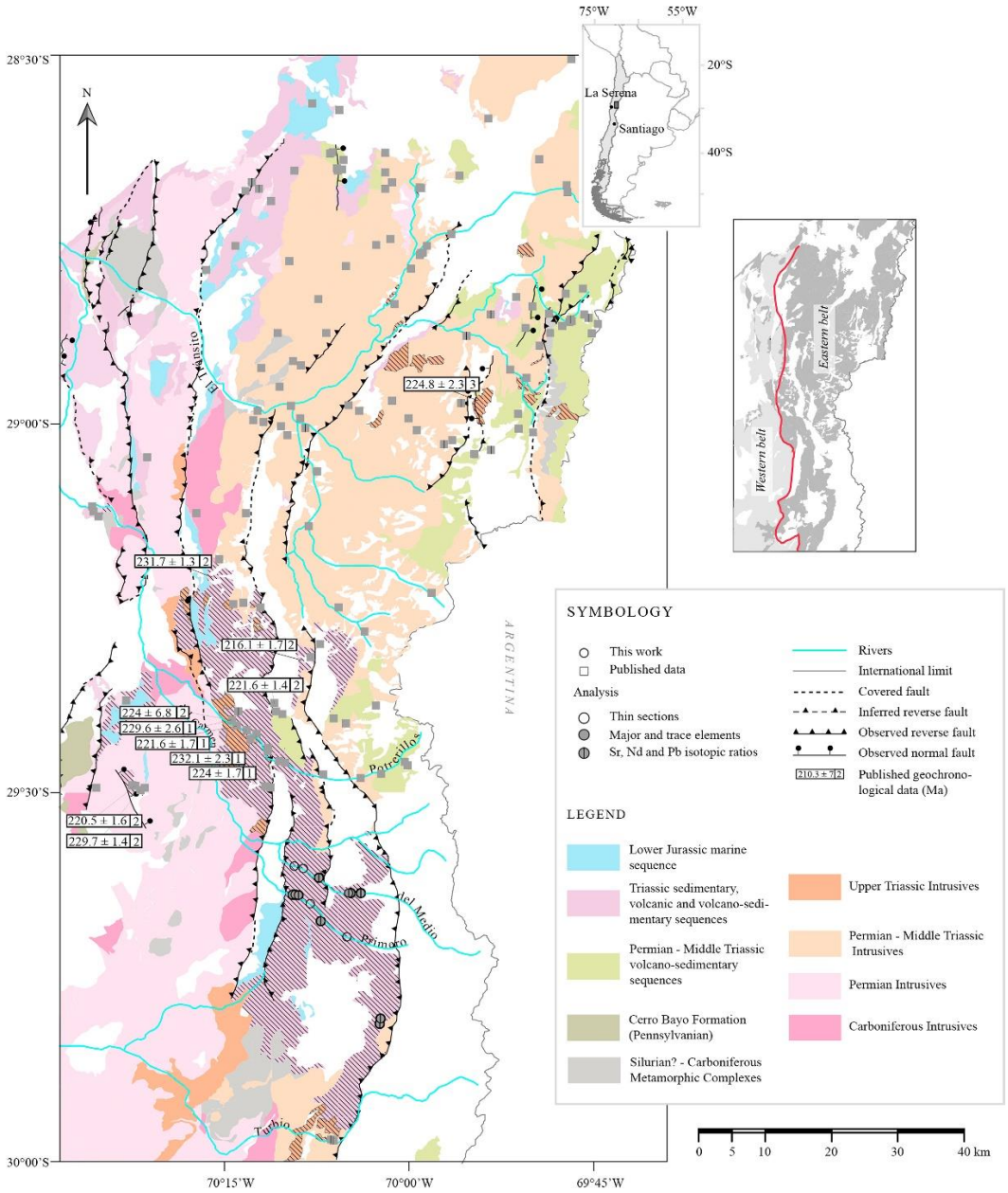

Figure 4.1. Geological map compiled of the updated geological cartography carried out by the Chilean Geology and Mining Survey (Salazar et al., 2013, Ortiz and Merino, 2015, Salazar and Coloma, 2016, Murillo et al., 2017) at Chilean High Cordillera and Precordillera, between 28°30′S and 30°S, including Middle Paleozoic to Jurassic units. The hatched polygons highlight the two units studied in this work: the Pastos Blancos Formation (purple colour) and the Colorado Syenogranites (orange colour). The published geochronological data for these units are included (1: Maksaev et al., 2014; 2: Ortiz and Merino, 2015; 3: Salazar and Coloma, 2016). The samples of this work are symbolized with circles and the samples published, with squares (Creixell et al., 2009, Salazar et al., 2013, Ortiz and Merino, 2015, Salazar and Coloma, 2016, Oliveros et al., 2016, Coloma et al., 2017). The samples with petrographic description have a black border, the filled symbols correspond to the samples with elemental geochemistry and the filled symbols with a line in the middle correspond to samples with isotopic (Sr, Nd and Pb) data. At the top right, a diagram showing the two belts of igneous rocks is shown.

biotite and amphibole tonalites, granodiorites, monzogranites, syenogranites, melanocratic diorites and two-mica granodiorites and monzogranites (Salazar et al., 2013, Ortiz and Merino, 2015, Coloma et al., 2017, Murillo et al., 2017).

The Early to Middle Triassic (249–236 Ma) Chollay Plutonic Complex (CPC) is main unit of the eastern belt between 28°20′S and 29°30′S (Salazar et al., 2013). The CPC is composed of five lithologies: a) monzogranites with scarce biotite and amphibole, b) amphibole and biotite granodiorites with minor muscovite, c) biotite and amphibole tonalites, d) diorites and gabbros with variable contents of pyroxene and olivine, and e) hornblende syenogranites (Salazar et al., 2013, Ortiz and Merino, 2015, Coloma et al., 2017). The CPC intrudes Upper Devonian? – Cisuralian quartz-feldspathic sandstones and metapelites and other Paleozoic to Mid-Permian units (Fig. 4.1). This complex also intrudes into Permian – Middle Triassic volcanic and volcanoclastic rocks: the Laguna Chica Formation (Artinskian – Wordian) composed of vitric and lithic rhyodacitic lapilli tuffs, pyroclastic breccias and minor andesites (Salazar and Coloma, 2016); and the Guanaco Sonso Formation (Lopingian – Ladinian) composed of rhyolitic-dacitic ash, lapilli tuffs and lavas with minor detritic and epiclastic rocks (Ortiz and Merino, 2015). South of 29°30′S, the Lower-Middle Triassic Intrusive units are more restricted (Murillo et al., 2017).

The Pastos Blancos Formation (236–216 Ma) comprises a stratified sequence, with a basal section of mafic lavas, pyroclastic rocks and stocks, and an upper section of rhyolitic lavas and welded rhyolitic pyroclastic rocks, that unconformably and nonconformably overlays the Laguna Chica and Guanaco Sonso formations and the CPC (Ortiz and Merino, 2015, Salazar and Coloma, 2016). This unit is spatially and temporally related to small syenogranitic and monzogranitic plutons with graphic and perthitic textures of a typical brick red colour, that intrude all the units of the eastern belt and are known as the Colorado Syenogranites (229–219 Ma) (Salazar et al., 2013, Ortiz and Merino, 2015, Salazar and Coloma, 2016). Several intermediate to felsic dikes of the same brick red colour that intruded into Pastos Blancos Formation, have been considered as part of Colorado Syenogranites as well (Martin et al., 1999).

Contemporary to the Guanaco Sonso and Pastos Blancos extrusion (i.e. Late Permian to Late Triassic), on the western edge of the Frontal Cordillera, a succession of marine and continental rocks was deposited in the extensional San Félix basin from ca. 253 Ma to 237 Ma (Salazar et al., 2013). Nonconformably over the Chollay Plutonic Complex and unconformably over the Laguna Chica and Guanaco Sonso formations rests a Norian andesitic–basaltic volcanic sequence, with lavas and thick volcanic breccias, interbedded with lithic arkoses, lapilli and ash tuffs and rhyolitic domes, called La Totora Formation. This sequence underlies with a slight unconformity, Jurassic marine carbonate rocks (von Hillebrandt, 1973, Jensen, 1976, Salazar et al., 2013, Ortiz and Merino, 2015).

4.3. Samples and methods

Geological data from the Pastos Blancos Formation and the felsic-mafic dikes related to Colorado Syenogranites were collected during field mapping of the studied area. Twenty-five samples were collected for petrographic analysis and eleven samples were selected for chemical (major and trace elements) and isotopic (Sr-Nd-Pb) composition. The thin sections were analyzed under the polarized-light microscope for a textural and mineralogical characterization. Due to the common alteration, the selected samples were crushed under 5 mm fraction and fresh fragments were handpicked under binocular lens for geochemical analyses. The fresh fragments were powdered to a fraction below 50 µm. The powered samples were mixed with a flux of lithium metaborate and lithium tetraborate, and fused in an induction furnace. The resulting molten was poured into a solution of 5% nitric acid and mixed until completely dissolved. The samples were run on Varian V735 ICP-OES and Perkin-Elmer Elan 6000 ICP/MS at Activation Laboratories, Ontario, Canada.

Whole-rock Sr, Nd, and Pb isotope ratios were obtained through thermal ionization mass spectrometry (TIMS) on a Triton plus instrument (Thermo Scientific) at the Isotope Geochemistry Laboratory of MARUM, University of Bremen. Approximately 100 mg of the pulverized samples were dissolved in a mixture of triple distilled HF and HNO_3 in 5:1 proportion, dried and re-dissolved in 1000 µl of 2 m HNO_3 for chemical separation. Sr and Pb were isolated from the other elements using miniaturized

columns with 70 µl of Sr- and Pb-specific resin (Sr.spec 50–100 µm). The Sr and Pb simultaneous separation from silicate samples using Sr.spec in a single stage column was developed and detailed by Deniel and Pin (2001) and was adapted to the smaller resin volumes. The light rare earth elements (LREE) were isolated from Sr elute, using TRU.Spec (50–100 µm) followed by Nd and Sm isolation via LN.Spec (50–100 µm). The setup of LREE and Sm-Nd separation columns and separation procedure were adapted from Pin and Zalduegui (1997) and Miková and Denková (2007). Total procedure blanks of Sr, Nd, and Pb were <180 pg, <80 pg and <40 pg respectively, being insignificant in relation to the amount of material used in the analyses. Hence, no blank corrections have been applied to analyzed ratios. Strontium was loaded with a Ta-oxide emitter and 0.1 m phosphoric acid on Re single filaments and Neodymium with 0.1 m phosphoric acid on a Re double filament configuration. These elements were analyzed by TIMS in dynamic multi-collection mode. Instrumental mass fractionation of Sr and Nd isotope ratios was normalized to $^{86}Sr/^{88}Sr$ of 0.1194 and $^{146}Nd/^{144}Nd$ of 0.7219, respectively. Lead was loaded onto Re single filaments with 0.1 m phosphoric acid and silica emitter, and its isotopic ratios were analyzed at pyrometer-controlled temperature of ~1250 °C in static multi-collection mode. Instrumental mass-fractionation of Pb has been corrected using 0.1% per atomic mass unit. This factor was derived from repeated analyses of NIST 981 and comparison of analyzed and certified Pb isotope ratios. The overall error including the correction for mass-fractionation is better than 0.1% of the respective isotope ratio.

4.4 Results

4.4.1 Field and stratigraphic constrains

The Pastos Blancos Formation is distributed along a roughly N-S trending block where large thicknesses are preserved (a maximum of 1000 m, Murillo et al., 2017). This block is limited to the west and east by regional scale faults with reverse displacements occurred during Cenozoic orogenic stages (Cembrano et al., 2003, Lossada et al., 2017). Outside these limits, thickness of the Pastos Blancos Formation are drastically reduced to <400 m, where is conformably and unconformably overlying by Jurassic marine strata (Fig. 4.2A). The crystalline basement of the Pastos Blancos Formation

corresponds to Ordovician – Carboniferous metamorphic complex and Carboniferous to Middle Triassic intrusive rocks. The southern limit for the distribution of the Pastos Blancos Formation is marked by a W-E lineament at 30°S, which could correspond to a normal fault with nearly vertical dip, that puts this unit in contact with Permian – Middle Triassic Intrusives (Murillo et al., 2017.). However, the Pastos Blancos Formation also overlays the intrusives (Fig. 4.2B) suggesting a fast exhumation process during the 239–235 Ma time span. To the north, the volcanic rocks are limited by near vertical contacts interpreted as normal faults that control the large exposures of this unit over Carboniferous to Triassic intrusives (Nasi et al., 1990, Murillo et al., 2017).

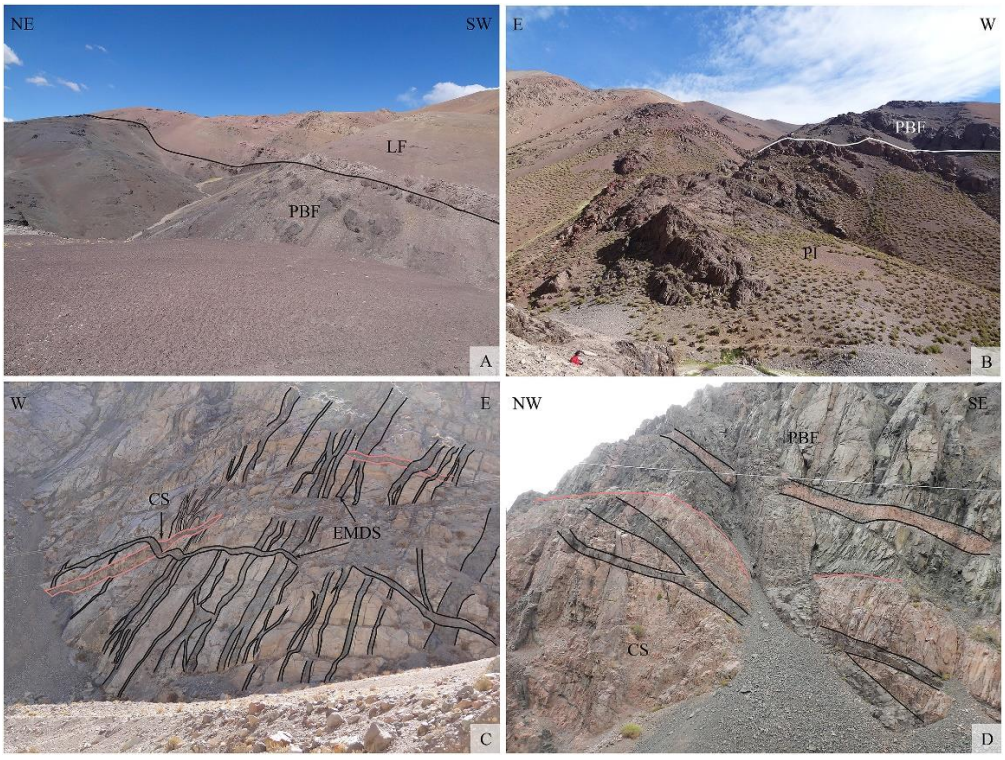

Figure. 4.2. Stratigraphic relationships of the Pastos Blancos Formation in the vicinity of the Río del Medio, Río Primero, Turbio Valley and Potrerillos Valley. A. Concordant depositional contact between the Pastos Blancos Formation (PBF) and the Lautaro Formation (LF). B. Layers of the Pastos Blancos Formation deposited in nonconformity on the Permian granodioritic intrusive (PI) at the Río del Medio. C. Crosscutting relationship between the Elqui Mafic Dike Swarm (EMDS) with black edges and the intermediate to felsic dikes related to Colorado Syenogranites (CS) with red edges, at Turbio Valley. D. Pastos Blancos Formation intruded by a pluton of Colorado Syenogranites at Potrerillos Valley.

Dikes of variable composition are an essential component of the magmatism of the Pastos Blancos Formation. The best and most voluminous dike exposures are

recognized along the upper stream of the Turbio Valley, where a large number of mafic dikes, assigned to the Elqui Mafic Dike Swarm (Creixell et al., 2009), intrude mostly the CPC and to a less extent the Colorado Syenogranites. Mafic dike swarms that crop out along the western stream of the Turbio Valley and intrude Upper Triassic granitoids (215 Ma) are considered Jurassic in age (Murillo et al., 2017.), and are not considered in this study. Along the same section, outcrops of the Pastos Blancos Formation are very restricted and intruded by mafic dikes and felsic dikes and plutons of Upper Triassic Colorado Syenogranites. To the north, along the Río Primero and Río del Medio valleys, there is a minor quantity of mafic dikes (<1% of the outcrops). Locally, intermediate and felsic dikes of red brick colour are abundant, and considered here and in previous works (Martin et al., 1999) as part of the Colorado Syenogranites. The dikes intrude the Pastos Blancos Formation, some with sharp borders and straight geometries, but other with remarkable irregular geometries, suggesting a possible contemporaneity between the dikes and the country rock, likely due to low viscosity contrast (Emerman and Marrett, 1990). These red brick dikes usually show mutual crosscutting relationship with mafic dikes (Fig. 4.2C), indicating that the EMDS and the Colorado Syenogranites are roughly contemporaneous, as noted previously by Martin et al. (1999). Approximately 15 km to the north of Río del Medio, along the Potrerillos Valley, the Pastos Blancos Formation is intruded by dikes and plutons of the Colorado Syenogranites (Ortiz and Merino, 2015) (Fig. 4.2D). In several locations felsic dikes with mafic lobulated enclaves and composite dikes with mafic borders and granitic centers are recognized.

4.4.2 Crustal extension approach: Elqui mafic dike swarm (EMDS)

The most spectacular and voluminous exposures of the EMDS are found along the Turbio Valley at 30°S, in the International road to Argentina, across the Agua Negra Pass. A total of 229 mafic dikes were measured systematically along several sections in the Turbio Valley. The geometry of each dike was characterized in the field by its orientation and thickness. The resulting database (Appendix 4.A) is used to calculate statistical populations of dike orientations and to estimate dike injection densities

across the sections, as a proxy to crustal dilation caused by dike emplacement (e.g., Marinoni, 2001, Klausen and Larsen, 2002).

On the eastern belt there are at least two mafic dike generations that intrude into the Chollay Plutonic Complex, the Pastos Blancos Formation and the Colorado Syenogranites and at the same time is intruded by red brick dikes of the Colorado Syenogranites. These crosscutting relationships indicate that in this area, the EMDS is Late Triassic in age. Most specimens of mafic dikes are roughly N-S oriented, with a minor population of roughly E-W trending dikes. The strikes of the dominant group commonly plots between N10°E and N20°E, but the mean trend vector is 184°/80° (Fig. 4.3). The older population represents less than 5% of the total dike volume and is distributed highly oblique to the main population. Locally, we recognized small gabbro stocks from where dikes are injected into the country rock. Also at local scale, we can observe several units of subparallel mafic dikes intruded one close to another, and can be considered as syntaxial intrusions, in the sense of Bartley et al. (2006). In lithological terms, the mafic dikes vary between andesite and basaltic andesite, and are mostly aphyric or with plagioclase and clinopyroxene phenocrysts and only a few dikes contain amphibole phenocrysts. The fine-grained groundmass is commonly altered to chlorite and minor epidote and sericite. Compositional differences between the differently oriented groups are absent.

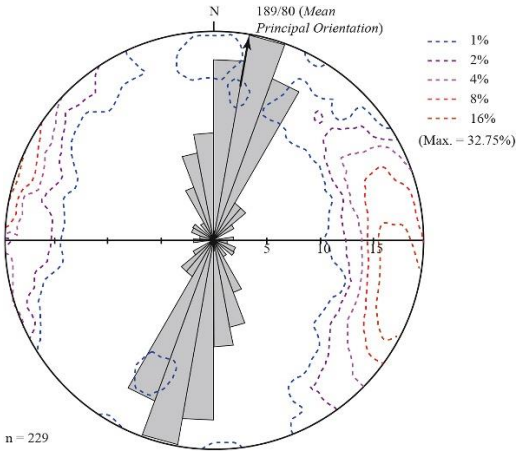

Figure 4.3. Rose diagram of strike and contoured density distributions of poles showing the attitudes of intrusion planes of the 229 dikes from the eastern section of EMDS. Stereographic equal area projection. Mean orientation is 189/80

Table 4.1. Summary by section of the measurements made in the eastern segment of the EMDS to estimate the percentage of cortical dilation. The thickness of the dikes is in centimetres and the length of each section is in meters.

Section	Start coordinate	End coordinate	Number of dikes	Total dikes thickness (m)	Section length (m)	Dilation (%)
1	394235	394121	22	15.09	114	13.24
	6683359	6683353				
2	394057	393926	25	20.16	131	15.39
	6683388	6683411				
3	393689	393596	25	36.81	93	39.58
	6683412	6683442				
4	393523	393470	24	15.23	53	28.74
	6683463	6683534				
5	393232	393154	19	19.29	78	24.73
	6683770	6683788				
6	393150	392598	35	47.23	630	7.50
	6683789	6683784				
7	392565	392398	11	21.81	180	12.12
	6683756	6683773				
8	392174	391693	34	59.89	530	11.30
	6683735	6683845				
9	391329	391192	8	15.21	137	11.10
	6684139	6684258				
10	387782	387650	22	27.13	132	20.55
	6685533	6685672				
11	387213	387148	9	7.30	65	11.23
	6685718	6685726				

Individual dike thickness shows large variations across the eastern segment of the Río Turbio profile, between a minimum of 30 cm and a maximum value of 10 m. The frequency distribution of the dike occurrence per meter of country rock shows a good negative correlation with dike thickness values (i.e. the thicker the dikes, the lower the density in the country rock). The thickest dikes are found along the central portion of the EMDS, with several dikes >6 m. The studied EMDS segment along the Turbio Valley was divided in eleven sections of different lengths, separated from each other

by covered stretches (e.g. alluvial fans). The dilation percentage was calculated for each section as the ratio between the total thickness of the dikes (summation of the thicknesses of all the dikes exposed in section) and the length of the section (Klausen and Larsen, 2002). The values obtained vary mainly between 11% and 25% (Table 4.1), where the largest value is reached near the eastern limit of the EMDS, in the same place where syntaxial dikes and gabbroic stocks were observed. The sum of each dike thickness along the eastern section is 285 m, but this remains a minimum value, since we were not able to measure several segments along the EMDS.

4.4.3 Petrography

The main lithologies in the Pastos Blancos Formation are partially welded rhyodacitic ash and lapilli tuffs, interbedded with andesitic and dacitic lavas, rhyolitic domes, volcanic breccias and agglomerates, and volcanoclastic rocks with high contents of epiclastic components.

The volcanoclastic rocks correspond to vitric, crystal-vitric, lithic-vitric and lapilli tuffs, according to the classification of Pettijohn (1975). They are composed of fragmented crystals of plagioclase altered to clays and sericite with a local alteration to calcite and epidote, fragmented crystals of embayed quartz, scarce sanidine altered to clays and sericite in its pertites. Mafic minerals are replaced by chlorite, biotite, and opaque minerals (Fig. 4.4A and B). Lithic components are mainly volcanic clasts of intermediate to silicic compositions, but there are volcanoclastic, intrusive and, to a lesser extent, sedimentary lithics as well. The glass is devitrified, altered to clays or limonite; scarce spherical spherulites are recognized. The mineralogy of rocks with high epiclastic rework do not differ much from pyroclastic rocks, but lithics are more rounded and possible glass is in some cases completely replaced by calcareous cement.

Andesitic lavas have seriate porphyritic and locally glomero-porphyritic texture, with subhedral to euhedral plagioclase phenocrysts altered to clays, sericite and minor epidote and calcite. Mafic phenocrysts are often completely altered to calcite or chlorite. In one sample, phenocrysts of fresh clinopyroxene and orthopyroxene are replaced by zeolites, chlorite and serpentine (Fig. 4C). The groundmass is hialophytic or pylotaxitic with plagioclase, opaque minerals and devitrified glass altered to clays or chlorite. The

dacites also have a porphyritic and locally glomero-porphyritic texture with subhedral to euhedral plagioclase phenocrysts altered to clays and sericite (Fig. 4D), immersed in a felsitic groundmass with veinlets filled by zeolites and calcite. The rhyolites are characterized by their perlitic cracks and banded texture with alternating bands of different sized crystals.

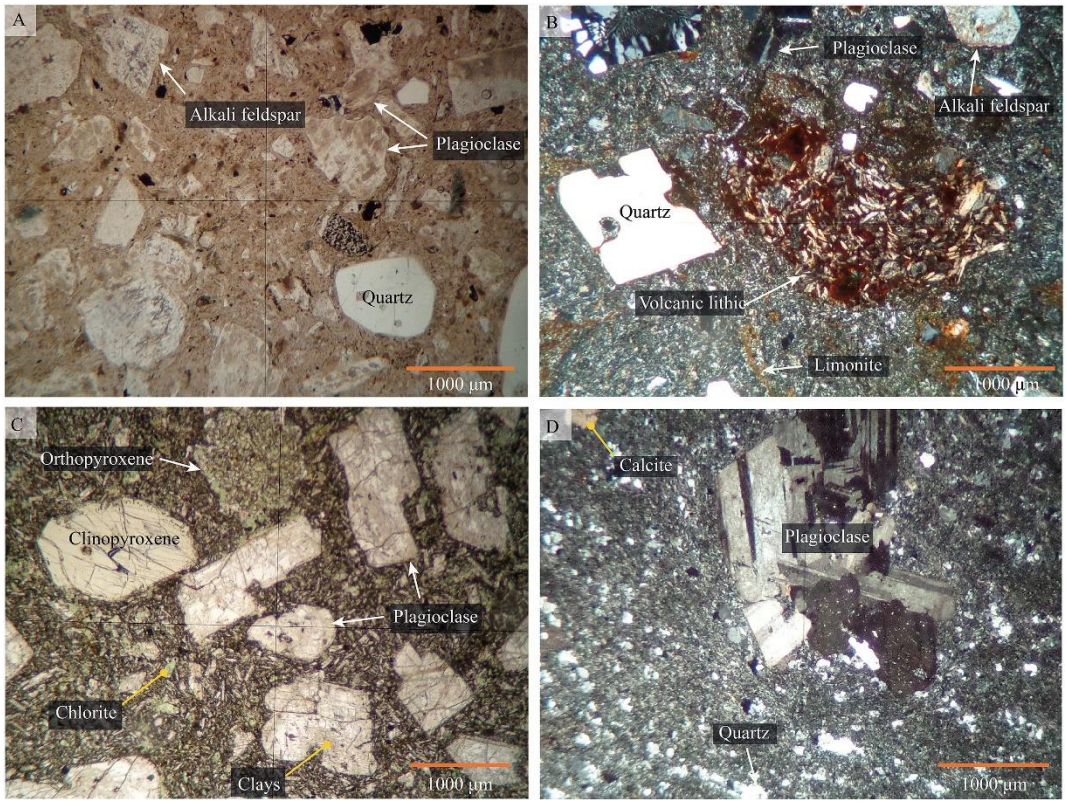

Figure 4.4. Microphotographs of the Pastos Blancos Formation samples. A. Rhyodacitic crystal-vitric tuff, with a moderate alteration to clays (GUC-45). B. Rhyodacitic vitric lapilli tuff, with glass partially replaced by limonite (GUC-41). C. Pyroxene-bearing andesite, with plagioclase, clinopyroxene and bastitized orthopyroxene phenocrystals (GUC-32). D. Dacite with a locally glomero-porphiritic texture and a felsitic groundmass (GUC-47).

In the Río Primero and Río del Medio areas, one intermediate and three felsic dikes were sampled. The intermediate dike intrudes rhyolites with sinuous contacts (Fig. 4.5A), and corresponds to a porphyritic andesitic rock, with euhedral plagioclase phenocrysts altered to clay and sericite, and amphibole with rounded edges slightly altered to calcite in a holocrystalline groundmass composed of plagioclase, mafic minerals replaced by chlorite and titanite.

One of the felsic dikes sampled has straight and sharp contacts with tuffs of the Pastos Blancos Formation (Fig. 4.5B) and abundant centimetric mafic enclaves, some of them with lobulated borders (Fig. 4.5C). It corresponds to a quartziferous monzonitic porphyry, with euhedral plagioclase phenocrysts with intense orange borders, altered strongly to clay and weakly to sericite, quartz phenocrysts with rounded shapes and locally embayed edges in a holocrystalline groundmass composed by plagioclase, quartz, alkali feldspar, opaque minerals and a mafic mineral completely replaced by chlorite. In thin section, the mafic enclaves have diffused boundaries and are composed of plagioclase, non-identified mafic mineral replaced by chlorite, opaque minerals, titanite, and quartz. The plagioclase reaction rims and lobulated enclaves are typical features of magma mixing. The remaining samples were taken from the centers and edges of two felsic dikes, one 4 m thick that intruded into the tuffs of the volcanic sequence and another 1 m thick dike that cuts into the previous dike (Fig. 4.5D). Both dikes show a decrease in the crystal size from the center to the edges, and have a monzonitic composition with plagioclase, alkali feldspar and opaque minerals and without mafic enclaves.

Figure 4.5. Photographs of dikes related to Colorado Syenogranites that intrude the Pastos Blancos Formation at Primero and del Medio rivers. A. Felsic dikes related to Colorado Syenogranites and mafic dikes crosscutting with sinuous margins and intruding rhyolites of the volcano-sedimentary sequence. B. Felsic dikes in sharp contacts with Pastos Blancos tuffs. C. Mafic enclaves with lobulated borders and porphyritic texture in the same dike. D) Felsic dike, intruding a tuff, with sharp contacts.

4.4.4 Geochemistry

The results of the major and trace elements whole-rock analysis of eight samples from Pastos Blancos Formation and three samples from dikes related to Colorado Syenogranites, are presented in Table 4.2 and in Fig. 4.6, Fig. 4.7, Fig. 4.8. These figures show also the published geochemical data from the aforementioned units (Salazar et al., 2013, Ortiz and Merino, 2015, Oliveros et al., 2016).

Table 4.2. ICP-MS and ICP-OES geochemical results for analyzed samples.

	Unit		**Pastos Blancos Formation**								**Dikes of Colorado Syenogranites**		
Sample		DL	GUC-05	GUC-32	GUC-33	GUC-38B	GUC-41	GUC-45	GUC-46	GUC-47	GUC-34	GUC-37A	GUC-37C
Major elements (wt%)	SiO_2	0.01	79.94	51.10	75.18	62.96	71.28	72.36	67.73	79.57	50.67	74.98	70.43
	Al_2O_3	0.01	10.93	18.32	12.56	13.93	13.59	14.15	14.72	10.81	17.74	12.84	13.55
	Fe_2O_{3T}	0.01	0.77	8.02	2.21	6.61	4.02	2.45	3.61	1.20	9.38	1.92	2.87
	MnO	0.001	0.025	0.151	0.068	0.101	0.037	0.052	0.066	0.011	0.173	0.037	0.060
	MgO	0.01	0.06	5.85	0.20	2.74	0.16	0.54	0.68	0.04	3.88	0.62	0.48
	CaO	0.01	0.22	8.63	0.80	3.23	1.41	0.62	2.32	0.22	4.81	1.10	1.30
	Na_2O	0.01	5.40	3.63	4.36	5.75	4.25	4.09	4.96	3.38	4.21	3.67	4.57
	K_2O	0.01	0.52	1.06	3.23	0.06	4.24	3.49	3.25	3.86	3.07	3.30	3.72
	TiO_2	0.001	0.144	1.164	0.139	1.234	0.793	0.362	0.694	0.147	1.167	0.352	0.462
	P_2O_5	0.01	0.02	0.25	0.03	0.42	0.32	0.05	0.19	0.01	0.36	0.07	0.10
	LOI		0.46	2.58	1.14	3.03	0.58	1.53	2.73	0.77	4.09	1.98	2.39
	Total		98.48	100.70	99.90	100.10	100.70	99.69	101.00	100.00	99.55	100.90	99.94
Trace elements (ppm)	Sc	1	3	24	8	19	12	5	9	3	18	6	8
	Be	1	3	1	3	2	3	3	3	2	4	2	2
	V	5	7	202	8	121	50	41	61	18	171	29	28
	Cr	20	<20	150	<20	20	<20	<20	<20	<20	<20	<20	<20
	Co	1	<1	30	<1	14	2	4	4	<1	23	3	3
	Ni	20	<20	80	<20	20	<20	<20	<20	<20	<20	<20	<20
	Cu	10	<10	50	<10	<10	<10	<10	<10	10	20	<10	<10

Zn	30	<30	80	80	70	80	80	80	<30	70	40	60
Ga	1	12	20	20	16	20	16	17	10	20	15	17
Ge	0.5	3.4	2.3	2.1	3.4	1.9	2.4	1.6	2.1	3.1	2	1.9
As	5	<5	5	<5	5	11	<5	<5	<5	<5	<5	<5
Rb	1	18	41	113	1	150	108	98	116	117	126	111
Sr	2	49	642	85	155	126	148	185	115	672	127	125
Y	0.5	19.5	19.8	40.0	22.6	36.7	28.3	29.0	24.7	21.5	25.8	48.9
Zr	1	114	129	284	187	337	167	278	135	137	228	351
Nb	0.2	7.2	4.2	10.9	7.0	13.5	4.1	5.4	4.9	9.8	8.8	11.0
Ag	0.5	1.4	1.6	2.9	1.9	2.6	<0.5	<0.5	<0.5	1.4	1.7	2.8
Sn	1	3	2	5	2	3	2	2	4	1	4	4
Sb	0.2	0.4	0.7	0.2	0.7	0.8	<0.2	<0.2	<0.2	0.3	0.2	0.3
Cs	0.1	0.7	14.0	2.0	0.5	3.6	3.6	6.4	1.6	8.9	3.4	2.7
Ba	3	152	409	680	25	1093	934	763	3289	1104	1966	574
La	0.05	28.7	16.4	30.4	11.1	33.3	37.3	34.7	26.5	16.7	19.3	36.8
Ce	0.05	51.4	36.8	66.3	25.6	72.9	66.1	69.7	49.9	37.6	40.3	74.3
Pr	0.01	6.32	5.11	8.53	3.69	9.60	8.58	9.00	6.37	5.30	4.99	8.93
Nd	0.05	22.5	22.1	36.3	17.4	40.0	31.8	34.3	23.5	23.0	18.7	34.6
Sm	0.01	4.01	4.90	7.40	4.73	8.55	6.14	7.04	4.70	5.20	4.17	7.76
Eu	0.005	0.532	1.580	1.480	1.470	1.640	1.400	1.630	0.615	1.630	0.732	1.690
Gd	0.01	3.26	4.16	6.70	4.51	7.54	5.95	6.02	3.74	4.48	3.75	7.58
Tb	0.01	0.53	0.67	1.10	0.72	1.23	0.94	0.98	0.76	0.67	0.69	1.35
Dy	0.01	3.25	3.67	6.77	4.16	6.94	4.87	5.46	4.35	3.93	4.24	7.54
Ho	0.01	0.66	0.70	1.41	0.83	1.38	0.91	1.07	0.96	0.74	0.86	1.42
Er	0.01	1.89	2.03	4.24	2.26	3.92	2.86	3.28	2.65	2.15	2.59	3.94
Tm	0.005	0.307	0.290	0.683	0.342	0.576	0.439	0.476	0.433	0.324	0.404	0.548
Yb	0.01	2.11	1.88	4.65	2.16	3.96	2.85	3.02	2.98	2.09	2.73	3.62
Lu	0.002	0.321	0.260	0.648	0.308	0.577	0.397	0.445	0.446	0.327	0.389	0.509
Hf	0.1	3.5	2.9	7.1	4.2	8.0	3.8	6.1	3.7	3.4	5.6	7.7
Ta	0.01	0.69	0.32	0.88	0.52	0.95	0.54	0.56	0.67	0.66	0.79	2.94
W	0.5	1.9	2.6	2.6	3.2	6.1	3.4	2.2	1.5	2.8	5.1	3.1
Tl	0.05	0.30	0.40	0.73	0.22	1.00	0.42	0.47	0.56	0.86	0.81	0.84
Pb	5	18	11	6	<5	27	10	11	12	<5	<5	7
Bi	0.1	0.2	<0.1	<0.1	<0.1	<0.1	0.2	0.2	0.2	<0.1	<0.1	<0.1
Th	0.05	10.60	3.68	12.80	4.25	9.19	10.20	8.51	9.90	3.25	15.10	11.50
U	0.01	2.52	0.96	2.72	0.89	2.70	2.19	1.92	2.00	0.88	3.40	2.58

continued Table 4.2

4.4.4.1 Alteration

According to the petrographic descriptions, the volcanic and volcano sedimentary rocks from Pastos Blancos Formation and dikes related with Colorado Syenogranites, exhibit a wide variety of secondary minerals that include clays, sericite, quartz, opaque minerals, limonite, celadonite, calcite, epidote and chlorite. The volume of alteration minerals in general is high and can be up to the 50% of the total rock volume (see Appendix 4.B for the specific proportions of these minerals in each sample). The geochemical analyses show low loss on ignition values ranging from 0.46 wt% to 4.09 wt% (only two samples have LOI > 3%) and its increment is related with the calcite or chlorite abundance in the samples.

4.4.4.2. Major elements

The major-element oxide concentrations have been recalculated to 100% on an anhydrous basis, and the Fe_2O_3 and FeO abundances have been estimated from the analytical data expressed as $Fe_2O_{3(T)}$. The SiO_2 content of the analyzed samples varies between 52.05 wt% and 81.55 wt%, with most values between 71 wt% and 76 wt%, and have total alkali contents between 4.78 wt% and 8.50 wt%. Most samples belong to the calc-alkaline and high-K calc-alkaline series and only two samples plot on the low-K tholeiite series (Fig. 4.6). The Al_2O_3 (10.89–18.66 wt%), MgO (0.04–5.96 wt%), FeO* (0.73–9.12 wt%) CaO (0.22–8.79 wt%) and TiO_2 (0.14–1.27 wt%) contents decrease with increasing SiO_2. The overall trends of P_2O_5 (0.01–0.43 wt%) and Na_2O (2.80–5.92 wt%) are also decreasing, but only from SiO_2 contents > 65 wt% probably controlled by the crystallization of apatite and K-feldspar, respectively once that SiO_2 content is exceeded. In contrast, the K_2O (0.06–4.23 wt%) data show a rise in their concentrations as SiO_2 increases. The Na_2O and K_2O data are more dispersed values, probably due to the alteration processes.

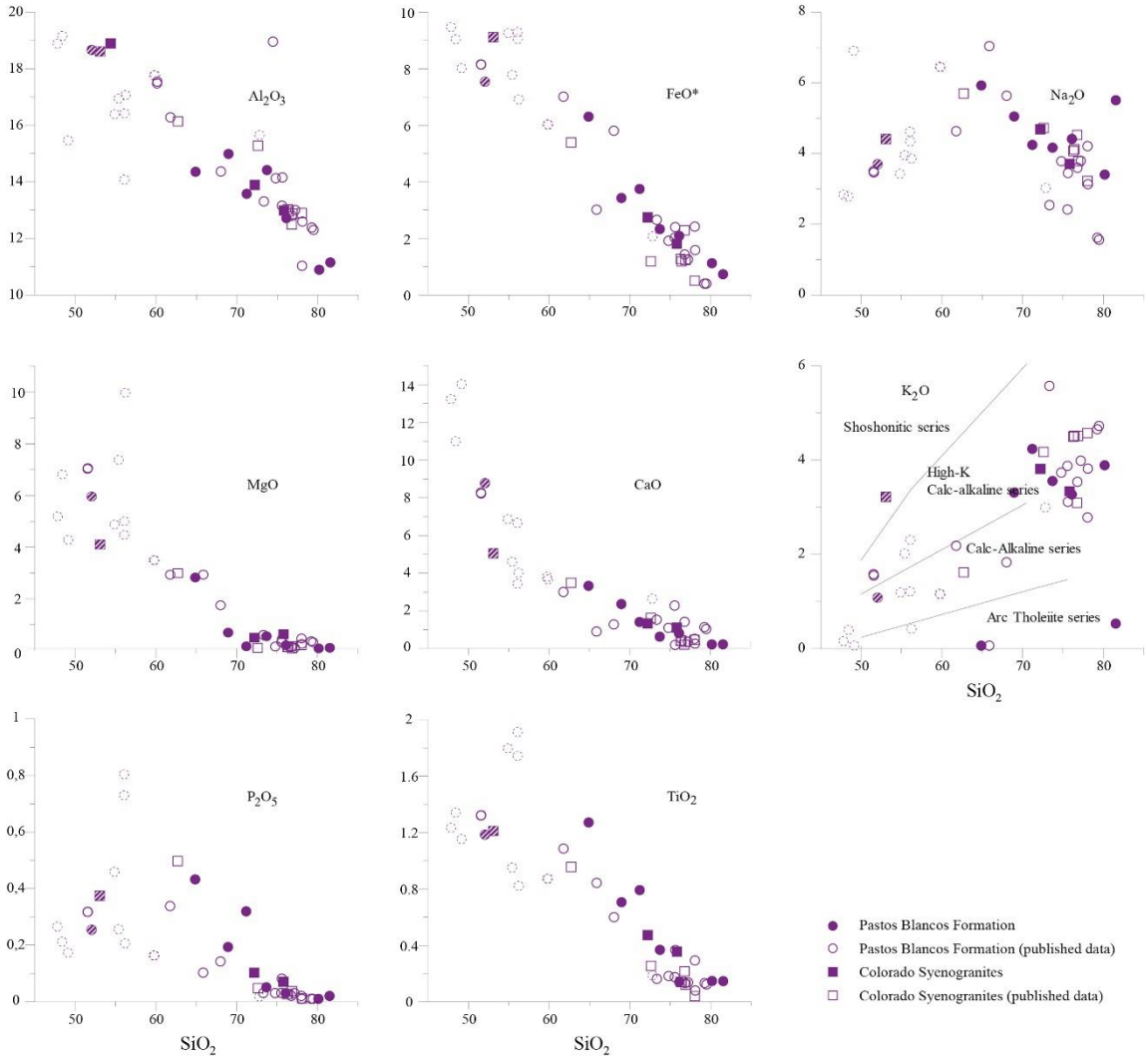

Figure 4.6. Harker diagrams of the analyzed samples and previously published data (Salazar et al., 2013, Ortiz and Merino, 2015, Oliveros et al., 2016) for Pastos Blancos Formation, Colorado Syenogranites and related dikes. The symbols with dashed edges and filled with white diagonal stripes correspond published data and samples from this study with LOI >3%, respectively. The subdivisions of the K_2O versus SiO_2 diagram are those defined by Peccerillo and Taylor (1976).

The comparison of our samples with previous published data from the same suites shows that the SiO_2 content varies between 47.84% and 81.55%. The new analyses fit the covariations of all the elements with SiO_2 as an indicator of progressive magmatic differentiation in the larger data set.

In TAS (total alkali versus silica) classification diagram, the Pastos Blancos Formation and Colorado Syenogranites show a subalkaline trend, with only one of the analyzed samples and one of the published data in the alkaline field (Fig. 4.7A and 4.B). All subalkaline rocks are calc-alkaline in the AFM diagram (Fig. 4.7C). From the analyzed

dikes of Colorado Syenogranites, there are two metaluminous and one peraluminous (Fig. 4.7D) and the published data of this unit are also divided into both fields.

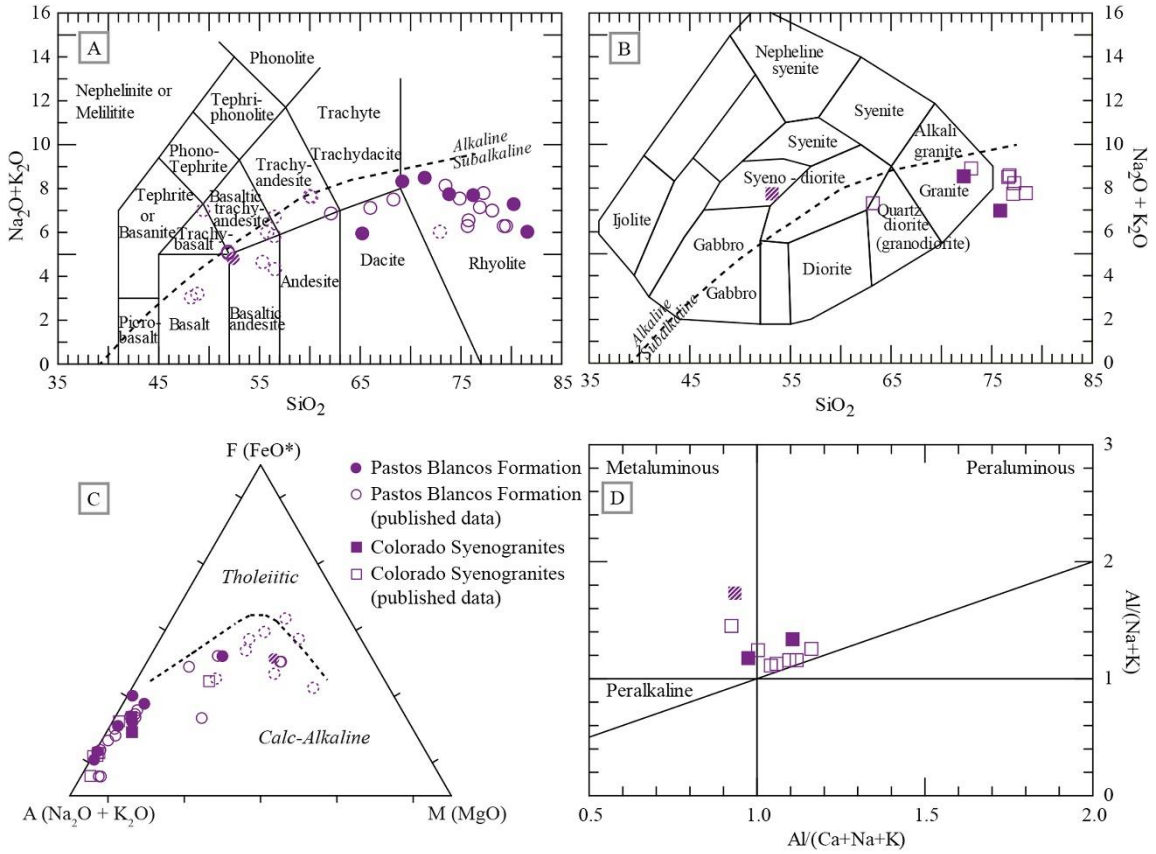

Figure 4.7. Classification diagrams for the analyzed samples and previously published data of Pastos Blancos Formation, Colorado Syenogranites and related dikes (references as in Fig. 6). A. Total alkalis versus silica diagram for volcanic rocks (TAS, Le Maitre et al., 1989) uses the subdivision between the alkaline and subalkaline series defined by Irvine and Baragar (1971). B. Total alkalis versus silica diagram for intrusive rocks (Cox et al., 1979 adapted by Wilson (1989)). C. AFM diagram, division between tholeiitic and calc-alkaline series proposed by Irvine and Baragar (1971). D. Diagram of the aluminium saturation index for plutonic rocks (Shand, 1927).

4.4.4.3. Trace elements

Primitive mantle normalized plots (Fig. 4.8A and B) show that all the samples are enriched in large ion lithophile elements (LILE) and Pb respect to high field strength elements (HFSE). Nb and Ta troughs are ubiquitous, although one sample has anomalously high Ta/Nb ratio. Our data have lower Y contents and less pronounced negative Sr anomalies than the published data for the Pastos Blancos Formation, but otherwise share the characteristics mentioned above. The published data of the Colorado Syenogranites show lower LILE and Zr contents and higher Pb contents compared to the analyzed samples, in addition to pronounced Sr, P and Ti troughs.

Light rare earth elements are enriched respect to the heavy rare earth elements, with relatively flat chondrite-normalized patterns (La_N/Yb_N: 3.44–9.10) and negative Eu anomalies poorly pronounced in most of them (Eu/Eu*: 0.45–0.98), except for two that have a slight positive anomaly (Eu/Eu*: 1.04 and 1.08) (Fig. 4.8C and 4.D). The Eu/Eu* ratio decreases smoothly as the SiO_2 content increases, suggesting plagioclase fractionation to the evolution of the magmas, evidenced in the direct correlation between the Eu/Eu* and the content of Sr. A mild concave depression is also common in the middle rare earth elements, which could reflect amphibole fractionation.

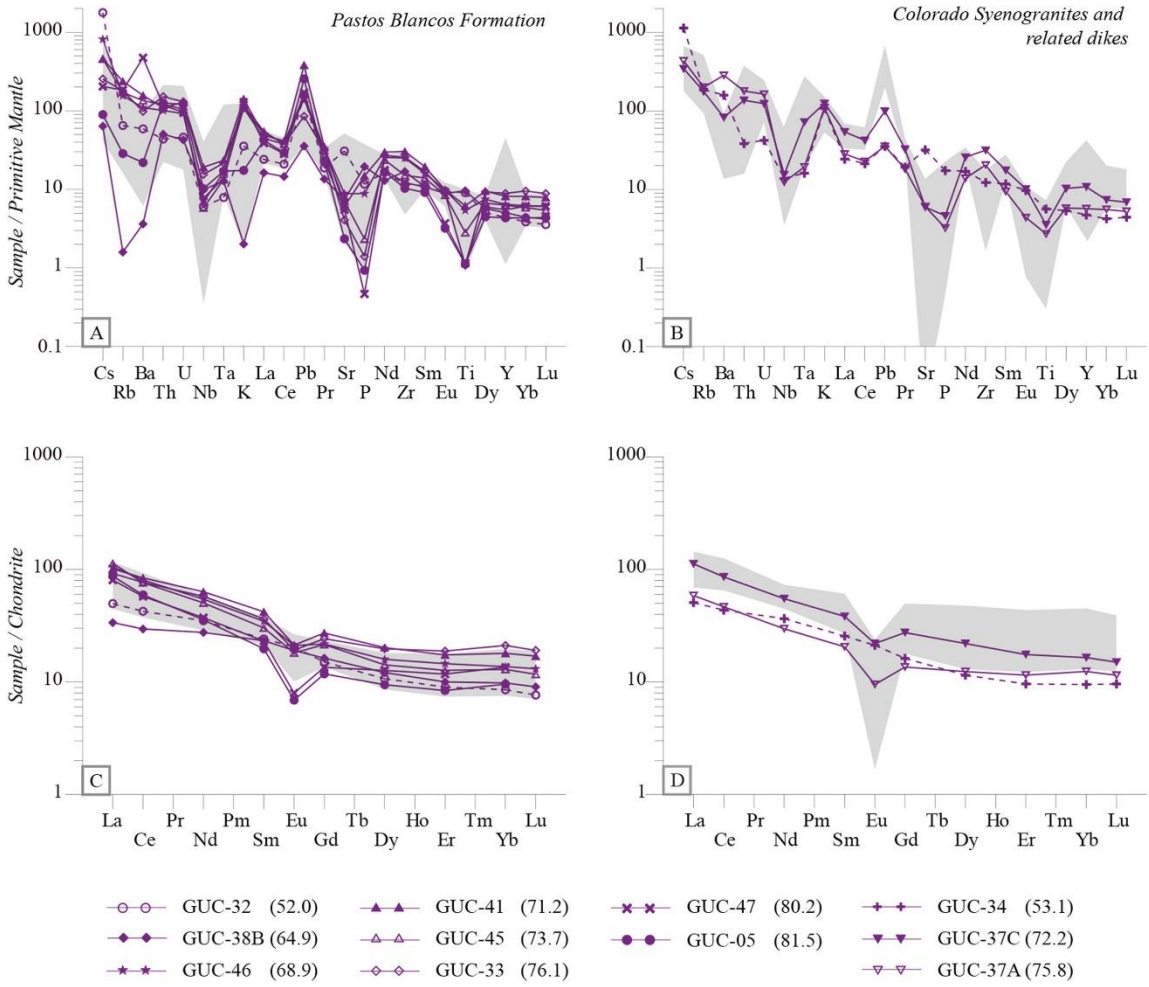

Figure 4.8. Multi-element diagrams normalized to the primitive mantle (Sun and McDonough, 1989) for Pastos Blancos Formation (A) and dikes related to Colorado Syenogranites (B). Rare Earth Elements diagrams normalized to chondrite (Nakamura, 1974) for Pastos Blancos Formation (C) and dikes related to Colorado Syenogranites (D). The samples with LOI >3% are represented with dashed lines. The gray areas represent published data for both units, references as in Fig. 4.6. These data were filtered out by removing the samples with outliers.

4.4.4.4. Isotopes

The initial isotopic ratios were calculated using the isotopic ratios analyzed by TIMS, the contents of Rb, Sr, Sm, Nd, U, Th and Pb analyzed by ICP-MS, and average ages of the Pastos Blancos Formation, the Colorado Syenogranites and related dikes, estimated from the published radiometric ages of both units (Table 4.3). Initial $^{87}Sr/^{86}Sr$ ratios are between 0.7038 and 0.7076 with the exception of sample GUC-41, which has a value of 0.7012. The initial ratios of $^{143}Nd/^{144}Nd$ are between 0.512281 and 0.512572, with calculated εNd_i between −1.3 and + 1.5. The initial ratios of $^{206}Pb/^{204}Pb$, $^{207}Pb/^{204}Pb$ and $^{208}Pb/^{204}Pb$ range between 16.56 and 18.49, 15.47–15.59 and 35.49–38.35, respectively. The Sr and Nd initial ratios of the analyzed samples, tend to concentrated between the fields defined for the Upper Paleozoic and the Jurassic-Cretaceous magmatism that crop out in the north of Chile (Fig. 4.9A), and therefore, between the Lower Paleozoic crust, defined by the gneisses and metabasites of northern Chile and Argentina and the MORB fields. In the $^{207}Pb/^{204}Pbi$ vs $^{206}Pb/^{204}Pbi$ diagram, the studied samples are close to the Paleozoic and Jurassic – Cretaceous magmatism (Fig. 4.9B).

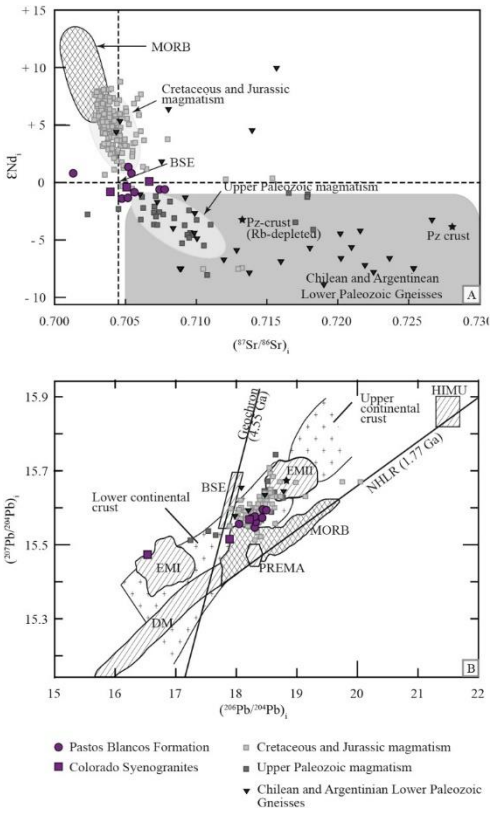

Figure 4.9. Initial isotopic compositions of samples from Pastos Blancos Formation and dikes related to Colorado Syenogranites compared with the isotopic composition of Chilean Upper Paleozoic, Jurassic and Cretaceous magmatism and Chilean-Argentinian Lower Paleozoic Gneisses (Beccio et al., 1999, Lucassen et al., 1999, Parada et al., 1999, Parada, 2013, Oliveros et al., 2016). Pz-crust correspond to the average of Early Paleozoic crust (Rb depleted) and upper crust (Lucassen et al., 2001). A. ƐNdi versus $^{87}Sr/^{86}Sri$ diagram including the isotopic composition of mid-ocean ridge basalt (MORB) and the Bulk Silicate Earth (Workman and Hart, 2005, White, 2013). B. $^{207}Pb/^{204}Pb$ versus $^{206}Pb/^{204}Pb$ with the isotopic composition of the mantle reservoirs proposed by Zindler and Hart (1986): depleted mantle (DM), bulk silicate earth (BSE), mantle with high U/Pb ratio (HIMU), enriched mantle I (EMI), enriched mantle II (EMII) and observed prevalent mantle composition (PREMA). Also, isotopic composition of mid-ocean ridge basalt (MORB) is included.

Table 4.3. Initial Sr, Nd and Pb isotope ratios, calculated from the measurements of the current isotope ratios (TIMS), the Rb, Sr, Sm, Nd, U, Th and Pb concentrations in ppm (ICP-MS) and the average ages of the Pastos Blancos Formation and of the Colorado Syenogranites.

Sample	Age (Ma)	Rb (ppm)	Sr (ppm)	$^{87}Sr/^{86}Sr$	Standard error	$^{87}Rb/^{86}Sr$	$^{87}Sr/^{86}Sr$ initial	Sm (ppm)	Nd (ppm)	$^{143}Nd/^{144}Nd$	Standard error	$^{147}Sm/^{144}Nd$	$^{143}Nd/^{144}Nd$ initial	εNd initial
GUC-05q	224	18	49	0.710619	2.37×10^{-6}	1.063	0.707232	4.01	22.5	0.512494	1.86×10^{-5}	0.108	0.512324	−0.50
GUC-32q	224	41	642	0.705657	2.49×10^{-6}	0.185	0.705069	4.90	22.1	0.512623	3.16×10^{-6}	0.134	0.512427	1.50
GUC-33q	224	113	85	0.716861	4.02×10^{-6}	3.850	0.704596	7.40	36.3	0.512462	1.74×10^{-6}	0.123	0.512281	−1.34
GUC-38Bq	224	1	155	0.705615	1.99×10^{-6}	0.019	0.705556	4.73	17.4	0.512554	2.45×10^{-6}	0.164	0.512313	−0.72
GUC-41q	224	150	126	0.712184	2.96×10^{-6}	3.446	0.701206	8.55	40.0	0.512586	1.58×10^{-6}	0.129	0.512396	0.91
GUC-45q	224	108	148	0.712055	2.58×10^{-6}	2.112	0.705326	6.14	31.8	0.512565	2.33×10^{-6}	0.117	0.512394	0.87
GUC-46q	224	98	185	0.709997	2.56×10^{-6}	1.533	0.705113	7.04	34.3	0.512468	3.93×10^{-6}	0.124	0.512286	−1.24
GUC-47q	224	116	115	0.716998	1.27×10^{-6}	2.921	0.707692	4.70	23.5	0.512497	1.92×10^{-6}	0.121	0.512320	−0.58
GUC-34q	224	117	672	0.706581	1.92×10^{-6}	0.504	0.704977	5.20	23.0	0.512772	1.47×10^{-6}	0.137	0.512572	4.33
GUC-37Aq	224	126	127	0.715666	3.09×10^{-6}	2.873	0.706514	4.17	18.7	0.512533	2.75×10^{-6}	0.135	0.512335	−0.29
GUC-37Cq	224	111	125	0.711957	3.12×10^{-6}	2.570	0.703769	7.76	34.6	0.512560	1.69×10^{-6}	0.136	0.512361	0.22

Sample	U (ppm)	Th (ppm)	Pb (ppm)	$^{206}Pb/^{204}Pb$	Standard error	$^{206}Pb/^{204}Pb$ initial	$^{207}Pb/^{204}Pb$	Standard error	$^{207}Pb/^{204}Pb$ initial	$^{208}Pb/^{204}Pb$	Standard error	$^{208}Pb/^{204}Pb$ initial
GUC-05q	2.52	10.60	18	18.72	2.35×10^{-4}	18.40	15.59	2.17×10^{-4}	15.57	38.61	6.12×10^{-4}	38.17
GUC-32q	0.96	3.68	11	18.63	3.92×10^{-3}	18.43	15.61	3.21×10^{-3}	15.60	38.46	8.49×10^{-3}	38.21
GUC-33q	2.72	12.80	6	19.29	2.94×10^{-4}	18.24	15.62	2.68×10^{-4}	15.57	39.53	6.75×10^{-4}	37.93
GUC-38Bq	0.89	4.25	2.5	18.86	6.98×10^{-4}	18.05	15.60	6.66×10^{-4}	15.56	38.94	1.56×10^{-3}	37.69
GUC-41q	2.70	9.19	27	18.72	3.35×10^{-4}	18.50	15.60	2.19×10^{-4}	15.59	38.61	7.25×10^{-4}	38.36
GUC-45q	2.19	10.20	10	18.81	1.43×10^{-4}	18.31	15.57	1.40×10^{-4}	15.54	38.69	3.91×10^{-4}	37.94
GUC-46q	1.92	8.51	11	18.72	4.04×10^{-4}	18.32	15.58	3.70×10^{-4}	15.56	38.65	1.15×10^{-3}	38.08
GUC-47q	2.00	9.90	12	18.69	3.39×10^{-4}	18.31	15.60	2.51×10^{-4}	15.58	38.69	8.57×10^{-4}	38.08

4.5. Discussion

4.5.1. Source of Late Triassic magmatism in the High Andes

The Late Triassic magmatism has a broad and continuous compositional spectrum, ranging from basaltic to rhyolitic composition with predominance of silicic lithologies, but no bimodal SiO_2 distribution. Most of the samples from the Pastos Blancos Formation and dikes related to Colorado Syenogranites, are subalkaline and differentiate along calc-alkaline trends. The studied rocks show LILE (e.g. Rb, Ba, and K) enrichments with respect to HFSE. Nb-Ta troughs and Pb enrichment are present in all samples, and Sr, P, and Ti troughs are common, which is the typical pattern of subduction-related magmatism (Wilson, 1989, Stern, 2002). The REE chondrite normalized patterns for these units have shallow slopes ($1.53 < La_N/Yb_N < 13.34$) and flat patterns for the HREE ($1.35 < Sm_N/Yb_N < 4.71$), suggesting that the generation of the Upper Triassic magmas took place below a non-thickened crust, with an estimated thickness of approximately 40 km using the procedure described by Profeta et al. (2015). Another characteristic of the REE patterns is the mild concavity in the MREE (Fig. 4.8C and D), suggesting amphibole and titanite fractionation in the source area (Bachmann et al., 2005), which is typical of an oxidized and wet environment for the magma genesis (Bachmann and Bergantz, 2008). The predominantly subalkaline and calc-alkaline nature of these rocks, added to the contents and patterns of the trace elements, suggest that this magmatism is the result of the melting of a depleted mantle, induced by the action of fluids released by the dehydration of the subducted plate, which would explain the LILE enrichments.

The stratified sequences and intrusions representing the Upper Triassic magmatism overlie or intrude igneous rocks of the Lower - Middle Triassic. However, an event of fast exhumation that may have taken place prior to the genesis of the studied magmatism (Section 4.4.1) suggest that these current host rocks were likely not at an appropriate crustal level to be assimilated or melted during the late Triassic magmatic activity. We consider that the Paleozoic continental crust is the most probable contaminant for the Upper Triassic magmatism due to the fact that there is a large volume of Paleozoic rocks to the west (Carboniferous and Permian Intrusives) and to

the east (Las Placetas Formation and Colangüil Batholith) of the Carnian – Norian magmatism and therefore much of the unexposed crust could be Paleozoic in age. The less evolved initial isotopic composition of the Pastos Blancos Formation and Colorado Syenogranites compared to that of the Upper Paleozoic magmatism and the Lower Paleozoic basement located further north (Beccio et al., 1999, Lucassen et al., 1999, Parada et al., 1999, Parada, 2013, Oliveros et al., 2016), suggest that the Paleozoic crust could not have been the sole source of the Upper Triassic magmatism, and the participation of a more depleted source is also required. Therefore, the Upper Triassic magmatism isotope composition is better explained as a mixture between a depleted mantle and the Paleozoic continental crust. The moderate values of $^{87}Sr/^{86}Sr_i$ (~0.705) together with the slightly negative values of εNd_i (~−1) in the studied magmatism suggest that the contribution of the Paleozoic crust during the genesis of Upper Triassic magmatism was restricted, unless the assimilated crust had a less evolved (low ^{87}Sr, high ^{143}Nd) isotopic composition (e.g. lower crust).

As mentioned above, the Carnian - Norian magmatism is characterized by a continuous and broad compositional spectrum. However, as seen in Fig. 4.7A, there is a predominance of silicic compositions. This characteristic is not typical of the continental arcs, where the intermediate compositions are the most frequent, but the presence of silicic magmatism in Phanerozoic arcs has been recognized in others magmatic provinces (e.g. silicic volcanism in the Andean Central Volcanic Zone, de Silva, 1989, Schnurr et al., 2007). The origin of siliceous rocks has been explained by two mechanisms: (1) the fractional crystallization of basaltic magmas derived from the mantle accompanied or not by cortical assimilation or (2) crustal anatexis induced by basaltic mantle-derived magmas. The isotopy of the studied magmatism suggests that the most likely mechanism for generating the rocks of rhyolitic composition corresponds to fractional crystallization, probably accompanied by crustal assimilation. Given that there is no correlation between the isotopic composition and the degree of differentiation of the studied samples, especially in terms of the εNd which is insensitive to post-magmatic alteration, and the fact that even the most silicic rocks have an isotopic signature less evolved that the Paleozoic basement, crustal anatexis does not seem to have played a role in the generation of the Upper Triassic magmas.

4.5.2. Comparison of studied units with contemporaneous and Late Permian-Middle Triassic magmatism

Published data from four Late Permian - Triassic magmatic units exposed between the 28°30′S and 30°S are used for comparison: the Guanaco Sonso Formation, Chollay Plutonic Complex, the eastern section of the Elqui Mafic Dike Swarm and La Totora Formation (Creixell et al., 2009, Salazar et al., 2013, Ortiz and Merino, 2015, Salazar and Coloma, 2016, Oliveros et al., 2016, Coloma et al., 2017). The locations of the samples included in the comparison are shown in Fig. 4.1. The major elements were normalized on an anhydrous basis and the isotopic ratios were corrected for in-situ decay to the respective crystallization ages.

The Late Permian – Lower-Middle Triassic volcanic and volcano-sedimentary rocks of the Guanaco Sonso Formation and the CPC share many compositional characteristics with the Carnian-Norian magmatism, such as the continuous spectrum of compositions with a predominance of subalkaline, silicic rocks of calc-alkaline affinity. Trace element patterns normalized to primitive mantle show enrichment LILE over HFSE and troughs in Nb and Ta, (not show) and are predominantly assigned by their chemical composition to an active continental margin geotectonic setting (Coloma et al., 2017). Only few samples plot in the within-plate and syn-collisional fields on tectonic discrimination diagrams for volcanic and plutonic rocks (Fig. 4.10).

Unlike the units described above, the dikes of the eastern section of the EMDS and the volcanic rocks of the Norian La Totora Formation are mainly basaltic to basaltic-andesitic, but they also are subalkaline. Mafic dykes have tholeiitic affinities, a weak enrichment in LILE with respect to HFSE and mild depressions in Nb and Ta. The samples from La Totora Formation have calc-alkaline evolution trend and exhibit enrichment of LILE over HSFE, with a subtle pronounced Pb enrichment. Both units plot mainly in the fields of volcanic arcs in the tectonic discrimination diagrams with a few samples of La Totora Formation in the within-plate field (Fig. 4.10).

From Late Permian to Late Triassic, the magmatism isotopic composition shows a slight increase in the $\varepsilon Nd_{Initial}$ together with a decrease in the $^{87}Sr/^{86}Sr_{Initial}$, suggesting a reduction in the crustal component in younger magmatism, in agreement

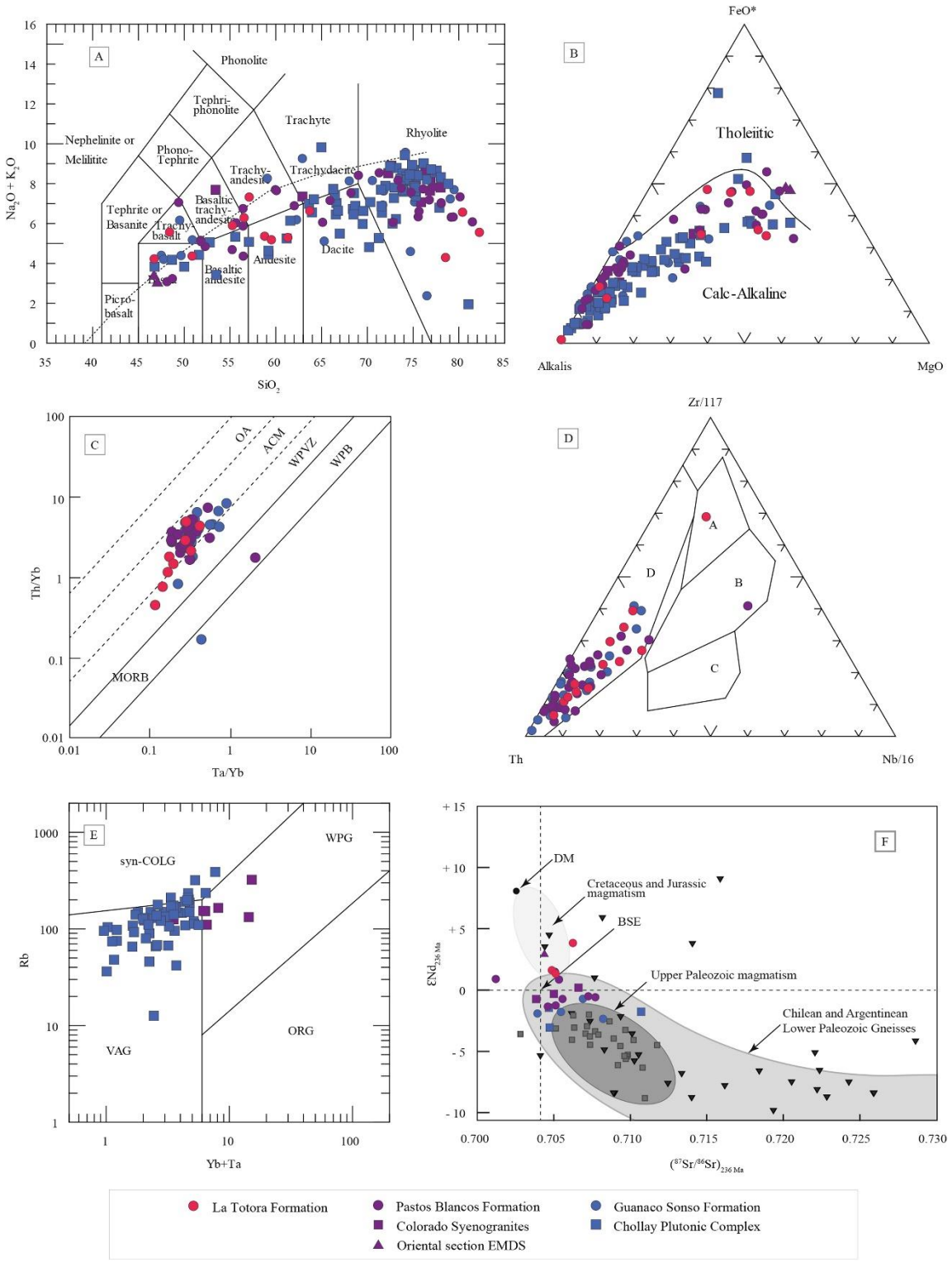

Figure 4.10. Geochemical comparison between studied Carnian – Norian magmatism and Lopingian – Lower-Middle Triassic and Upper Triassic magmatic rocks exposed in the High Andes (28°30′S – 30°S). A. Total alkalis versus silica diagram (TAS, Le Maitre et al., 1989) for all samples including volcanic and intrusive rocks. The dashed line divides alkaline and subalkaline series (Irvine and Baragar, 1971). B. AFM diagram, division between tholeiitic and calcalkaline series (Irvine and Baragar, 1971). C. Th/Yb vs

Ta/Yb tectonic discrimination diagram for intermediate and silicic volcanic rocks (Gorton and Schandl, 2000), the fields correspond to: oceanic arc (OA), active continental margins (ACM), within-plate volcanic zones (WPVZ), within-plate basalt (WPB) and mid-ocean ridge basalt (MORB). D. Th - Zr - Nb tectonic discrimination diagram for silicic, intermediate and basic volcanic rocks (Wood, 1980), the field correspond to: N-type MORB (A), E-type MORB and tholeiitic within-plate basalts and differentiates (B), alkaline within-plate basalts and differentiates (C) and destructive plate-margin basalts and differentiates (D). E. Rb versus Yb + Ta tectonic discrimination diagram for granitic rocks (Pearce et al., 1984), the fields correspond to: ocean ridge granites (ORG), volcanic arc granites (VAG), within plate granites (WPG) and syn-collision granites (syn-COLG). F. ℇNd versus 87Sr/86Sr diagram. The isotopic ratios of magmatism older than the studied units were recalculated at the average age of the Pastos Blancos Formation (236 Ma), as well as the isotopic ratios of the Chilean and Argentine Lower Paleozoic gneisses. The youngest magmatism is plotted with its initial isotopic ratios. The values of the Depleted Mantle (DM) and the Bulk Silicate Earth (BSE) were taken from Workman and Hart (2005).

with the progressive sources change from Carboniferous to Early Jurassic in the magmatism exposed in the Chilean Costal and Frontal Ranges, based on its $\delta^{18}O$ and ℇHf in zircon composition (Hervé et al., 2014, del Rey et al., 2016). The $(La/Yb)_N$ ratios for Late Permian – Lower-Middle Triassic magmatism range between 0.82 and 40.6, but most samples are between 3.5 and 10, whereas the Upper Triassic ratios range from 1.5 to 9.6 with most samples between 2.5 and 8.0, also suggesting a slight trend of diminished crustal thickness in the younger rocks. The increase in the mantle component of the magmatism sources could have been due to steepening of the subducted plate that triggered extension and thinning of the continental crust (del Rey et al., 2016) (Fig. 4.11).

4.5.3. Geotectonic setting for the Upper Triassic magmatism in the western margin of Gondwana

The Late Permian – Triassic magmatism described above (Guanaco Sonso and Pastos Blancos formations, Chollay Plutonic Complex and Colorado Syenogranites) was assigned to the “Pastos Blancos Group” and the “Ingaguás Superunit” (Nasi et al., 1985), and interpreted as equivalents of the Choiyoi Group magmatism (Kay et al., 1989, Mpodozis and Kay, 1990, Mpodozis and Kay, 1992) based on the predominance of silicic compositions and their ages. The Choiyoi magmatism has been divided into two sections (Llambías et al., 1993, Sato and Llambías, 1993): a lower section (280–260 Ma) of andesitic composition with calcalkaline affinities, related to the last stages of the subduction, and an upper section (259–247 Ma) of silicic and post-orogenic compositions, which marks the transition towards an intraplate magmatism developed

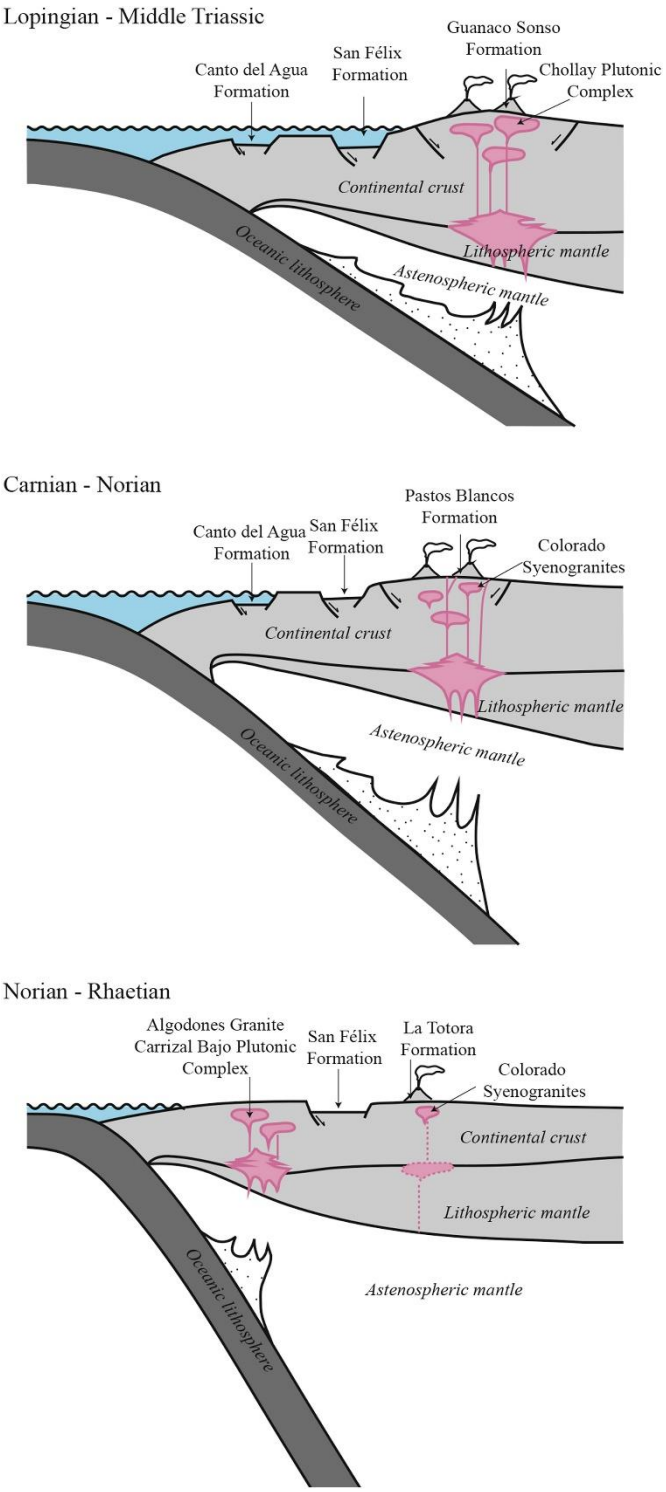

Figure 4.11. Geotectonic evolution proposed for the southwestern of Gondwana margin between actual 28°30′ – 30°S, during Lopingian – Upper Triassic. We propose a continuous subduction during this period with a progressive slab steepening and crustal thinning. A. Lopingian – Middle Triassic: the magmatic arc was situated in the High Andes and would be represented by the Chollay Plutonic Complex and Guanaco Sonso Formation (Coloma et al., 2017). B. Carnian – Norian: the position of the magmatic arc migrated slightly to the west and would be represented by the Pastos Blancos Formation and Colorado Syenogranites. C. Rhaetian: The magmatic front migrated to the Coastal Range, represented by Algodones Granite and Carrizal Bajo Plutonic Complex. La Totora Formation could corresponds to the remnants of the arc previously situated in the Frontal Cordillera.

in an extensional setting (Kay et al., 1989, Mpodozis and Kay, 1992, Llambías and Sato, 1995, Martínez et al., 2006, Kleiman and Japas, 2009). Taking into account the updated geochronological framework for the Chilean units, the Guanaco Sonso Formation can be considered as part of the Upper Choiyoi magmatism, and the Chollay

Plutonic Complex, Pastos Blancos and La Totora Formations are part of the post-Choiyoi magmatism.

The new and published data for the Upper Triassic magmatism, do not support previous models that invoked crustal melting as the mechanism responsible for the Choiyoi magmatism and decompression melting of asthenospheric mantle for the post-Choiyoi magmatism, in the context of inactive subduction (Kay et al., 1989, Mpodozis and Kay, 1992, Martin et al., 1999). The major and trace element composition of the studied magmatism, show characteristics of a magmatism generated in an active continental margin and its isotopic composition demonstrates that this was generated from a mixture of sources that correspond to a MORB-like depleted mantle source and the Paleozoic continental crust. Although the intraplate signal is present in some samples of the Chilean post-Choiyoi magmatism studied in this work (Fig. 4.10), they represent a restricted volume compared to the magmatism that can be related with the arc activity in an active continental margin. Taking this into account, we propose that during the Carnian – Norian the subduction along this section of the Andean margin was an active process. Furthermore, our data do not fit the model proposed by Martin et al. (1999) which suggested that the important volume of basaltic magmas represented by the current exposed dikes in the study area would be related to basaltic underplating that facilitated crustal melting and thereby generated the Upper Triassic magmatism.

The Pastos Blancos Formation shows important variations in thickness, which suggests that accumulation of the volcanic material occurred in a volcanic basin with an N-S axis, limited by faults that are probably inverted during Cenozoic compressional tectonic events (Ortiz and Merino, 2015). Secondary normal faults and high angle contacts trending ca. WNW-ESE are also recognized outside the main axis of the possible basin, where the Pastos Blancos Formation is deposited over the Chollay Plutonic Complex and older units. To the south, near 30° S, the contact between this formation and the country rock is also controlled by a E-W trending normal fault that limit the deposits to the south (Murillo et al., 2017). The accumulation of the volcanic deposits in an extensional basin occurs contemporaneously with the intrusion of the EMDS. The distribution of dikes indicates that near-horizontal crustal dilation associated with the

injection of the mafic dikes. The cumulative dike thickness indicates crustal dilation by dike injection between 7.5% and 39.58% in the studied section, with an absolute minimum extension value of 285 m, a value comparable to crustal dilation associated to magma injection below volcanic centers (i.e. Marinoni, 2001). However, this value is much smaller than values calculated from extension in continental rift zones and oceanic expansion areas (Klausen and Larsen, 2002, Bell et al., 2011). In spite of this, is still unclear how much extension accumulated along possible normal faults in the area. The dominant distribution of dikes in the EMDS, suggest that extension was mainly associated with a WNW-ESE extensional strain vector. This extensional deformation field apparently prevailed during large periods of the Triassic in the Vallenar-La Serena area according to the geometrical features of the San Felix and La Totora formations in the High Andes (Salazar et al., 2013) and the Carrizal Bajo Plutonic Complex in the Coastal Cordillera (Grocott et al., 2009).

4.6. Conclusions

The Pastos Blancos Formation corresponds to a mainly volcanic sequence that is composed of lavas ranging from andesites to rhyolites, and pyroclastic rocks, specifically rhyodacitic and rhyolitic tuffs. Thickness variations in this sequence from north to south suggest that it was deposited in a basin with an N-S axis limited by normal faults. The Pastos Blancos Formation accumulation is associated with the penecontemporaneous mafic and felsic dike injection, and with restricted monzogranitic and syenogranitic intrusive bodies belonging to the Colorado Syenogranites.

The studied Carnian – Norian magmatism has features that are characteristic of a subduction-related magmatism, such as a continuous compositional spectrum, calcalkaline affinities, enrichment of LILE with respect to HFSE and depressions in Nb-Ta and Ti. The REE patterns of the analyzed samples suggest that this magmatism was generated under a normal thickness crust. This is consistent with extensional dynamics and the development of the Pastos Blancos Formation basin and the injection of mafic dikes. The calculated amount of crustal extension due to dike injection of the

Elqui Mafic Dike Swarm, is far below the amounts of extension in typical continental rift zones.

The magmatism of the Lopingian – Lower-Middle Triassic exposed between 28°30′ S and 30° S has geochemical characteristics very similar to those of the studied magmatism, and has been proposed as a subduction zone magmatism (Coloma et al., 2017). Isotopic compositions of the Lopingian - Triassic igneous rocks indicate that the sources of the magmas correspond to mixing of a depleted mantle and the regional older continental crust.

Apart from the compositional similarity of Lopingian – Lower-Middle Triassic and Carnian - Norian magmatism, subtle differences exist between the two-time sections. The Carnian – Norian magmatism has flatter REE patterns, lower $^{87}Sr/^{86}Sr$ ratios, and higher ƐNd values and some samples with potential intraplate affinities in the rocks than the older group. We interpreted this as an increasing influence of the depleted mantle source in the hybrid magmas, which could be due to steepening of the subducted plate that triggered extension and thinning of the continental crust.

Ackowledgements

This research was funded through the Plan Nacional de Geología of the Chilean Geological and Mining Survey (Servicio Nacional de Geología y Minería, SNGM), the Fondecyt grant 1120715 and the Doctoral fellowship of the National Commission for Scientific and Technological Research (Comisión Nacional de Investigación Científica y Tecnológica, CONICYT), grant no. 21150502. Felipe Coloma, Esteban Salazar, Miguel Ortiz, Roberto Merino and Ismael Murillo are thanked for the fruitful discussions on the updated geological mapping in northern Chile.

4.7 References

Arriagada, C., Cobbold, P.R., Roperch, P., 2006. Salar de Atacama basin: A record of compressional tectonics in the central Andes since the mid-Cretaceous. Tectonics 25, 1–19. doi:10.1029/2004TC001770

Bachmann, O., Bergantz, G.W., 2008. Rhyolites and their Source Mushes across Tectonic Settings. J. Petrol. 49, 2277–2285. doi:10.1093/petrology/egn068

Bachmann, O., Dungan, M.A., Bussy, F., 2005. Insights into shallow magmatic processes in large silicic magma bodies: The trace element record in the Fish Canyon magma body, Colorado. Contrib. to Mineral. Petrol. 149, 338–349. doi:10.1007/s00410-005-0653-z

Bartley, J.M., Coleman, D.S., Glazner, A.F., 2006. Incremental pluton emplacement by magmatic crack-seal. Trans. R. Soc. Edinb. Earth Sci. 97, 383–396. doi:10.1017/S0263593300001528

Beccio, R., Lucassen, F., Kasemann, S., Franz, G., Viramonte, J., 1999. Geochemistry and isotope systematics of Early Paleozoic metamorphic rocks Northwest Argentina and North Chile (21° – 27°S). Acta Geológica Hispana. 34, 273–299.

Bell, R.E., McNeill, L.C., Henstock, T.J., Bull, J.M., 2011. Comparing extension on multiple time and depth scales in the Corinth Rift, Central Greece. Geophys. J. Int. 186, 463–470. doi:10.1111/j.1365-246X.2011.05077.x

Cembrano, J., Zentilli, M., Grist, A., Yáñez, G., 2003. Nuevas edades de trazas de fisión para Chile Central (30-34°S): Implicancias en el alzamiento y exhumación en los Andes desde el Cretácico. 10th Congreso Geológico Chileno, Concepción, Chile.

Charrier, R.; Pinto, L.; Rodríguez, M. 2007. Tectonostratigraphic evolution of the Andean Orogen in Chile. The Geology of Chile. (Moreno, T.; Gibbons, W., editors). The Geological Society: 21 – 114. London. doi:10.1144/GOCH.3

Charrier, R., Ramos, V.A., Tapia, F., Sagripanti, L., 2014. Tectono-stratigraphic evolution of the Andean Orogen between 31 and 37°S (Chile and Western Argentina). Geol. Soc. London, Spec. Publ. 399, 13–61.

Coira, B., Davidson, J., Mpodozis, C., Ramos, V., 1982. Tectonic and Magmatic Evolution of the Andes of Northern Argentina and Chile. Earth Sci. Rev. 18, 303–332. doi:10.1016/0012-8252(82)90042-3

Coloma, F., Valin, X., Oliveros, V., Vásquez, P., Creixell, C., Salazar, E., Ducea, M.N., Vallejos, D., 2017. Geochemistry of Permian to Triassic igneous rocks from

northern Chile (28°-30°15'S): Implications on the dynamics of the proto-Andean margin. Andean Geol. 44, 147–178. doi:10.5027/andgeoV44n2-a03

Cox, K.G., Bell, J.D., Pankhurst, R.J., 1979. The Interpretation of Igneous Rocks. Springer Netherlands.

Creixell, C., Parada, M.Á., Morata, D., Roperch, P., Arriagada, C., 2009. The genetic relationship between mafic dike swarms and plutonic reservoirs in the mesozoic of central chile (30°-33°45'S): insights from AMS and geochemistry. Int. J. Earth Sci. 98, 177–201. doi:10.1007/s00531-007-0240-9

de Silva, S.L., 1989. Altiplano-Puna volcanic complex of the central Andes. Geology 17, 1102–1106. doi:10.1130/0091-7613(1989)017<1102

del Rey, A., Deckart, K., Arriagada, C., Martínez, F., 2016. Resolving the paradigm of the late Paleozoic - Triassic Chilean magmatism: Isotopic approach. Gondwana Res. 37, 172–181. doi:10.1016/j.gr.2016.06.008

Deniel, C., Pin, C., 2001. Single-stage method for the simultaneous isolation of lead and strontium from silicate samples for isotopic measurements. Anal. Chim. Acta 426, 95–103. doi:10.1016/S0003-2670(00)01185-5

Emerman, S.H., Marrett, R., 1990. Why dikes? Geology 18, 231–233. doi:10.1130/0091-7613(1990)018<0231

Franzese, J.R., Spalletti, L.A., 2001. Late Triassic- early Jurassic continental extension in southwestern Gondwana: tectonic segmentation and pre-break-up rifting. J. South Am. Earth Sci. 14, 257–270. doi:10.1016/S0895-9811(01)00029-3

Gorton, M.P., Shandl, E.S., 2000. From continents to island arcs: A geochemical index of tectonic setting for arc-related and within-plate felsic to intermediate volcanic rocks. Can. Mineral. 38, 1065–1073. doi:10.2113/gscanmin.38.5.1065

Grocott, J., Arévalo, C., Welkner, D., Cruden, A., 2009. Fault-assisted vertical pluton growth: Coastal Cordillera, north Chilean Andes. J. Geol. Soc. London. 166, 295–301. doi:10.1144/0016-76492007-165

Hervé, F., Fanning, C.M., Calderón, M., Mpodozis, C., 2014. Early Permian to Late Triassic batholiths of the Chilean Frontal Cordillera (28°-31°S): SHRIMP U-Pb zircon ages and Lu-Hf and O isotope systematics. Lithos 184–187, 436–446. doi:10.1016/j.lithos.2013.10.018

Irvine, T.N., Baragar, W.R.A., 1971. A Guide to the Chemical Classification of the Common Volcanic Rocks. Can. J. Earth Sci. 8, 523–548. doi:10.1139/e71-055

Jensen, O., 1976. Geología de las nacientes del río Copiapó, entre los 27°53' y 28°20' de latitud sur. Provincia de Atacama, Chile. Universidad de Chile.

Kay, S.M., Ramos, V.A., Mpodozis, C., Sruoga, P., 1989. Late Paleozoic to Jurassic silicic magmatism at the Gondwana margin: Analogy to the Middle Proterozoic in North America? Geology 17, 324–328. doi:10.1130/0091-7613(1989)017<0324:LPTJSM>2.3.CO;2

Klausen, M., Larsen, H., 2002. East Greenland coast-parallel dike swarm and its role in continental break-up. Geol. Soc. Am. Spec. Pap. 362, 133–158.

Kleiman, L.E., Japas, M.S., 2009. The Choiyoi volcanic province at 34°S – 36°S (San Rafael, Mendoza, Argentina): Implications for the Late Palaeozoic evolution of the southwestern margin of Gondwana. Tectonophysics 473, 283–299. doi:10.1016/j.tecto.2009.02.046

Kramer, W., Siebel, W., Romer, R.L., Haase, G., Zimmer, M., Ehrlichmann, R., 2005. Geochemical and isotopic characteristics and evolution of the Jurassic volcanic arc between Arica (18°30'S) and Tocopilla (22°S), North Chilean Coastal Cordillera. Chemie der Erde 65, 47–78. doi:10.1016/j.chemer.2004.01.002

Le Maitre, R.., Bateman, P., Dudek, A., Keller, J., Lameyre, M., Le Bas, M.J., Sabine, P.A., Schmid, R., Sørensen, H., Streckeisen, A., Woolley, A.R., Zanettin, B., 1989. A Classification of Igneous Rocks and a Glossary of Terms. Recommendations of the International Union of Geological Sciences Subcommission on the Systematics of Igneous Rocks. Blackwell Scientific Publications, Oxford.

Llambías, E.J., Sato, A.M., 1995. El Batolito de Colangüil: Transición entre orogénesis y anorogénesis. Rev. la Asoc. Geológica Argentina 50, 111–131.

Llambías, E.J., Kleiman, L.E., Salvarredy, J., 1993. El magmatismo Gondwánico. In: Ramos, V.A. (Ed.), Geología y Recursos Naturales de Mendoza, Relatorio 12° Congreso Geológico Argentino y 2° Congreso de Exploración de Hidrocarburos, Mendoza, pp. 53-64.

Lucassen, F., Franz, G., Thirlwall, M.F., Mezger, K., 1999. Crustal Recycling of Metamorphic Basement: Late Palaeozoic Granitoids of Northern Chile (~ 22°S). Implications for the Composition of the Andean Crust. J. Petrol. 40, 1527–1551.

Lucassen, F., Becchio, R., Harmon, R., Kasemann, S., Franz, G., Trumbull, R., Wilke, H., Romer, R.L., Dulski, P., 2001. Composition and density model of the continental crust at an active continental margin — the Central Andes between 21° and 27° S. Tectonophysics 341, 195–223.

Lucassen, F., Kramer, W., Bartsch, V., Wilke, H.G., Franz, G., Romer, R.L., Dulski, P., 2006. Nd, Pb, and Sr isotope composition of juvenile magmatism in the Mesozoic large magmatic province of northern Chile (18-27°S): Indications for a uniform subarc mantle. Contrib. to Mineral. Petrol. 152, 571–589. doi:10.1007/s00410-006-0119-y

Lossada, A.C., Giambiagi, L., Hoke, G.D., Fitzgerald, P.G., Creixell, C., Murillo, I., Mardonez, D., Velásquez, R., Suriano, J. 2017. Thermochronologic evidence for late Eocene Andean mountain building at 30°S. Tectonics. 36. doi: 10.1002/2017TC004674.

Maksaev, V., Munizaga, F., Tassinari, C., 2014. Timing of the magmatism of the paleo-Pacific border of Gondwana: U-Pb geochronology of Late Paleozoic to Early Mesozoic igneous rocks of the north Chilean Andes between 20° and 30°S. Andean Geol. 41, 447–506. doi:10.5027/andgeoV41n3-a01

Marinoni, L.B., 2001. Crustal extension from exposed sheet instrusions: review and method proposal. J. Volcanol. Geotherm. Res. 107, 27–46. doi:10.1016/S0377-0273(00)00318-8

Martin, M.W., Clavero R, J., Mpodozis M, C., 1999. Late Paleozoic to Early Jurassic tectonic development of the high Andean Principal Cordillera, El Indio Region, Chile (29 - 30°S). J. South Am. Earth Sci. 12, 33–49.

Martínez, A., Barredo, S., Giambiagi, L., 2006 Modelo geodinámico para la evolución magmática Permo-Triásica entre los 32° y 34° S, Cordillera Frontal de Mendoza, Argentina. XIII Reunión de Tectónica, San Luis, Argentina.

Míková, J., Denková, P., 2007. Modified chromatographic separation scheme for Sr and Nd isotope analysis in geological silicate samples. J. Geosci. 52, 221–226. doi:10.3190/jgeosci.015

Mpodozis, C., Kay, S.M., 1992. Late Paleozoic to Triassic evolution of the Gondwana margin: evidence from Chilean Frontal cordilleran batholiths (28°S to 31°S). Geol. Soc. Am. Bull. 104, 999–1014. doi:10.1130/0016-7606(1992)104<0999:LPTTEO>2.3.CO;2

Mpodozis, C., Cornejo, P., 1988. Hoja Pisco Elqui. IV Región de Coquimbo, Servicio Nacional de Geología y Minería. Carta Geológica de Chile 68. map scale 1:250.000.

Mpodozis, C., Kay, S.M., 1990. Provincias magmáticas ácidas y evolución tectónica de Gondwana: Andes Chilenos (28-31°S). Rev. Geol. Chile 17, 153–180. doi:10.5027/andgeoV17n2-a03

Mpodozis, C., Ramos, V., 1989. The Andes of Chile and Argentina, in: Ericksen, G.E., Cañas Pinochet, M.T., Reinemund, J.A. (Eds.), Geology of the Andes and Its Relation to Hydrocarbon and Mineral Resources. Circum-Pacific Council for Energy and Mineral Resources Earth Science Series, Houston, Texas, pp. 59–90.

Murillo, I., Velásquez, R., Creixell, C., in press. Geología del área Guanta - Paso de Vacas Heladas. Serv. Nac. Geol. y Minería. Cart. Geológica Chile, Ser. Geol. Básica . map scale 1:100.000.

Nakamura, N., 1974. Determination of REE, Ba, Fe, Mg, Na and K in carbonaceous and ordinary chondrites. Geochim. Cosmochim. Acta 38, 757–775. doi:10.1016/0016-7037(74)90149-5

Nasi, C., Moscoso, R., Maksaek, V., 1990. Hoja Guanta. Región de Coquimbo. Serv. Nac. Geol. y Minería. Cart. Geológica Chile 67. map scale 1:250.000.

Nasi, C., Mpodozis, C., Cornejo, P., Moscoso, R., Maksaev, V. 1985. El Batolito Elqui-Limarí (Paleozoico Superior – Triásico): características petrográficas, geoquímicas y significado tectónico. Rev. Geológica Chile 25-26, 77-111.

Oliveros, V., Morata, D., Féraud, G., Fornari, M., 2007. Jurassic to Early Cretaceous subduction-related magmatism in the Coastal Cordillera of northern Chile (18°30'-24°S): geochemistry and petrogenesis. Rev. Geológica Chile 34, 209–232. doi:10.4067/S0716-02082007000200003

Oliveros, V., González, J., Espinoza, M., Vásquez, P., Rossel, P., Creixell, C., Sepúlveda, F., Bastías, F., 2017. The early stages of the magmatic arc in the Southern Central Andes, in Folguera et al., (eds.): The Evolution of the Chilean-Argentinean Andes. Springer. Berlín, 185 – 212.

Oliveros, V., Vásquez, P., Creixell, C., Lucassen, F., Ducea, M., González, J., Ciocca, I., 2016. Lithospheric evolution at the Early Andean convergent margin, Chile. Goldschmidt2016 Conference. Geochemical Society and European Association of Geochemistry, Yokohama, 2382.

Ortiz, M., Merino, R., 2015. Geología de las áreas Río Chollay - Matancilla y Cajón del Encierro. Regiones de Atacama y Coquimbo, Servicio Nacional de Geología y Minería. Carta Geológica de Chile, Serie Geología Básica 175-176. map scale 1:100.000.

Parada, F., 2013. Geoquímica de las rocas ígneas del Carbonífero - Triásico de la Alta Cordillera, Región de Atacama, Chile. Memoria para optar al título de Geólogo, Universidad de Chile.

Parada, M.A., Nyström, J.O., Levi, B., 1999. Multiple sources for the Coastal Batholith of central Chile (31 – 34°S): geochemical and Sr – Nd isotopic evidence and tectonic implications. Lithos 46, 505–521.

Pearce, J.A., Harris, N.B.W., Tindle, A.G., 1984. Trace Element Distribution Diagrams for the Tectonic Interpretation of Granitic Rocks. J. Petrol. 25, 956–983. doi:10.1093/petrology/25.4.956

Peccerillo, A., Taylor, S.R., 1976. Geochemistry of Eocene Calc-Alkaline Volcanic Rocks from the Kastamonu Area, Northern Turkey. Contrib. to Mineral. Petrol. 58, 63–81. doi:10.1007/BF00384745

Pettilohn, F.J., 1975. Sedimentary rocks. Harper & Row, New YorkPin, C., Santos Zalduegui, J.F., 1997. Sequential separation of light rare-earth elements, thorium and uranium by miniaturized extraction chromatography: Application to isotopic analyses of silicate rocks. Anal. Chim. Acta 339, 79–89. doi:10.1016/S0003-2670(96)00499-0

Poma, S., Zappettini, E.O., Quenardelle, S., Santos, J.O., Koukharsky, M., Belousova, E., McNaughton, N., 2014. Geochemistry, U-Pb SHRIMP zircon dating and Hf isotopes of the Gondwanan magmatism in NW Argentina: petrogenesis and geodynamic implications. Andean Geol. 41, 267–292. doi:10.5027/andgeoV41n2-a01

Profeta, L., Ducea, M.N., Chapman, J.B., Paterson, S., Henríquez González, S.M., Kirsch, M., Patrescu, L., DeCelles, P.G., 2015. Quantifying crustal thickness over time in magmatic arcs. Sci. Rep. 5, 1–7. doi:10.1038/srep17786

Ramos, V.A., Folguera, A., 2009. Andean flat-slab subduction through time. Geol. Soc. London, Spec. Publ. 327, 31–54. doi:10.1144/SP327.3

Ribba, L., Mpodozis, C., Hervé, F., Nasi, C., Moscoso, R., 1988. El Basamento del Valle del Tránsito, Cordillera de Vallenar: Eventos Magmáticos y Metamórficos y su relación con la evolución de los Andes chileno-argentinos. Rev. Geológica Chile 15, 129–149.

Salazar, E., Coloma, F., 2016. Geología del área Cerros de Cantaritos-Laguna Chica. Región de Atacama, Servicio Nacional de Geología y Minería. Carta Geológica de Chile, Serie Geología Básica 181. map scale 1:100.000.

Salazar, E., Coloma, F., Creixell, C., 2013. Geología del área El Tránsito - Lagunillas, Región de Atacama, Servicio Nacional de Geología y Minería. Carta Geológica de Chile, Serie Geología Básica 149. map scale 1:100.000.

Sato, A.M., Llambías, E.J., 1993. El Grupo Choiyoi, provincia de San Juan: equivalentes efusivos del batolito Colangüil. In: 12° Congreso Geológico Argentino y 2° Congreso de Exploración de Hidrocarburos (Mendoza), Actas 4, pp. 156 – 165.

Sato, A.M., Llambías, E.J., Basei, M.A.S., Castro, C.E., 2015. Three stages in the Late Paleozoic to Triassic magmatism of southwestern Gondwana, and the relationships with the volcanogenic events in coeval basins. J. South Am. Earth Sci. 63, 48–69. doi:10.1016/j.jsames.2015.07.005

Shand, S.J., 1927. On the Relations between Silica, Alumina, and the Bases in Eruptive Rocks, considered as a Means of Classification. Geol. Mag. 64, 446–449. doi:10.1017/S0016756800103760

Stern, R.J., 2002. Subduction zones. Rev. Geophys. 40, 3-1-3–38. doi:10.1029/2001RG000108

Suárez, M., Bell, C.M., 1992. Triassic rift-related sedimentary basins in northern Chile (24° – 29°S). J. South Am. Earth Sci. 6 (3), 109 – 121.

Sun, S. -s., McDonough, W.F., 1989. Chemical and isotopic systematics of oceanic basalts: implications for mantle composition and processes. Geol. Soc. London, Spec. Publ. 42, 313–345. doi:10.1144/GSL.SP.1989.042.01.19

Thiele, R., 1964. Reconocimiento geológico de la Alta Cordillera de Elqui. Universidad de Chile.

Vásquez, P., Glodny, J., Franz, G., Frei, D., Romer, R.L., 2011. Early Mesozoic Plutonism of the Cordillera de la Costa (34°–37°S), Chile: Constraints on the Onset of the Andean Orogeny. J. Geol. 119, 159–184. doi:10.1086/658296

Vilas, J.F.A., Valencio, D.A., 1978. Palaeomagnetism of South American and African rocks and the age of the South Atlantic. Rev. Bras. Geociencias 8, 3–10.

White, W. 2013. Geochemistry. Wiley-Blackwell, Oxford.

Wilson, M., 1989. Igneous Petrogenesis a global tectonic approach. Springer, London.

von Hillebrandt, 1973. Neue Ergebnisse über den Jura in Chile und Argentinien. Münstersche Forschungen zur Geologie und Paläontologie 31(32), 167-199.

Wood, D.A., 1980. The application of a Th-Hf-Ta diagram to problems of tectonomagmatic classification and to establishing the nature of crustal contamination of basaltic lavas of the British Tertiary Volcanic Province. Earth Planet. Sci. Lett. 50, 11–30

Workman, R.K., Hart, S.R., 2005. Major and trace element composition of the depleted MORB mantle (DMM). Earth Planet. Sci. Lett. 231, 53–72. doi:10.1016/j.epsl.2004.12.005

Zindler, A., Hart, S., 1986. Chemical Geodynamics. Annu. Rev. Earth Planet. Sci. 14, 493–571. doi:10.1146/annurev.earth.14.1.493

CAPÍTULO V: MAGMATISMO DEL CHOIYOI

Manuscript title: Volumetric and compositional estimation of the Choiyoi Magmatic Province and its comparison with other Silicic Large Igneous Provinces.

Authors: Francisco Bastías-Mercado1, Javiera González1, Verónica Oliveros1*

[1] Departamento Ciencias de la Tierra, Universidad de Concepción, Casilla 160-C, Concepción, Chile.

Published as: Bastías-Mercado, F.; González, J.; Oliveros, V. (2020): Volumetric and compositional estimation of the Choiyoi Magmatic Province and its comparison with other Silicic Large Igneous Provinces., Journal of South American Earth Sciences, 103: 102749.

Abstract

The Choiyoi Magmatic Province (ChMP) is a major feature of southern South America comprising volcanic and plutonic rocks from the Early Permian to the Early Triassic (286-247 Ma), prior to the Andean subduction. Its outcrops are exposed from northern Chile (~20°S) down to southwestern Argentina in Patagonia (~44°S), and from the Andean region to the foreland in southeastern Argentina. These rocks can be subdivided in three main regions: Andes, La Pampa Permian-Triassic Magmatic Corridor (CMPT-LP) and North Patagonia. Despite the three regions have similar lithological composition and timing, the deformation style and geochemical features of the CMPT-LP rocks suggest that they may represent an event of magmatism distinct from the Andes region. On the other hand, the rocks from North Patagonia and the Andes regions are considered to be part of the same geotectonic setting, the Orogenic Choiyoi, even though North Patagonia exhibits a more complex deformation pattern. A compilation of published ages and lithological data for all the units that compose the ChMP, allowed an estimation of its areal extent (909,250 km^2), the volume of its volcanic products, and the compositional variation through time. The volcanic products of Choiyoi Magmatic Province (ChMP-V) are composed of 51% rhyolite, 26% dacite, 22% andesite and 1% basalts, but the early stages of the volcanism were dominated by andesitic products. The plutonic rocks make up the 25% of the total area of the ChMP and they are dominated by granites (~65%) and granodiorites (~30%), although the units representing the early stages of the ChMP are composed up to 60% of granodiorites, tonalites and diorites. It is thus evident that the Choiyoi magmatism, in its whole extension, transitioned from dominantly intermediate to more rhyolitic at its final stages. When considering the ChMP-V, their estimated volume (947,553 km^3) and time span are akin to a Silicic Large Igneous Province (SLIP). However, their lithological composition through time and especially the large amount of intermediate rocks in the first stage of the ChMP-V differ from typical SLIPs, in which rhyolitic and bimodal (rhyolite-basalt) compositions dominate. The largest preserved silicic province identified so far, the Okhotsk-Chukotka Volcanic Belt (OCVB) in Siberia, has nonetheless a compositional pattern very similar to the ChMP-V with an early stage in which the magmatism was dominantly intermediate in composition (~47% of outcrops),

followed by a more volumetric and mostly rhyolitic stage. The fact that the OCVB and other silicic provinces related to convergent margins, such as the Sikote-Alin Belt or the Taupo Volcanic Zone have a similar evolution than the ChMP-V, suggests that the Choiyoi Magmatic Province could have been partly generated in a subduction zone setting.

Keywords: Permian, Subduction magmatism, Lithological evolution, Southwestern Gondwana

5.1 Introduction

Silicic Large Igneous Provinces (SLIPs) are important features of the continental crust, they are defined as high volume (>0.25x106 km^3) provinces of dominantly rhyolite-dacite (>80%) magmatism, spanning at least 40 Myr of magmatic activity (Byran, 2007). SLIPs are less abundant in the geological record than the continental flood basalts that compose the mafic Large Igneous Provinces (LIPs) and although they may be associated to continental rifting, their precise geotectonic setting is debated (Bryan and Ernst, 2013; Tikhomirov, 2010). Furthermore, given the degree of continental crust assimilation needed for the formation of the large felsic sequences, unlike LIPs, the net contribution of SLIPs to crustal growth is currently unknown (Bryan, 2007). In general, SLIPs cover large volumes of the continental masses and thus represent intense magmatic activity, although developed during a longer lifespan than the more mafic counterparts (<5 Myr).

In Southwestern Gondwana (present-day South America), only one SLIP is currently recognized: the Jurassic Chon Aike Province in Patagonia, Argentina, which developed in response to the thermal anomaly of the Karoo plume and immediately postdate the emplacement of the Karoo LIP and subsequent continental rifting (Pankhurst et al. 1998; Navarrete et al., 2019). However, another large exposure of intermediate and felsic magmatism is observed to the north of Chon Aike outcrops in Chile and Argentina, the Middle Permian to Lower Triassic Choiyoi Magmatic Province (ChMP; Fig. 5.1; Llambías and Sato, 2011; Sato et al. 2015; Spalletti and Limarino, 2017). The ChMP is dominated by highly siliceous igneous rocks, such as dacite and rhyolite, and its activity spans ca. 40 Myr (Sato et al., 2015), suggesting that it may correspond to a SLIP

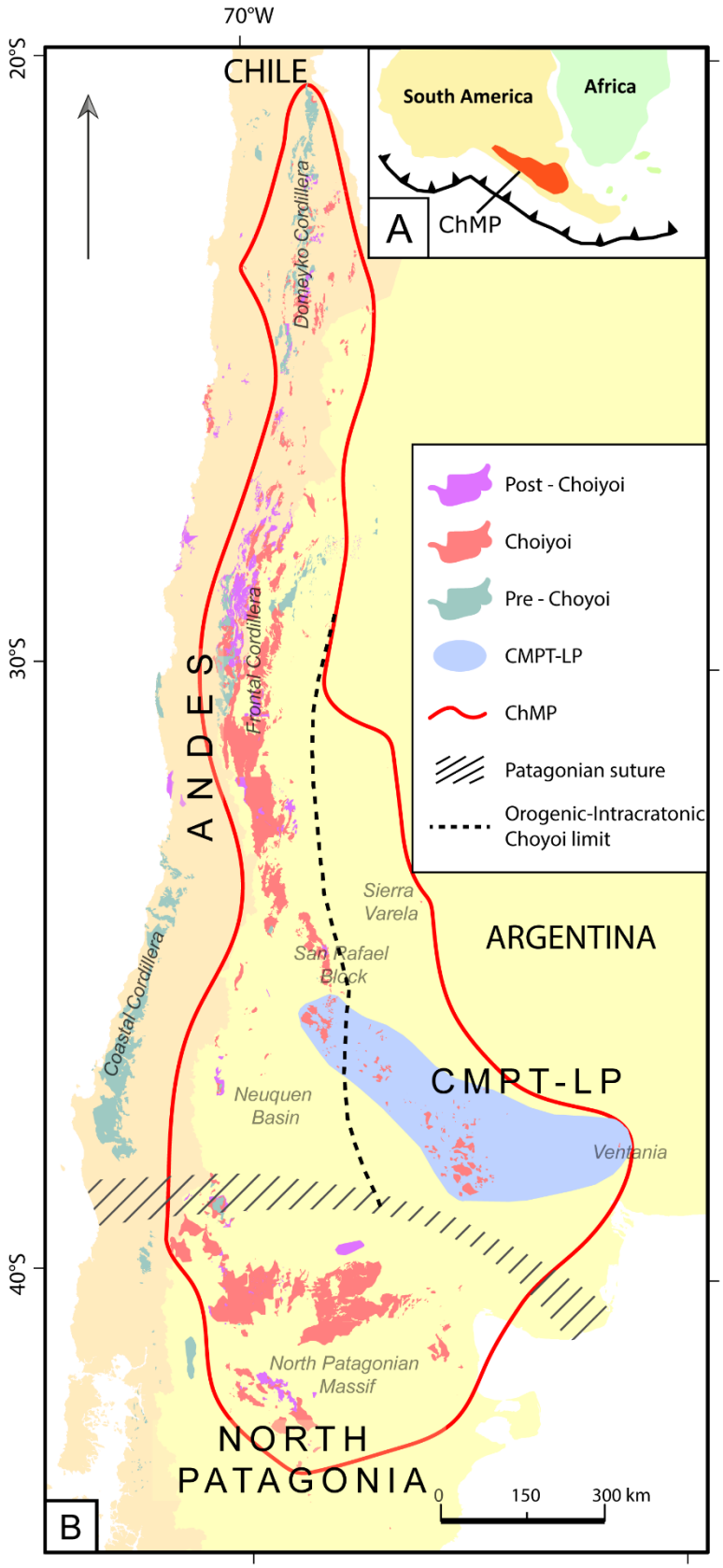

Figure 5.1. (a) Location of the Choiyoi Magmatic Province (ChMP) in SW Gondwana during the Permian-Lower Triassic. Modified from Nelson and Cottle (2019). (b) Distribution of volcanic and plutonic outcrops from Carboniferous-Triassic magmatism, separated according to the three stages proposed by Sato et al. (2015): pre-Choiyoi, Choiyoi (286-247 Ma) and post-Choiyoi. Intracratonic outcrops from CMPT-LP (Chernicoff et al., 2019) are grouped. The Orogenic Choiyoi limit was taken from Llambías and Sato (2011). Also, the possible Patagonian suture zone is demarcated (Pankhurst et al., 2006; Ramos, 2010; Martínez Dopico et al., 2017). It is not clear whether the northwestern outcrops of the North Patagonia region –southern Neuquén province– would be a southern extension of Andes region or not. The present-day continuity gap between their outcrops could be the result of buried sequences during the Neuquén basin subsidence (Howell et al. 2011). In this work, because of its disconnection with the rest of the Carboníferous-Permian magmatism, these outcrops have been assigned to the North Patagonia region.

(Bryan, 2007; Bryan and Ernst, 2008). It has been proposed that the ChMP may have contributed to the end-Permian mass extinction by means of releasing large volumes of CO_2 and CH_4 through magmatic emplacement in carboniferous sedimentary rocks with high organic material content (Spalletti and Limarino, 2017). Furthermore, the geotectonic setting of the ChMP magmatism, though still debated, would have been associated to the extensional collapse of Early Permian orogeny known as the "San Rafael orogenic phase" (Mpodozis and Kay, 1992; Llambías and Sato 1995, Llambías et al., 2003; Martínez, 2004; Kleiman and Japas, 2009; Sato et al. 2015) and would have involved significant amounts of crustal reworking (Sato et al., 2015).

The volume of magmatism generated during the ChMP lifespan may have been as high as 1.23x106 km^3 (Spalletti and Limarino, 2017) and its ashfall deposits have been reported even in the Paraná basin, south of Brazil, and the Karoo Basin in South Africa (Sato et al., 2015). In spite of the large exposure area of the ChMP units and its relevance in the geotectonic evolution of southern South America (Oliveros et al., 2020), the amount of available geochemical data from the ChMP volcanic and plutonic rocks is strikingly low (n<450 for major elements, n<350 for trace elements, n<50 for Sr-Nd-Pb-Hf isotopic composition and n<150 radiometric ages) and mostly restricted to the Frontal Cordillera and San Rafael Block (Fig. 5.1b; see Sato et al. 2015, Martínez and Giambiagi 2010; Kleiman and Japas, 2009; Rocher et al., 2015 and Oliveros et al., 2020 for recent compilations of ChMP data). In contrast with other LIPs (Karoo n>1,000; Deccan Traps n>10,000) and SLIPs (Sierra Madre Occidental n>4,000, Whitsunday n>1,000, Okhotsk-Chukotka Volcanic Belt n>400) with larger geochemical and geochronological databases (Georoc database, Ferrari et al., 2018), the lack of statistically significant geochemical data for the ChMP prevents a proper assessment of the geotectonic setting for the magmatism and its evolution through time. This is important because some units of the ChMP have been interpreted as subduction-related magmatism (Llambías and Sato 1995; Rocher et al., 2015) while other have either a clear anorogenic or within plate affinity or transitional character (Llambías et al., 2003; Tobares et al., 2015; Chernicoff et al., 2019). Interestingly, most SLIPs are linked to within plate magmatism (e.g. Chon Aike Province, Whitsunday, Sierra Madre Occidental (Bryan, 2007), but others such as the volcanic belts of Kazakhstan, East

Sikhote-Alin, SW China and Okhotsk-Chukotka (OCVB) have been recently considered typical examples of subduction-related magmatism (Tikhomirov, 2010; Tikhomirov et al., 2016).

In this work we have performed a detailed quantification of the present-day outcrops of the Carboniferous to Triassic igneous rocks in Chile and Argentina in order to characterize the petrological composition of the Choiyoi Magmatic Province (ChMP) as a whole and also of its three main geographical divisions (Fig. 5.1b): the Andes region, the La Pampa Permian-Triassic Magmatic Corridor (CMPT-LP, Chernicoff et al., 2019) and North Patagonia region. In addition, we examine the total volume of Choiyoi volcanism, as well as the temporal and spatial variations in the composition of the magmas and compare these features to other SLIPs worldwide. Our aim is to assess the magmatic evolution of the SW Gondwana margin during that time, the most likely tectonic setting for the generation of the ChMP, and the crustal contribution to the magmatism. For this purpose, we use the only available data that is evenly distributed throughout the province, which are the lithology and geochronological/stratigraphic age of its outcrops.

5.2 Geological setting

The southwestern portion of the Gondwana continent (present-day South America, Fig. 5.1a) was built during the phanerozoic through the development of magmatic arcs on its western margin from the Cambrian to the Early Devonian, and through the accretion of allochthonous terrains (Ramos et al., 1986). After a period of tectonic quiescence during the Devonian, subduction resumed along the proto-Andean margin in the Carboniferous (Mpodozis and Ramos, 1990). During the Permian and the Triassic, an intense magmatic activity took place, whose present-day record consists of mostly plutonic rocks representing the early stages of magmatism, and large volumes of volcanic rocks of younger ages (Fig. 5.1b; Sato et al. 2015). This igneous record is known as the Choiyoi Magmatic Province (ChMP; Kay et al., 1989; Sato et al., 2015) and its outcrops can be found from Northern Chile (22°S) down to the North Patagonian Massif in Argentina (43°S), and from the Principal and Frontal Cordillera to the

Pampean and the Ventania Ranges (70-62°W) to the east (Fig. 5.1b), making up a continuous andesitic-rhyolitic plateau that was built during 39 Myr of magmatic activity.

The term Choiyoi was initially assigned to the Triassic volcanic sequences that crop out in the Neuquen area and the northwestern Patagonia in Argentina (Fig. 5.1b; the "Choiyoitense" Groeber, 1946, 1951). Afterwards, the name was widely used in reference to the Permian volcanic and plutonic rocks of the San Rafael Block and the Frontal Cordillera in northwestern Argentina and Chile (Rolleri and Criado Roqué, 1970). These two uses of the term Choiyoi created a certain confusion with its specific meaning, until the Triassic volcanics were finally reassigned to the Upper Triassic-Jurassic pre-Cuyo cycle (Gulisano, 1981), defining a separate volcanic event distinguished from the Permian to Middle Triassic magmatism grouped by Kay et al. (1989) into the Choiyoi Magmatic Province.

The tectonic-magmatic evolution of the Late Paleozoic to Triassic magmatism can be separated into three stages, according to Sato et al. (2015). The first, pre-Choiyoi (Fig. 5.1b), spans the late Early Carboniferous to the Early Permian (Guadalupian) and is mainly represented by supra subduction plutonic rocks exposed along the western flank of the Frontal Cordillera in the Chile-Argentina border (28º-31ºS), the Coastal Cordillera in Chile (32º-38ºS), and northwestern Patagonia (38º30'-42ºS), and by volcanic and shallow plutonic rocks along the Precordillera in Chile (20°-30S°). The second stage corresponds to Choiyoi magmatism, developed between 286 and 247 Ma after the deformation of the San Rafael orogenic phase in an increasingly extensional setting (Heredia et al., 2002; Giambiagi and Martínez, 2008), with mostly ignimbritic deposits (Spalletti and Limarino, 2017). Its products are located to the east and southeast of the pre-Choiyoi (Fig. 5.1b). Finally, an early to Middle-Triassic extensional phase (Huarpica phase) marks the beginning of post-Choiyoi magmatism, whose products are exposed from Domeyko Cordillera to Northwestern Patagonia in the Chile-Argentina border region (22°-39°S), extending east to the North Patagonian Massif.

In the San Rafael Block (Fig. 5.1b), Kleiman and Japas (2009) further divided the Choiyoi outcrops into: a lower section (ca. 280-265 Ma) of intermediate composition with a calc-alkaline signature, medium to high K, metaluminous to peraluminous, high

LILE/HFSE and Nb-Ta troughs, and an upper section (ca. 265-250 Ma) of rhyolitic-dacitic composition, high K, peraluminous and with alkaline affinities (Kleiman and Japas, 2009; Sato et al., 2015). Also, on the basis of their Nb, Y and Zr contents (diagrams of Pierce et al., 1984 and Macdonald et al., 1992) rocks from the lower section plot in the field of a volcanic arc in an active continental margin, whereas the dacitic-rhyolitic upper section shows a signature transitional to within plate magmatism, especially in the younger terms (Kleiman and Japas, 2009). This compositional differences of the Choiyoi sequences are observed in several localities along the Andean margin, but with different temporal constraints for the shift from intermediate to silicic rocks, (Rocha-Campos et al., 2011; Llambías and Sato, 2011; Strazzere and Gregori, 2011) and is not always as clear as in the Frontal Cordillera and San Rafael Block (Iriarte et al., 1996; Tomlinson et al., 1999; Mpodozis et al., 2012; Niemeyer, 2013; Venegas et al., 2013; Henríquez et al., 2014; Maksaev et al., 2014).

The outcrops assigned to ChMP extend from the Andes to the foreland (Fig. 5.1b), including isolated rhyolites from the Sierra de Varela (Martínez et al., 2012; Tobares et al., 2015) and reaching the Ventania Ranges in the cratonic part of Argentina (Fig. 5.1b). Recent works however have questioned the incorporation of some of these foreland units into the silicic province. For example, based on new geochronological and geochemical data of igneous rocks from the La Pampa area, Chernicoff et al. (2019) suggested that the intracratonic magmatism exposed from the southern San Rafael Block to the southeast, would correspond to a different event: the La Pampa Permian-Triassic Magmatic Corridor (CMPT-LP). The plutonic rocks of CMPT-LP (Fig. 5.1b) show anorogenic affinities (A1-type granites), with high K content and alkalinity, suggesting a different setting than the Andes region. Also, the deformation associated with the San Rafael orogenic phase, featured in many of the Choiyoi-related units in the Andes region, is very weak (e.g. Chadileuvú Block and Southern Sierras, Llambías et al., 2003; Kleiman and Japas, 2009; Sato et al., 2015) or absent (Chernicoff et al. 2019) in the rocks overlied or intruded by the CMPT-LP.

On the other hand, the North Patagonia region comprises the outcrops of southern Neuquén and the North Patagonian Massif (Fig. 5.1). In northern North Patagonia

(~41°S-68°30'W), the Los Menucos Group (257-248 Ma) is another penecontemporaneous unit associated with the Choiyoi magmatism, and would represent the effusive expressions of the Middle Permian-Early Middle Triassic La Esperanza Plutonic Complex (Luppo et al., 2018; Martínez Dopico et al., 2017, 2019; Supplementary Material 5.1). The deformation pattern in this region is more complex than in the rest of the ChMP, in which the San Rafael and Huarpica phases bracket the magmatism. Although in the Los Menucos-La Esperanza area there is no evidence of deformed plutons, in the eastern North Patagonian Massif (Fig. 5.1b) the undeformed Navarrete Plutonic Complex (281±3 Ma, U-Pb, Pankhurst et al., 2006; López de Luchi et al., 2010) is close to highly deformed orthogneisses (260-245 Ma, Chernicoff et al., 2013; Pankhurst et al., 2014; Martínez Dopico et al., 2016; Supplementary Material 5.1) which have been associated with a Permian continental collision (Chernicoff et al., 2013; Rapalini et al., 2010).

The tectonic setting for the Choiyoi magmatism has been traditionally interpreted as an extensional collapse developed after the San Rafael orogenic phase without subduction involved (Nasi et al., 1990; Mpodozis and Kay, 1992; Charrier et al., 2007). However, recent works suggest that the most likely tectonic setting would imply a continuous subduction throughout the Permian and Triassic in SW Gondwana (Poma et al., 2014; Rocher et al., 2015; del Rey et al., 2016; 2019; Coloma et al., 2017; González et al., 2018; Oliveros et al., 2018; 2020).

5.3 Methodology

We performed an estimation of the areal distribution of the Carboniferous to Triassic plutonic and volcanic rocks exposed in Chile and Argentina, north of 45ºS (Fig. 5.1b); grouping the outcrops by age and composition. The information has been compiled mostly from the geological maps published by the Chilean Geological and Mining Service (1:50,000, 1:100,000, 1:250,000) and the Argentinean Geological Service (1:100,000, 1:250,000) (Supplementary Material 5.1).

5.3.1 Area calculation

For a precise estimation of the total area of the Carboniferous to Triassic igneous outcrops, a revision of the published geological maps (1:100:000 and 1:250.000) covering the western part of South America between 20º and 45ºS was made. Geological maps at scales other than 1:100.000 or 1:250.000 were used only for complementing the information. Updated or more detailed geological maps from scientific publications were used when available. Facies subdivisions in some units were considered while calculating the total area of the corresponding unit, eliminating from the calculation those whose origin was not entirely co-magmatic (for example: highly reworked volcano-sedimentary facies). The area of each unit was then calculated through the ArcGIS 10.1 software (Datum WGS84, Zone 18S, 19S and 20S). In some cases, the available geodatabase was used.

5.3.2 Age and composition

The area of each unit was further divided according to the reported dominant composition for each collected polygon. Lithological subdivisions are basalt, andesite, dacite, rhyolite, for volcanic outcrops, and gabbro, diorite, granodiorite, granite and tonalite for plutonic outcrops. Each part (lithological subdivision of a unit) was grouped into one of five intervals of either 50 (350-300 Ma) or 25 Myr (300-200 Ma), according to the age assigned to the unit in the literature. These regular intervals are independent of the three Choiyoi stages (pre-Choiyoi, Choiyoi, and post-Choiyoi). This distribution allows us to visualize the magmatic evolution of the SW Gondwana margin, expanding and refining the method proposed by Oliveros et al. (2018). In addition, the compiled outcrops were grouped into three geographical regions: Andes, Permian-Triassic Intracratonic magmatic corridor of La Pampa (CMPT-LP, *sensu* Chernicoff et al., 2019) and North Patagonia. The volcanic outcrops assigned to the ChMP in Argentina, and their equivalents in Chile (286-247 Ma, Sato et al., 2015), were also grouped to be distinguished from the pre and post-Choiyoi magmatism.

Whenever the age range of a unit spanned more than one of the defined time intervals, its area was either assigned as a whole to a single interval, or divided in equal parts into two intervals, if none of the intervals cover more than 75% of the age range. A

detailed description of the methodology for the age-composition estimation can be found in the Supplementary Material 5.2.

5.3.3 Volume calculation

The volume for the volcanic outcrops of the ChMP was estimated based on thickness data from different localities of the Andean margin (Fig. 5.2). The area covered by these outcrops depicts the volcanic part of the ChMP (ChMP-V) which can be further subdivided into nine zones with specific, and relatively homogeneous, thickness. The addition of each independent calculated volume results in the total volume of the ChMP-V. Based on geological criteria (see section 5.5.1), the units cropping out in the Andes and North Patagonia regions have been grouped into one province corresponding to the orogenic part of Choiyoi magmatism (Fig. 5.2). This province named Orogenic Choiyoi excludes the eastern intracratonic outcrops from CMPT-LP and the isolated rhyolites from Sierra de Varela (Fig. 5.1b; Tobares et al., 2015; Supplementary Material 5.1). An explanation of how the thicknesses were assigned to each zone can be found in the Supplementary Materials 5.2, 5.3.

5.4. Results

5.4.1 Temporal evolution of the Carboniferous to Triassic magmatism

The total area covered by outcrops of Carboniferous to Triassic igneous rocks in the studied region is ca. 108,146 km^2, of which 48,104 km^2 (45%) correspond to volcanic and 60,042 km^2 (55%) to intrusive rocks. The estimation of temporal and geographical variation of outcrops allows to evaluate the evolution of magmatism in the SW Gondwana margin from 350 to 200 Ma, according to the intervals defined in Section 5.3.2 (Fig. 5.4). The volcanic rocks increase from 350 to 250 Ma with a peak in the 275-250 Ma interval (ca. 30,600 km^2, 69% of the total volcanic outcrops). This time interval records the highest proportion of felsic rocks, with rhyolite and dacite composing the 81% of the outcrops (Fig. 5.3a). Subsequently, there is a significant decrease in the volcanic outcrops in the time intervals corresponding to Triassic (250-200 Ma). Moreover, much of the triassic volcanic rocks were extruded during Lower Triassic and early Middle Triassic. Basaltic rocks are scarce (<3%) prior to 225-200 Ma, an interval

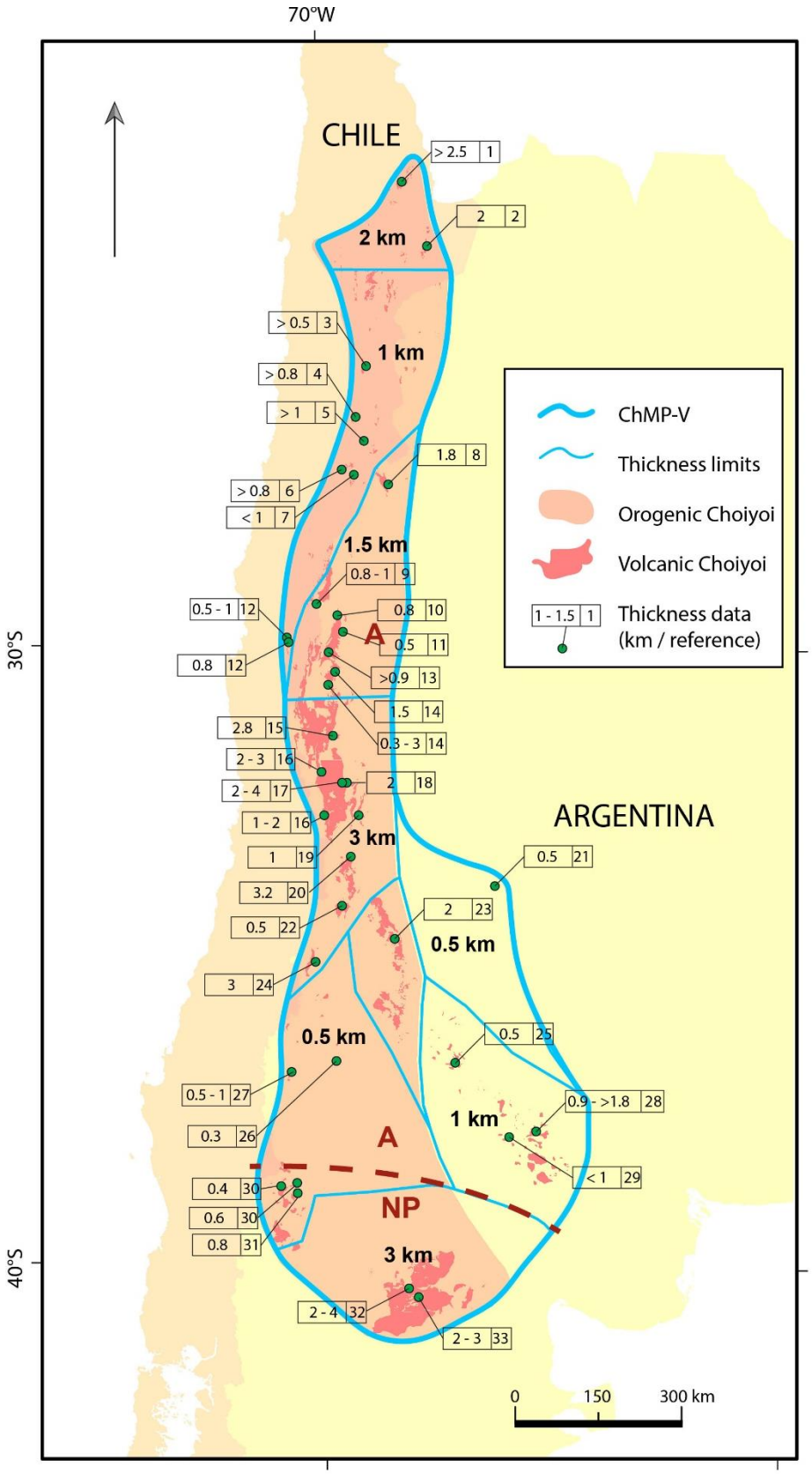
70°W
CHILE
ARGENTINA
30°S
40°S
2 km
1 km
1.5 km
3 km
0.5 km
0.5 km
1 km
3 km
A
A
NP
> 2.5 1
2 2
> 0.5 3
> 0.8 4
> 1 5
1.8 8
> 0.8 6
< 1 7
0.8 - 1 9
0.5 - 1 12
0.8 10
0.8 12
0.5 11
>0.9 13
1.5 14
2.8 15
0.3 - 3 14
2 - 3 16
2 - 4 17
2 18
1 - 2 16
1 19
3.2 20
0.5 21
0.5 22
2 23
3 24
0.5 25
0.5 - 1 27
0.9 - >1.8 28
0.3 26
< 1 29
0.4 30
0.6 30
0.8 31
2 - 4 32
2 - 3 33
ChMP-V
Thickness limits
Orogenic Choiyoi
Volcanic Choiyoi
1 - 1.5 1
Thickness data
(km / reference)
0
150
300 km

Figure 5.2. Volcanic outcrops from the Choiyoi magmatic province defining the Choiyoi Volcanic Province (ChMP-V). Nine zones with different thickness of the volcanic sequences have been identified inside the ChMP-V. The Andes and North Patagonia subdivisions are grouped into the Orogenic Choiyoi, excluding the eastern foreland outcrops from the CMPT-LP and Sierra Varela. A: Andes region, NP: North Patagonia region. (1) Raczynnski, 1963; (2) Breitkreuz and van Schmus, 1996; (3) Cornejo et al., 2009; (4) Tomlinson et al., 1999; (5) Cornejo et al., 1998; (6) Iriarte et aI., 1996; (7) Mpodozis et al., 2012; (8) Koukharsky, 1969; Rubiolo et al., 2003; (9) Ortiz and Merino, 2015; Martin et al., 1999; (10) Sato and Llambías, 1993; (11) Cardó et al., 2007; (12) Pineda and Emparan, 2006; (13) Malizia et al., 1999; (14) Rodríguez Fernández et al., 1996; (15) Rocher et al., 2015; (16) Ramos et al., 1996; (17) Cortés, 1985; (18) Cortés et al., 1997; (19) Folguera et al., 2004; (20) Martínez and Giambiagi, 2010; (21) Flores and Criado Roque, 1972 (22) Volkheimer, 1978; (23) Kleiman and Japas, 2009; Kleiman, 1999; (24) Nullo et al. 2005; López Fontenla, 1984; (25) Barrionuevo et al., 2013; (26) Narciso et al., 2004; (27) Llambías et al., 2007; Suárez et al., 2007; (28) Linares et al., 1980; Sruoga and Llambías, 1992; (29) Espejo and Silva Nieto, 2007; (30) Freytes, 1969; (31) Leanza, 1985, 1992; Cucchi et al., 2005; (32) Luppo et al., 2018; (33) Lema et al., 2009. Detailed localization of data in Supplementary Material 5.3.

in which they constitute 30% of the total area and along with andesites represent the majority of volcanic activity. Thus, the 225 Ma age marks an important change in magmatism composition, with a more balanced distribution of mafic, intermediate and felsic rocks (Fig. 5.3a). The time frame of the Choiyoi magmatism was defined by Sato et al. (2015) between ca. 286 and 247 Ma (Fig. 5.3). The volcanic outcrops that have been assigned to the Choiyoi stage (equivalent to the ChMP-V defined in Section 5.3.3) cover a total area of ca. 37,000 km^2, of which 77% are felsic rocks (rhyolite-dacite) and more specifically, 51% corresponds to rhyolites. Andesites represent 22% of the total area and basalts do not exceed 1%.

Regarding plutonic outcrops, they concentrate in the 350-250 Ma time span (Fig. 5.3b). They are considerably more abundant than volcanic rocks in the range of 350-275 Ma, reaching over 14,000 km^2 for each 25 Myr interval, even in the period of more intense volcanic activity (275-250 Ma). The area of plutonic rocks of Triassic age is significantly smaller (ca. 9,000 km^2 between 250-200 Ma). Prior to 275 Ma, granodiorite is the dominant lithology, with an important amount of tonalite in the 350-300 Ma time interval and of granite between 300 and 275 Ma. After 275 Ma, granites comprise more than 60% of the total area for each time interval. Diorite represents a subordinate lithology along the studied time span, and only by Late Triassic the outcrops of this composition represent more than 10% of the total area. Gabbros do not exceed 2% of the quantified rocks between 350 and 200 Ma.

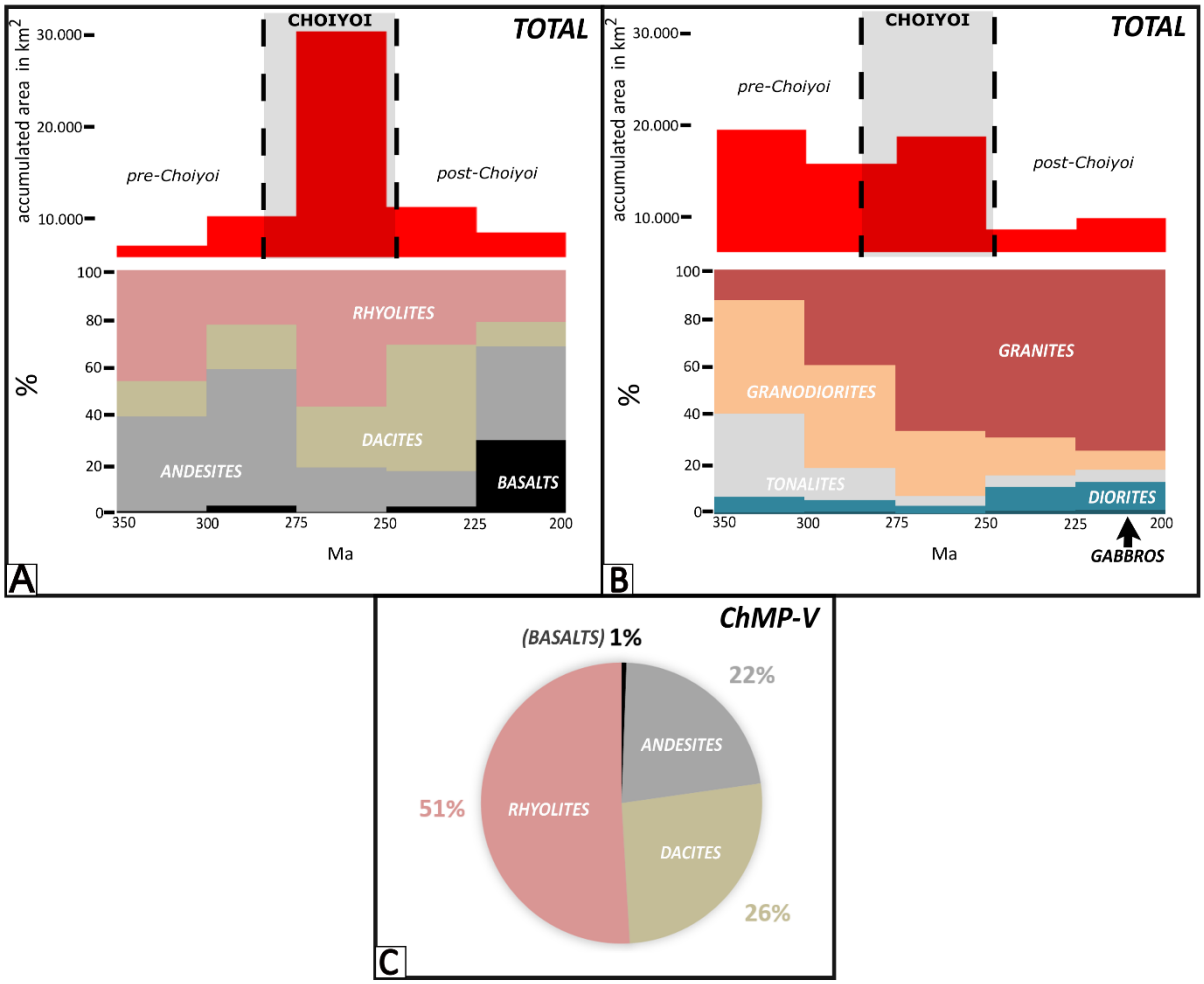

Figure 5.3. Compositional distribution of Carboniferous-Triassic outcrops in SW Gondwana and its accumulated area in each of the five age intervals. (a) shows the volcanic outcrops and (b) the plutonic. The Choiyoi stage is demarcated according to the ages of Sato et al. (2015). (c) Composition of the ChMP-V outcrops.

5.4.2 Geographical distribution of magmatism

When comparing the proposed geographical division of the ChMP outcrops -Andes, North Patagonia and CMPT-LP it is noteworthy that the volcanic and plutonic rocks of the CMPT-LP cover a small proportion of the total outcrop area (<5,000 km^2). So the great majority of outcrops are located either in the Andes or North Patagonia regions, and in both cases the magmatism spans the Carboniferous to Triassic periods (Fig. 5.4).

The peak of felsic volcanism at the 275-250 Ma interval is observed in the three areas, marked by the upper section of Choiyoi Group in the Andes region, the Los Menucos

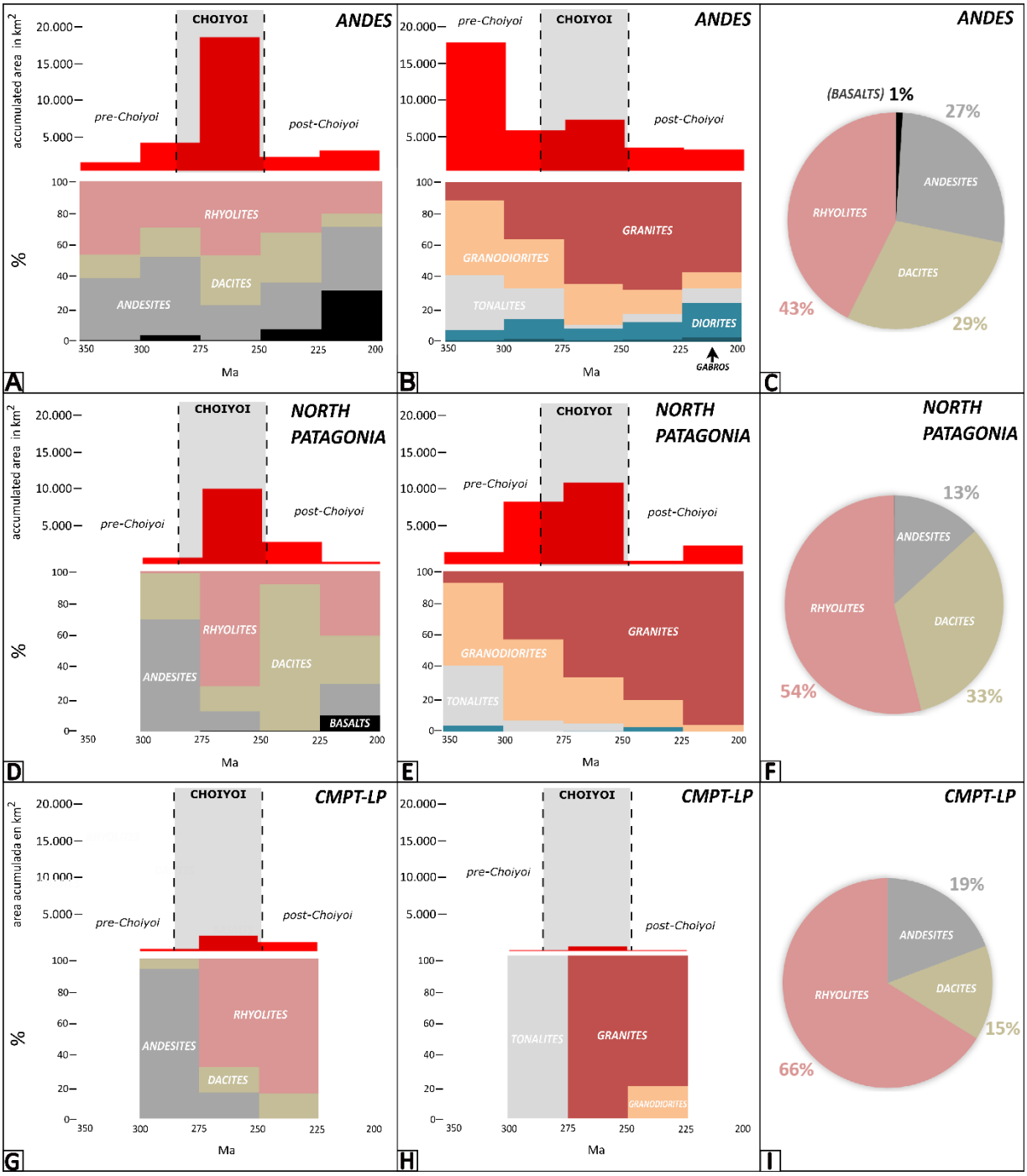

Figure 5.4. Compositional distribution of Carboniferous-Triassic outcrops in SW Gondwana and its accumulated area in each of the five age intervals, separated into three geographic divisions: Andes, North Patagonia, and CMPT-LP. (a), (d) and (g) show the volcanic outcrops and (b), (e) and (h) the plutonic. (c), (f) and (i) show the composition of volcanic rocks inside the age limits of the Choiyoi Magmatic Province for each geographic division (286-247 Ma, Sato et al., 2015).

Group in North Patagonia (Luppo et al., 2018) and the Choique Mahuida Fm. in the CMPT-LP (e.g. Espejo and Silva Nieto, 1996; Supplementary Material 5.1). Both North Patagonia and the CMPT-LP have few to none Upper Triassic volcanic outcrops and no Carboniferous volcanism. In these two areas the dominant lithologies are rhyolite and dacite, particularly in the 275-225 Ma time intervals, period where most of their volcanic activity took place, a slightly younger peak compared with the Andes region (300-250 Ma). Andesites dominate the rock record between 300-275 Ma (ca. 56%) and 225-200 Ma (ca. 38%). The latter interval also records the peak of basic magmatism, mostly in the Andes region, where basalts represent 30% of the total area.

Plutonic record comprise mainly granodiorites and tonalites during the Carboniferous, period in which the magmatism is concentrated in the Andes region, specifically in the southern Coastal Cordillera in Chile (Deckart et al., 2014). From 300-275 Ma, granites are increasingly dominant and plutonic outcrops are widely spread in Andes and particularly in North Patagonia. The granitic plutonic rocks in the CMPT-LP are restricted to the 300-225 Ma time interval (Fig. 5.4h), which contrasts to the rather constant plutonic activity for the rest of the margin (Fig. 5.4b, f).

The volcanic rocks of the Choiyoi magmatism, that constitute the ChMP-V, are distributed as follows: ca. 20,700 km^2 in the Andes region, ca. 13,600 km^2 in North Patagonia and ca. 4,000 km^2 (all its outcrops) in the CMPT-LP. The southernmost outcrops in the San Rafael Block were assigned to both the Andes and CMPT-LP regions, as they are in the transition of these geographic divisions (Chernicoff et al., 2019).

North Patagonia and CMPT-LP are largely rhyolitic (>50% total area; Fig. 5.4f,i), whereas andesite represent a smaller part of the rock record (<20%) compared to the Andes region (Fig. 5.4c), underscoring the felsic character of these two regions. 87% of the outcrops in North Patagonia are rhyolitic-dacitic, mostly represented by the Los Menucos Group and equivalent rocks, which cover 6,500 km^2 (Supplementary Material 5.1). Even though the predominance of acidic rocks, along with an important andesitic fraction (>13%) and almost no basalts, is common to the three regions, the volcanic activity is diachronic and started somewhat later in North Patagonia and CMPT-LP in

comparison to the Andes. Based on a U-Pb age for the Choique Mahuida Fm. (Supplementary Material 5.1), Chernicoff et al. (2019) suggest that the volcanism of the CMPT-LP extends until ca. 239 Ma, placing this unit beyond the temporal limits defined by Sato et al. (2015), although its lithological and structural characteristics are very similar to the upper section of Choiyoi magmatism from the San Rafael Block and Frontal Cordillera (Llambías et al., 2003; Barrionuevo et al., 2013). For purposes of this study, this formation has been entirely assigned to the ChMP-V (Fig. 5.3c, 5.4i).

Mafic rocks are very scarce in the ChMP-V, and the Andes is the only region that has a significant area of basalts (ca. 1% of total area) cropping out in small isolated bodies or within the felsic rocks of the ChMP-V (Supplementary Material 5.1). In North Patagonia there are barely a few basaltic outcrops associated with the Los Menucos Group, none of them larger than 1 km^2 (Supplementary Material 5.1). In Figure 5.5, the volcanic outcrops of North Patagonia and Andes are grouped into the Orogenic Choiyoi, which excludes the CMPT-LP and Sierra de Varela foreland outcrops (Fig. 5.2), in order to evaluate the impact of removing the eastern extension of the ChMP-V. It is possible to observe that the proportion of basic, intermediate and felsic rocks of the ChMP do not vary when excluding the CMPT-LP and Sierra de Varela outcrops.

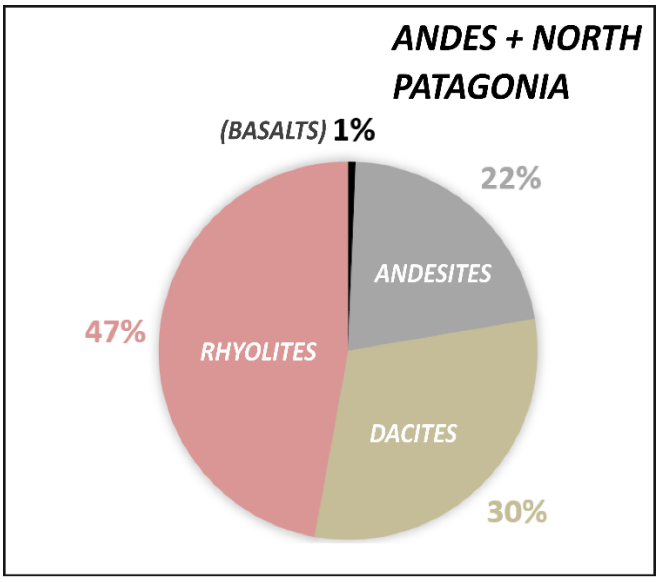

Figure 5.5. Composition of volcanic rocks from Andes and Patagonia regions between the age limits of the Choiyoi Magmatic Province (286-247 Ma, Sato et al., 2015).

5.4.3 Volume quantification

The ChMP has an approximate extension of over 900,000 km^2 (Fig. 5.1, Table 5.1); the union of its volcanic outcrops delimits a province of 610,173 km^2 (ChMP-V, Fig. 5.2). Exposed volcanic sequences have different thicknesses depending on their location in the margin, and according to this were grouped into 9 zones (Fig. 5.2). The addition of the volumes calculated for each zone gives a total estimated volume of 947,553 km^3 (Table 5.1). The volume for the Orogenic Choiyoi volcanics was further distinguished from the foreland Choiyoi volcanism (CMPT-LP and Sierra de Varela.), totaling 799,231 km^3 (Table 5.1).

Table 5.1. Area and volume estimation for the Choiyoi Magmatic Province (ChMP), the Choiyoi Volcanic Province (ChMP-V) and the Orogenic Choiyoi composed of Andes and North Patagonia regions.

Province	Area	Volume
ChMP	909,250 km^2	-
ChMP-V	610,173 km^2	947,553 km^3
Andes + North Patagonia (Orogenic Choiyoi)	455,234 km^2	799,231 km^3

5.5. Discussion

5.5.1 La Pampa Permian-Triassic Intracratonic Magmatic Corridor (CMPT-LP) and North Patagonia, part of the Choiyoi Magmatic Province?

The original extension of the ChMP according to Kay et al. (1989) and Sato et al. (2015) includes, in addition to the orogenic rocks close to the margin in the Frontal Cordillera, Precordillera and San Rafael Block (Andes region), the eastern outcrops reaching to the Ventania Ranges which are located in an intracratonic setting (Fig. 5.1b). These outcrops have recently been renamed as the CMPT-LP (La Pampa Permian-Triassic Magmatic Corridor, according to Chernicoff et al., 2019). The outcrops located in southern Neuquén and the North Patagonian Massif (Fig. 5.1b) are also included in the

original definition of ChMP and have been grouped in this work within the North Patagonia region.

The magmatic activity of the CMPT-LP started with a limited volcanism and plutonism at 300-275 Ma, and its peak (Fig. 5.4g,h) coincides with the late stage of the ChMP in the Andes region (the dominantly felsic upper section). However, U-Pb dating carried out in the younger stages of CMPT-LP magmatism yielded Middle Triassic ages (239 Ma, Chernicoff et al., 2019) and suggest that this magmatism would be out of the time frame for the Choiyoi event. The lithologies and their evolution over time in the CMPT-LP are similar to those of the ChMP outcrops in the Andes region, but the tectonic setting and deformation style would have been different. The strong anorogenic signature of this magmatism (Chernicoff et al. 2019) contrasts with the late stages of the ChMP magmatism in the Andes region, which is calc-alkaline to transitional to alkaline in affinity (Fig. 5.6; Llambías and Sato, 1995; Rocher et al., 2015) and isotopically less evolved (Hervé et al., 2014), even though they are partly contemporaneous (Llambías et al., 2003; Chernicoff et al. 2019). The San Rafael orogenic phase deformation is very weak (e.g. Chadileuvú Block and Southern Sierras, Llambías et al., 2003; Kleiman and Japas, 2009; Sato et al., 2015) or absent (Chernicoff et al. 2019) in the rocks predating the CMPT-LP and thus the CMPT-LP magmatism cannot be attributed to relaxation after a compressional event (Llambías et al. 2003). The area covered by the CMPT-LP, along with the isolated rhyolites from Sierra Varela, represents a small part of the total exposed rocks of the ChMP-V (<11%; Fig. 5.1b), but if it is excluded from the areal estimation, the eastern prolongation of the province decreases dramatically (Fig. 5.2), reducing the extrapolated extension of the ChMP-V by 24% (Table 5.1).

The magmatic activity in the North Patagonia region shows clear temporal similarities to the Andes region (Fig. 5.4d,e), only with some slight delay: the area covered by plutonic rocks has a maximum between 300-250 Ma and the volcanic rocks are concentrated between 275-225 Ma. The Los Menucos Group (Luppo et al., 2018; Supplementary Material 5.1) from the northern North Patagonian Massif (Fig. 5.1b) was extruded during 257-248 Ma and has a rhyolitic-dacitic composition, having a similar

time span and lithology than the upper section of Choiyoi magmatism in the Andes region. The Los Menucos Group and equivalent units represent the majority of volcanic rocks in North Patagonia. The plutonic rocks in North Patagonia also show a compositional evolution similar to that of the Andes region, with increasing granites towards younger ages (Fig. 5.4b,e).

On the other hand, the San Rafael orogenic phase is recognized in a wide area within the North Patagonian region (e.g. Giacosa et al., 1997; von Gosen, 2003; García-Sansegundo et al., 2009). However, the deformation pattern in this region is more complex than in the rest of the ChMP, with deformed orthogneisses that have been associated to an Upper Permian continental collision (Chernicoff et al., 2013; Rapalini et al., 2010; Pankhurst et al., 2014; Martínez Dopico et al., 2016), implying that at least a part of northern Patagonia underwent distinct tectonic processes than the rest of the margin.

The absence of Carboniferous volcanism and low volume of Early Permian volcanism in both the CMPT-LP and North Patagonia (Fig. 5.4d,g) compared to the Andes region (Fig. 5.4a), would support the idea of a southeast expansion of magmatism from the Frontal Cordillera and northern Chile in the Early-Middle Permian (Maksaev et al., 2014). The greater proportion of silicic rocks in the CMPT-LP and North Patagonia may be explained by the younger ages of the volcanism, coeval to the upper section of Choiyoi from the Andes region. The particular structural style, the strong anorogenic signature and the more isotopically evolved character of the CMPT-LP rocks (Chernicoff et al., 2019) suggest that this magmatism would be distinct from that of the Andes and North Patagonia regions. The outcrops of the North Patagonia region have been considered as an integral part of the ChMP in previous works (e.g. Sato et al., 2015; Rocher et al., 2015). For these reasons, two configurations of the ChMP are considered when comparing it to other SLIPs: the ChMP-V, which includes all volcanic outcrops assigned to the ChMP, and the Orogenic Choiyoi, which excludes the outcrops assigned to the CMPT-LP.

5.5.2 Estimation of total area for SLIPs and related silicic provinces worldwide

The 610,173 km^2 comprising the ChMP-V (Table 5.1), according to the estimate in this work, is more than 16th fold the area of exposed volcanic rocks at present, and more than 13^{th} fold the Orogenic Choiyoi. A similar area is covered by the largest SLIP in the world, the Whitsunday province in Australia, whose outcrops represent a minor fraction (~22,500 km^3) of the total extrusive volume proposed for the event (2,500,000 km^3, Bryan et al., 2012). The estimation of present-day outcrops for this province includes sedimentary successions in nearby basins and submarine remnants that would have been separated from eastern Australia during continental rifting (Bryan et al., 2012). Furthermore, the 7,500 km^2 covered by volcanic outcrops represent a minor fraction of the total 180,000 km^2 estimation for the Whitsunday Volcanic Province (WVP, Fig, 5.7a,b) composed by all preserved igneous rocks in the margin (Bryan et al., 2012). In the case of the Chon Aike Province in Patagonia (CAP, Fig. 5.7a,c), the area covered by its outcrops from northern Patagonia down to the Antarctic Peninsula is about 20% of the total area estimated for the entire province (Pankhurst et al. 1998). The Sierra Madre Occidental in North America (SMO, Fig. 5.7a,d) is a relatively continuous belt of silicic rocks located in the continental margin, whose outcrops represent almost the total area attributed to the entire province (> 450,000 km^2, Bryan et al., 2008). The Okhotsk–Chukotka Volcanic Belt (OCVB, Fig. 5.7a,e) is also a continuous, thin, well-preserved arc that extends for ~3,200 kms, whose estimated area is similar to that of the SMO (Table 5.2). The thickness range for the outcrops is 2-4 km which implies that the province has an estimated volume of over 1,000,000 km^3, being thus one of the largest silicic provinces identified so far (Tikhomirov et al., 2012). If one considers that the OCVB area is represented in a vast majority by its outcrops, unlike the WVP or the CAP whose estimations are extrapolated from present-day exposures, the volume of the OCVB could be far larger than any other known silicic province.

It is thus evident that the criteria for estimating areas and volumes of SLIPs and related silicic provinces vary significantly, both in methodology and precision. When comparing SLIPs such as WVP or ChMP to the OCVB, it is assumed that the former were once a continuous volcanic plateau of silicic composition (ignibritic plateau) that covered an

area now extrapolated from the isolated remaining outcrops (Fig 5.1b). This seems, nonetheless, a fair approximation to the total area of ancient, not well preserved, volcanic provinces. In this context, the ChMP, with an estimated volume ranging between ~800,000 and ~950,000 km^3, would be among the largest SLIPs.

5.5.3 Comparison of the ChMP-V and Orogenic Choiyoi to other SLIPs and related silicic provinces

The ChMP-V is in many aspects similar to other SLIPs worldwide (Table 5.2), such as its location near the continental margin and the dominant extensional tectonic setting during its emplacement (Bryan, 2007; Bryan and Ferrari, 2013) but it differs in the composition of its volcanic products, with an anomalous high proportion of intermediate (andesitic) rocks. In any case, the 610,173 km^2 of total area (947,553 km^3 total volume), the ~77% of silicic volcanic rocks, the fact that most of its outcrops are ignimbrites (Spalletti and Limarino, 2017) and the ca. 40 Myr of magmatic activity, are compatible features with the definition of SLIP (Bryan, 2007; Bryan and Ernst, 2008). This character akin to a SLIP is maintained even if the foreland magmatism of the CMPT-LP and Sierra de Varela is excluded from the calculations of area and volume.

Table 5.2 Comparison of silicic provinces: ChMP-V, Orogenic Choiyoi (Sato et al., 2015; this work); OCVB (Tikhomirov et al., 2012, 2016); CAP (Pankhurst et al., 1998, 2000; Riley et al., 2001); WVP (Bryan et al., 2000, 2012); SMO (Bryan et al., 2007; Ferrari et al., 2018); TVZ (Wilson et al., 1995; Deering et al., 2011).

Silicic province	Age (Ma)	Composition	Volcanic area	Thickness / Volume	Tectonic context
Choiyoi Volcanic Province (ChMP-V)	286-247	77% rhyolites-dacites, 22% de andesites, 1% basalts	Outcrops: 37,300 km^2 Province: 610,173 km^2	0.5-3 km/ 947,553 km^3	Post orogenic lithospheric extension
Andes + North Patagonia (Orogenic Choiyoi)	286-247	77% rhyolites-dacites, 22% de andesites, 1% basalts	Outcrops: 34,400 km^2	0.5-1.5 km/ 799,231 km^3	Post orogenic lithospheric extension

			Province: 455,234 km^2		
Okhotsk–Chukotka Volcanic Belt (OCVB)	106-79 (74)*	53% silicic rocks (>70% volume), 47% andesites	>450,000 km^2	2-4 km/ 1,000,000 km^3	Subduction related arc magmatism
Whitsunday Volcanic Province (WVP)	132-95	From rhyolitic-dacitic to bimodal	180,000 km^2 (900x200 km)	~3 km/ >540,000 km^3	Intraplate magmatism, continental break-up related rifting
Chon Aike Province (CAP)	188-153	Overwhelmingly silicic, with scarce intermediate and mafic compositions	702,000 km^2	>230,000 km^3	Intraplate magmatism in a continental break-up context
Sierra Madre Occidental (SMO)	38-18	Strongly silicic, transition to bimodal magmatism	>450,000 km^2	~1 km/ 450,000 km^3	Slab window and piecemeal removal of the slab
Taupo Volcanic Zone (TVZ)	2-present	>90% rhyolitic. Initially andesitic, then bimodal	8,000 km^2	~2 km/ 15,000 km^3	Arc and back-arc rifting, fast extension

Geochemically, the rocks of the ChMP are dominantly rhyolites and dacites, with less andesites, according to the TAS classification diagram (Fig. 5.6a). Even though the number of analysed samples is not representative of the entire province (n<400, mostly from the Frontal Cordillera and San Rafael areas), the absence of basalts and the moderate proportion of andesites is consistent with the petrographic distribution obtained from this work (Fig. 5.5). The majority of the rocks are calc-alkaline (Fig. 5.6b) and plot in the continental arc fields for basic-intermediate (Fig. 5.6c,d) and silicic rocks (Fig. 6e). A minor proportion of the analysed rocks, mostly belonging to the upper section of the Choiyoi magmatism in the Frontal Cordillera and San Rafael Block (Martínez, 2004; Kleiman and Japas, 2009; Martinez and Giambiagi, 2010; Rocha-Campos et al., 2011; Rocher et al., 2015), plot in fields akin to transitional to within-

plate magmatism (Fig. 5.6d,e). The rocks of the CMPT-LP plot mostly in the fields of continental arcs (Fig. 5.6d,e).

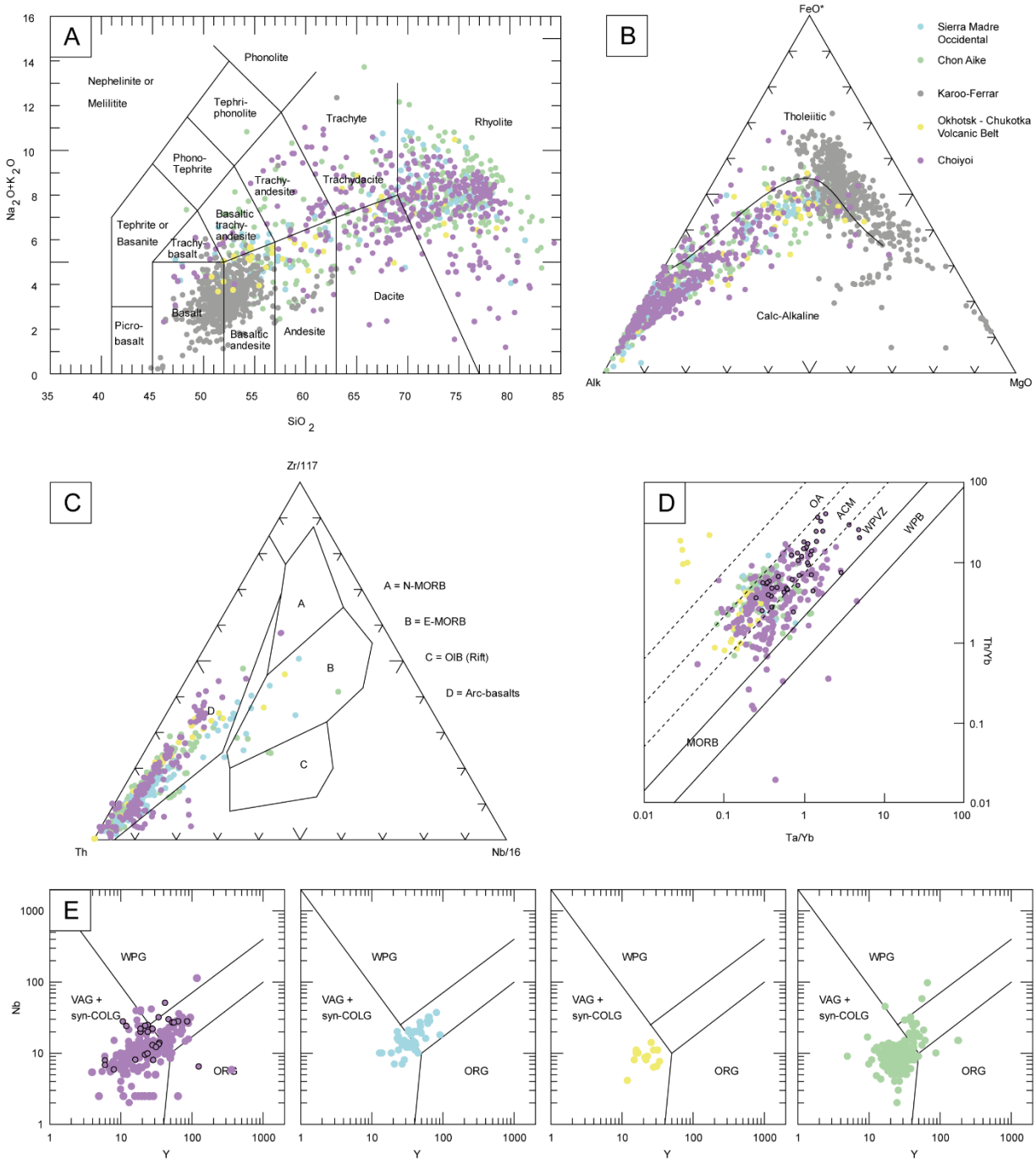

Figure 5.6. Geochemical comparison between ChMP-V and other magmatic provinces. All geochemical data and their references can be found in the Supplementary Material 5.4. a) Total alkalis versus silica diagram (TAS, Le Maitre et al., 1989). b) AFM diagram, division between tholeiitic and calc-alkaline series (Irvine and Baragar 1971). c) Th-Zr-Nb tectonic discrimination diagram for silicic, intermediate and basic volcanic rocks (Wood, 1980). d) Th/Yb vs Ta/Yb tectonic discrimination diagram for intermediate and silicic volcanic rocks (Gorton and Schandl, 2000), the fields correspond to: oceanic arc (OA), active

continental margins (ACM), within-plate volcanic zones (WPVZ), within-plate basalt (WPB) and mid-ocean ridge basalt (MORB). e) Nb vs Y tectonic discrimination diagram for granitic rocks (Pearce et al., 1984), the fields correspond to: ocean ridge granites (ORG), volcanic arc granites (VAG), within plate granites (WPG) and syn-collision granites (syn-COLG). The circles with black borders correspond to samples from CMPT-LP.

5.5.3.1. SLIPs related to continental breakup

The Whitsunday and the Chon Aike Magmatic (CAP) provinces are two SLIPs, associated to continental extension or breakup, to which the ChMP-V can be compared given the similar features they exhibit (Fig. 5.7). In the case of Whitsunday (Fig. 5.7b) the comparison is done taking into account the volcanic outcrops of the province (WVP, Table 5.2). The WVP is defined by a series of outcrops forming a magmatic belt of ~900 km long and 200 km wide (180.000 km^2) that record an initial stage of dacitic composition followed by bimodal volcanism; intermediate rocks are scarce throughout the sequence (Bryan et al., 2000, 2012). The CAP, located immediately to the south of the ChMP-V (Fig. 5.7c) has rhyolitic composition, with subordinate dacite and very minor intermediate and basic rocks (Pankhurst et al., 1998; Riley et al., 2001). This almost entirely rhyolitic to bimodal character of the volcanic sequences in both provinces is the main difference with the ChMP-V, because the latter has an important volume of andesitic rocks (~22%) especially in its lower section. The total volumes of magmatism in the WVP and the CAP are smaller than the ChMP-V, even if just Orogenic Choiyoi is considered. The area covered by the CAP is 15% larger than ChMP-V, and 54% larger than Orogenic Choiyoi. In terms of the duration of the silicic magmatism, the three provinces record very similar time spans: 39 Myr for the Choiyoi, 37 Myr for Whitsunday and 35 Myr for Choin Aike.

5.5.3.2 Silicic provinces related to convergent margins

The Sierra Madre Occidental (SMO), located in western North America (Fig. 5.7d), is compositionally similar to SLIPs associated to continental breakup. It is highly silicic in a pre-extensional stage and bimodal in the syn-extensional stage, although its duration is shorter than other SLIPs (~20 Myr, Table 5.2; Bryan et al., 2007; Ferrari et al., 2018). The volcanism of the SMO shows little to no petrogenetic relation to an active convergent margin, notwithstanding its adjacency to a subducting plate. The calc-alkaline signature (Fig. 5.6) and LILE-LREE enrichment over HFSE, would be due to

the metasomatized lithospheric mantle from previous subduction processes (Ferrari et al., 2018). Furthermore, the high Nb content (>20 ppm) of its rocks, the fayalite-bearing rhyolites and the occurrence of rhyolites with a ferroan character are features that link

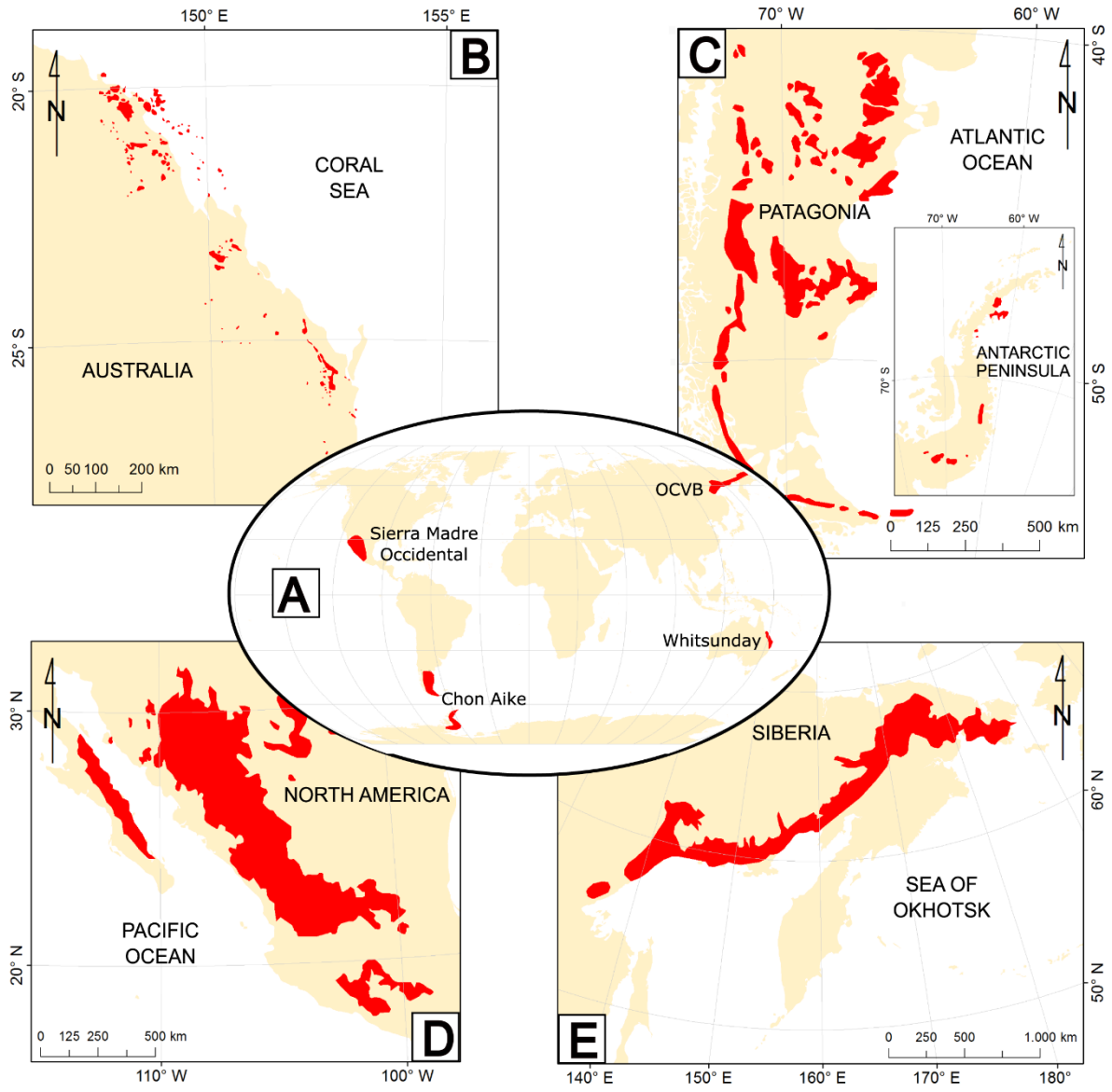

Figure 5.7. Location (a) and outcrops of four silicic provinces: b) Whitsunday Volcanic Province, modified from Bryan et al. (2012); c) Chon Aike Province, modified from Pankhurst et al. (1998); d) Sierra Madre Occidental, modified from Bryan et al. (2007); e) Okhotsk-Chukotka Volcanic Belt, modified from Tikhomirov et al. (2016).

this province with intraplate magmatism (Ferrari et al., 2018). The mechanism by which the SMO magmas were generated would have been the thinning of the upper plate and

establishment of a shallow asthenospheric mantle beneath the continent, during progressive slab tearing and detachment (Ferrari et al., 2018). Before the first ignimbrite flare-ups, intermediate intrusive and volcanic rocks generated in the margin. Unlike the andesite-dominated lower section of Choiyoi magmatism, it developed far from the paleo-trench (ca. 480-730 km) and represents a diffuse, low-volume event linked to the first stages of slab tearing (Ferrari et al., 2018). The total volume of magmatism of the SMO is similar to that of the WVP and CAP, and the more restricted presence of intermediate rocks is also a feature that shares with the other two provinces (Fig.5.6a,b; Bryan et al., 2012; Pankhurst et al., 1998; Riley et al., 2001). Taking into account that the SMO lasted only 20 Myr, its magmatic rates are very similar to those of the Orogenic Choiyoi (Table 5.2).

The Taupo Volcanic Zone (TVZ) in New Zealand is another silicic province developed since 2 Ma in a subduction setting with rifting due to fast extension (Wilson et al., 1995; Deering et al., 2011). Its magmatism is bimodal in composition with >90% of rhyolites, although the volcanism of the first stage from 2.0 to 0.9 Ma has intermediate composition and an arc signature (Table 5.2). The transition from andesitic arc volcanism to voluminous rift-related rhyolitic volcanism mimics the evolution of the ChMP but in a much shorter timescale. On the other hand, the magnitude of the lithospheric extension in the TVZ is greater compared to the ChMP because the former has developed active rifting and bimodal magmatism.

5.5.3.3 The Okhotsk-Chukotka Volcanic Belt

The traditional SLIP definition underscore its relationship to within plate magmatism (e.g. CAP, WVP, SMO; Bryan, 2007), but recently several phanerozoic magmatic provinces of Central- Eastern Asia have been attributed to subduction zones (Tikhomirov, 2010), and they cover areas that are comparable, though mostly smaller, to the typical SLIPs. Among those provinces, the most prominent is the Okhotsk–Chukotka Volcanic Belt, whose geochemical signature resembles an Andean-type volcanism, with Nb-Ta troughs, high Pb content, high LILE/HFSE and calc-alkaline affinities (Fig. 5.6; Tikhomirov et al., 2016).

The province exceeds 450,000 km^2 of volcanic rocks and considering 2-4 km of mean thickness, its volume is >1,000,000 km^3 (Table 5.2). Its outcrops comprise basalts to rhyolites, with the latter being more than the 53% of the total area (>90% in some localities) and likely more than the 70% of the estimated volume of volcanic rocks (Tikhomirov et al., 2016). The large proportion of andesitic outcrops is the main difference of the OCVB with other SLIPs, and alike the ChMP-V, it shows a temporal evolution with an initial stage of intermediate arc volcanism that transitions to dominantly rhyolitic-dacitic volcanism. The magmatic activity of the OCVB is 27 Myr, but if the final mafic stage of the arc is taken into account it expands to 31 Myr (Akinin and Miller, 2011; Tikhomirov et al., 2016) which is still a shorter time span than the ChMP. This late mafic rocks are known as the “upper basalts”, and has been attributed to the ending of the OCBV arc by a trenchward shift of the subduction zone or a collision of a continental block (Tikhomirov et al., 2016 and references therein).

Another, smaller, province in Eastern Asia that is associated to subduction is the East Sikhote-Alin Belt (Sakhno and Akinin, 2008; Khanchuk et al., 2016), whose outcrops range in composition from basalts to rhyolites, representing the latter more than the 70% of the total area, and has a duration of 34 Ma. The Southeast China Belt is composed of >2.000.000 km^3 of bimodal magmatism generated during 59 Ma of activity, in a tectonic setting of convergence with strong lithospheric extension (Zinin et al., 1991; Zhou et al., 2006; Sakhno and Akinin, 2008).

The ChMP-V estimated rates for volcanism are comparable to either the SLIPs associated to within-plate processes or those linked to convergent margin setting, regardless of the CMPT-LP being included or not in the rates calculation. However, the transition from early intermediate calc-alkaline magmatism to a more felsic one and the scarce mafic rocks, that are characteristics of the OCVB, makes it more similar to the ChMP-V. It is then plausible that a convergent margin, with subduction zone magmatism, would have been the tectonic setting of the ChMP given its similarities to the Central-Eastern Asia magmatic provinces.

5.5.4. Role of the continental crust and the Carboniferous magmatism in the origin of the ChMP

The huge volumes of felsic magmas present in all the SLIPs require an important contribution from the continental crust for their formation. Bryan et al. (2002, 2008) consider that the melt degree reached by the crust depends mainly on the water contained in the crustal protolith. This is consistent with the position of all SLIPs in phanerozoic consolidation tectonic zones, containing subduction associated complexes, typically hydrated, unlike the cratonic environments in which the basaltic plateaus of the LIPs are located. Tikhomirov (2010) suggests that another factor that affects the volume of crust-derived magmas is the thermal history of the basement in which the SLIP is located. A crust heated by a recent major previous magmatic event would be decisive in allowing large volumes of felsic magmas. The ChMP would comply with the factors previously indicated for the SLIP generation. On the one hand, it is located covering continental terranes accreted on the western margin of South America during the Paleozoic (Ramos, 2010); and on the other, prior to its formation, extensive subduction-related magmatism developed along the southwestern margin of Gondwana during Carboniferous. This magmatism is mostly exposed close to the margin, particularly in Chile (32°S–40°S), and has been grouped in the pre-Choiyoi stage (Fig. 5.1b).

The scarce basalts erupted on the continental surface until Upper Triassic (Fig. 5.3c) could be explained by a density barrier produced by a large amount of partial fusion in the lower crust, preventing the rise of mafic magmas and favouring their underplating (Mpodozis and Kay, 1992; Bryan et al., 2002). The heat source for this partial melting process has been associated with the cessation of subduction after the compressional event of the San Rafael orogenic phase, where slab detachment would have caused the asthenospheric upwelling (e.g. Mpodozis and Kay, 1990; Kleiman and Japas, 2009). Tikhomirov (2010) suggests that under the conditions of a preheated and hydrated crust, such as that of the southwestern margin of Gondwana by the Middle Permian, a similar model could be applied to a continuous subduction setting. This would be the case for some large provinces of silicic volcanism from Asia, including the

OCVB. As discussed before, the latter have a similar volume and lithological evolution to that of the ChMP-V, with an important andesitic lower section followed by an even more volumetric silicic stage, in a time span similar to that of SLIPs (Tikhomirov, 2010; Tikhomirov et al., 2016).

The units of the ChMP-V and the OCVB are similar in their lithology and, to a lesser extent, geochemistry (Table 5.2, Fig. 5.6), and the magmatism of both provinces emplaced in a preheated and hydrated crust. These similarities open the possibility that ChMP-V magmatism would be related to subduction, especially considering that the lower section of the ChMP has already been interpreted as a typical volcanic arc in an active continental margin (Rocher et al., 2015; Kleiman and Japas, 2009). In this potential tectonic scenario, the progressive injection of heat into the hydrated crust by the ongoing subduction-related magmatism plus the high temperature gradient from the previous, mostly plutonic event, would have produced a large-scale partial melting of the lower crust with inevitable mixing of crustal and underplated material (Tikhomirov, 2010). This would have resulted in abnormally high volumes of felsic magmatism (upper section of Choiyoi), a process that could have been boosted by an increase of the subduction angle during the Permian (rollback, e.g. del Rey et al., 2016; Rocher et al., 2015). The chemistry of the CMPT-LP rocks suggest that in this region the magmatism would have had a different genesis, more akin to within-plate, extensional, processes (Llambías, et al., 2003; Chernicoff et al., 2019).

Although a more representative set of geochemical, and especially isotopic data are needed to support the hypothesis, the lithological evolution of the ChMP suggest that the mechanism for magma generation from the Early Permian to the Early Triassic in the southwestern margin of Gondwana would have been an active subduction zone (Rocher et al., 2015; Del Rey et al. 2016, 2019; González et al. 2018; Oliveros et al., 2020). The combination with a hydrated and previously heated crust would have allowed the generation of huge volumes of siliceous magmas.

5.6. Concluding remarks

The Choiyoi Magmatic Province (ChMP) is a continuous rhyolitic plateau that can be further subdivided in three main regions: Andes, La Pampa Permo-Triassic Magmatic

Corridor (CMPT-LP) and North Patagonia. The age, composition and deformation styles of the CMPT-LP units suggest that they would not be associated with the Choiyoi events, even though they are penecontemporaneous to the ChMP. The units assigned to the ChMP in the Andes and North Patagonia regions (Orogenic Choiyoi) are very similar in composition and temporal evolution. However, the deformation styles of the North Patagonia region are more complex than the Andean region, where the San Rafael orogenic phase is clearly distinguished as the main deformation event. In spite of this, the magmatism in both regions is considered as equivalent.

A compilation of published age and lithological data on all the units that compose the ChMP, allowed an estimation of its areal extent (909,250 km^2), the volume of its volcanic products, and the compositional variation through time. The ChMP-V is composed of 51% rhyolite, 26% dacite, 22% andesite and 1% basalts, but the early stages of the volcanism were dominated by andesitic products (~60%). The plutonic rocks make up the 25% of the total area of the ChMP and they are dominated by granites (~65%) and granodiorites (~30%), although the units representing the early stages of the ChMP are composed up to 60% of granodiorites, tonalites and diorites. It is thus evident that the Choiyoi magmatism, in its whole extension, transitioned from dominantly intermediate to more rhyolitic at its final stages.

When considering the volcanic products of the Choiyoi province (ChMP-V), their estimated volume (947,553 km^3) and time span are akin to a Silicic Large Igneous Provinces (SLIP). However, their lithological composition, geochemical signature and especially the large amount of intermediate rocks in the first stage of the ChMP-V, markedly differ from typical SLIPs, in which the rhyolitic magmatism is far more abundant and exhibits within plate affinities. The largest silicic province identified so far, the Okhotsk-Chukotka Volcanic Belt (OCVB) in Siberia, has nonetheless a compositional pattern very similar to the ChMP-V, with more restricted rhyolitic volcanism (~53% of the total volume) and an early stage in which the magmatism was dominantly intermediate in composition. The fact that the OCVB and other silicic provinces related to convergent margins, such as the Sikote-Alin Belt or the Taupo Volcanic Zone, are more similar to the ChMP-V than the typical intracratonic SLIPs,

suggests that the Choiyoi Magmatic Province could have been partly generated in a subduction zone setting.

Acknowledgements

This work was funded by the Fondecyt Grant 1120715 (VO), the University of Concepción grant 218.040.025-1.0 (VO) and the Doctoral fellowship of the National Agency for Research and Development (ANID), grant 21150502 (JG).

5.7 References

Akinin, V.V.; Andronikov, A.V.; Mukasa, and S.B.; Miller, E.L. (2013) Cretaceous lower crust of the continental margins of the northern pacific: Petrological and geochronological data on lower to middle crustal xenoliths. Petrology, 21, 28–65.

Akinin, V.V., and Miller, E.L. (2011) Evolution of calc-alkaline magmas of the Okhotsk-Chukotka volcanic belt. Petrology, 19, 237–277.

Barrionuevo, M., Arnosio, M., and Llambías, E. J. (2013). Nuevos datos geocronológicos en subsuelo y afloramientos del Grupo Choiyoi en el oeste de La Pampa: implicancias estratigráficas.

Breitkreuz, C. and Van Schmus, W. R. (1996). U-Pb geochronology and significance of Late Permian ignimbrites in Northern Chile. Journal of South American Earth Sciences, 9(5-6), 281-293.

Bryan, S. E., (2007). Silicic large igneous provinces. Episodes, 30, 20.

Bryan, S. E., Cook, A., Allen, C. M., Siegel, C., Purdy, D., Greentree, J., and Uysal, T. (2012). Early-mid Cretaceous tectonic evolution of eastern Gondwana: from silicic LIP magmatism to continental rupture. Episodes, 35, 142–152.

Bryan, S. E., and Ernst, R. E. (2008). Revised definition of large igneous provinces (LIPs). Earth-Science Reviews, 86, 175–202.

Bryan, S. E., Ferrari, L., Reiners, P. W., Allen, C. M., Petrone, C. M., Ramos-Rosique, A., and Campbell, I. H. (2008). New insights into crustal contributions to large-

volume rhyolite generation in the mid-Tertiary Sierra Madre Occidental province, Mexico, revealed by U–Pb geochronology. Journal of Petrology, 49, 47–77.

Cardó, R., I. N. Díaz, O. Limarino, V. Litvak, S. Poma and G. Santamaria, (2007). Hoja Geológica 2969-III, Malimán, provincias de San Juan y La Rioja. Instituto de Geología y Recursos Minerales, Servicio Geológico Minero Argentino. Boletín 320, 52p. Buenos Aires.

Charrier, R., Pinto, L., and Rodríguez, M. P. (2007). Tectonostratigraphic evolution of the Andean Orogen in Chile. In The geology of Chile (Moreno, T; Gibbons, W., eds), 21–114.

Chernicoff, C.J., Zappettini, E.O., Santos, J.O.S., McNaughton, N.J., Belousova, E., 2013. Combined U-Pb SHRIMP and Hf isotope study of the Late Paleozoic Yaminué Complex, Río Negro Province, Argentina: implications for the origin and evolution of the Patagonia composite terrane. Geosci. Front. 4, 37–56.

Chernicoff, C.J., Zappettini, E.O., Santos, J.O.S. and McNaughton, N.J., (2016), Las Matras pluton, Cuyania terrane, Argentina: is it truly Mesoproterozoic,or is it Early Permian derived from Mesoproterozoic?. In 35 International Geological Congress: Cape Town, Actas en GEOREF (American Geological Institute), Record ID: 0784662019.

Chernicoff, C. J., Zappettini, E. O., Santos, J. O., and McNaughton, N. (2019). El Corredor Magmático Intracratónico Pérmico-Triásico de la provincia de La Pampa, Argentina: nuevas edades U-Pb SHRIMP, composición isotópica de Hf e implicancias geodinámicas. Revista Mexicana de Ciencias Geologicas, 36, 13–26.

Coloma, F., Valin, X., Oliveros, V., Vásquez, P., Creixell, C., Salazar, E., and Ducea, M. N. (2017). Geochemistry of Permian to Triassic igneous rocks from northern Chile (28º-30º15'S): Implications on the dynamics of the proto-Andean margin. Andean Geology, 44, 147–178.

Cornejo, P., Mpodozis, C., and Tomlinson, A. (1998). Hoja Salar de Maricunga, Región de Atacama, Servicio Nacional de Geología y Minería (Chile). Mapas Geológicos, mapa escala, 1(100.000).

Cornejo, P.; Mpodozis, C.; Rivera, O. and Matthews, S. (2009). Carta Exploradora, Regiones de Antofagasta y Atacama. Chilean Geological and Mining Service, Geologic Chart of Chile, Basic Geology Series 119: 103 p., 1 map scale 1:100,000. Santiago.

Cortés, J. M. (1985). Volcanitas y sedimentitas lacustres en la base del Grupo Choiyoi al sur de Estancia Tambillos, Mendoza, Argentina, en4 Congreso Geológico Chileno, Antofagasta: Antofagasta, Chile. Sociedad Geológica de Chile, Actas, 1, 89-108.

Cortés, J. M., González Bonorino, G., Koukharsky, M. M. L., Pereyra, F. X., Brodtkorb, A., and Ingeoma, S. (1997). Hoja Geológica 3369-09 Uspallata, Provincia de Mendoza.

Courtillot, V. E., Renne, P. R. (2003). On the ages of flood basalt events. Comptes Rendus Geoscience, 335, 113–140.

Cucchi, R., Leanza, H. A., Repol, D., Escosteguy, L., González, R., and Daniela, J. C. (2005). Hoja Geológica 3972-IV Junín de los Andes, provincia del Neuquén. SEGEMAR. Programa Nacional de Cartas Geológicas de la República Argentina, escala, 1(250.000).

Deckart, K., Hervé, F., Fanning, M., Ramírez, V., Calderón, M., and Godoy, E. (2014). U-Pb geochronology and Hf-O isotopes of zircons from the Pennsylvanian Coastal Batholith, south-central Chile. Andean Geology, 41, 49–82.

Deering, C. D.; Bachmann, O.; Dufek, J., Gravley, D. M. (2011) Rift-related transition from andesite to rhyolite volcanism in the Taupo Volcanic Zone (New Zealand) controlled by crystal– melt dynamics in mush zones with variable mineral assemblages. Journal of Petrology, 52, 2243–2263.

del Rey, A., Deckart, K., Arriagada, C., and Martínez, F. (2016). Resolving the paradigm of the late Paleozoic–Triassic Chilean magmatism: Isotopic approach. Gondwana Research, 37, 172–181.

del Rey, Á., Deckart, K., Planavsky, N., Arriagada, C., and Martínez, F. (2019). Tectonic evolution of the southwestern margin of Pangea and its global implications: Evidence from the mid Permian–Triassic magmatism along the Chilean-Argentine border. Gondwana Research, 76, 303–321.

Espejo M. P. and D. G. Silva Nieto, (2007). Hoja Geológica 3966-I, Gobernador Duval, provincias de La Pampa y Río Negro. Instituto de Geología y Recursos Minerales, Servicio Geológico Minero Argentino. Boletín 368, 67 pp. Buenos Aires.

Ferrari, L., Orozco-Esquivel, T., Bryan, S. E., López-Martínez, M., and Silva-Fragoso, A. (2018). Cenozoic magmatism and extension in western Mexico: Linking the Sierra Madre Occidental silicic large igneous province and the Comondú Group with the Gulf of California rift. Earth-Science Reviews, 183, 115–152.

Folguera, A., M. Etcheverría, P. J. Pazos, L. Giambiagi, L. Fauqué, J. M. Cortés, M. F. Rodríguez, M. V. Irigoyen and C. Fusari (2003). Hoja Geológica 3369-15, Potrerillos. Provincia de Mendoza. Instituto de Geología y Recursos Minerales, Servicio Geológico Minero Argentino. Boletín 301, 144 p. Buenos Aires.

Freytes, E. (1969). Estratigrafía y relaciones de contacto de los afloramientos del Grupo Choiyoi (Serie Porfirítica) en el sur de Mendoza, norte de Neuquén y sudoeste de La Pampa. Yacimientos Petrolíferos Viento, provincia del Neuquén. Revista de la Asociación Geológica Argentina, 41(1-2), 22-32.

García-Sansegundo, J., Farias, P., Gallastegui, G., Giacosa, R.E. and Heredia, N. (2009). Structure and metamorphism of the Gondwanan basement in the Bariloche region (North patagonian Argentine Andes). International Journal of Earth Sciences, 98, 1599–1608.

Giacosa, R. (1997). Geología y petrología de las rocas pre-cretácicas de la región de Sierra Pailemán, Provincia de Río Negro. Revista Asocación Geológica Argentina, 52, 65–80.

Giambiagi, L., and Martínez, A.N., (2008), Permo-Triassic oblique extension in the Potrerillos-Uspallata area, western Argentina: Journal of South American Earth Sciences, 26, 252–260.

González, J., Oliveros, V., Creixell, C., Velásquez, R., Vásquez, P., and Lucassen, F. (2018). The Triassic magmatism and its relation with the Pre-Andean tectonic evolution: Geochemical and petrographic constrains from the High Andes of north central Chile (29° 30′–30° S). Journal of South American Earth Sciences, 87, 95–112.

Gorton, M. P., and Schandl, E. S. (2000). From continents to island arcs: a geochemical index of tectonic setting for arc-related and within-plate felsic to intermediate volcanic rocks. The Canadian Mineralogist, 38(5), 1065-1073.

Gulisano, C. A. (1981). El Ciclo Cuyano en el norte de Neuquén y sur de Mendoza. In Congreso Geológico Argentino (Vol. 8, pp. 579–592).

Henríquez, S. M., Becerra, J., and Arriagada, C. (2014). Geología del área San Pedro de Atacama, Región de Antofagasta. Servicio Nacional de Geología y Minería. Carta Geológica de Chile, Serie Geología Básica, 1.

Heredia, N., Rodríguez Fernández, L.R., Gallastegui, G., Busquets, P., Colombo, F. (2002). Geological setting of the Argentine Frontal Cordillera in the flat-slab segment (30°00-31°30'S latitude): Journal of South AmericanEarth Sciences, 15, 79–99.

Iriarte, S.; Arévalo, C.; Mpodozis, M. and Rivera, O. (1996). Mapa geológico de la Hoja Carrera Pinto. Chilean Geological and Mining Service, Geologic Maps 3, 1 map scale 1:100,000. Santiago.

Irvine, T. N. J., and Baragar, W. R. A. (1971). A guide to the chemical classification of the common volcanic rocks. Canadian journal of earth sciences, 8(5), 523-548.

Kay, S. M., Ramos, V. A., Mpodozis, C., and Sruoga, P. (1989). Late Paleozoic to Jurassic silicic magmatism at the Gondwana margin: Analogy to the Middle Proterozoic in North America?. Geology, 17, 324–328.

Khanchuk, A.I.; Kemkin, I.V. Y Kruk, N.N. (2016) The Sikhote-Alin orogenic belt, Russian South East: Terranes and the formation of continental lithosphere based on geological and isotopic data. Journal of Asian Earth Sciences, 120, 117–138.

Kleiman, L. E. (1999). Mineralogía y petrología del volcanismo permo-triásico del bloque de San Rafael en el área de Sierra Pintada, Provincia de Mendoza y su relación con las mineralizaciones de uranio (Doctoral dissertation, Universidad de Buenos Aires. Facultad de Ciencias Exactas y Naturales).

Kleiman, L. E., and Japas, M. S. (2009). The Choiyoi volcanic province at 34 S–36 S (San Rafael, Mendoza, Argentina): Implications for the Late Palaeozoic evolution of the southwestern margin of Gondwana. Tectonophysics, 473, 283–299.

Koukharsky, M. M. L. (1969). Perfiles Geológicos Realizados en los Ríos Cazadero Grande y Tres Quebradas y en el Camino de los Patos, Provincia de Catamarca.

Le Maitre, R.W., editor, (1989), A classification of igneous rocks and glossary of terms, in Recommendations of the International Union of Geological Sciences Subcommission on the systematics of igneous rocks: Oxford, Blackwell, 193 p.

Leanza, H. A. (1985). Descripción geológica de la Hoja 36b, cerro Chachil, provincia del Neuquén. Servicio Geologico Nacional.

Leanza, H. A. (1992). Estratigrafía del Paleozoico y Mesozoico anterior a los Movimientos Intermálmicos en la comarca del Cerro Chachil, provincia del Neuquén. Revista de la Asociación Geológica Argentina 45 (3-4) : 272-299. Buenos Aires.

Lema, H. A., Busteros, A. G., Giacosa, R. E., Cucchi, R. J., Zubía, M. A., Dalponte, M. R., Di Tommaso, I. M., Espejo, P. M., and Franchi, M. (2009). Hojas Geológicas 4169-17 Cerro Abanico y 4169-18 Colonia Ganzú Lauquén. Servicio Geológico Minero Argentino. Instituto de Geología y Recursos Minerales.

Linares, E., Llambías, E. J., and Latorre, C. O. (1980). Geología de la provincia de La Pampa, República Argentina, y geocronología de sus rocas metamórficas y eruptivas. Revista de la Asociación Geológica Argentina, 35(1):87-146. Buenos Aires.

Llambías, E. J., and Sato, A. M., (1995). El batolito de Colangüil: transición entre orogénesis y anorogénesis. Revista de la Asociación Geológica Argentina 50, 111–131.

Llambías, E. J., Quenardelle, S., and Montenegro, T. (2003). The Choiyoi Group from central Argentina: A subalkaline transitionalto alkaline association in the craton adjacent to the active margin of the Gondwana continent. Journal of South American Earth Sciences 16, 243–257.

Llambías, E. J., Leanza, H. A., and Carbone, O. (2007). Evolución tectono-magmática durante el Pérmico al Jurásico temprano en la Cordillera del Viento (37 05'S-37 15'S): Nuevas evidencias geológicas y geoquímicas del inicio de la Cuenca Neuquina. Revista de la Asociación Geológica Argentina, 62(2), 217-235.

Llambías, E. J., and Sato, A. M. (2011). Ciclo Gondwánico: La Provincia Magmática Choiyoi en Neuquén Geología Y Recursos Naturales De La Provincia Del Neuquén. In Relatorio del VXIII Congreso Geológico Argentino, Buenos Aires, HA Leanza, C. Arregui, O. Carbone, JC Danieli, JM Vallés (Eds.) (pp. 53–62).

López de Luchi, M.G., Rapalini, A.E., Tomezzoli, R.N., (2010). Magnetic fabric and microstructures of Late Paleozoic granitoids from the North Patagonian Massif: evidence of a collision between Patagonia and Gondwana? Tectonophysics 494, 118–137.

López Fontenla, E.J.J. (1984). Geología de los Arroyos El Desecho y de los Corralitos, Departamento Malargüe, provincia de Mendoza. Final Degree Report,

Facultad de Ciencias Exactas y Naturales, Universidad de Buenos Aires (unpublished), 84 p., Buenos Aires.

Luppo, T., de Luchi, M. G. L., Rapalini, A. E., Dopico, C. I. M., and Fanning, C. M. (2018). Geochronologic evidence of a large magmatic province in northern Patagonia encompassing the Permian-Triassic boundary. Journal of South American Earth Sciences, 82, 346–355.

Maksaev, V., Munizaga, F., and Tassinari, C. (2014). Timing of the magmatism of the paleo-Pacific border of Gondwana: U-Pb geochronology of Late Paleozoic to Early Mesozoic igneous rocks of the north Chilean Andes between 20 and 31 S.

Malizia, D., Limarino, C. O., Sosa-Gómez, J., Kokot, R., Nullo, F. E., and Gutiérrez, P. R. (1999). Hoja Geológica 3169-2 Paso del Agua Negra, Provincia de San Juan.

Martin, M. W., Clavero, J., and Mpodozis, C. (1999). Late Paleozoic to early Jurassic tectonic development of the high Andean principal Cordillera, El Indio region, Chile (29–30 S). Journal of South American Earth Sciences, 12(1), 33-49.

Martínez, A. (2004). Secuencias volcánicas permo-triásicas de los cordones del Portillo y del Plata, Cordillera Frontal, Mendoza: su interpretación tectónica. Unpublished PhD Thesis, Universidad de Buenos Aires, Buenos Aires, 275.

Martínez, A., and Giambiagi, L. (2010). Evolución petrológica y geoquímica del magmatismo bimodal Permo-Triásico del Grupo Choiyoi en el cordón del Portillo, Mendoza, Argentina. Trabajos de geología, 30(30).

Martínez, A. N., Laura Tobares, M., Giaccardi, A., Aguilera, D., Roquet, M. B., and Giambiagi, L. (2012). Depósitos piroclásticos gondwánicos en el sur de la sierra de Varela, provincia de San Luis: su petrografía y geoquímica. Instituto Superior de Correlación Geológica, Serie Correlacion Geológica, 28(1).

Martínez Dopico, C. I., Tohver, E., López de Luchi, M. G., Wemmer, K., Rapalini, A. E., Cawood, P. (2016). Jurassic cooling ages in paleozoic to early mesozoic

granitoids of northeastern Patagonia: 40Ar/39Ar, 40K-40Ar mica and U-Pb zircon evidence. International Journal of Earth Sciences, 106, 2343–2357.

Martínez Dopico, C. I., de Luchi, M. G. L., Rapalini, A. E., Wemmer, K., Fanning, C. M., Basei, M. A. (2017). Emplacement and temporal constraints of the Gondwanan intrusive complexes of northern Patagonia: La Esperanza plutono-volcanic case. Tectonophysics, 712, 249–269.

Martínez Dopico, C. I., de Luchi, M. G. L., Rapalini, A. E., Fanning, C. M., and Antonio, P. Y. (2019). Geochemistry and geochronology of the shallow-level La Esperanza magmatic system (Permian-Triassic), Northern Patagonia. Journal of South American Earth Sciences, 96, 102347.

Mpodozis, C., and Kay, S. M. (1992). Late Paleozoic to Triassic evolution of the Gondwana margin: Evidence from Chilean Frontal Cordilleran batholiths (28°S to 31°S). Geological Society of America Bulletin, 104, 999–1014.

Mpodozis, C., Ramos, V.A. (1990). The Andes of Chile and Argentina, in: Geology of the Andes and its Relation to Hydrocarbon and Mineral Resources 11, 59–90.

Mpodozis, C.; Iriarte, S.; Gardeweg, M. and Valenzuela, M. (2012). Carta Laguna del Negro Francisco Región de Atacama. Chilean Geological and Mining Service, Geologic Chart of Chile, Basic Geology Series 145: 41 p., 1 map scale 1:100,000. Santiago.

Nasi, C., Moscoso, R., and Maksaev, V. (1990). Hoja Guanta: regiones de Atacama y Coquimbo. Servicio nacional de geologia y mineria.

Navarrete, C., Gianni, G., Encinas, A., Márquez, M., Kamerbeek, Y., Valle, M., Folguera, A. (2019). Triassic to Middle Jurassic geodynamic evolution of southwestern Gondwana: From a large flat-slab to mantle plume suction in a rollback subduction setting. Earth-science reviews, 194, 125-159.

Niemeyer, H. R. (2013). Geología del Área Cerro Lila-Peine, Región de Antofagasta. Servicio Nacional de Geología y Minería, Serie Geológica Básica 147: xxx p., 1 mapa escala 1: 100.000.

Nullo, F. E., G. Stephens, A. Combina, L. Dimieri, P. Baldauf, P. Bouza and Zanettini, J. C. M. (2005). Hoja Geológica 3569-III / 3572IV, Malargüe, provincia de Mendoza. Servicio Geológico Minero Argentino. Instituto de Geología y Recursos Minerales, Boletín 346, 85 p. BuenosAires.

Oliveros, V., González, J., Vargas, M. E., Vásquez, P., Rossel, P., Creixell, C., Sepúlveda, F., and Bastias, F. (2018). The early stages of the magmatic arc in the Southern Central Andes. In The Evolution of the Chilean-Argentinean Andes (pp. 165–190). Springer, Cham.

Oliveros, V., Vásquez, P., Creixell, C., Lucassen, F., Ducea, M. N., Ciocca, I., González, J., Espinoza, M., Salazar, E., Coloma, F., and Kasemann, S. A. (2019). Lithospheric evolution of the Pre-and Early Andean convergent margin, Chile. Gondwana Research, 80, 202–227.

Ortiz, M. and Merino, R.N. (2015). Geología de las áreas Río Chollay-Matancilla y Cajón del Encierro, Regiones de Atacama y Coquimbo.Chilean Geological and Mining Service, Geologic Chart of Chile, Basic Geology Series 175 and 176: 230 pp. 1 map scale 1:100,000. Santiago.

Pankhurst, R. J., Leat, P. T., Sruoga, P., Rapela, C. W., Márquez, M., Storey, B. C., and Riley, T. R. (1998). The Chon Aike province of Patagonia and related rocks in West Antarctica: A silicic large igneous province. Journal of Volcanology and Geothermal Research, 81, 113–136.

Pankhurst, R. J., Riley, T. R., Fanning, C. M., and Kelley, S. P. (2000). Episodic silicic volcanism in Patagonia and the Antarctic Peninsula: chronology of magmatism associated with the break-up of Gondwana. Journal of Petrology, 41, 605–625.

Pankhurst, R.J., Rapela, C.W., Fanning, C.M., Marquez, M. (2006). Gondwanide continental collision and the origin of Patagonia. Earth-Sciences Review, 76, 235–257.

Pankhurst, R. J., Rapela, C. W., De Luchi, M. L., Rapalini, A. E., Fanning, C. M., and Galindo, C. (2014). The Gondwana connections of northern Patagonia. Journal of the Geological Society, 171, 313–328.

Pearce, J. A., Harris, N. B., and Tindle, A. G. (1984). Trace element discrimination diagrams for the tectonic interpretation of granitic rocks. Journal of petrology, 25(4), 956-983.

Pineda, G. and Emparan, C. 2006. Geología del área Vicuña-Pichasca, Región de Coquimbo. Chilean Geological and Mining Service, Geologic Chart of Chile, Basic Geology Series 97: 40 pp. 1 map scale 1:100,000. Santiago.

Poma, S., Zappettini, E., Quenardelle, S., Santos, J., Koukharsky, M., Belousova, E., and McNaughton, N. (2014). Geochemistry, U-Pb SHRIMP zircon dating and Hf isotopes of the Gondwanan magmatism in NW Argentina: petrogenesis and geodynamic implications. Andean Geology, 41, 267–292.

Raczynnski, A. (1963). Geología del distrito minero de Tuina. Memoria de Título, Univ. Chile, Depto. Geología, 117 p., Santiago.

Ramos, V. A., Jordan, T. E., Allmendinger, R. W., Mpodozis, C., Kay, S. M., Cortés, J. M., Palma, M. (1986), Paleozoic terranes of the central Argentine-Chilean Andes. Tectonics, 5, 855– 880.

Ramos, V. A., Aguirre-Urreta, M. B., Álvarez, P. P., Cegarra, M. I., Cristallini, E. O., Kay, S. M., Lo Forte, G. L., Pereyra, F. X. and Pérez, D. J. (1996). Geología de la Región del Aconcagua. Provincias de San Juan y Mendoza.

Ramos, V. A. (2008). Patagonia: a Paleozoic continent adrift?. Journal of South American Earth Sciences, 26, 235–251.

Ramos, V.A. (2009) Anatomy and global context of the Andes: main geologic features and the Andean orogenic cycle. In: Kay, S.M., Ramos, V.A., Dickinson, W.R. (Eds.), Backbone of the Americas: Shallow Subduction, Plateau Uplift, and Ridge and Terrane Collision, Geological Society of America Memoir 204, pp. 31–65.

Rapalini, A. E., de Luchi, M. L., Dopico, C. M., Klinger, F. L., Giménez, M. E., and Martínez, P. (2010). Did Patagonia collide with Gondwana in the Late

Paleozoic? Some insights from a multidisciplinary study of magmatic units of the North Patagonian Massif. Geologica Acta, 8, 349–371.

Rocha-Campos, A. C., Basei, M. A., Nutman, A. P., Kleiman, L. E., Varela, R., Llambias, E., Canile, F.M., and Da Rosa, O. D. C. (2011). 30 million years of Permian volcanism recorded in the Choiyoi igneous province (W Argentina) and their source for younger ash fall deposits in the Paraná Basin: SHRIMP U–Pb zircon geochronology evidence. Gondwana Research, 19, 509–523.

Rocher, S., Vallecillo, G., Castro de Machuca, B., and Alasino, P. (2015). El Grupo Choiyoi (Pérmico temprano-medio) en la Cordillera Frontal de Calingasta, San Juan, Argentina: volcanismo de arco asociado a extensión. Revista mexicana de ciencias geológicas, 32, 415–432.

Rodríguez Fernández, L. R., N. Heredia, G. Marín, C. Quesada, A. Robador, D. Ragona and R. Cardó, (1996). Tectonoestratigrafía y estructura de los Andes argentinos entre los 30° 30’ y 31° 00’ de latitud sur. Actas 13° Congreso Geológico Argentino y 3° Congreso de Exploración de Hidrocarburos, 2: 111 - 124. Buenos Aires.

Rolleri, E. O., and Criado Roqué, P. (1970). Geología de la Provincia de Mendoza. IV Jornadas Geológicas Argentinas (Mendoza, 1969), II: 1–60. Buenos Aires.

Rubiolo, R.; L. Martínez and F. Pereyra. (2003). Fiambalá 2769-IV, Provincias de Catamarca y La Rioja. Instituto de Geología y Recursos Minerales, Servicio Geológico Minero Argentino. Boletín N° 421, 78 pp. Buenos Aires.

Sakhno, V.G. y Akinin, V.V. (2008) First U-Pb dating of volcanics from the East Sikhote-Alin belt. Doklady Earth Sciences. SP MAIK Nauka/Interperiodica, 418, 32–36.

Sato, A. M., and Llambías, E. J. (1993). El grupo Choiyoi, provincia de San Juan: equivalente efusivo del batolito de Colangüil. In Congreso Geológico Argentino (No. 12, pp. 156-165).

Sato, A. M., Llambías, E. J., Basei, M. A., and Castro, C. E. (2015). Three stages in the Late Paleozoic to Triassic magmatism of southwestern Gondwana, and the

relationships with the volcanogenic events in coeval basins. Journal of South American Earth Sciences, 63, 48–69.

Silva Nieto, D. G. and Espejo, P. M. (1996). Puelches. Programa Nacional de Cartas Geológicas de la República Argentina 1:250.000. Hoja Geológica 3966-II. Provincias de La Pampa y Río Negro. Boletín; 216. Buenos Aires, Servicio Geológico Minero Argentino. Instituto de Geología y Recursos Minerales.

Spalletti, L.A., Limarino, C.O., 2017. The Choiyoi magmatism in south western Gondwana : implications for the end-permian mass extinction - a review. Andean Geology, 44, 328–338.

Sruoga, P., and Llambías, E. J. (1992). Permo-Triassic leucorhyolitic ignimbrites at Sierra de Lihue Calel, La Pampa Province, Argentina. Journal of South American earth sciences, 5(2), 141-152.

Strazzere, L., and Gregori, D. (2011). Estratigrafía y evolución del Grupo Choiyoi entre Rincón de los Vallecitos (Cordillera Frontal) y Pampa de Canota (Precordillera Mendocina) provincia de Mendoza (resumen), en 18 Congreso Geológico Argentino, Neuquén: Neuquén, Argentina. Asociación Geológica Argentina, Actas, 1514.

Suárez, M. (2007): Geología del área Andacollo -parte sur-, Cordillera del Viento, Neuquén, Argentina. MAGSA-Andacollo, (unpublished), 50 p.

Tikhomirov, P. L. (2010). Largest Phanerozoic provinces of silicic volcanism: Tectonic position and genetic prerequisites. Moscow University Geology Bulletin, 65, 194–202.

Tikhomirov, P. L.; Kalinina, E. A.; Moriguti, T.; Makishima, A.; Kobayashi, K.;Cherepanova, I. Y.; Nakamura, E. (2012) The Cretaceous Okhotsk–Chukotka Volcanic Belt (NE Russia): Geology, geochronology, magma output rates, and implications on the genesis of silicic LIPs. Journal of Volcanology and Geothermal Research, 221, 14–32.

Tikhomirov, P. L., Kalinina, E. A., Moriguti, T., Makishima, A., Kobayashi, K., Nakamura, E. (2016). Trace element and isotopic geochemistry of Cretaceous magmatism in NE Asia: Spatial zonation, temporal evolution, and tectonic controls. Lithos, 264, 453–471.

Tobares, M. L., Martinez, A., Gallardo, A. H., Aguilera, D. (2015). Petrography and geochemical characterisation of the Permo-Triassic in the Sierra de Varela, San Luis, Argentina. Revista de la Sociedad Geológica de España, 28, 2.

Tomlinson, A. J.; Cornejo, P. and Mpodozis, C. (1999). Hoja Potrerillos, Región de Atacama. Chilean Geological and Mining Service, Geologic Maps 14, 1 map scale 1:100,000.

Venegas, C., Cervetto, M., Astudillo, N., Espinoza, F., Cornejo, P., Mpodozis, C., and Rivera, O. (2013). Carta Sierra Vaquillas Altas, Regiones de Antofagasta y Atacama. Servicio Nacional de Geología y Minería. Carta Geológica de Chile, Serie Geología Básica, 159(1), 100-000.

Volkheimer, W. (1978). Descripción Geológica de la Hoja 27b, Cerro Sosneado. Boletín n° 151 del Servicio Geológico Nacional. 80 p. Buenos Aires.

von Gosen, W. (2003). Thrust tectonics in the North Patagonian Massif (Argentina): implications for a Patagonian plate. Tectonics, 22, 1005.

Wilson, C. J. N.; Houghton, B. F.; Mcwilliams, M. O.; Lanphere, M. A.; Weaver, S. D., and Briggs, R.M. (1995). Volcanic and structural evolution of Taupo Volcanic Zone, New Zealand: a review. Journal of volcanology and geothermal research, 68, 1–28.

Wood, D. A. (1980). The application of a Th-Hf-Ta diagram to problems of tectonomagmatic classification and to establishing the nature of crustal contamination of basaltic lavas of the British Tertiary Volcanic Province. Earth and planetary science letters, 50(1), 11-30.

Zhou, B. X.; Sun, T .; Shen, W.; Shu, L., and Niu, Y. (2006) Petrogenesis of Mesozoic granitoids and volcanic rocks in South China: a response to tectonic evolution. Episodes, 29, 26– 86

Zinin, S. S.; Govorov, I.N., and Sakhno, V. G. (1991) The Pacific Margin of Asia: Magmatism. Nauka. 262 pp. Moscow.

CAPÍTULO VI: DISCUSIÓN Y CONCLUSIONES

Tal como se mencionó en el capítulo I, la configuración geotectónica del margen occidental de Sudamérica ha sido clásicamente propuesto como un límite de placas periódicamente activo tras la acreción de sucesivos terrenos autóctonos y para-autóctonos durante el Paleozoico. Según el modelo clásico propuesto por Mpodozis & Kay (1992), basado en el estudio de rocas intrusivas expuestas en la Alta Cordillera Chilena (28°S - 31°S), la subducción durante el ciclo Pre-Andino habría cesado tras la colisión de un último terreno (Terreno X) al margen occidental de Gondwana, provocando el quiebre del slab, el ascenso de grandes volúmenes de magmas basálticos que habrían quedado estancados en la base de la corteza, provocando la fusión de ésta. Por lo que el magmatismo Pre-Andino, fue atribuido a una extensa fusión cortical, explicando los grandes volúmenes de magmatismo silíceo observado en este periodo y atribuyéndolos al Grupo Choiyoi. Otros modelos más recientes, han planteado escenarios en los que la subducción no habría cesado durante este ciclo tectónico, proponiendo que la subducción a lo largo del margen habría sido un proceso continuo desde el Carbonífero hasta el Presente.

El estudio de las rocas ígneas bien preservadas por las condiciones áridas y semiáridas que predominan en el Norte de Chile, específicamente en la Cordillera Frontal entre los 28°30’S y los 30°30’S, han permitido aportar a esta discusión y proponer un contexto geotectónico basado en numerosas descripciones petrográficas, análisis geoquímicos e isotópicos con un control exhaustivo de la geología de campo, de unidades específicas que son clave para el entendimiento del Ciclo Pre.Andino, tales como los complejos plutónicos Chollay y Piuquenes del Triásico Inferior – Triásico Medio, y la Formación Pastos Blancos y Sienogranitos Colorado del Triásico Superior, dados sus extensos afloramientos. También se ha caracterizado el magmatismo del Choiyoi, que corresponde al magmatismo Pre-Andino Pérmico, en términos composicionales y volumétricos, con la finalidad de compararlos con provincias magmáticas silíceas que se han originado en ambientes anorogénicos y en zonas de subducción activa. Por último, se han contrastado los registros magmáticos de los tres ciclos tectónicos: Gondwánico, Pre-Andino y Andino para generar un modelo

geotécnico que permite explicar las variaciones composicionales e isotópicas que se observan en el tiempo.

Los principales resultados obtenidos en esta investigación se resumen a continuación:

Al contrastar la petrografía y geoquímica de las rocas ígneas generadas en los ciclos Gondwánico, Pre-Andino y Andino temprano, expuestas entre los 18°S – 40°S en Chile y Argentina, es posible reconocer que en términos composicionales presentan una variación gradual, siendo las rocas del Ciclo Gondwánico predominantemente intermedias a ácidas; las del Ciclo Pre-Andino, ácidas a intermedias; y las del Ciclo Andino temprano, intermedias a básicas. La señal geoquímica elemental e isotópica y la petrografía de estas rocas sugieren que el ambiente geotectónico más probable para generar este registro magmático es una subducción activa, reconociéndose afinidades subacalinas, enriquecimientos en LILE respecto a los HFSE y depresiones en Nb-Ta, además de texturas porfídicas y litologías ricas en minerales máficos hidratados (hornblenda y biotita).

También es posible detectar algunas variaciones en las razones La_N/Yb_N y Sr/Y en las que se reconoce un incremento progresivo desde los 350 Ma hasta los 285 Ma, aproximadamente alcanzando su valor máximo tras la Orogenia San Rafael, y posteriormente una disminución sistemática de la razón $^{87}Sr/^{86}Sr_i$ y La_N/Yb_N, y el incremento del εNd_i desde los 285 Ma a los 150 Ma, lo que apunta a una disminución progresiva del componente cortical o litosférico al magmatismo o un incremento de la fuente mantélica deprimida, que es consistente con el cambio de una tectónica compresiva desde el Carbonífero al Pérmico Temprano, hacia una tectónica transtensional durante el Pérmico Medio – Jurásico.

Estos resultados permiten proponer que el margen occidental de Gondwana, al menos en el segmento estudiado, fue un margen activo entre el Carbonífero y el Jurásico y que las variaciones isotópicas registradas podrían estar sujetas a cambios en la geometría de la zona de subducción en la que el término del Ciclo Gondwánico estaría marcada por una subducción plana que habría generado la Orogenia San Rafael, para luego dar paso a un *roll-back* del *slab*, induciendo una extensión en la corteza, y

pérdida de parte de la litósfera por delaminación o erosión termal durante el Ciclo Pre-Andino y parte del Ciclo Andino.

El magmatismo Pre-Andino que abarca desde el Lopingiano al Triásico Inferior (286 – 247 Ma, Sato et al., 2015), forma parte del magmatismo del Choiyoi y se expone en dos zonas principales: en la zona andina (Cordillera Frontal, Cordillera de Domeyko, Bloque San Rafael), y en la Patagonia Norte (Macizo Norpatagónico y parte de la Cuenca Neuquina). Está representado principalmente por rocas volcánicas (~70% de los afloramientos) que en términos composicionales, se encuentran dominadas por riolitas y dacitas (77%), seguidas por andesitas (26%) y escasos basaltos (1%). Las rocas intrusivas que forman parte de este magmatismo, son principalmente granitos y granodioritas (~95%), con tonalitas y dioritas subordinadas (< 5%). La composición de las fases iniciales del magmatismo del Choiyoi es principalmente intermedia, pasando a una composición riolítica en sus etapas finales.

En términos volumétricos (~947.500 km^3) y en rangos de edad (~40 Ma), el magmatismo del Choiyoi es compatible con una SLIP (*Silicic Large Igneous Province)*. Sin embargo, la ausencia de señales intraplaca y el predominio de composiciones intermedias en las primeras etapas del magmatismo del Choiyoi, lo diferencian de las SLIPs. Esta característica se encuentra presente en otras provincias silíceas relacionadas a márgenes convergentes, tales como Okhotsk-Chukotka Volcanic Belt o Sikote-Alin Belt o la Zona Volcánica Taupo, permitiendo proponer que el magmatismo Pérmico del Ciclo Pre-Andino, podría haberse originado en un margen continental activo.

El magmatismo Pre-Andino, del Triásico Inferior – Triásico Medio, representado por las rocas intrusivas de los complejos plutónicos Chollay y Piuquenes, se distribuyen en una franja de orientación NNE-SSW al Este del arco del Ciclo Gondwánico representado por los complejos plutónicos Guanta y Chanchoquín, intruyéndolos. También es posible reconocer en el sector occidental de estos complejos, grandes xenolitos de rocas metamórficas paleozoicas (Complejo Metamórfico El Cepo y Gneisses La Pampa) definiendo un crecimiento antitaxial. En la zona central del Complejo Plutónico Chollay se reconocen cuerpos subverticales de diferentes

composiciones que definen un emplazamiento sintaxial. En términos petrográficos, las rocas que componen a los complejos corresponden principalmente a granodioritas y monzogranitos hololeucocráticos y leucocráticos con anfíboles cálcicos y biotita como minerales máficos, aunque también se reconocen cuerpos dioríticos, tonalíticos y monzograníticos. Geoquímicamente abarcan un amplio espectro composicional (desde gabros hasta granitos) y corresponden principalmente a rocas subalcalinas, con un *trend* de evolución calcoalcalino. Son peraluminosas a metaluminosas y presentan un enriquecimiento en LILE respecto a los HFSE, con depresiones en Nb-Ta, P y Ti. Clasifican en los diagramas de discriminación tectónica como rocas de arco con escasas muestras en el campo de los granitos intraplaca. En cuanto a su composición isotópica en Sr-Nd-Pb, presentan valores iniciales que representan una mezcla entre una fuente mantélica deprimida y la litósfera continental. Dentro del Complejo Plutónico Chollay es posible detectar una variación en la composición isotópica donde se reconoce un mayor aporte cortical en la zona de crecimiento antitaxial.

Por otro lado, el magmatismo Pre-Andino del Triásico Superior (Cárnico – Nórico) representado por las rocas de la Formación Pastos Blancos y Sienogranitos Colorado, también exhiben un amplio y continuo espectro composicional, un *trend* de diferenciación calcoalcalino, un enriquecimiento en LILE respecto a los HFSE y depresiones en Nb-Ta y Ti. Su composición isotópica, al igual que el magmatismo del Triásico Inferior – Triásico Medio, requiere de la participación de dos fuentes: un manto deprimido y de la litósfera continental.

El emplazamiento del magmatismo triásico estudiado ocurrió en un contexto extensional, en el que se desarrollaron cuencas de antearco y de trasarco. Sin embargo, el grado de extensión, estimado a partir del estudio estadístico de diques máficos contemporáneos al emplazamiento de los Sienogranitos Colorado, es menor que el requerido para un proceso de rift continental, escenario geotectónico que se había propuesto para este ciclo tectónico.

En términos generales, es posible mencionar que el magmatismo Pre-Andino estudiado, presenta una composición más silícea que la esperada para un arco.

También se detectan algunas muestras con señales geoquímicas que apuntan a un ambiente geotectónico anorogénico. Sin embargo, estas muestras son poco abundantes dentro de cada unidad, y, por otro lado, tienden a concentrarse en el Triásico Superior (Formación La Ternera, Formación Pastos Blancos, Sienogranitos Colorado, Complejo Plutónico Los Carricitos), representando un magmatismo transicional previo al establecimiento del arco en la actual Cordillera de la Costa, marcando el inicio del Ciclo Andino.

Si bien la subducción activa durante este periodo ya había sido planteada en otros trabajos basados en estudios petrográficos y geoquímicos elementales e isotópicos en rocas ígneas expuestas entre los 21°S - 40°S en las cordilleras de la Costa y Frontal (Chilena y Argentina), (e.g. Coloma et al., 2017; del Rey et al., 2016, 2019; Rocher et al., 2015), en el análisis sedimentológico de la Cuenca de Domeyko (Espinoza et al., 2019), y en reconstrucciones globales de placas (Riel et al., 2018; Young et al., 2019), en esta investigación se realizaron estudios petrográficos y geoquímicos de detalle, en unidades clave (complejos plutónicos Chollay y Piuquenes) en las que se desafió el modelo clásico donde se plantea el cese de la subducción a causa de la acreción del terreno X al margen occidental de Gondwana (Mpodozis & Kay, 1992).

A diferencia de lo que se plantea en el trabajo desarrollado por Mpodozis y Kay (1992), en esta investigación se reconocieron granodioritas, monzogranitos, sienogranitos, dioritas y monzogranitos, estas últimas dos no descritas anteriormente, ampliando el espectro composicional de las unidades analizadas. Además, las litologías dominantes dentro de los complejos corresponden a las granodioritas y monzogranitos. De esta manera, las rocas que componen a los complejos plutónicos Chollay y Piuquenes no corresponden únicamente a litologías extremadamente silíceas, como se había definido previamente. Por otro lado, la isotopía (Sr-Nd-Pb) menos evolucionada de estas rocas en comparación con las rocas del Carbonífero o Pérmico, permite descartar la fusión cortical como proceso petrogenético principal, como se había propuesto en el modelo en el que se interrumpe la subducción y la génesis de los magmas habría estado vinculada a una extensa anatexia cortical por el estancamiento

de magmas basálticos en la base de la corteza, tras el quiebre del slab (Mpodozis & Kay, 1992, 1990).

Por otro lado, en este trabajo se ha podido contrastar el magmatismo de los tres ciclos geotectónicos en términos petrográficos y geoquímicos mediante una extensa base de datos, poniendo en evidencia que los cambios observados son graduales y consistentes con una subducción prolongada a lo largo del margen.

Las principales conclusiones que dan respuesta a las interrogantes que guiaron esta investigación, centrada en las rocas ígneas triásicas expuestas en la Cordillera Frontal Chilena, se listan a continuación:

1. Las rocas de los complejos plutónicos Chollay y Piuquenes forman parte del arco del Triásico Inferior - Triásico Medio, y se caracterizan por presentar un amplio espectro composicional, que varía desde dioritas hasta granitos, generalmente leucocráticos, con biotita y anfíbol como minerales maficos. Presentan una señal calcoalcalina, son meta a ligeramente peraluminosas, con un enriquecimiento en LILE respecto a los HFSE, depresiones en Nb-Ta, P y T. Además, sus contenidos en La/Yb y Sr/Y, permiten estimar un espesor cortical ligeramente engrosado de aproximadamente 45 km.

2. La Formación Pastos Blancos y los Sienogranitos Colorado, ambas unidades del Triásico Superior, carecen de una bimodalidad composicional, abarcando desde andesitas basálticas a riolitas en el caso de la Formación Pastos Blancos, y monzo a sienogranitos hololeucocráticos a leucocráticos, en los Sienogranitos Colorado. La mayoría de las muestras analizadas presentan características geoquímicas de haber sido extruidas y emplazadas en un contexto de subducción. Sin embargo, escasas muestras presentan afinidades alcalinas. Por otro lado, los proxies empleados para estimar el espesor cortical, sugieren que la corteza presentaba un espesor normal.

3. El grado de extensión estimado a partir del análisis de los diques máficos contemporáneos a la intrusión de los Sienogranitos Colorado, pertenecientes al

Enjambre de Diques Máficos del Elqui, se encuentra muy por debajo de la extensión en zonas donde se ha generado un rift continental.

4. El magmatismo Pre-Andino estudiado posee un contenido en SiO_2 más elevado que el esperado para las rocas de arco. Sin embargo, no es posible reconocer una distribución bimodal en términos composicionales, que había sido previamente descrito en el magmatismo Triásico y que es propio de los magmas generados en un contexto de rift continental

5. Al contrastar el magmatismo Pre-Andino con aquel del ciclo Gondwánico y Andino temprano, se detectan variaciones graduales en cuanto a su composición, pasando de un magmatismo principalmente silíceo (ciclo Gondwánico) a un magmatismo intermedio a básico (ciclo Andino temprano). El magmatismo generado entre el Carbonífero y el Jurásico Inferior, expuesto en el norte de Chile entre los 22° - 31°S, presenta señales geoquímicas consistentes con un magmatismo generado en un contexto de subducción, tales como afinidades calcoalcalinas, enriquecimiento en LILE respecto a los HFSE, depresiones en Nb-Ta y anomalías negativas de Eu.

6. La composición isotópica en Sr-Nd-Pb de las rocas ígneas del Carbonífero al Jurásico Inferior sugiere la participación de dos fuentes en la génesis de los magmas: un manto deprimido y la corteza/litosfera continental. Por otro lado, se reconoce un cambio gradual desde el Carbonífero hasta el Jurásico, donde el componente cortical va disminuyendo y la fuente mantélica aumentando de manera progresiva.

Referencias

Álvarez, J., Mpodozis, C., Arriagada, C., Astini, R., Morata, D., Salazar, E., Valencia, V. A., & Vervoort, J. D. (2011). Detrital zircons from late Paleozoic accretionary complexes in north-central Chile (28°-32°S): Possible fingerprints of the Chilenia terrane. Journal of South American Earth Sciences, 32(4), 460–476. https://doi.org/10.1016/j.jsames.2011.06.002

Arriagada, C., Roperch, P., Mpodozis, C., & Fernandez, R. (2006). Paleomagnetism and tectonics of the southern Atacama Desert (25-28°S), northern Chile. Tectonics, 25(4). https://doi.org/10.1029/2005TC001923

Bahlburg, H., Vervoort, J. D., du Frane, S. A., Bock, B., Augustsson, C., & Reimann, C. (2009). Timing of crust formation and recycling in accretionary orogens: Insights learned from the western margin of South America. In Earth-Science Reviews (Vol. 97, pp. 215–241). https://doi.org/10.1016/j.earscirev.2009.10.006

Barbarin, B. (1999). A review of the relationships between granitoid types, their origins and their geodynamic environments. Lithos, 46, 605–626.

Charrier, R., Pinto, L., & Pía Rodríguez, M. (2007). Tectonostratigraphic evolution of the Andean Orogen in Chile. In The Geology of Chile (pp. 21–114). https://www.researchgate.net/publication/279890158

Charrier, R., Pinto, L., & Rodríguez, M. P. (2007). Tectonostratigraphic evolution of the Andean Orogen in Chile. In T. Moreno & W. Gibbons (Eds.), The Geology of Chile (pp. 21–114). The Geological Society.

Charrier, R., Ramos, V. A., Tapia, F., & Sagripanti, L. (2014). Tectono-stratigraphic evolution of the Andean Orogen between 31 and 37°S (Chile and Western Argentina). Geological Society Special Publication, 399, 13–61. https://doi.org/10.1144/SP399.20

Coira, B., Davidson, J., Mpodozis, C., Ramos, V., 1982. Tectonic and Magmatic Evolution of the Andes of Northern Argentina and Chile. Earth Sci. Rev. 18, 303–332. doi:10.1016/0012-8252(82)90042-3

Coloma, F., Ortíz, M., Creixell, C., Salazar, E., & Merino, R. (2015). Nuevos antecedentes geológicos del Complejo Plutónico Chollay y Estratos del Paso del Guanaco Sonso (Triásico inferior – medio), Cordillera de Vallenar, 28°30’ – 29°30’. XIV Congreso Geológico Chileno.

Deckart, K., Hervé, F., Fanning, C. M., Ramírez, V., Calderón, M., & Godoy, E. (2014a). Geocronología U-Pb e isótopos de Hf-O en circones del batolito de la Costa Pensilvaniana, Chile. Andean Geology, 41(1), 49–82. https://doi.org/10.5027/andgeoV41n1-a03

Deckart, K., Hervé, F., Fanning, C. M., Ramírez, V., Calderón, M., & Godoy, E. (2014b). Geocronología U-Pb e isótopos de Hf-O en circones del batolito de la Costa Pensilvaniana, Chile. Andean Geology, 41(1), 49–82. https://doi.org/10.5027/andgeoV41n1-a03

del Rey, A., Deckart, K., Arriagada, C., & Martínez, F. (2016). Resolving the paradigm of the late Paleozoic–Triassic Chilean magmatism: Isotopic approach. Gondwana Research, 37, 172–181. https://doi.org/10.1016/j.gr.2016.06.008

del Rey, A., Deckart, K., Planavsky, N., Arriagada, C., & Martínez, F. (2019). Tectonic evolution of the southwestern margin of Pangea and its global implications: Evidence from the mid Permian–Triassic magmatism along the Chilean-Argentine border. Gondwana Research, 76, 303–321. https://doi.org/10.1016/j.gr.2019.05.007

Ducea, M. N., Saleeby, J. B., & Bergantz, G. (2015). The architecture, chemistry, and evolution of continental magmatic arcs. Annual Review of Earth and Planetary Sciences, 43, 299–331. https://doi.org/10.1146/annurev-earth-060614-105049

Franzese, J. R., & Spalletti, L. A. (2001). Late Triassic - early Jurassic continental extension in southwestern Gondwana: tectonic segmentation and pre-break-up rifting. Journal of South American Earth Sciences, 14, 257–270. www.elsevier.com/locate/jsames

González, J. (2015). Petrografía y geoquímica del Triásico Superior de la Alta Cordillera (28°45’ – 30°02’S), Región de Coquimbo, Chile [Memoria para optar al título de Geólogo]. Universidad de Concepción.

Hervé, F., Fanning, C. M., Calderón, M., & Mpodozis, C. (2014). Early Permian to Late Triassic batholiths of the Chilean Frontal Cordillera (28°-31°S): SHRIMP U-Pb zircon ages and Lu-Hf and O isotope systematics. Lithos, 184–187, 436–446. https://doi.org/10.1016/j.lithos.2013.10.018

Hyppolito, T., García-Casco, A., Juliani, C., Meira, V. T., & Hall, C. (2014). Late Paleozoic onset of subduction and exhumation at the western margin of Gondwana (Chilenia Terrane): Counterclockwise P-T paths and timing of metamorphism of deep-seated garnet-mica schist and amphibolite of Punta Sirena, Coastal Accretionary Complex, central Chile (34° S). Lithos, 206–207, 409–434. https://doi.org/10.1016/j.lithos.2014.07.023

Kay, S., Ramos, V., Mpodozis, C., & Sruoga, P. (1989). Late Paleozoic to Jurassic silicic magmatism at the Gondwana margin: Analogy to the Middle Proterozoic in North America? Geology, 17, 324–328.

Kleiman, L. E., & Japas, M. S. (2009). The Choiyoi volcanic province at 34°S-36°S (San Rafael, Mendoza, Argentina): Implications for the Late Palaeozoic evolution of the southwestern margin of Gondwana. Tectonophysics, 473(3–4), 283–299. https://doi.org/10.1016/j.tecto.2009.02.046

Llambías, E. J., & Sato, A. M. (1995). El batolito de Colangüil: transición entre orogénesis y anorogénesis. Revista de La Asociación Geológica Argentina, 50(1–4), 111–131. https://www.researchgate.net/publication/285007862

Lucassen, F., Franz, G., Thirlwall, M. F., & Mezger, A. K. (1999). Crustal Recycling of Metamorphic Basement: Late Palaeozoic Granitoids of Northern Chile (~22°S). Implications for the Composition of the Andean Crust. Journal of Petrology, 40, 1527–1551.

Lucassen, F., Kramer, W., Bartsch, V., Wilke, H. G., Franz, G., Romer, R. L., & Dulski, P. (2006). Nd, Pb, and Sr isotope composition of juvenile magmatism in the Mesozoic large magmatic province of northern Chile (18-27°S): Indications for a uniform subarc mantle. Contributions to Mineralogy and Petrology, 152(5), 571–589. https://doi.org/10.1007/s00410-006-0119-y

Maksaev, V., Munizaga, F., & Tassinari, C. (2014). Timing of the magmatism of the paleo-pacific border of Gondwana: U-Pb geochronology of Late Paleozoic to Early Mesozoic igneous rocks of the north Chilean Andes between 20° and 31°S. Andean Geology, 41(3), 447–506. https://doi.org/10.5027/andgeoV41n3-a01

Martin, M. W., Clavero, J. R., & Mpodozis, C. M. (1999). Late Paleozoic to Early Jurassic tectonic development of the high Andean Principal Cordillera, El Indio Region, Chile (29-30°S). Journal of South American Earth Sciences, 12, 33–49.

Martínez, A. (2004). Secuencias volcánicas permo-triásicas de los cordones del Portillo y del Plata, Cordillera Frontal, Mendoza: su Interpretación Tectónica. Universidad de Buenos Aires.

Mpodozis, C., & Kay, S. (1992). Late Paleozoic to Triassic evolution of the Gondwana margin: Evidence from Chilean Frontal Cordilleran batholiths (28°S to 31°S). Geological Society of America Bulletin, 104, 999–1014.

Mpodozis, C., & Kay, S. M. (1990). Provincias magmáticas ácidas y evolución tectónica de Gondwana: Andes Chilenos (28°-31°S). Revista Geológica de Chile, 17(2), 153–180.

Mpodozis, C., & Ramos, V. A. (1989). The Andes of Chile and Argentina. In G. Ericksen, M. Cañas, & J. Reinemund (Eds.), Geology of the Andes and its Relation to Hydrocarbon and Mineral Resources (Vol. 11, pp. 59–90). Circum-Pacific Council for Energy and Mineral Resources Earth Science Series. https://www.researchgate.net/publication/284756949

Murillo, I., Velásquez, R., & Creixell, C. (2017). Geología de las áreas Guanta - Los Cuartitos y Paso de Vacas Heladas, Regiones de Atacama y Coquimbo. Servicio Nacional de Geología y Minería. Carta Geológica de Chile. Serie Geología Básica N°192-193. Escala 1:100.000.

Oliveros, V., González, J., Espinoza-Vargas, M., Vásquez, P., Rossel, P., Creixell, C., Sepúlveda, F., & Bastías, F. (2018). The Early Stages of the Magmatic Arc in the Southern Central Andes. In A. Folguera, E. Contreras-Reyes, N. Heredia, A. Encinas, S. Iannelli, V. Oliveros, F. M. Dávila, G. Collo, L. Giambiagi, A. Maksymowicz, M. P.

Iglesia Llanos, M. M. Turienzo, M. Naipauer, D. Orts, V. D. Litvak, O. Álvarez, & C. Arriagada (Eds.), The Evolution of the Chilean-Argentinean Andes (pp. 185–212). Springer International Publishing. http://www.springer.com/series/10178

Oliveros, V., Morata, D., & Aguirre, L. (2007). Jurassic to Early Cretaceous subduction-related magmatism in the Coastal Cordillera of northern Chile (18°30'-24°S): geochemistry and petrogenesis. Revista Geológica de Chile, 34(2), 209–232.

Oliveros, V., Vásquez, P., Creixell, C., González, J., Espinoza, M., Lucassen, F., & Ducea, M. (2015). Lithospheric loss in the Andean convergent margin during the Triassic: geochemical evidence from igneous rocks of northern Chile (24°30' – 30°00'S). . XIV Congreso Geológico Chileno.

Ortiz, M., & Merino, R. (2015). Geología de las áreas Río Chollay - Matancilla y Cajón del Encierro, Regiones de Atacama y Coquimbo. Servicio Nacional de Geología y Minería. Carta Geológica de Chile. Serie Geología Básica N°175-176. Escala 1:100.000.

Parada, F. (2013). Geoquímica de las rocas ígneas del Carbonífero – Triásico de la Alta Cordillera, Región de Atacama, Chile. [Memoria para optar al título de Geólogo]. Universidad de Chile.

Parada, M. A., Nystrom, J. O., & Levi, B. (1999). Multiple sources for the Coastal Batholith of central Chile (31-34°S): geochemical and Sr-Nd isotopic evidence and tectonic implications. Lithos, 46, 505–521.

Pearce, J., & Peate, D. (1995). Tectonic implications of the composition of volcanic arc magmas. Annual Review Earth Planetary Sciences, 23, 251–285.

Philpotts, A., & Ague, J. (2009). Principles of Igneous and Metamorphic Petrology (Second Edition). Cambridge University.

Ramos, V. (1988). Late Proterozoic-Early Paleozoic of South America - a Collisional History. Episodes, 11(3), 168–174.

Ramos, V. A., & Folguera, A. (2009). Andean flat-slab subduction through time. Geological Society Special Publication, 327, 31–54. https://doi.org/10.1144/SP327.3

Ramos, V. A., Jordan, T. E., Allmendinger, R. W., Mpodozis, C., Kay, S. M., Cortes, J. M., & Palma, M. (1986). Paleozoic terranes of the central Argentine-Chilean Andes. Tectonics, 5(6), 855–880.

Riel, N., Jaillard, E., Martelat, J. E., Guillot, S., & Braun, J. (2018). Permian-Triassic Tethyan realm reorganization: Implications for the outward Pangea margin. Journal of South American Earth Sciences, 81, 78–86. https://doi.org/10.1016/j.jsames.2017.11.007

Rossel, P., Oliveros, V., Ducea, M. N., Charrier, R., Scaillet, S., Retamal, L., & Figueroa, O. (2013). The Early Andean subduction system as an analog to island arcs: Evidence from across-arc geochemical variations in northern Chile. Lithos, 179, 211–230. https://doi.org/10.1016/j.lithos.2013.08.014

Salazar, E., & Coloma, F. (2016). Geología del área Cerros de Cantaritos-Laguna Chica, Región de Atacama. Servicio Nacional de Geología y Minería. Carta Geológica de Chile. Serie Geología Básica N°181. Escala 1:100.000.

Salazar, E., Coloma, F., & Creixell, C. (2013). Geología del área El Tránsito-Lagunillas, Región de Atacama. Servicio Nacional de Geología y Minería. Carta Geológica de Chile. Serie Geología Básica N°149. Escala 1:100.000.

Sato, A. M., Llambías, E. J., Basei, M. A. S., & Castro, C. E. (2015). Three stages in the Late Paleozoic to Triassic magmatism of southwestern Gondwana, and the relationships with the volcanogenic events in coeval basins. In Journal of South American Earth Sciences (Vol. 63, pp. 48–69). Elsevier Ltd. https://doi.org/10.1016/j.jsames.2015.07.005

Stern, R. J. (2002). Subduction zones. Reviews of Geophysics, 40(4), 3-1-3–38. https://doi.org/10.1029/2001RG000108

Suarez, M., & Bell, C. M. (1992). Triassic rift-related sedimentary basins in northern Chile (24°-29°S). Journal of South American Earth Sciences, 6(3), 109–121.

Valin, X. (2014). Geoquímica de las unidades del Triásico a Jurásico Inferior en el Norte de Chile (28°00’ – 29°30’S): Implicancias para el inicio de la subducción. [Memoria para optar al título de Geólogo]. Universidad de Concepción.

Velásquez, R., Coloma, F., Murillo, I., Merino, R., & Ortiz, M. (2021). Geología de las áreas Pisco Elqui y Paso del Agua Negra. Servicio Nacional de Geología y Minería. Carta Geológica de Chile. Serie Geología Básica N°211-212. Escala 1:100.000.

Vilas, J. F. A., & Valencio, D. A. (1978). Palaeomagnetism of South American and African rocks and the age of the South Atlantic. Revista Brasileira de Geociências, 8, 3–10.

White, W. (2013). Geochemistry. Wiley-Blackwell.

Willner, A. P., Massonne, H. J., Ring, U., Sudo, M., & Thomson, S. N. (2012). P-T evolution and timing of a late Palaeozoic fore-arc system and its heterogeneous Mesozoic overprint in north-central Chile (latitudes 31-32°S). Geological Magazine, 149(2), 177–207. https://doi.org/10.1017/S0016756811000641

Wilson, M. (1989). Igneous Petrogenesis A global tectonic approach. Springer.

Young, A., Flament, N., Maloney, K., Williams, S., Matthews, K., Zahirovic, S., & Müller, R. D. (2019). Global kinematics of tectonic plates and subduction zones since the late Paleozoic Era. Geoscience Frontiers, 10, 989–1013. https://doi.org/10.1016/j.gsf.2018.05.011

Apéndice Capítulo II

Supplementary Material 2.1. Table listing the mineral components of the studied rocks expressed as % of volume of the total rock. The first and third TOTAL columns refer to the total amount of igneous and alteration components, respectively, present in the rock, regardless of the domain in which they occur. The second TOTAL column refers to the different igneous minerals detectable at micro scale. In the case of phaneritic rocks, igneous crystals are listed in the column “phenocrysts”. For volcanic rocks, the vitric component occurs as part of the groundmass. Phn = Phenocyrsts, Gls = Glass, Lith = Lithics, Gdms = Groundmass, Mtr = Matrix, Pl = plagioclase, Qz = quartz, Ort = orthoclase, Mic = microcline, Bt = biotite, Amp = amphibole, Mv = muscovite, Cpx = clinopyroxene, Opx = orthopyroxene, Ol = olivine, Indet = mafic undetermined, opa = opaque mineral undetermined, Sph = sphene, Ap = apatite, Rut = rutile, Q = quartz, A = alkaline feldspar, P = plagioclase (for Streickesen classification of phaneritic rocks with % of mafic minerals under 90%), Cc = calcite/carbonate undetermined, Ser = sericite, Chl = chlorite, Ep = epidote, Qz = quartz (chalcedony, amorphous silica), Ttn = titanite, Cl = clays, Bt = biotite, Fe-ox = Fe oxides/hydroxides, opa = opaque mineral undetermined. Ill = illlite. Analyzed samples not listed in this table are described in Ortiz and Merino (2015), Salazar and Coloma (2016) and Coloma et al. (2017).

Sample	Lithology	Location		Unit	Igneous components					
		E	N		Phn	Gls	Lith	Gdms	Mtr	TOTAL
CPV-12-01	Diabase	257848	6780649	La Vaca Granodiorite	1	0	0	0	0	1,00
CPV-12-03	Granodiorite	264762	6778121	La Vaca Granodiorite	1	0	0	0	0	1,00
CPV-12-26B	Andesite (breccia fragment)	359110	6779598	Algarrobal Formation	0,25	0,03	0	0,72	0	1,00
CPV-12-28x	Basaltic Andesite	361226	6778404	Algarrobal Formation	0,12	0,08	0	0,8	0	1,00
CPV-12-30x	Andesite	359946	6778193	Algarrobal Formation	0,33	0,05	0	0,62	0	1,00
CPV-12-90	Lithic tuff	306157	6873300	Canto del Agua Formation	0,16	0	0,12	0	0,72	1,00
CPV-14-159	Basaltic andesite (Agglomerate matrix)	486567	7248856	Cerro Guanaco Formation	0,25	0,2	0	0,55	0	1,00
CPV-14-164	Basalt	486491	7248161	Cerro Guanaco Formation	0,25	0,33	0	0,42	0	1,00
CPV-14-166	Andesite	486526	7248012	Cerro Guanaco Formation	0,16	0,29	0	0,55	0	1,00
CPV-14-167	Andesite	489308	7242948	Cerro Guanaco Formation	0,19	0,05	0	0,78	0	1,02
CPV-14-169A	Andesite	489086	7243400	Cerro Guanaco Formation	0,29	0,11	0	0,6	0	1,00
CPV-14-172	Andesite	488824	7243423	Cerro Guanaco Formation	0,15	0,09	0	0,76	0	1,00
CPV-14-173	Andesite	488614	7243452	Cerro Guanaco Formation	0,29	0,03	0	0,68	0	1,00
CPV-14-176	Rhyolitic tuff	480403	7272029	La Tabla Formation	0,67	0,33	0	0	0	1,00
CPV-14-180A	Monzogranite	335853	7160972	Cifuncho Plutonic Complex	1	0	0	0	0	1,00
CPV-14-181B	Monzodiorite	342187	7138664	Sierra Esmeralda Plutonic Complex	1	0	0	0	0	1,00
CPV-14-182B	Tonalite	342760	7134508	Sierra Esmeralda Plutonic Complex	1	0	0	0	0	1,00
CPV-14-184	Andesite (porphyry)	340042	7134594	Cifuncho Formation	0,39	0,05	0	0,56	0	1,00
CPV-14-187	Andesite	339123	7134911	Cifuncho Formation	0,4	0,5	0	0,1	0	1,00
CPV-14-190	Dacite (porphyry)	337489	7133332	Cifuncho Formation	0,67	0,04	0	0,29	0	1,00
CPV-14-191	Monzogranite	331989	7133968	Cifuncho Plutonic Complex	1	0	0	0	0	1,00
CPV-14-192	Granite	344202	7119705	Pan de Azúcar Pluton	1	0	0	0	0	1,00

CPV-14-194	Dacitic tuff	346064	7116574	Agua Chica Formation	0,62	0,33	0	0,05	0	1,00
CPV-14-198	Andesite	345848	7117138	Agua Chica Formation	0,58	0,05	0	0,37	0	1,00
CPV-14-245	Basaltic Andesite	476322	7196656	Quebrada del Salitre Formation	0,84	0,16	0	0	0	1,00
CPV-14-247	Lapilli tuff	478187	7202622	Quebrada del Salitre Formation	0,22	0,2	0,58	0	0	1,00
CPV-14-249	Rhyolitic tuff	477668	7201891	La Tabla Formation	0,4	0,05	0	0,55	0	1,00
CPV-14-253	Basalt	476972	7201597	Quebrada del Salitre Formation	0,15	0,04	0	0,81	0	1,00
CPV-14-256	Basaltic andesite	469978	7201796	Quebrada del Salitre Formation	0,17	0,14	0	0,69	0	1,00
CPV-14-263	Dacite	480329	7252855	Cerro Ratones Beds	0,6	0	0	0,4	0	1,00
CPV-15-271	Basalt	405540	6897409	La Ternera Formation	0,1	0,05	0	0,85	0	1,00
CPV-15-274	Basalt	438698	6931859	La Ternera Formation	0	0,05	0	0,95	0	1,00
CPV-15-278	Andesite	451252	6927171	La Ternera Formation	0,3	0,1	0	0,6	0	1,00
CPV-15-279	Dacitic tuff	448251	6933987	La Ternera Formation	0,1	0,55	0,01	0	0,34	1,00
CPV-15-280	Andesitic tuff	442475	6933547	La Ternera Formation	0,3	0,15	0,3	0	0,25	1,00
CPV-15-281	Andesite	427604	7000335	La Ternera Formation	0,1	0,1	0,05	0	0,75	1,00
CPV-15-284	Basalt	429399	7000568	La Ternera Formation	0,3	0	0	0,7	0	1,00
CPV-15-285	Lapilli tuff	429399	7000568	La Ternera Formation	0,1	0,05	0,7	0	0,15	1,00
CPV-15-287	Basaltic andesite	429509	7000612	La Ternera Formation	0,05	0	0	0,95	0	1,00
CPV-15-303	Basaltic andesite	467920	7113259	Quebrada del Salitre Formation	0,22	0,08	0	0,7	0	1,00
CPV-15-310	Rhyolite	462332	7114194	Quebrada del Salitre Formation	0,22	0,05	0	0,73	0	1,00
CPV-15-311	Basalt	467495	7132147	Quebrada del Salitre Formation	0,29	0,05	0	0,66	0	1,00
CPV-15-312	Andesite	471764	7136501	Quebrada del Salitre Formation	0,38	0	0	0,62	0	1,00
CPV-15-314	Rhyolite (dome)	467881	7125180	Quebrada del Salitre Formation	0,11	0,2	0	0,69	0	1,00
CPV-15-319	Dacite	465751	7126652	Quebrada del Salitre Formation	0,7	0,02	0	0,28	0	1,00
CPV-15-320	Quartz Monzodiorite	465519	7125144	Sierra de Doña Inés Chica Plutonic Complex	1	0	0	0	0	1,00
CPV-15-322	Andesite	460777	7123933	Quebrada del Salitre Formation	0,02	0	0	0,98	0	1,00
CPV-15-330	Lithic tuff	475259	7226802	Quebrada del Salitre Formation	0,25	0,2	0,55	0	0	1,00
CPV-15-332	Dacite	475197	7226045	Quebrada del Salitre Formation	0,32	0,1	0	0,58	0	1,00
CPV-15-337	Andesitic breccia	476243	7225507	Quebrada del Salitre Formation	0,34	0,28	0,38	0	0	1,00
CPV-15-353	Dacite	471839	7201617	La Tabla Formation	0,35	0	0	0,65	0	1,00
CPV-15-359	Basalt	471835	7201594	Quebrada del Salitre Formation	0	0	0	1	0	1,00
CPV-15-365	Granodiorite	475235	7200650	Punta del Viento Plutonic Complex	1	0	0	0	0	1,00
CPV-15-386	Basalt	471710	7201470	Quebrada del Salitre Formation	0	0	0	1	0	1,00
RCM-61q	Syenogranite	381620	6744026	Colorado Syenogranite	1	0	0	0	0	1,00
RCM-78q	Andesite	379914	6748141	Pastos Blancos Formation	0,49	0,32	0	0,19	0	1,00
SCL-28q	Rhyolitic tuff	423238	6807445	Guanaco Sonso Formation	0,53	0,47	0	0	0	1,00
SCL-96	Dacitic tuff	425477	6807665	Guanaco Sonso Formation	0,03	0,65	0,02	0	0,3	1,00

Sample	Igneous minerals														
	Pl	Qz	Ort	Mic	Bt	Amp	Mv	Cpx	Opx	Ol	Indet	Opa	Ap	Zr	TOTAL
CPV-12-01	0,47	0	0	0	0,19	0	0	0,1	0	0	0	0,11	0	0	0,87
CPV-12-03	0,35	0,25	0,1	0	0,1	0	0	0,15	0	0	0	0,03	0	0	0,98
CPV-12-26B	0,72	0	0	0	0	0	0	0	0	0	0	0,09	0	0	0,81
CPV-12-28x	0,6	0	0	0	0	0	0	0	0	0	0,11	0	0	0	0,71
CPV-12-30x	0,55	0	0	0	0,03	0	0	0,1	0	0	0,1	0	0	0	0,78
CPV-12-90	0,08	0,05	0	0	0	0	0	0	0	0	0,03	0	0	0	0,16
CPV-14-159	0,56	0	0	0	0	0	0	0	0	0	0,08	0,03	0	0	0,67
CPV-14-164	0,4	0	0	0	0	0	0	0,06	0	0,07	0	0,04	0	0	0,57
CPV-14-166	0,55	0,08	0	0	0	0,09	0	0	0	0	0	0	0	0	0,72
CPV-14-167	0,59	0	0	0	0	0	0	0	0	0	0	0,05	0	0	0,64
CPV-14-169A	0,37	0	0	0	0,08	0,14	0	0	0	0	0	0,03	0	0	0,62
CPV-14-172	0,37	0,07	0	0	0	0,13	0	0	0	0	0	0,07	0	0	0,64
CPV-14-173	0,65	0	0	0	0	0,02	0	0	0	0	0,04	0,01	0	0	0,72
CPV-14-176	0,42	0,08	0	0	0,12	0,03	0	0	0	0	0	0,02	0	0	0,67
CPV-14-180A	0,27	0,36	0,15	0,04	0,09	0	0	0	0	0	0	0	0	0	0,91
CPV-14-181B	0,43	0,03	0,08	0	0	0,06	0,05	0	0	0	0	0,03	0	0	0,68
CPV-14-182B	0,34	0,26	0,05	0	0,09	0,1	0	0	0	0	0	0,02	0	0	0,86
CPV-14-184	0,5	0,03	0	0	0,14	0	0	0	0	0	0	0,01	0	0	0,68
CPV-14-187	0,43	0,01	0	0	0,01	0	0	0	0	0	0,15	0	0	0	0,60
CPV-14-190	0,45	0,21	0	0	0,02	0,13	0	0	0	0	0	0,03	0	0	0,84
CPV-14-191	0,2	0,36	0,12	0	0,08	0,02	0	0	0	0	0	0,01	0,01	0	0,80
CPV-14-192	0,16	0,31	0,31	0	0	0	0,08	0	0	0	0	0	0,01	0	0,87
CPV-14-194	0,52	0	0	0	0,06	0,1	0	0	0	0	0	0,02	0	0	0,70
CPV-14-198	0,35	0	0	0	0,07	0,15	0	0	0	0	0	0,03	0	0	0,60
CPV-14-245	0,56	0	0	0	0	0	0	0,04	0	0	0	0,01	0	0	0,61
CPV-14-247	0,47	0,03	0	0	0	0	0	0	0	0	0,18	0,03	0	0	0,71
CPV-14-249	0,12	0,3	0,19	0	0	0	0	0	0	0	0,03	0,2	0	0	0,84
CPV-14-253	0,51	0	0	0	0	0	0	0	0	0	0,09	0,02	0	0	0,62
CPV-14-256	0,55	0	0	0	0	0	0	0	0	0	0,02	0,03	0	0	0,60
CPV-14-263	0,2	0,29	0,04	0	0,03	0,06	0	0	0	0	0	0,02	0	0,01	0,65
CPV-15-271	0,49	0	0	0	0	0	0	0,07	0	0,06	0	0,03	0	0	0,65
CPV-15-274	0,49	0	0	0	0	0	0	0,07	0	0	0,06	0,03	0	0	0,65
CPV-15-278	0,47	0	0	0	0	0	0	0,07	0	0	0,03	0,07	0	0	0,64
CPV-15-279	0,08	0,39	0,08	0	0	0	0	0	0	0	0	0	0	0	0,55
CPV-15-280	0,47	0,13	0	0	0	0	0	0	0	0	0,08	0,04	0	0	0,72
CPV-15-281	0,26	0,32	0	0	0	0	0	0	0	0	0	0,06	0	0	0,64
CPV-15-284	0,5	0	0	0	0	0	0	0,07	0	0,1	0	0,01	0	0	0,68
CPV-15-285	0,48	0	0	0	0	0	0	0	0	0	0,09	0,03	0	0	0,60
CPV-15-287	0,39	0	0	0	0	0	0	0,05	0	0	0,03	0,02	0	0	0,49

CPV-15-303	0,63	0	0	0	0	0	0	0	0	0,05	0	0	0	0	0,68
CPV-15-310	0,09	0,28	0	0	0	0	0	0	0	0	0	0,02	0	0	0,39
CPV-15-311	0,41	0	0	0	0	0	0	0,09	0	0,03	0	0,08	0	0	0,61
CPV-15-312	0,39	0,1	0,03	0	0	0,11	0	0	0,03	0	0	0	0	0	0,66
CPV-15-314	0,6	0	0	0	0	0	0	0	0	0	0	0,01	0	0	0,61
CPV-15-319	0,59	0	0	0	0	0	0	0	0	0	0	0,04	0	0	0,63
CPV-15-320	0,22	0,35	0,07	0	0,06	0,01	0	0,01	0	0	0	0	0	0	0,72
CPV-15-322	0,3	0	0	0	0	0	0	0,06	0	0,02	0	0,02	0	0	0,40
CPV-15-330	0,25	0,04	0	0	0	0	0	0,02	0,02	0	0	0	0	0	0,33
CPV-15-332	0,38	0,18	0	0	0	0	0	0	0	0	0,12	0	0	0	0,68
CPV-15-337	0,4	0	0	0	0	0	0	0	0	0	0	0,05	0	0	0,45
CPV-15-353	0,51	0	0	0	0,03	0,03	0	0	0	0	0,05	0,03	0	0	0,65
CPV-15-359	0,53	0	0	0	0	0	0	0	0	0	0,07	0,02	0	0	0,62
CPV-15-365	0,44	0,23	0,13	0	0	0	0	0,02	0	0	0	0	0	0	0,82
CPV-15-386	0,67	0	0	0	0	0	0	0,13	0	0	0	0	0	0	0,80
RCM-61q	0,15	0,22	0,29	0	0,01	0	0,01	0	0	0	0	0,02	0	0	0,70
RCM-78q	0,54	0	0	0	0,01	0	0	0	0	0	0,08	0,04	0	0	0,67
SCL-28q	0,04	0,4	0,1	0	0	0	0	0	0	0	0,01	0,05	0	0	0,60
SCL-96	0,02	0,17	0	0	0	0	0	0	0	0	0	0,01	0	0	0,20

Sample	Alteration minerals											
	Cc	Ser	Chl	Ep	Qz	Ttn	Cl	Bt	Amp	Fe-mx	Opa	TOTAL
CPV-12-01	0	0	0	0	0	0	0,03	0	0,1	0	0	0,13
CPV-12-03	0	0,02	0	0	0	0	0	0	0	0	0	0,02
CPV-12-26B	0,07	0	0	0,01	0	0	0,1	0	0	0,01	0	0,19
CPV-12-28x	0,1	0	0,03	0	0	0	0,08	0	0	0,08	0	0,29
CPV-12-30x	0,08	0	0,07	0	0	0	0,02	0	0	0,05	0	0,22
CPV-12-90	0,05	0,25	0	0	0	0	0,125	0,05	0	0,025	0	0,50
CPV-14-159	0,1	0	0,05	0	0	0	0,1	0	0	0,08	0	0,33
CPV-14-164	0,07	0	0,07	0	0,02	0	0,27	0	0	0	0	0,43
CPV-14-166	0	0,03	0,03	0	0	0	0,22	0	0	0	0	0,28
CPV-14-167	0,16	0	0	0	0	0	0,2	0	0	0	0	0,36
CPV-14-169A	0,07	0,04	0	0	0	0	0,27	0	0	0	0	0,38
CPV-14-172	0,2	0	0,02	0,03	0	0	0,09	0	0	0,02	0	0,36
CPV-14-173	0,09	0	0,02	0,01	0	0,03	0,05	0	0	0,08	0	0,28
CPV-14-176	0	0,04	0,08	0,12	0	0	0,09	0	0	0	0	0,33
CPV-14-180A	0	0,05	0,02	0	0	0	0,02	0	0	0	0	0,09
CPV-14-181B	0,05	0,07	0,02	0	0	0,03	0,1	0	0	0,05	0	0,32
CPV-14-182B	0	0	0,02	0	0	0	0,12	0	0	0	0	0,14
CPV-14-184	0,02	0	0,04	0,1	0	0	0,16	0	0	0	0	0,32
CPV-14-187	0,05	0	0	0,02	0	0	0,15	0	0	0,08	0	0,30

CPV-14-190	0,06	0	0	0,02	0	0	0,04	0	0	0,04	0	0,16
CPV-14-191	0	0,07	0,05	0,08	0	0	0	0	0	0	0	0,20
CPV-14-192	0	0,08	0	0	0	0	0	0	0	0	0,05	0,13
CPV-14-194	0,1	0	0,03	0,05	0	0	0,1	0	0	0,02	0	0,30
CPV-14-198	0,07	0	0	0	0	0	0,2	0	0	0,13	0	0,40
CPV-14-245	0,26	0	0	0	0	0	0,13	0	0	0	0	0,39
CPV-14-247	0	0	0,05	0	0	0	0,24	0	0	0	0	0,29
CPV-14-249	0	0,2	0,05	0	0,1	0	0	0	0	0	0,01	0,36
CPV-14-253	0,04	0	0,07	0,02	0	0	0,23	0	0	0,02	0	0,38
CPV-14-256	0,15	0,1	0,07	0	0	0	0,08	0	0	0	0	0,40
CPV-14-263	0	0,08	0,12	0,05	0,05	0	0,05	0	0	0	0	0,35
CPV-15-271	0	0	0,2	0	0	0,05	0	0	0	0	0,1	0,35
CPV-15-274	0,1	0	0,08	0	0,1	0	0	0	0	0,07	0	0,35
CPV-15-278	0,1	0,11	0	0	0	0	0	0	0	0,15	0	0,36
CPV-15-279	0,2	0	0,05	0	0	0	0,15	0	0	0,05	0	0,45
CPV-15-280	0,05	0,01	0,05	0	0	0,02	0,05	0	0	0,07	0,03	0,28
CPV-15-281	0,05	0,05	0,15	0	0	0	0	0	0	0,1	0,01	0,36
CPV-15-284	0	0	0,15	0	0	0	0,02	0	0	0,05	0,1	0,32
CPV-15-285	0,05	0	0,05	0	0,1	0,05	0	0	0	0,05	0,1	0,40
CPV-15-287	0,03	0,2	0,03	0	0	0	0,2	0	0	0,05	0	0,51
CPV-15-303	0,09	0,07	0,05	0	0	0	0,1	0	0	0,01	0	0,32
CPV-15-310	0,3	0,03	0	0	0	0	0,28	0	0	0	0	0,61
CPV-15-311	0,14	0,21	0,03	0	0	0	0	0	0	0,01	0	0,39
CPV-15-312	0,2	0,04	0	0	0	0	0,1	0	0	0	0	0,34
CPV-15-314	0,19	0	0	0	0	0	0,1	0	0	0	0	0,29
CPV-15-319	0,25	0,08	0,04	0	0	0	0	0	0	0	0	0,37
CPV-15-320	0	0,03	0,08	0,07	0	0	0,1	0	0	0	0	0,28
CPV-15-322	0,1	0,3	0,15	0	0	0	0	0	0	0	0,05	0,60
CPV-15-330	0,12	0,02	0,02	0	0	0	0,05	0	0	0	0	0,21
CPV-15-332	0,2	0	0,02	0	0	0	0,1	0	0	0	0	0,32
CPV-15-337	0,2	0,02	0	0	0	0	0,1	0	0	0	0	0,32
CPV-15-353	0,05	0,05	0	0,02	0,03	0	0,05	0	0	0	0,15	0,35
CPV-15-359	0,15	0,02	0,1	0	0,05	0,03	0	0	0	0	0,03	0,38
CPV-15-365	0	0,05	0	0,01	0	0	0,12	0	0	0	0	0,18
CPV-15-386	0	0,04	0,04	0,06	0	0,03	0	0	0	0	0	0,17
RCM-61q	0	0,03	0,02	0	0	0	0,25	0	0	0	0	0,30
RCM-78q	0,1	0,08	0	0,01	0,01	0,03	0,1	0	0	0	0	0,33
SCL-28q	0	0,01	0	0	0	0	0,39	0	0	0	0	0,40
SCL-96	0	0	0	0	0	0	0,03	0	0	0	0	0,03

Suppementary Material 2.2. Age data for the analyzed samples. Column "Age dating" refers to the radiometric age obtained for the listed sample in the same publication of the geochemical data. Column "Age reference" refers to the radiometric age assigned to the listed sample by the authors of the same publication of the geochemical data based on the literature. Usually, it corresponds to the geographically/stratigraphically closest sample with a published radiometric age available. Columns "Age min" and "Age max" are referred to the stratigraphic age assigned (by the authors of the publication in which the geochemical data is reported) to the unit to which the sample belongs or to an interval of radiometric ages of the same unit, if the sample cannot be related to a single radiometric age. Columns "Preferred age max" and "Preferred age min" refer to the age interval assigned in this work to the listed sample based on stratigraphical or geological criteria. References at the bottom of the table.

Sample	Unit	Petrography	East	North	Age (Ma) dating	±	Age (Ma) reference	±	Reference
CPV-12-23	La Totora Formation	Andesite	376484	6814323	N.D.	N.D.	N.D.	N.D.	N.D.
CPV-12-24	La Totora Formation	Andesite	383333	6826718	N.D.	N.D.	N.D.	N.D.	N.D.
CPV-12-38	San Félix Formation	Lithic tuff	362530	6778657	N.D.	N.D.	N.D.	N.D.	N.D.
CPV-12-49b	San Félix Formation	Lithic tuff	359174	6805415	N.D.	N.D.	N.D.	N.D.	N.D.
CPV-12-60	La Totora Formation	Basalt	382348	6827655	N.D.	N.D.	N.D.	N.D.	N.D.
CPV-12-91A	Carrizal Bajo Complex	Diorite	301526	6884546	N.D.	N.D.	N.D.	N.D.	N.D.
CPV-12-91B	Carrizal Bajo Complex	Tonalite	301526	6884546	N.D.	N.D.	N.D.	N.D.	N.D.
CPV-12-92	Algodones Granite	Quartz diorite	298038	6887501	N.D.	N.D.	N.D.	N.D.	N.D.
CPV-12-93	Carrizal Bajo Complex	Granite	288859	6878634	N.D.	N.D.	N.D.	N.D.	N.D.
SCL-02q	Chollay Plutonic Complex	Monzogranite	410948	6804964	N.D.	N.D.	245,5	N.D.	Salazar et al. 2013
SCL-09q	Chollay Plutonic Complex	Granodiorite	410315	6794865	N.D.	N.D.	245,5	N.D.	Salazar et al. 2013
SCL-26q	La Totora Formation	Rhyolitic tuff	414172	6808064	N.D.	N.D.	217,9	2,20	N.D.
O7-06	Montegrande Granite	Granite	357424	6668630	N.D.	N.D.	214,7	N.D.	Coloma et al. 2017
O7-07	Montegrande Granite	Granite	361047	6666761	N.D.	N.D.	214,7	N.D.	Coloma et al. 2017
O7-10	La Laguna Gabbro	Gabbro	396451	6669570	N.D.	N.D.	218,1	N.D.	Coloma et al. 2017
O7-11	La Laguna Gabbro	Gabbro	396266	6669913	N.D.	N.D.	218,1	N.D.	Coloma et al. 2017
O7-13	Guanta Plutonic Complex	Graniodiorite	368473	6695942	N.D.	N.D.	290,0	N.D.	Coloma et al. 2017
O7-15	Guanta Putonic Complex	Tonalite	366163	6697056	N.D.	N.D.	296,0	N.D.	Coloma et al. 2017
CPV-12-105	Llano de Chocolate Beds	Rhyolite	286402	6789103	N.D.	N.D.	318,8	N.D.	Creixell et al. 2016
CPV-12-12	Llano de Chocolate Beds	Dacite	289084	6794562	N.D.	N.D.	303,8	N.D.	Creixell et al. 2016
CPV-12-127	Llano de Chocolate Beds	Rhyolitic tuff	287052	6792338	N.D.	N.D.	291,4	0,80	Creixell et al. 2016
CPV-12-01	La Vaca Granodiorite	Diabase	257848	6780649	N.D.	N.D.	180,00	N.D.	Creixell et al. 2012
CPV-12-03	La Vaca Granodiorite	Granodiorite	264762	6778121	N.D.	N.D.	198,00	N.D.	Creixell et al. 2012
CPV-12-26B	Algarrobal Formation	Andesite (breccia fragment)	359110	6779598	N.D.	N.D.	152,70	2,30	Rossel et al. 2013
CPV-12-28x	Algarrobal Formation	Basaltic Andesite	361226	6778404	N.D.	N.D.	152,70	2,30	Rossel et al. 2013
CPV-12-30x	Algarrobal Formation	Andesite	359946	6778193	N.D.	N.D.	152,70	2,30	Rossel et al. 2013

CPV-12-90	Canto del Agua Formation	Lithic tuff	306157	6873300	N.D.	N.D.	212,75	4,38	Salazar et al. 2019
CPV-14-176	La Tabla Formation	Rhyolitic tuff	480403	7272029	N.D.	N.D.	295,10	2,80	Venegas et al. 2013
CPV-14-180A	Cifuncho Plutonic Complex	Monzogranite	335853	7160972	N.D.	N.D.	284,8	N.D.	Contreras et al. 2013
CPV-14-181B	Sierra Esmeralda Plutonic Complex	Monzodiorite	342187	7138664	N.D.	N.D.	193,50	3,00	Contreras et al. 2013
CPV-14-182B	Sierra Esmeralda Plutonic Complex	Tonalite	342760	7134508	N.D.	N.D.	193,50	3,00	Contreras et al. 2013
CPV-14-184	Cifuncho Formation	Andesite (porphyry)	340042	7134594	N.D.	N.D.	212,00	4,80	Contreras et al. 2013
CPV-14-187	Cifuncho Formation	Andesite	339123	7134911	N.D.	N.D.	210,10	4,00	Contreras et al. 2013
CPV-14-190	Cifuncho Formation	Dacite (porphyry)	337489	7133332	N.D.	N.D.	212,00	4,80	Contreras et al. 2013
CPV-14-191	Cifuncho Plutonic Complex	Monzogranite	331989	7133968	N.D.	N.D.	N.D.	N.D.	N.D.
CPV-14-192	Pan de Azúcar Pluton	Granite	344202	7119705	N.D.	N.D.	N.D.	N.D.	N.D.
CPV-14-194	Agua Chica Formation	Dacitic tuff	346064	7116574	N.D.	N.D.	200,40	2,10	Espinoza et al. 2015
CPV-14-198	Agua Chica Formation	Andesite	345848	7117138	N.D.	N.D.	200,40	2,10	Espinoza et al. 2015
CPV-14-245	Quebrada del Salitre Formation	Basaltic Andesite	476322	7196656	N.D.	N.D.	212,00	N.D.	N.D.
CPV-14-247	Quebrada del Salitre Formation	Lapilli tuff	478187	7202622	N.D.	N.D.	212,00	N.D.	N.D.
CPV-14-249	La Tabla Formation	Rhyolitic tuff	477668	7201891	N.D.	N.D.	N.D.	N.D.	N.D.
CPV-14-253	Quebrada del Salitre Formation	Basalt	476972	7201597	N.D.	N.D.	212,00	N.D.	N.D.
CPV-14-256	Quebrada del Salitre Formation	Basaltic andesite	469978	7201796	N.D.	N.D.	233,00	N.D.	N.D.
CPV-14-263	Cerro Ratones Beds	Dacite	480329	7252855	N.D.	N.D.	N.D.	N.D.	N.D.
CPV-15-271	La Ternera Formation	Basalt	405540	6897409	N.D.	N.D.	N.D.	N.D.	3.4
CPV-15-274	La Ternera Formation	Basalt	438698	6931859	N.D.	N.D.	N.D.	N.D.	N.D.
CPV-15-278	La Ternera Formation	Andesite	451252	6927171	N.D.	N.D.	N.D.	N.D.	N.D.
CPV-15-279	La Ternera Formation	Dacitic tuff	448251	6933987	N.D.	N.D.	N.D.	N.D.	N.D.
CPV-15-280	La Ternera Formation	Andesitic tuff	442475	6933547	N.D.	N.D.	N.D.	N.D.	N.D.
CPV-15-281	La Ternera Formation	Andesite	427604	7000335	N.D.	N.D.	N.D.	N.D.	N.D.
CPV-15-284	La Ternera Formation	Basalt	429399	7000568	N.D.	N.D.	N.D.	N.D.	N.D.
CPV-15-285	La Ternera Formation	Lapilli tuff	429399	7000568	N.D.	N.D.	N.D.	N.D.	N.D.
CPV-15-287	La Ternera Formation	Basaltic andesite	429509	7000612	N.D.	N.D.	N.D.	N.D.	N.D.
CPV-15-303	Quebrada del Salitre Formation	Basaltic andesite	467921	7113260	N.D.	N.D.	N.D.	N.D.	N.D.
CPV-15-310	Quebrada del Salitre Formation	Rhyolite	462332	7114194	N.D.	N.D.	N.D.	N.D.	N.D.
CPV-15-311	Quebrada del Salitre Formation	Basalt	467495	7132147	N.D.	N.D.	N.D.	N.D.	N.D.
CPV-15-312	Quebrada del Salitre Formation	Andesite	471764	7136501	N.D.	N.D.	N.D.	N.D.	N.D.
CPV-15-314	Quebrada del Salitre Formation	Rhyolite (dome)	467881	7125180	N.D.	N.D.	N.D.	N.D.	N.D.
CPV-15-319	Quebrada del Salitre Formation	Dacite	465751	7126652	N.D.	N.D.	N.D.	N.D.	N.D.
CPV-15-320	Sierra de Doña Inés Chica Plutonic Complex	Quartz Monzodiorite	465519	7125144	N.D.	N.D.	285,30	6,40	Cornejo and Mpodozis 1996

CPV-15-322	Quebrada del Salitre Formation	Andesite	460778	7123934	N.D.	N.D.	N.D.	N.D.	N.D.
CPV-15-330	Quebrada del Salitre Formation	Lithic tuff	475260	7226802	N.D.	N.D.	N.D.	N.D.	N.D.
CPV-15-332	Quebrada del Salitre Formation	Dacite	475197	7226045	N.D.	N.D.	N.D.	N.D.	N.D.
CPV-15-337	Quebrada del Salitre Formation	Andesitic breccia	476244	7225507	N.D.	N.D.	N.D.	N.D.	N.D.
CPV-15-353	La Tabla Formation	Dacite	471839	7201617	N.D.	N.D.	N.D.	N.D.	Venegas et al. 2013
CPV-15-359	Quebrada del Salitre Formation	Basalt	471835	7201594	N.D.	N.D.	N.D.	N.D.	N.D.
CPV-15-365	Punta del Viento Plutonic Complex	Granodiorite	475235	7200650	N.D.	N.D.	N.D.	N.D.	N.D.
CPV-15-386	Quebrada del Salitre Formation	Basalt	471710	7201470	N.D.	N.D.	N.D.	N.D.	N.D.
CPV-15-410	La Ternera Formation	Andesite	429359	7000950	N.D.	N.D.	N.D.	N.D.	N.D.
RCM-61q	Colorado Syenogranite	Syenogranite	381620	6744026	N.D.	N.D.	N.D.	N.D.	N.D.
RCM-78q	Pastos Blancos Formation	Andesite	379914	6748141	N.D.	N.D.	N.D.	N.D.	N.D.
SCL-28q	Guanaco Sonso Formation	Rhyolitic tuff	423238	6807445	N.D.	N.D.	249,10	1,30	Ortiz and Merino 2015
MCM-010q	El León Monzogranites	Monzogranite	385798	6747866	N.D.	N.D.	252,30	1,90	Ortiz and Merino 2015
MCM-022q	Chollay Plutonic Complex	Syenogranite	396485	6760228	N.D.	N.D.	248,20	2,10	Ortiz and Merino 2015
MCM-129q	Chanchoquín Plutonic Complex	Quartz monzodiorite	368977	6772428	N.D.	N.D.	N.D.	N.D.	N.D.
MCM-159q	Guachicay Pluton	Tonalite	365695	6776725	N.D.	N.D.	303,60	1,80	Ortiz and Merino 2015
MCM-168 Bq	Quebrada Pinte Diorite	Diorite	375805	6786355	N.D.	N.D.	324,00	4,10	Ortiz and Merino 2015
MCM-205q	Guanta Plutonic Complex	Granodiorite	363509	6737985	N.D.	N.D.	291,30	1,30	Ortiz and Merino 2015
MCM-265q	Chollay Plutonic Complex	Monzogranite	388323	6790790	N.D.	N.D.	239,70	1,90	Ortiz and Merino 2015
MCM-280q	Guanta Plutonic Complex	Granodiorite	368652	6736827	N.D.	N.D.	300,90	1,00	Ortiz and Merino 2015
RCM-015q	Guanta Plutonic Complex	Syenogranite	358677	6736102	N.D.	N.D.	293,80	4,00	Ortiz and Merino 2015
RCM-040q	Chollay Plutonic Complex	Tonalite	406713	6788541	N.D.	N.D.	234,90	0,50	Ortiz and Merino 2015
RCM-077q	Chacaicito Pluton	Syenogranite	380434	6748991	N.D.	N.D.	329,00	2,60	Ortiz and Merino 2015
RCM-133q	Chanchoquín Plutonic Complex	Granodiorite	365378	6767843	N.D.	N.D.	293,20	1,10	Ortiz and Merino 2015
RCM-150q	Guanaco Sonso Formation	Rhyolitic tuff	412909	6787833	N.D.	N.D.	252,40	1,80	Ortiz and Merino 2015
SCL-96	Guanaco Sonso Formation	Dacitic tuff	425477	6807665	N.D.	N.D.	248,80	1,20	Ortiz and Merino 2015

Sample	**Age max (Ma)**	**±**	**Age min (Ma)**	**±**	**Reference**	**Preferred Age max (Ma)**	**±**	**Preferred Age min (Ma)**	**±**	**Reference(s)**	**Radiometric dating technique**	**Dated material**
CPV-12-23	221	2,6	210,4	2,9	Salazar et al. 2013	N.D.	N.D.	N.D.	N.D.	N.D.	U-Pb	Zircon
CPV-12-24	221	2,6	210,4	2,9	Salazar et al. 2013	N.D.	N.D.	N.D.	N.D.	N.D.	U-Pb	Zircon
CPV-12-38	252	0,1	237	0	Salazar et al. 2013	N.D.	N.D.	N.D.	N.D.	N.D.	Stratigraphic	N.D.

CPV-12-49b	252	0,1	237	0	Salazar et al. 2013	N.D.	N.D.	N.D.	N.D.	N.D.	Stratigraphic	N.D.
CPV-12-60	221	2,6	210,4	2,9	Salazar et al. 2013	N.D.	N.D.	N.D.	N.D.	N.D.	U-Pb	Zircon
CPV-12-91A	208	5	204,9	3,8	Arévalo and Welkner 2008	N.D.	N.D.	N.D.	N.D.	N.D.	Ar-Ar, U-Pb	Biotite, Zircon
CPV-12-91B	208	5	204,9	3,8	Arévalo and Welkner 2008	N.D.	N.D.	N.D.	N.D.	N.D.	Ar-Ar, U-Pb	Biotite, Zircon
CPV-12-92	203	5	199	3	Arévalo and Welkner 2008	N.D.	N.D.	N.D.	N.D.	N.D.	Ar-Ar, K-Ar	Biotite, Amphibole
CPV-12-93	206,2	0,6	202,1	3,6	Arévalo and Welkner 2008	N.D.	N.D.	N.D.	N.D.	N.D.	Ar-Ar, U-Pb	Biotite, Hornblende, Zircon
SCL-02q	N.D.	N.D.	N.D.	N.D.	N.D.	249,3	0,7	233,8	1	Álvarez et al. 2013; Salazar et al. 2013; Ortiz and Merino 2015; Salazar and Coloma 2016	U-Pb	Zircon
SCL-09q	N.D.	N.D.	N.D.	N.D.	N.D.	249,3	0,7	233,8	1	Álvarez et al. 2013; Salazar et al. 2013; Ortiz and Merino 2015; Salazar and Coloma 2016	U-Pb	Zircon
SCL-26q	221	2,6	210,4	2,9	Martin et al. 1999	N.D.	N.D.	N.D.	N.D.	N.D.	K-Ar, U-Pb	Biotite, Zircon
O7-06	N.D.	N.D.	N.D.	N.D.	N.D.	N.D.	N.D.	N.D.	N.D.	N.D.	U-Pb	Zircon
O7-07	N.D.	N.D.	N.D.	N.D.	N.D.	N.D.	N.D.	N.D.	N.D.	N.D.	U-Pb	Zircon
O7-10	218,0	N.D.	218,0	N.D.	N.D.	N.D.	N.D.	N.D.	N.D.	N.D.	U-Pb	Zircon
O7-11	N.D.	N.D.	N.D.	N.D.	N.D.	N.D.	N.D.	N.D.	N.D.	N.D.	U-Pb	Zircon
O7-13	N.D.	N.D.	N.D.	N.D.	N.D.	N.D.	N.D.	N.D.	N.D.	N.D.	U-Pb	Zircon
O7-15	N.D.	N.D.	N.D.	N.D.	N.D.	300,9	1	291,3	1	Ortiz and Merino 2015	U-Pb	Zircon
CPV-12-105	N.D.	N.D.	N.D.	N.D.	N.D.	N.D.	N.D.	N.D.	N.D.	N.D.	U-Pb	Zircon
CPV-12-12	N.D.	N.D.	N.D.	N.D.	N.D.	N.D.	N.D.	N.D.	N.D.	N.D.	U-Pb	Zircon
CPV-12-127	N.D.	N.D.	N.D.	N.D.	N.D.	N.D.	N.D.	N.D.	N.D.	N.D.	U-Pb	Zircon
CPV-12-01	N.D.	N.D.	N.D.	N.D.	N.D.	193	N.D.	191	N.D.	Creixell et al. 2012	N.D.	N.D.
CPV-12-03	N.D.	N.D.	N.D.	N.D.	N.D.	193	N.D.	191	N.D.	Creixell et al. 2012	N.D.	N.D.
CPV-12-26B	N.D.	N.D.	N.D.	N.D.	N.D.	154,3	1,9	135	2	Salazar 2012; Salazar et al. 2013; Rossel et al. 2013; Maksaev et al. 2014; Ortiz and Merino 2015	U-Pb	Zircon
CPV-12-28x	N.D.	N.D.	N.D.	N.D.	N.D.	154,3	1,9	135	2	Salazar 2012; Salazar et al. 2013; Rossel et al. 2013; Maksaev et al. 2014; Ortiz and Merino 2015	U-Pb	Zircon

CPV-12-30x	N.D.	N.D.	N.D.	N.D.	N.D.	154,3	1,9	135	2	Salazar 2012; Salazar et al. 2013; Rossel et al. 2013; Maksaev et al. 2014; Ortiz and Merino 2015	U-Pb	Zircon
CPV-12-90	N.D.	N.D.	N.D.	N.D.	N.D.	N.D.	N.D.	N.D.	N.D.	N.D.	U-Pb	Zircon
CPV-14-176	328,3	3,4	259	3,4	Hervé et al. 2012; Naranjo et al. 2013; Venegas et al. 2013; Maksaev et al. 2014; González et al. 2015	290	2	289	2	González et al. 2015	U-Pb	Zircon
CPV-14-180A	285	1	255	1	Contreras et al. 2013	284,8	6,6	256	2,5	Contreras et al. 2013	U-Pb	Zircon
CPV-14-181B	N.D.	N.D.	N.D.	N.D.	N.D.	N.D.	N.D.	N.D.	N.D.	N.D.	U-Pb	Zircon
CPV-14-182B	N.D.	N.D.	N.D.	N.D.	N.D.	N.D.	N.D.	N.D.	N.D.	N.D.	U-Pb	Zircon
CPV-14-184	N.D.	N.D.	N.D.	N.D.	N.D.	N.D.	N.D.	N.D.	N.D.	N.D.	U-Pb	Zircon
CPV-14-187	N.D.	N.D.	N.D.	N.D.	N.D.	N.D.	N.D.	N.D.	N.D.	N.D.	U-Pb	Zircon
CPV-14-190	N.D.	N.D.	N.D.	N.D.	N.D.	N.D.	N.D.	N.D.	N.D.	N.D.	U-Pb	Zircon
CPV-14-191	265	N.D.	250	N.D.	N.D.	284,8	6,6	256	2,5	Contreras et al. 2013	U-Pb	Zircon
CPV-14-192	276,6	N.D.	265,5	N.D.	N.D.	276,6	3,6	269,5	4	Maksaev et al. 2014	U-Pb	Zircon
CPV-14-194	237	N.D.	201	N.D.	N.D.	N.D.	N.D.	N.D.	N.D.	N.D.	U-Pb	Zircon
CPV-14-198	237	N.D.	201	N.D.	N.D.	N.D.	N.D.	N.D.	N.D.	N.D.	U-Pb	Zircon
CPV-14-245	N.D.	N.D.	N.D.	N.D.	N.D.	214,2	2	212,8	2	Venegas et al. 2013	U-Pb	Zircon
CPV-14-247	N.D.	N.D.	N.D.	N.D.	N.D.	214,2	2	212,8	2	Venegas et al. 2014	U-Pb	Zircon
CPV-14-249	307	N.D.	277	N.D.	Cornejo et al. 2009; Venegas et al. 2013; Astudillo et al. 2017	326	3	259	3,4	Hervé et al. 2012; Naranjo et al. 2013; Venegas et al. 2013; Maksaev et al. 2014; González et al. 2015	U-Pb	Zircon
CPV-14-253	N.D.	N.D.	N.D.	N.D.	N.D.	214,2	2	212,8	2	Venegas et al. 2014	U-Pb	Zircon
CPV-14-256	N.D.	N.D.	N.D.	N.D.	N.D.	214,2	2	212,8	2	Venegas et al. 2014	U-Pb	Zircon
CPV-14-263	328,3	3,4	259	3,4	Astudillo et al. 2015	N.D.	N.D.	N.D.	N.D.	N.D.	U-Pb	Zircon
CPV-15-271	237	N.D.	201	N.D.	N.D.	237	0	199,6	0,3	Peña et al. 2013	Stratigraphic	N.D.
CPV-15-274	237	N.D.	201	N.D.	N.D.	237	0	199,6	0,3	Peña et al. 2013	Stratigraphic	N.D.
CPV-15-278	237	N.D.	201	N.D.	N.D.	237	0	199,6	0,3	Peña et al. 2013	Stratigraphic	N.D.
CPV-15-279	237	N.D.	201	N.D.	N.D.	237	0	199,6	0,3	Peña et al. 2013	Stratigraphic	N.D.
CPV-15-280	237	N.D.	201	N.D.	N.D.	237	0	199,6	0,3	Peña et al. 2013	Stratigraphic	N.D.
CPV-15-281	237	N.D.	201	N.D.	N.D.	237	0	199,6	0,3	Peña et al. 2013	Stratigraphic	N.D.

CPV-15-284	237	N.D.	201	N.D.	N.D.	237	0	199,6	0,3	Peña et al. 2013	Stratigraphic	N.D.
CPV-15-285	237	N.D.	201	N.D.	N.D.	237	0	199,6	0,3	Peña et al. 2013	Stratigraphic	N.D.
CPV-15-287	237	N.D.	201	N.D.	N.D.	237	0	199,6	0,3	Peña et al. 2013	Stratigraphic	N.D.
CPV-15-303	232,9	0,2	212,1	1,7	Cornejo et al. 2009; Venegas et al. 2013; this work	N.D.	N.D.	N.D.	N.D.	N.D.	U-Pb	Zircon
CPV-15-310	232,9	0,2	212,1	1,7	Cornejo et al. 2009; Venegas et al. 2013; this work	N.D.	N.D.	N.D.	N.D.	N.D.	U-Pb	Zircon
CPV-15-311	232,9	0,2	212,1	1,7	Cornejo et al. 2009; Venegas et al. 2013; this work	N.D.	N.D.	N.D.	N.D.	N.D.	U-Pb	Zircon
CPV-15-312	232,9	0,2	212,1	1,7	Cornejo et al. 2009; Venegas et al. 2013; this work	N.D.	N.D.	N.D.	N.D.	N.D.	U-Pb	Zircon
CPV-15-314	232,9	0,2	212,1	1,7	Cornejo et al. 2009; Venegas et al. 2013; this work	N.D.	N.D.	N.D.	N.D.	N.D.	U-Pb	Zircon
CPV-15-319	232,9	0,2	212,1	1,7	Cornejo et al. 2009; Venegas et al. 2013; this work	N.D.	N.D.	N.D.	N.D.	N.D.	U-Pb	Zircon
CPV-15-320	262,6	6,4	259	6	Cornejo and Mpodozis 1996	N.D.	N.D.	N.D.	N.D.	N.D.	K-Ar	Hornblende
CPV-15-322	N.D.	N.D.	N.D.	N.D.	N.D.	232,9	0,2	212,1	1,7	Cornejo et al. 2009; Venegas et al. 2013	U-Pb	Zircon
CPV-15-330	N.D.	N.D.	N.D.	N.D.	N.D.	214,2	2	212,8	2	Venegas et al. 2013	U-Pb	Zircon
CPV-15-332	N.D.	N.D.	N.D.	N.D.	N.D.	214,2	2	212,8	2	Venegas et al. 2013	U-Pb	Zircon
CPV-15-337	N.D.	N.D.	N.D.	N.D.	N.D.	214,2	2	212,8	2	Venegas et al. 2013	U-Pb	Zircon
CPV-15-353	328,3	3,4	259	3,4	Hervé et al. 2012; Naranjo et al. 2013; Venegas et al. 2013; Maksaev et al. 2014; González et al. 2015	326	3	259	3,4	Hervé et al. 2012; Naranjo et al. 2013; Venegas et al. 2013; Maksaev et al. 2014; González et al. 2015	U-Pb	Zircon
CPV-15-359	N.D.	N.D.	N.D.	N.D.	N.D.	214,2	2	212,8	2	Venegas et al. 2013	U-Pb	Zircon
CPV-15-365	323,9	2,6	277	0	Marinovic et al. 1995; Venegas et al. 2013	295,6	2,6	289,8	0,9	Marinovic et al. 1995; Venegas et al. 2013	Ar-Ar, U-Pb	Biotite, Zircon
CPV-15-386	N.D.	N.D.	N.D.	N.D.	N.D.	214,2	2	212,8	2	Venegas et al. 2013	U-Pb	Zircon
CPV-15-410	237	N.D.	201	N.D.	N.D.	237	N.D.	199,6	5	Peña et al. 2013	Stratigraphic	N.D.
RCM-61q	235	5	210	1	Martin et al. 1999	229,6	2,6	214,6	2,6	Maksaev et al. 2014; Ortiz and Merino 2015; Salazar and Coloma 2016	K-Ar, U-Pb	Biotite, Zircon
RCM-78q	235	5	210	1	Martin et al. 1999	231,7	1,3	216,1	2	Maksaev et al. 2014; Ortiz	K-Ar, U-Pb	Biotite, Zircon

										and Merino 2015		
SCL-28q	N.D.	N.D.	N.D.	N.D.	N.D.	253,9	2,8	240,6	4	Ortiz and Merino 2015; Sazalar and Coloma 2016	U-Pb	Zircon
MCM-010q	248	N.D.	237	N.D.	Ortiz and Merino 2015	252,3	1,9	239,5	2	Ortiz and Merino 2015; Murillo et al. in prep	U-Pb	Zircon
MCM-022q	248	N.D.	237	N.D.	Ortiz and Merino 2015	249,3	0,7	233,8	1	Álvarez et al. 2013; Salazar et al. 2013; Ortiz and Merino 2015; Salazar and Coloma 2016	U-Pb	Zircon
MCM-129q	297	N.D.	285	N.D.	Ortiz and Merino 2015	296,1	4,8	285,7	2	Pankhurst et al. 1996; Salazar et al. 2013; Maksaev et al. 2014; Ortiz and Merino 2015	U-Pb	Zircon
MCM-159q	315	N.D.	303	N.D.	Ortiz and Merino 2015	315,7	2,3	303,6	18	Maksaev et al. 2014; Ortiz and Merino 2015; Salazar and Coloma 2016	U-Pb	Zircon
MCM-168 Bq	329	N.D.	324	N.D.	Ortiz and Merino 2015	327	N.D.	315,1	2,2	Murillo et al. 2013; Salazar et al. 2013; Ortiz and Merino 2015	U-Pb	Zircon
MCM-205q	301	N.D.	291	N.D.	Ortiz and Merino 2015	300,9	1	291,3	1	Ortiz and Merino 2015	Ar-Ar	Amphibole
MCM-265q	248	N.D.	237	N.D.	Ortiz and Merino 2015	249,3	0,7	233,8	1	Álvarez et al. 2013; Salazar et al. 2013; Ortiz and Merino 2015; Salazar and Coloma 2016	U-Pb	Zircon
MCM-280q	301	N.D.	291	N.D.	Ortiz and Merino 2015	300,9	1	291,3	1	Ortiz and Merino 2015	U-Pb	Zircon
RCM-015q	301	N.D.	291	N.D.	Ortiz and Merino 2015	300,9	1	291,3	1	Ortiz and Merino 2015	U-Pb	Zircon
RCM-040q	248	N.D.	237	N.D.	Ortiz and Merino 2015	249,3	0,7	233,8	1	Álvarez et al. 2013; Salazar et al. 2013; Ortiz and Merino 2015; Salazar and Coloma 2016	Ar-Ar	Biotite
RCM-077q	329	N.D.	324	N.D.	Ortiz and Merino 2015	329	2,6	324	4,1	Ortiz and Merino 2015	U-Pb	Zircon
RCM-133q	297	N.D.	285	N.D.	Ortiz and Merino 2015	296,1	4,8	285,7	2	Pankhurst et al. 1996; Salazar et al. 2013; Maksaev et al. 2014; Ortiz and Merino 2015	Ar-Ar	Amphibole
RCM-150q	265	N.D.	240	N.D.	Ortiz and Merino 2015	253,9	2,8	240,6	4	Ortiz and Merino 2015;	U-Pb	Zircon

										Sazalar and Coloma 2016		
SCL-96	N.D.	N.D.	N.D.	N.D.	N.D.	253,9	2,8	240,6	4	Ortiz and Merino 2015; Sazalar and Coloma 2016	U-Pb	Zircon

Álvarez, J., Mpodozis, C., Blanco-Quintero, I., García-Casco, A., Arriagada, C., Morata, D., 2013. U-Pb ages and metamorphic evolution of the La Pampa Gneisses: Implications for the evolution of the Chilenia Terrane and Permo-Triassic tectonics of north Central Chile. J. South Am. Earth Sci. 47, 100–115. doi:10.1016/j.jsames.2013.07.001

Arévalo, C.; Welkner, D. 2008. Geología del Área Carrizal Bajo-Chacritas, Región de Atacama. Servicio Nacional de Geología y Minería, Carta Geológica de Chile, Serie Geología Básica 111: 67 p.,

Astudillo, N., Ferrando, R., Montecinos, D., Espinoza, F:, Venegas, C., Matthews, S., Cornejo, P., Arévalo, C., 2017. Carta Augusta Victoria, Región de Antofagasta. Servicio Nacional de Geología y Minería, Carta Geológica de Chile, Serie Geología Básica, 189, 95 p.

Bahlburg, H., Vervoort, J.D., Du Frane, S.A., Bock, B., Augustsson, C., Reimann, C., 2009. Timing of crust formation and recycling in accretionary orogens: Insights learned from the western margin of South America. Earth-Science Rev. 97, 215–241. doi:10.1016/j.earscirev.2009.10.006

Contreras, J.C:, Espinoza, M., De La Cruz, R., Jorquera, R., Kraus, S., Ramírez, C., Naranjo, J.A., Escribano, J., Martínez, P., 2013. Carta Cifuncho, Regiones de Antofagasta y Atacama. Servicio Nacional de Geología y Minería, Carta Geológica de Chile, Serie Geología Básica, 161, 69 p.

Cornejo et al. 2009

Cornejo, P., Mpodozis, C., 1996. Geología de la Región de Sierra Exploradora (25-26 Lat. S). Servicio Nacional de Geología y Minería

Creixell, C., Ortiz, M., Arévalo, C., 2012. Geología del área Carrizalillo–El Tofo, Regiones de Atacama y Coquimbo. Servicio Nacional de Geología y Minería, Carta Geológica de Chile, Serie Geología Básica Nos. 133-134.

Creixell, C., Oliveros, V., Vásquez, P., Navarro, J., Vallejos, D., Valin, X., Godoy, E., N. Ducea, M., 2016. Geodynamics of Late Carboniferous–Early Permian forearc in north Chile (28°30′–29°30′S). J. Geol. Soc. London. 173

Espinoza, M.; Oliveros, V.; Vásquez, P.; Bechis, F. 2015 U-Pb geochronology and kinematic preliminary analyses of Late Triassic- Early Jurassic basins in northern Chile (24.5° -26°S). XIV Congreso Geologico Chileno, La Serena, Abstracts, 1, 840-843.

González, R., Wilke, G.-H., Riquelme, R., Menzies, A., Espinoza, F., Herrera, C., 2015. Carta Sierra de Varas, Región de Antofagasta. Servicio Nacional de Geología y Minería, Carta Geológica de Chile, Serie Geología Básica, 178, 81 p.

Hervé, F., Fanning, C.M., Calderón, M., Mpodozis, C., 2014. Early Permian to Late Triassic batholiths of the Chilean Frontal Cordillera (28°-31°S): SHRIMP U-Pb zircon ages and Lu-Hf and O isotope systematics. Lithos 184–187, 436–446. doi:10.1016/j.lithos.2013.10.018

Maksaev, V., Munizaga, F., Tassinari, C., 2014. Temporalidad del magmatismo del borde paleo-Pacífico de Gondwana: Geocronología U-Pb de rocas ígneas del Paleozoico tardío a Mesozoico temprano de los Andes del norte de Chile entre los 20o y 31oS, Andean Geology. doi:10.5027/andgeoV41n3-a01

Marinovic, N., Smoje, I., Hervé, M., Mpodozis, C., 1995. Hoja Aguas Blancas. Servicio Nacional de Geología y Minería. Carta Geológica de Chile, Serie Geología Básica, 70, 150 p.

Martin, M.W., Kato, T.T., Rodriguez, C., Godoy, E., Duhart, P., McDonough, M., Campos, A., 1999. Evolution of the late Paleozoic accretionary complex and overlying forearc-magmatic arc, south central Chile (38°–41°S): Constraints for the tectonic setting along the southwestern margin of Gondwana. Tectonics 18, 582. doi:10.1029/1999TC900021

Murillo, I., Velásquez, R., Creixell, C., 2017. Geología de las áreas Guanta–Los Cuartitos y Paso de Vacas Heladas, regiones de Atacama y Coquimbo. Servicio Nacional de Geología y Minería, Carta Geológica de Chile, Serie Geología Básica, 192-193, 96 p.

Naranjo, J.A., Villa, V., Venegas, C., 2013. Geología de las áreas Salar de Aguilar y Portezuelo de León Muerto, Región de Atacama. Servicio Nacional de Geología y Minería, Carta Geológica de Chile, Serie Geología Básica, 151-152, 96 p.

Ortiz, M., Merino, R.N., 2015. Geología de las áreas Río-Chollay y Matancillas y Cajón del Encierro, Regiones de Atacama y Coquimbo. Servicio Nacional de Geología y Minería, Carta Geológica de Cile, Serie Geología Básica 175-176.

Pankhurst, R., Millar, I., Hervé, F., 1996. A Permo-Carboniferous U-Pb age for part of the Guanta Unit of the Elqui-Limari Batholith at Rio del Transito, Northern Chile. Rev. Geol. Chile 23, 35–42

Peña, M., Becerra, J., Martínez, F., Arriagada, C., 2013. Geología del Área Yerbas Buenas-Tres Morros, Región de Atacama. Servicio Nacional de Geología y Minería, Carta Geológica de Chile, Serie Geología Básica 155. Servicio Nacional de Geología y Minería, Santiago.

Rossel, P., Oliveros, V., Ducea, M.N., Charrier, R., Scaillet, S., Retamal, L., Figueroa, O., 2013. The Early Andean subduction system as an analog to island arcs: Evidence from across-arc geochemical variations in northern Chile. Lithos 179, 211–230.

Salazar, E., Coloma, F., Creixell, C., 2013. Geología del Área El Tránsito-Lagunillas, Servicio Nacional de Geología y Minería-Gobierno Regional de Atacama. 1 Mapa escala 1:100.000. Santiago 1–113.

Salazar, E., Coloma, F., 2016. Geología del área Cerros de Cantaritos-Laguna Chica, Región de Atacama. Servicio Nacional de Geología y Minería, Carta Geológica de Chile, Serie Geología Básica 181. doi:10.13140/RG.2.2.30000.56327

Venegas, C., Cervetto, M., Astudillo, N., Espinoza, F., Cornejo, P., Mpodozis, C., Rivera, O., 2013. Carta Sierra Vaquillas Altas, Regiones de Antofagasta y Atacama. Servicio Nacional de Geología y Minería, Carta Geológica de Chile, Serie Geología Básica, 159, 86 p.

Supplementary Material 2.3. Elemental and isotopic composition and age data for Carboniferous to Upper Jurassic rocks cropping out in the Chilean and Argentinean Andes between 18ºS and 40ºS. Age data is reported following the same criteria as in Supplementary Material 2.2. References at the bottom of the table. Negative figures indicate element concentrations below the detection limit, with the absolute value as the half of the respective detection limit.

Ver apéndice digital

Supplementary Material 2.4. Discrimination diagrams of Whalen and Hildebrand (2019) for slab failure and A-type granites. Symbols and colours as in Figure 2.5.

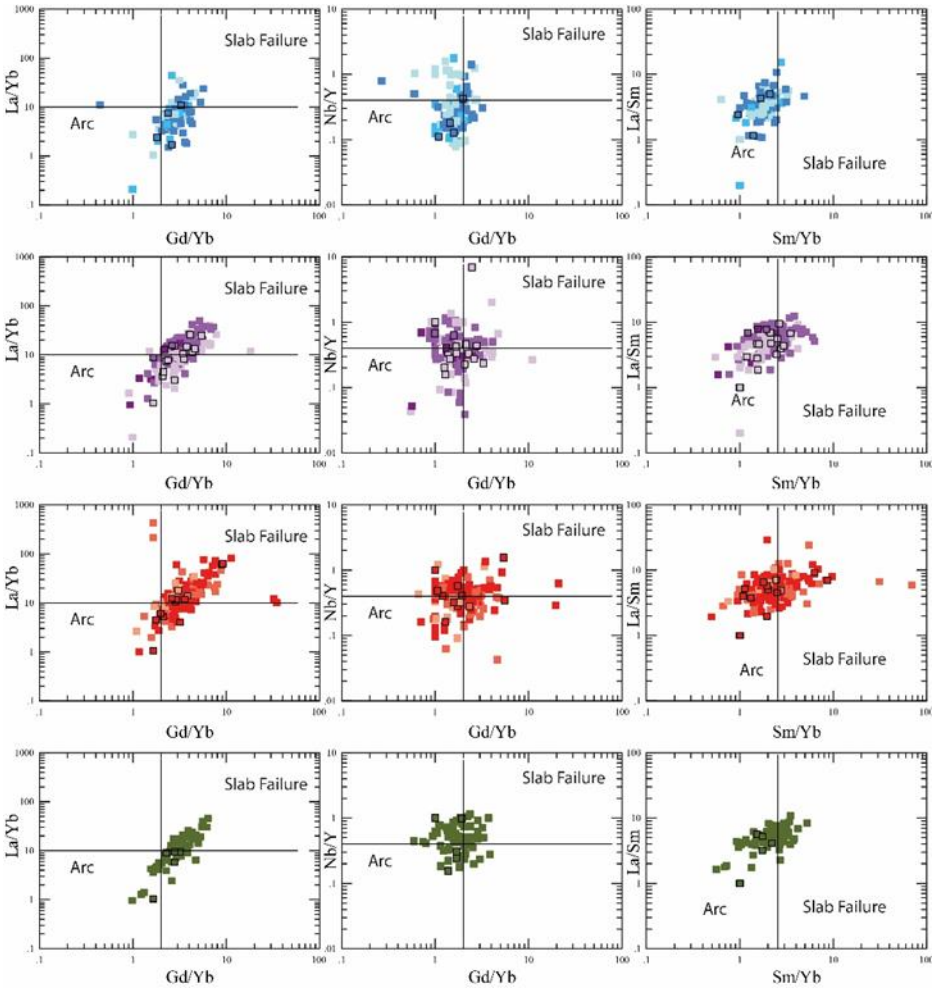

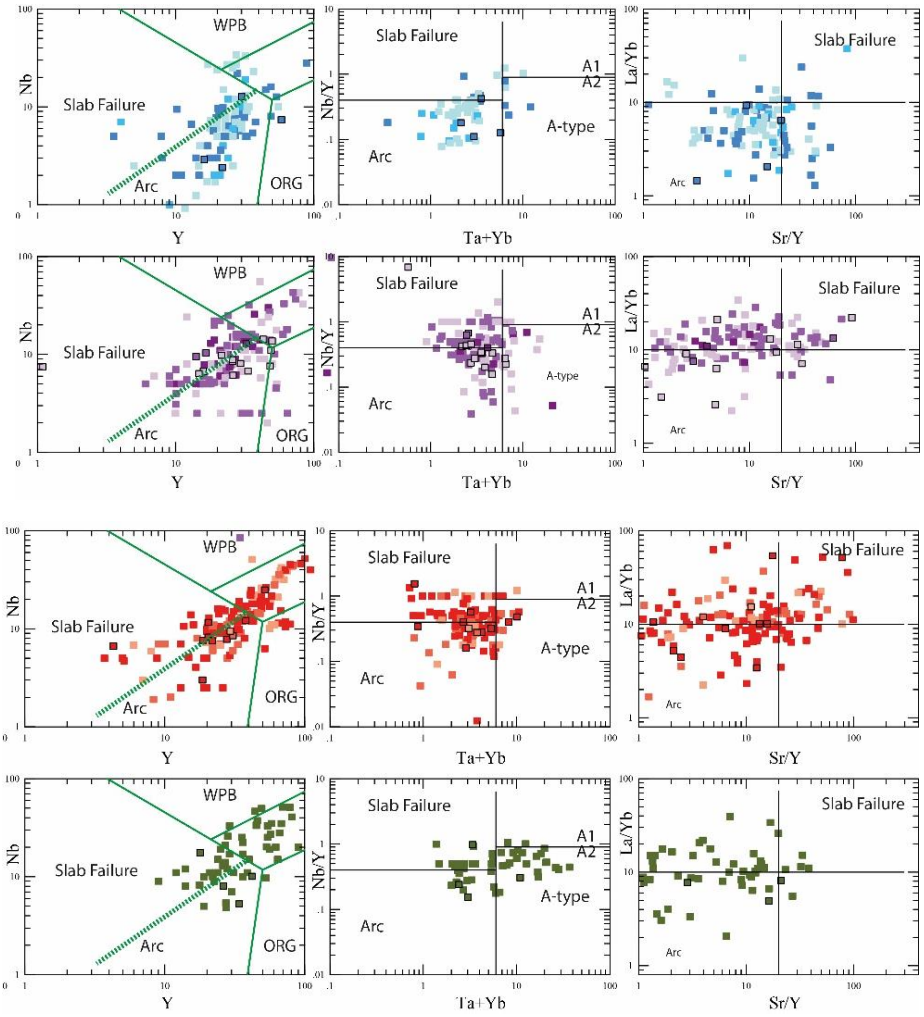
WPB
Slab Failure
Arc
ORG
Nb
Y
Slab Failure
A1
A2
A-type
Arc
Nb/Y
Ta+Yb
Slab Failure
Arc
La/Yb
Sr/Y

Apéndice Capítulo III

Appendix A. Analytical Methods.

Twenty-seven samples from CPC were collected for petrographic studies and nineteen were selected for whole-rock chemical (major and trace element) and isotopic composition (Sr-Nd-Pb). Thirty-three samples from CPC and eighteen samples from the Piuquenes Plutonic Complex (PPC) were collected by the SERNAGEOMIN during field mapping of the studied area (Murillo et al., 2017; Ortiz & Merino, 2015; Salazar et al., 2013; Salazar & Coloma, 2016; Velásquez et al., 2021) for petrographic analysis. The SERNAGEOMIN granted authorization to characterize petrographically these thin sections and facilitated part of sixteen samples to carry out whole rock isotopic analyses (Sr-Nd-Pb). The thin sections were studied under polarized-light microscope to characterize its mineralogy, texture and alteration degree. The modal classification was done using point count (~ 1300 – 2300 points per sample)..

Major and trace elements

Nineteen samples from CPC were selected to perform the whole-rock chemical analyses, including diorites (2), tonalites (2), granodiorites (4), granites (4), mafic enclaves (4) and dikes (3). They were crushed under 5 mm fraction and only fresh fragments were handpicked using binocular lens. These fragments were powdered below 50 µm, and 5 g of each sample were mixed with a flux of lithium metaborate and lithium tetraborate and fused in an induction furnace. The molten was poured into a solution of 5% nitric acid and mixed until completely dissolved. The samples were run on a combination simultaneous/sequential Varian Vista 735 ICP-OES and on a Perkin Elmer Sciex ELAN 6100 ICP-MS, for major and trace elements, respectively, at Actlabs, Ontario, Canada. In addition, to obtain the Pb concentrations in the samples, 0.25 g of each powdered sample were digested with hydrofluoric, nitric, perchloric and hydrofluoric acids. This solution was heated in several cycles until dried and then brought back into solution using hydrochloric and nitric acids. Digested samples were diluted and analysed by Perkin Elmer Sciex ELAN 9000 ICP-MS, in the aforementioned laboratory.

Whole-rock Sr, Nd and Pb isotopes

The nineteen samples subjected to major and trace elements analysis, were also selected for whole-rock isotopic analysis, along with twenty-three samples from those provided by the Chilean Geology and Mining Survey. Approximately 100 mg of pulverized sample were dissolved in a mixture of triple distilled hydrofluoric and nitric acid mixed in 5:1 proportion. The solution was dried and re-dissolved in 1000 µl of 2 m HNO3 for chemical separation. Strontium and lead were simultaneously isolated from the other elements using miniaturized columns with ~ 70 µl of Sr- and Pb-specific resin (Sr.spec 50 – 100 µm), following the procedure developed by Deniel & Pin (2001) adapted to smaller resin volumes. From the Sr elute, light rare earth elements (REE) were isolated using TRU.Spec (50 – 100 µm) resin, followed by Sm and Nd collection through LN.Spec (50 – 100 µm) resin. The setup of the LREE and Sm-Nd separation columns procedure, were adapted from Pin & Zalduegui (1997) and Míková & Denková

(2007). Total procedure blanks of Sr, Nd, and Pb were < 180 pg, < 80 pg and < 40 pg respectively, being insignificant in relation to the amount of material used in the analyses and hence, no blank corrections have been applied to analysed ratios.

The strontium concentrate was loaded on rhenium single filament with Ta-oxide emitter and 0.1 m phosphoric acid; and neodymium concentrate, on rhenium double filament with 0.1 phosphoric acid. The $^{87}Sr/^{86}Sr$ and $^{143}Nd/^{144}Nd$ ratios were measured through thermal ionization mass spectrometry (TIMS) on a Triton plus instrument (Thermo Scientific) in dynamic multi-collection mode, at the Isotope Geochemistry Laboratory of MARUM, University of Bremen. Instrumental mass fractionation of Sr and Nd isotope ratios were normalized to $^{86}Sr/^{88}Sr$ of 0.1194 and $^{146}Nd/^{144}Nd$ of 0.7219, respectively. The lead concentrate was loaded on rhenium single filament with silica emitter and 0.1 m phosphoric acid, and its isotopic ratios were measured at pyrometer-controlled temperature of ~ 1250°C in static multi-collection mode. Instrumental mass-fractionation of Pb was corrected using 0.1% per atomic mass unit.

Mineral composition

After petrographically characterizing the samples of Chollay Plutonic Complex (n=60), only three samples of different lithologies (quartz diorite, granodiorite and monzogranite) were selected for microprobe analyses, to estimate the crystallization pressure and temperature conditions. Polished thin sections of these samples were prepared at the Institute of Applied Economic Geology of the University of Concepción and covered with a 25 nm thick carbon layer. Backscattered electron images were used to select contiguous and free of alteration amphibole and plagioclase crystals. Major and minor elements were measured, at the same institution, using a JEOL JXA8600M electron microprobe provided with five wavelength dispersive spectrometers. Analyses were performed using a 15 kV accelerating voltage, a 20 nA beam current focused to a 5 µm spot and peak/background count times of 20-30/10-15 seconds. Accuracy of the analyzed major elements was ≤ 1.0% and ≤ 5 % for minor elements. Natural minerals and synthetic oxides were used as standards; those with USNM code were donated by the Smithsonian Institution, USA (Jarosewich et al., 1980): USNM diopside 117733 (Si, in amphiboles), USNM 137041 anorthite (Al), fayalite USNM 85276 (Fe), microcline USNM 143966 (K), chromite USNM 117075 (Cr), MnTiO3 (Ti), rhodonite (Mn), forsterite (Mg), jadeite (Na), wollastonite (Ca), sanidine (Si, plagioclase) and tugtupite (Cl). Data reduction was performed using the ZAF correction method.

References

Jarosewich, E., Nelen, J. A., & Norbers, J. A. (1980). Reference Samples for Electron Microprobe Analysis. Geostandards Newsletter, 4(1), 43–47.

Míková, J., & Denková, P. (2007). Modified chromatographic separation scheme for Sr and Nd isotope analysis in geological silicate samples. Journal of Geosciences, 52(3–4), 221–226. https://doi.org/10.3190/jgeosci.015

Murillo, I., Velásquez, R., & Creixell, C. (2017). Geología de las áreas Guanta - Los Cuartitos y Paso de Vacas Heladas, Regiones de Atacama y Coquimbo. Servicio Nacional de Geología y Minería. Carta Geológica de Chile. Serie Geología Básica N°192-193. Escala 1:100.000.

Ortiz, M., & Merino, R. (2015). Geología de las áreas Río Chollay - Matancilla y Cajón del Encierro, Regiones de Atacama y Coquimbo. Servicio Nacional de Geología y Minería. Carta Geológica de Chile. Serie Geología Básica N°175-176. Escala 1:100.000.

Pin, C., & Zalduegui, J. F. S. (1997). Sequential separation of light rare-earth elements, thorium and uranium by miniaturized extraction chromatography: Application to isotopic analyses of silicate rocks. Analytica Chimica Acta, 339, 79–89.

Salazar, E., & Coloma, F. (2016). Geología del área Cerros de Cantaritos-Laguna Chica, Región de Atacama. Servicio Nacional de Geología y Minería. Carta Geológica de Chile. Serie Geología Básica N°181. Escala 1:100.000.

Salazar, E., Coloma, F., & Creixell, C. (2013). Geología del área El Tránsito-Lagunillas, Región de Atacama. Servicio Nacional de Geología y Minería. Carta Geológica de Chile. Serie Geología Básica N°149. Escala 1:100.000.

Velásquez, R., Coloma, F., Murillo, I., Merino, R., & Ortiz, M. (2021). Geología de las áreas Pisco Elqui y Paso del Agua Negra. Servicio Nacional de Geología y Minería. Carta Geológica de Chile. Serie Geología Básica N°211-212. Escala 1:100.000.

Appendix B. Results of microprobe analyses on amphiboles (Table S2) and plagioclases (Table S1) of Chollay Plutonic Complex samples. The wt% of the major elements of plagioclase and amphibole, the recalculation of the atom per formula unit and the classification of each of the specimens are presented.

Table S2. Amphibole

Sample	CCL-65										
Zone	2	2	5	5	5	9	9	10	13	13	13
Spot	1.B	2	7	8.B	9	14	15	17	20	21.B	24
Classification	Mg-Fe-Hbl	Mg-Fe-Hbl	Mg-Fe-Hbl	Mg-Fe-Hbl	Mg-Fe-Hbl	Mg-Fe-Hbl	Mg-Fe-Hbl	Mg-Fe-Hbl	Mg-Fe-Hbl	Mg-Fe-Hbl	Mg-Fe-Hbl
Analysis (wt%)											
SiO2	47,570	48,850	49,760	48,270	48,360	49,460	46,320	48,420	48,110	49,510	48,840
TiO2	1,183	0,946	0,742	1,038	0,976	0,930	1,330	1,030	1,130	0,848	0,941
Al2O3	6,080	5,070	4,460	5,410	5,630	4,870	6,920	5,440	6,050	5,200	5,310
MnO	0,786	0,847	0,883	0,923	0,927	0,908	0,914	0,796	0,819	0,893	0,920
FeO	14,480	13,570	13,950	14,420	14,640	13,910	15,660	13,740	14,180	13,790	14,120
MgO	13,530	14,230	14,790	13,640	13,600	14,050	12,420	14,250	13,780	14,280	13,860
CaO	11,390	11,650	11,520	11,670	11,440	11,330	11,320	11,250	11,340	11,600	11,520
Na2O	1,270	0,968	0,881	1,083	0,951	0,903	1,301	1,301	1,103	0,882	0,951
K2O	0,577	0,448	0,390	0,492	0,501	0,432	0,667	0,367	0,554	0,448	0,468
Cl	0,167	0,103	0,065	0,111		0,092	0,161	0,134	0,126	0,070	0,113
O=F,Cl (calculated)	-0,04	-0,02	-0,010	-0,030	0	-0,020	-0,040	-0,030	-0,030	-0,020	-0,030
FeO calculated	11,642	10,815	9,877	11,594	11,141	11,142	12,544	10,731	11,089	10,784	11,211
Fe2O3 calculated	3,154	3,061	4,527	3,141	3,889	3,076	3,463	3,344	3,435	3,341	3,233
H2O+ calculated	2,000	2,030	2,050	2,020	2,050	2,040	1,990	2,020	2,020	2,040	2,020

Total	99,310	98,999	99,935	99,362	99,466	99,212	99,309	99,052	99,526	99,875	99,357
Formula Assignments											
T (ideally 8 apfu)											
Si	7,031	7,192	7,237	7,122	7,111	7,259	6,901	7,129	7,067	7,212	7,177
P	0,000	0,000	0,000	0,000	0,000	0,000	0,000	0,000	0,000	0,000	0,000
Be	0,000	0,000	0,000	0,000	0,000	0,000	0,000	0,000	0,000	0,000	0,000
Al	0,969	0,808	0,763	0,878	0,889	0,741	1,099	0,871	0,933	0,788	0,823
Ti	0,000	0,000	0,000	0,000	0,000	0,000	0,000	0,000	0,000	0,000	0,000
Fe3+	0,000	0,000	0,000	0,000	0,000	0,000	0,000	0,000	0,000	0,000	0,000
T subtotal	8,000	8,000	8,000	8,000	8,000	8,000	8,000	8,000	8,000	8,000	8,000
C (ideally 5 apfu)											
Ti	0,132	0,105	0,081	0,115	0,108	0,103	0,149	0,114	0,125	0,093	0,104
Zr	0,000	0,000	0,000	0,000	0,000	0,000	0,000	0,000	0,000	0,000	0,000
Al	0,090	0,072	0,002	0,062	0,087	0,101	0,116	0,073	0,114	0,105	0,097
Sc	0,000	0,000	0,000	0,000	0,000	0,000	0,000	0,000	0,000	0,000	0,000
V	0,000	0,000	0,000	0,000	0,000	0,000	0,000	0,000	0,000	0,000	0,000
Cr	0,000	0,000	0,000	0,000	0,000	0,000	0,000	0,000	0,000	0,000	0,000
Mn3+	0,000	0,000	0,000	0,000	0,000	0,000	0,000	0,000	0,000	0,000	0,000
Fe3+	0,351	0,340	0,495	0,348	0,430	0,340	0,388	0,370	0,380	0,367	0,357
Co	0,000	0,000	0,000	0,000	0,000	0,000	0,000	0,000	0,000	0,000	0,000
Ni	0,000	0,000	0,000	0,000	0,000	0,000	0,000	0,000	0,000	0,000	0,000
Zn	0,000	0,000	0,000	0,000	0,000	0,000	0,000	0,000	0,000	0,000	0,000
Mn2+	0,007	0,030	0,013	0,043	0,023	0,015	0,025	0,000	0,001	0,022	0,027
Fe2+	1,439	1,331	1,202	1,431	1,370	1,368	1,564	1,316	1,362	1,313	1,378
Mg	2,981	3,123	3,207	3,000	2,981	3,074	2,759	3,128	3,018	3,101	3,036
Li	0,000	0,000	0,000	0,000	0,000	0,000	0,000	0,000	0,000	0,000	0,000
C subtotal	5,000	5,001	5,000	4,999	4,999	5,001	5,001	5,001	5,000	5,001	4,999
B (ideally 2 apfu)											
Mn2+	0,092	0,076	0,096	0,072	0,092	0,097	0,090	0,099	0,101	0,089	0,087
Fe2+	0,000	0,000	0,000	0,000	0,000	0,000	0,000	0,006	0,000	0,000	0,000
Mg	0,000	0,000	0,000	0,000	0,000	0,000	0,000	0,000	0,000	0,000	0,000
Li	0,000	0,000	0,000	0,000	0,000	0,000	0,000	0,000	0,000	0,000	0,000
Ca	1,804	1,838	1,795	1,845	1,802	1,782	1,807	1,775	1,785	1,810	1,814
Sr	0,000	0,000	0,000	0,000	0,000	0,000	0,000	0,000	0,000	0,000	0,000
Na	0,104	0,086	0,109	0,083	0,105	0,121	0,103	0,120	0,114	0,101	0,099
B subtotal	2,000	2,000	2,000	2,000	1,999	2,000	2,000	2,000	2,000	2,000	2,000
A (from 0 to 1 apfu)											
Ca	0,000	0,000	0,000	0,000	0,000	0,000	0,000	0,000	0,000	0,000	0,000
Li	0,000	0,000	0,000	0,000	0,000	0,000	0,000	0,000	0,000	0,000	0,000
Na	0,260	0,190	0,139	0,227	0,166	0,136	0,273	0,251	0,200	0,148	0,172
Pb	0,000	0,000	0,000	0,000	0,000	0,000	0,000	0,000	0,000	0,000	0,000
K	0,109	0,084	0,072	0,093	0,094	0,081	0,127	0,069	0,104	0,083	0,088
A subtotal	0,369	0,274	0,211	0,320	0,260	0,217	0,400	0,320	0,304	0,231	0,260
O (non-W)											
O	22,000	22,000	22,000	22,000	22,000	22,000	22,000	22,000	22,000	22,000	22,000
W (ideally 2 apfu)											
OH	1,958	1,974	1,984	1,972	2,000	1,977	1,959	1,967	1,969	1,983	1,972
F	0,000	0,000	0,000	0,000	0,000	0,000	0,000	0,000	0,000	0,000	0,000
Cl	0,042	0,026	0,016	0,028	0,000	0,023	0,041	0,033	0,031	0,017	0,028
O	0,000	0,000	0,000	0,000	0,000	0,000	0,000	0,000	0,000	0,000	0,000
W subtotal	2,000	2,000	2,000	2,000	2,000	2,000	2,000	2,000	2,000	2,000	2,000
Sum T,C,B,A	15,369	15,275	15,211	15,319	15,258	15,218	15,401	15,321	15,304	15,232	15,259

Sample	CT-193											
Zone	4	4	4	4	2	2	2	2	2	5	5	5

Spot	1	2	3	7	8	9	10	11	12	13	15	17
Classification	Mg-Fe-Hbl	Mg-Hst	Mg-Fe-Hbl	Mg-Fe-Hbl	Mg-Fe-Hbl	Act	Mg-Fe-Hbl	Mg-Fe-Hbl	Mg-Fe-Hbl	Mg-Fe-Hbl	Mg-Fe-Hbl	Mg-Fe-Hbl
Analysis (wt%)												
SiO2	47,860	46,470	47,460	46,530	48,210	47,880	47,620	47,050	47,370	46,400	47,770	47,290
TiO2	0,899	1,063	1,031	0,925	0,850	0,855	0,809	0,733	0,782	0,959	0,881	1,062
Al2O3	5,980	6,210	5,580	6,040	5,520	5,510	5,530	5,680	5,510	6,240	5,460	5,820
MnO	1,160	1,138	1,100	1,146	1,264	1,145	1,228	1,262	1,227	1,152	1,134	1,200
FeO	18,350	17,780	17,470	17,500	17,780	16,970	17,590	17,550	17,350	18,010	17,580	17,650
MgO	10,870	11,280	11,500	11,320	11,210	12,100	11,780	11,420	11,560	11,350	11,570	11,230
CaO	11,370	11,010	11,130	11,350	11,180	11,360	11,160	11,240	11,370	11,040	11,170	10,880
Na2O	1,330	1,662	0,998	1,332	1,111	1,405	1,403	1,355	1,391	1,546	1,390	1,504
K2O	0,720	0,741	0,682	0,679	0,596	0,623	0,626	0,640	0,615	0,712	0,619	0,709
Cl	0,066	0,058	0,052	0,059	0,051	0,059	0,060	0,046	0,056	0,062	0,062	0,054
O=F,Cl (calculated)	-0,010	-0,010	-0,010	-0,010	-0,010	-0,010	-0,010	-0,010	-0,010	-0,010	-0,010	-0,010
FeO calculated	16,221	15,966	14,430	14,648	15,220	15,256	14,477	14,637	14,904	14,606	15,875	15,920
Fe2O3 calculated	2,366	2,015	3,378	3,170	2,845	1,905	3,460	3,238	2,719	3,783	1,895	1,922
H2O+ calculated	1,990	1,990	2,000	1,990	2,000	2,000	2,000	2,000	2,000	1,990	1,990	1,990
Total	100,822	99,593	99,331	99,179	100,047	100,088	100,143	99,291	99,494	99,830	99,806	99,571
Formula Assignments												
T (ideally 8 apfu)												
Si	7,102	6,995	7,106	7,009	7,171	7,122	7,086	7,073	7,103	6,955	7,141	7,096
P	0,000	0,000	0,000	0,000	0,000	0,000	0,000	0,000	0,000	0,000	0,000	0,000
Be	0,000	0,000	0,000	0,000	0,000	0,000	0,000	0,000	0,000	0,000	0,000	0,000
Al	0,898	1,005	0,894	0,991	0,829	0,878	0,914	0,927	0,897	1,045	0,859	0,904
Ti	0,000	0,000	0,000	0,000	0,000	0,000	0,000	0,000	0,000	0,000	0,000	0,000
Fe3+	0,000	0,000	0,000	0,000	0,000	0,000	0,000	0,000	0,000	0,000	0,000	0,000
T subtotal	8,000	8,000	8,000	8,000	8,000	8,000	8,000	8,000	8,000	8,000	8,000	8,000
C (ideally 5 apfu)												
Ti	0,100	0,120	0,116	0,105	0,095	0,096	0,091	0,083	0,088	0,108	0,099	0,120
Zr	0,000	0,000	0,000	0,000	0,000	0,000	0,000	0,000	0,000	0,000	0,000	0,000
Al	0,148	0,096	0,091	0,081	0,139	0,087	0,056	0,079	0,077	0,058	0,103	0,125
Sc	0,000	0,000	0,000	0,000	0,000	0,000	0,000	0,000	0,000	0,000	0,000	0,000
V	0,000	0,000	0,000	0,000	0,000	0,000	0,000	0,000	0,000	0,000	0,000	0,000
Cr	0,000	0,000	0,000	0,000	0,000	0,000	0,000	0,000	0,000	0,000	0,000	0,000
Mn3+	0,000	0,000	0,000	0,000	0,000	0,000	0,000	0,000	0,000	0,000	0,000	0,000
Fe3+	0,264	0,228	0,380	0,360	0,319	0,213	0,388	0,366	0,306	0,426	0,213	0,218
Co	0,000	0,000	0,000	0,000	0,000	0,000	0,000	0,000	0,000	0,000	0,000	0,000
Ni	0,000	0,000	0,000	0,000	0,000	0,000	0,000	0,000	0,000	0,000	0,000	0,000
Zn	0,000	0,000	0,000	0,000	0,000	0,000	0,000	0,000	0,000	0,000	0,000	0,000
Mn2+	0,070	0,014	0,039	0,068	0,068	0,023	0,051	0,072	0,075	0,040	0,021	0,028
Fe2+	2,013	2,010	1,808	1,844	1,893	1,898	1,801	1,841	1,870	1,831	1,985	1,997
Mg	2,405	2,531	2,567	2,542	2,486	2,683	2,613	2,559	2,584	2,536	2,578	2,512
Li	0,000	0,000	0,000	0,000	0,000	0,000	0,000	0,000	0,000	0,000	0,000	0,000
C subtotal	5,000	4,999	5,001	5,000	5,000	5,000	5,000	5,000	5,000	4,999	4,999	5,000
B (ideally 2 apfu)												
Mn2+	0,076	0,131	0,100	0,079	0,091	0,121	0,103	0,089	0,081	0,106	0,122	0,125
Fe2+	0,000	0,000	0,000	0,000	0,000	0,000	0,000	0,000	0,000	0,000	0,000	0,000
Mg	0,000	0,000	0,000	0,000	0,000	0,000	0,000	0,000	0,000	0,000	0,000	0,000
Li	0,000	0,000	0,000	0,000	0,000	0,000	0,000	0,000	0,000	0,000	0,000	0,000
Ca	1,808	1,776	1,785	1,832	1,782	1,810	1,779	1,810	1,827	1,773	1,789	1,749
Sr	0,000	0,000	0,000	0,000	0,000	0,000	0,000	0,000	0,000	0,000	0,000	0,000
Na	0,117	0,093	0,114	0,090	0,127	0,068	0,117	0,101	0,092	0,121	0,089	0,126

B subtotal	2,001	2,000	1,999	2,001	2,000	1,999	1,999	2,000	2,000	2,000	2,000	2,000
A (from 0 to 1 apfu)												
Ca	0,000	0,000	0,000	0,000	0,000	0,000	0,000	0,000	0,000	0,000	0,000	0,000
Li	0,000	0,000	0,000	0,000	0,000	0,000	0,000	0,000	0,000	0,000	0,000	0,000
Na	0,266	0,391	0,176	0,299	0,194	0,337	0,287	0,294	0,312	0,329	0,314	0,312
Pb	0,000	0,000	0,000	0,000	0,000	0,000	0,000	0,000	0,000	0,000	0,000	0,000
K	0,136	0,142	0,130	0,130	0,113	0,118	0,119	0,123	0,118	0,136	0,118	0,136
A subtotal	0,402	0,533	0,306	0,429	0,307	0,455	0,406	0,417	0,430	0,465	0,432	0,448
O (non-W)												
O	22,000	22,000	22,000	22,000	22,000	22,000	22,000	22,000	22,000	22,000	22,000	22,000
W (ideally 2 apfu)												
OH	1,983	1,985	1,987	1,985	1,987	1,985	1,985	1,988	1,986	1,984	1,984	1,986
F	0,000	0,000	0,000	0,000	0,000	0,000	0,000	0,000	0,000	0,000	0,000	0,000
Cl	0,017	0,015	0,013	0,015	0,013	0,015	0,015	0,012	0,014	0,016	0,016	0,014
O	0,000	0,000	0,000	0,000	0,000	0,000	0,000	0,000	0,000	0,000	0,000	0,000
W subtotal	2,000	2,000	2,000	2,000	2,000	2,000	2,000	2,000	2,000	2,000	2,000	2,000
Sum T,C,B,A	15,403	15,532	15,306	15,430	15,307	15,454	15,405	15,417	15,430	15,464	15,431	15,448

Sample	CPV-18-510											
Zone	6	6	6	6	6	10	10	10	10	10	10	15
Spot	1	2	3	4	10	13	14	15	16	18	19	21
Classification	Mg-Fe-Hbl	Mg-Fe-Hbl	Mg-Fe-Hbl	Mg-Fe-Hbl	Mg-Fe-Hbl	Mg-Fe-Hbl	Mg-Fe-Hbl	Mg-Fe-Hbl	Mg-Fe-Hbl	Mg-Fe-Hbl	Mg-Fe-Hbl	Mg-Fe-Hbl
Analysis (wt%)												
SiO2	47,750	47,480	48,120	47,240	44,000	44,400	43,690	44,920	43,360	45,440	44,830	44,940
TiO2	0,903	0,812	0,666	0,841	0,952	0,932	1,105	0,925	1,116	0,988	0,966	0,924
Al2O3	5,600	5,590	4,980	5,840	9,980	9,920	10,170	9,450	10,260	8,770	9,680	9,680
MnO	1,193	1,273	1,305	1,266	0,326	0,354	0,369	0,341	0,355	0,338	0,361	0,327
FeO	17,310	18,090	17,770	17,470	17,200	16,840	16,840	16,570	17,140	16,030	16,460	16,950
MgO	11,720	11,390	11,310	11,380	10,600	11,130	10,640	11,077	10,720	12,030	11,210	10,850
CaO	11,010	11,570	11,540	11,430	11,960	11,920	12,010	11,840	11,740	11,690	11,890	12,070
Na2O	1,543	1,331	1,170	1,340	1,054	1,035	1,120	1,019	1,121	0,974	1,049	1,012
K2O	0,664	0,597	0,564	0,610	0,717	0,704	0,752	0,687	0,794	0,562	0,700	0,681
Cl	0,055	0,052	0,051	0,059	0,047	0,041	0,050	0,040	0,043	0,035	0,043	0,044
O=F,Cl (calculated)	-0,010	-0,010	-0,010	-0,010	-0,010	-0,010	-0,010	-0,010	-0,010	-0,010	-0,010	-0,010
FeO calculated	15,544	15,051	15,549	14,937	13,485	12,579	13,438	13,322	12,769	11,654	12,987	13,780
Fe2O3 calculated	1,962	3,378	2,469	2,815	4,129	4,735	3,780	3,609	4,857	4,863	3,860	3,523
H2O+ calculated	2,000	1,990	2,000	1,990	2,000	2,010	2,000	2,010	2,000	2,030	2,010	2,010
Total	99,934	100,504	99,714	99,737	99,240	99,749	99,114	99,230	99,124	99,364	99,575	99,830
Formula Assignments												
T (ideally 8 apfu)												
Si	7,124	7,064	7,203	7,069	6,598	6,600	6,562	6,706	6,512	6,736	6,667	6,682
P	0,000	0,000	0,000	0,000	0,000	0,000	0,000	0,000	0,000	0,000	0,000	0,000
Be	0,000	0,000	0,000	0,000	0,000	0,000	0,000	0,000	0,000	0,000	0,000	0,000
Al	0,876	0,936	0,797	0,931	1,402	1,400	1,438	1,294	1,488	1,264	1,333	1,318
Ti	0,000	0,000	0,000	0,000	0,000	0,000	0,000	0,000	0,000	0,000	0,000	0,000

Fe3+	0,000	0,000	0,000	0,000	0,000	0,000	0,000	0,000	0,000	0,000	0,000	0,000
T subtotal	8,000	8,000	8,000	8,000	8,000	8,000	8,000	8,000	8,000	8,000	8,000	8,000
C (ideally 5 apfu)												
Ti	0,101	0,091	0,075	0,095	0,107	0,104	0,125	0,104	0,126	0,110	0,108	0,103
Zr	0,000	0,000	0,000	0,000	0,000	0,000	0,000	0,000	0,000	0,000	0,000	0,000
Al	0,108	0,044	0,081	0,099	0,361	0,338	0,362	0,369	0,328	0,268	0,363	0,379
Sc	0,000	0,000	0,000	0,000	0,000	0,000	0,000	0,000	0,000	0,000	0,000	0,000
V	0,000	0,000	0,000	0,000	0,000	0,000	0,000	0,000	0,000	0,000	0,000	0,000
Cr	0,000	0,000	0,000	0,000	0,000	0,000	0,000	0,000	0,000	0,000	0,000	0,000
Mn3+	0,000	0,000	0,000	0,000	0,000	0,000	0,000	0,000	0,000	0,000	0,000	0,000
Fe3+	0,220	0,379	0,278	0,317	0,466	0,529	0,428	0,405	0,548	0,542	0,431	0,394
Co	0,000	0,000	0,000	0,000	0,000	0,000	0,000	0,000	0,000	0,000	0,000	0,000
Ni	0,000	0,000	0,000	0,000	0,000	0,000	0,000	0,000	0,000	0,000	0,000	0,000
Zn	0,000	0,000	0,000	0,000	0,000	0,000	0,000	0,000	0,000	0,000	0,000	0,000
Mn2+	0,024	0,088	0,096	0,082	0,005	0,000	0,016	0,000	0,000	0,000	0,000	0,005
Fe2+	1,939	1,872	1,946	1,869	1,690	1,561	1,687	1,657	1,598	1,421	1,612	1,714
Mg	2,607	2,526	2,524	2,538	2,369	2,467	2,382	2,465	2,400	2,659	2,485	2,405
Li	0,000	0,000	0,000	0,000	0,000	0,000	0,000	0,000	0,000	0,000	0,000	0,000
C subtotal	4,999	5,000	5,000	5,000	4,998	4,999	5,000	5,000	5,000	5,000	4,999	5,000
B (ideally 2 apfu)												
Mn2+	0,126	0,073	0,070	0,078	0,037	0,045	0,031	0,043	0,045	0,042	0,045	0,036
Fe2+	0,000	0,000	0,000	0,000	0,000	0,003	0,000	0,006	0,007	0,024	0,004	0,000
Mg	0,000	0,000	0,000	0,000	0,000	0,000	0,000	0,000	0,000	0,000	0,000	0,000
Li	0,000	0,000	0,000	0,000	0,000	0,000	0,000	0,000	0,000	0,000	0,000	0,000
Ca	1,760	1,844	1,851	1,833	1,922	1,899	1,933	1,894	1,889	1,857	1,895	1,923
Sr	0,000	0,000	0,000	0,000	0,000	0,000	0,000	0,000	0,000	0,000	0,000	0,000
Na	0,114	0,083	0,080	0,089	0,042	0,054	0,036	0,057	0,059	0,076	0,056	0,041
B subtotal	2,000	2,000	2,001	2,000	2,001	2,001	2,000	2,000	2,000	1,999	2,000	2,000
A (from 0 to 1 apfu)												
Ca	0,000	0,000	0,000	0,000	0,000	0,000	0,000	0,000	0,000	0,000	0,000	0,000
Li	0,000	0,000	0,000	0,000	0,000	0,000	0,000	0,000	0,000	0,000	0,000	0,000
Na	0,333	0,301	0,260	0,299	0,264	0,244	0,290	0,238	0,267	0,203	0,246	0,251
Pb	0,000	0,000	0,000	0,000	0,000	0,000	0,000	0,000	0,000	0,000	0,000	0,000
K	0,126	0,113	0,108	0,116	0,137	0,133	0,144	0,131	0,152	0,106	0,133	0,129
A subtotal	0,459	0,414	0,368	0,415	0,401	0,377	0,434	0,369	0,419	0,309	0,379	0,380
O (non-W)												
O	22,000	22,000	22,000	22,000	22,000	22,000	22,000	22,000	22,000	22,000	22,000	22,000
W (ideally 2 apfu)												
OH	1,986	1,987	1,987	1,985	1,988	1,990	1,987	1,990	1,989	1,991	1,989	1,989
F	0,000	0,000	0,000	0,000	0,000	0,000	0,000	0,000	0,000	0,000	0,000	0,000
Cl	0,014	0,013	0,013	0,015	0,012	0,010	0,013	0,010	0,011	0,009	0,011	0,011
O	0,000	0,000	0,000	0,000	0,000	0,000	0,000	0,000	0,000	0,000	0,000	0,000
W subtotal	2,000	2,000	2,000	2,000	2,000	2,000	2,000	2,000	2,000	2,000	2,000	2,000
Sum T,C,B,A	15,458	15,414	15,369	15,415	15,400	15,377	15,434	15,369	15,419	15,308	15,378	15,380

Sample	CPV-18-510			
Zone	15	15	15	15

Spot	22	24	26	27
Classification	Mg-Fe-Hbl	Mg-Fe-Hbl	Mg-Fe-Hbl	Mg-Fe-Hbl
Analysis (wt%)				
SiO2	43,060	43,900	44,800	44,110
TiO2	1,087	1,044	1,041	1,027
Al2O3	10,170	10,020	9,610	10,190
MnO	0,381	0,335	0,353	0,392
FeO	16,930	16,800	16,600	17,920
MgO	10,390	11,020	11,210	10,810
CaO	11,770	11,910	11,850	12,090
Na2O	1,071	1,070	1,012	1,075
K2O	0,764	0,740	0,675	0,736
Cl	0,045	0,042	0,048	0,044
O=F,Cl (calculated)	-0,010	-0,010	-0,010	-0,010
FeO calculated	13,188	12,617	12,865	12,884
Fe2O3 calculated	4,158	4,649	4,151	5,596
H2O+ calculated	2,000	2,010	2,010	2,000
Total	98,075	99,347	99,614	100,944
Formula Assignments				
T (ideally 8 apfu)				
Si	6,541	6,562	6,660	6,513
P	0,000	0,000	0,000	0,000
Be	0,000	0,000	0,000	0,000
Al	1,459	1,438	1,340	1,487
Ti	0,000	0,000	0,000	0,000
Fe3+	0,000	0,000	0,000	0,000
T subtotal	8,000	8,000	8,000	8,000
C (ideally 5 apfu)				
Ti	0,124	0,117	0,116	0,114
Zr	0,000	0,000	0,000	0,000
Al	0,362	0,327	0,344	0,286
Sc	0,000	0,000	0,000	0,000
V	0,000	0,000	0,000	0,000
Cr	0,000	0,000	0,000	0,000
Mn3+	0,000	0,000	0,000	0,000
Fe3+	0,474	0,523	0,464	0,621
Co	0,000	0,000	0,000	0,000
Ni	0,000	0,000	0,000	0,000
Zn	0,000	0,000	0,000	0,000
Mn2+	0,010	0,000	0,000	0,008
Fe2+	1,676	1,576	1,591	1,592
Mg	2,353	2,456	2,484	2,379
Li	0,000	0,000	0,000	0,000
C subtotal	4,999	4,999	4,999	5,000
B (ideally 2 apfu)				
Mn2+	0,039	0,042	0,044	0,041
Fe2+	0,000	0,001	0,008	0,000
Mg	0,000	0,000	0,000	0,000
Li	0,000	0,000	0,000	0,000
Ca	1,916	1,908	1,887	1,913
Sr	0,000	0,000	0,000	0,000
Na	0,045	0,049	0,060	0,047
B subtotal	2,000	2,000	1,999	2,001

A (from 0 to 1 apfu)				
Ca	0,000	0,000	0,000	0,000
Li	0,000	0,000	0,000	0,000
Na	0,270	0,261	0,232	0,261
Pb	0,000	0,000	0,000	0,000
K	0,148	0,141	0,128	0,139
A subtotal	0,418	0,402	0,360	0,400
O (non-W)				
O	22,000	22,000	22,000	22,000
W (ideally 2 apfu)				
OH	1,988	1,989	1,988	1,989
F	0,000	0,000	0,000	0,000
Cl	0,012	0,011	0,012	0,011
O	0,000	0,000	0,000	0,000
W subtotal	2,000	2,000	2,000	2,000
Sum T,C,B,A	15,417	15,401	15,358	15,401

Table S1. Plagioclase

Sample	Zone	Spot	**Classification**	Analysis (wt%)							Formula Assignments (8O)						Classification (%)		
				SiO_2	Al_2O_3	Fe_2O_3	CaO	Na_2O	K_2O	**Total**	Si	Al	Fe^{3+}	Ca	Na	K	Ab	An	Or
CCL-65	2	1.B	**Oligoclase**	63,760	22,490	0,225	3,360	9,990	0,114	**99,940**	2,820	1,172	0,008	0,159	0,856	0,006	0,838	0,156	0,006
CCL-65	2	2	**Oligoclase**	63,180	23,300	0,272	4,470	9,220	0,320	**100,762**	2,780	1,208	0,009	0,211	0,786	0,018	0,775	0,207	0,018
CCL-65	5	7	**Oligoclase**	63,270	22,490	0,215	3,530	9,890	0,212	**99,607**	2,812	1,178	0,007	0,168	0,852	0,012	0,826	0,152	0,022
CCL-65	5	8.B	**Oligoclase**	63,020	22,780	0,253	4,290	9,420	0,313	**100,076**	2,793	1,190	0,008	0,204	0,809	0,018	0,785	0,197	0,017
CCL-65	5	9	**Oligoclase**	63,470	23,010	0,372	4,280	9,350	0,329	**100,811**	2,792	1,193	0,012	0,202	0,797	0,019	0,783	0,198	0,018
CCL-65	9	14	**Oligoclase**	63,300	22,650	0,328	4,360	9,200	0,315	**100,153**	2,801	1,181	0,011	0,207	0,789	0,018	0,779	0,204	0,018
CCL-65	9	15	**Oligoclase**	63,250	23,210	0,347	4,500	9,440	0,327	**101,074**	2,779	1,202	0,012	0,212	0,804	0,018	0,854	0,135	0,011
CCL-65	10	17	**Oligoclase**	63,080	22,320	0,387	4,450	9,160	0,304	**99,701**	2,805	1,170	0,013	0,212	0,790	0,017	0,775	0,208	0,017
CCL-65	13	20	**Oligoclase**	61,340	23,510	0,403	5,350	8,640	0,294	**99,537**	2,741	1,239	0,014	0,256	0,749	0,017	0,733	0,251	0,016
CCL-65	13	21.B	**Oligoclase**	64,970	21,080	0,405	2,751	10,190	0,131	**99,526**	2,876	1,100	0,014	0,131	0,875	0,007	0,864	0,129	0,007
CCL-65	13	24	**Oligoclase**	61,440	23,920	0,238	5,670	8,570	0,222	**100,060**	2,731	1,253	0,008	0,270	0,739	0,013	0,723	0,264	0,012
CT-193	4	1	**Labradorite**	54,780	27,740	0,234	10,710	5,460	0,090	**99,015**	2,494	1,489	0,008	0,522	0,482	0,005	0,478	0,517	0,005
CT-193	4	2	**Labradorite**	55,130	28,210	0,288	11,050	5,400	0,119	**100,197**	2,483	1,497	0,010	0,533	0,471	0,007	0,466	0,527	0,007
CT-193	4	3	**Labradorite**	54,610	28,110	0,261	11,260	5,360	0,124	**99,726**	2,474	1,501	0,009	0,547	0,471	0,007	0,460	0,533	0,007
CT-193	4	7	**Labradorite**	55,130	27,730	0,188	10,730	5,640	0,087	**99,505**	2,499	1,481	0,006	0,521	0,496	0,005	0,485	0,510	0,005
CT-193	2	8	**Labradorite**	54,340	28,890	0,228	11,060	5,190	0,104	**99,813**	2,456	1,539	0,008	0,536	0,455	0,006	0,457	0,537	0,006
CT-193	2	9	**Labradorite**	54,300	28,120	0,258	11,030	5,440	0,112	**99,260**	2,471	1,509	0,009	0,538	0,480	0,007	0,468	0,525	0,007
CT-193	2	10	**Labradorite**	54,380	28,290	0,237	11,060	5,260	0,107	**99,334**	2,471	1,515	0,008	0,538	0,463	0,006	0,460	0,534	0,006
CT-193	2	11	**Labradorite**	53,760	28,350	0,253	11,340	5,280	0,074	**99,057**	2,454	1,526	0,009	0,555	0,467	0,004	0,455	0,541	0,004
CT-193	2	12	**Labradorite**	52,960	29,100	0,294	11,890	4,920	0,085	**99,249**	2,417	1,565	0,010	0,581	0,436	0,005	0,426	0,569	0,005
CT-193	5	13	**Labradorite**	54,950	27,940	0,197	10,800	5,490	0,114	**99,491**	2,491	1,493	0,007	0,524	0,482	0,007	0,476	0,518	0,006
CT-193	5	15	**Labradorite**	54,950	28,070	0,183	10,780	5,530	0,143	**99,656**	2,487	1,498	0,006	0,523	0,486	0,008	0,478	0,514	0,008
CT-193	5	17	**Labradorite**	54,370	28,090	0,247	10,740	5,540	0,088	**99,074**	2,477	1,508	0,009	0,524	0,489	0,005	0,480	0,515	0,005
CPV-18-510	6	1	**Oligoclase**	65,240	21,160	0,354	2,930	10,120	0,289	**100,093**	2,877	1,100	0,012	0,138	0,865	0,016	0,848	0,136	0,016
CPV-18-510	6	2	**Oligoclase**	65,390	21,070	0,359	2,995	10,110	0,253	**100,178**	2,881	1,094	0,012	0,141	0,864	0,014	0,847	0,139	0,014

CPV-18-510	6	3	**Oligoclase**	65,220	21,290	0,430	2,811	10,100	0,179	**100,031**	2,875	1,106	0,014	0,133	0,863	0,010	0,858	0,132	0,010
CPV-18-510	6	4	**Oligoclase**	64,130	22,630	0,288	3,970	9,230	0,266	**100,514**	2,820	1,173	0,010	0,187	0,787	0,015	0,796	0,189	0,015
CPV-18-510	6	10	**Oligoclase**	65,740	21,060	0,318	2,284	10,740	0,129	**100,270**	2,890	1,091	0,011	0,108	0,916	0,007	0,889	0,104	0,007
CPV-18-510	10	13	**Oligoclase**	65,070	21,340	0,290	2,791	10,250	0,136	**99,878**	2,873	1,111	0,010	0,132	0,877	0,008	0,863	0,128	0,009
CPV-18-510	10	14	**Oligoclase**	64,260	21,660	0,305	3,730	9,790	0,197	**99,942**	2,844	1,130	0,010	0,177	0,840	0,011	0,817	0,172	0,011
CPV-18-510	10	15	**Oligoclase**	64,540	21,450	0,522	3,330	9,820	0,176	**99,838**	2,856	1,119	0,017	0,158	0,843	0,010	0,834	0,156	0,010
CPV-18-510	10	16	**Oligoclase**	65,640	21,410	0,501	2,824	10,280	0,205	**100,859**	2,872	1,104	0,017	0,132	0,872	0,011	0,858	0,130	0,012
CPV-18-510	10	18	**Oligoclase**	65,640	21,710	0,379	2,823	10,240	0,181	**100,973**	2,867	1,118	0,013	0,132	0,867	0,010	0,859	0,131	0,010
CPV-18-510	10	19	**Oligoclase**	65,730	21,670	0,330	2,739	10,200	0,191	**100,861**	2,872	1,116	0,011	0,128	0,864	0,011	0,861	0,128	0,011
CPV-18-510	15	21	**Oligoclase**	69,390	19,510	0,205	0,375	11,710	0,028	**101,219**	2,996	0,993	0,007	0,017	0,981	0,002	0,873	0,120	0,007
CPV-18-510	15	22	**Oligoclase**	65,780	21,240	0,300	2,497	10,470	0,114	**100,401**	2,886	1,098	0,010	0,117	0,891	0,006	0,878	0,116	0,006
CPV-18-510	15	24	**Oligoclase**	65,580	20,790	0,297	2,408	10,360	0,461	**99,896**	2,896	1,082	0,010	0,114	0,887	0,026	0,864	0,111	0,025
CPV-18-510	15	26	**Oligoclase**	65,950	21,390	0,280	2,550	10,650	0,163	**100,983**	2,880	1,101	0,009	0,119	0,901	0,009	0,875	0,116	0,009
CPV-18-510	15	27	**Oligoclase**	65,160	21,210	0,292	2,702	10,570	0,175	**100,109**	2,874	1,103	0,010	0,128	0,904	0,010	0,868	0,123	0,009

Apéndice Capítulo IV

Appendix 4.A. Measurements made in the eastern segment of the EMDS. The data includes the strike, dip (determined by the right-hand rule) and thickness (in cm) for each of the dikes and the rock to which they intrude. The data are organized according to the subdivision into eleven sections within the segment.

Section	Strike	Dip	Thickness (cm)	Host rock	Section	Strike	Dip	Thickness (cm)	Host rock
1	128	62	48	Permian – Mid. Tr Intrusives	3	166	73	68	Permian – Mid. Tr Intrusives
1	152	68	82	Permian – Mid. Tr Intrusives	3	181	77	270	Permian – Mid. Tr Intrusives
1	132	61	32	Permian – Mid. Tr Intrusives	3	173	74	540	Permian – Mid. Tr Intrusives
1	157	66	9,5	Permian – Mid. Tr Intrusives	3	204	77	11	Permian – Mid. Tr Intrusives
1	152	68	12	Permian – Mid. Tr Intrusives	3	13	88	22	Permian – Mid. Tr Intrusives
1	157	60	62	Permian – Mid. Tr Intrusives	3	192	87	126	Permian – Mid. Tr Intrusives
1	176	74	270	Permian – Mid. Tr Intrusives	3	87	87	182	Permian – Mid. Tr Intrusives
1	294	57	30	Permian – Mid. Tr Intrusives	3	190	68	124	Permian – Mid. Tr Intrusives
1	295	76	28	Permian – Mid. Tr Intrusives	3	167	77	90	Permian – Mid. Tr Intrusives
1	205	66	146	Permian – Mid. Tr Intrusives	3	177	77	4	Permian – Mid. Tr Intrusives
1	145	50	53	Permian – Mid. Tr Intrusives	3	181	82	190	Permian – Mid. Tr Intrusives
1	207	76	9	Permian – Mid. Tr Intrusives	3	187	76	52	Permian – Mid. Tr Intrusives
1	168	69	194	Permian – Mid. Tr Intrusives	3	77	67	11	Permian – Mid. Tr Intrusives
1	182	72	119	Permian – Mid. Tr Intrusives	3	201	87	33	Permian – Mid. Tr Intrusives
1	203	78	107	Permian – Mid. Tr Intrusives	4	186	84	14	Permian – Mid. Tr Intrusives
1	202	82	48	Permian – Mid. Tr Intrusives	4	182	81	46	Permian – Mid. Tr Intrusives
1	202	86	73	Permian – Mid. Tr Intrusives	4	170	75	14	Permian – Mid. Tr Intrusives
1	198	68	51	Permian – Mid. Tr Intrusives	4	196	87	84	Permian – Mid. Tr Intrusives
1	219	59	3	Permian – Mid. Tr Intrusives	4	123	60	154	Permian – Mid. Tr Intrusives
1	197	77	63	Permian – Mid. Tr Intrusives	4	207	76	103	Permian – Mid. Tr Intrusives
1	184	88	22	Permian – Mid. Tr Intrusives	4	190	74	64	Permian – Mid. Tr Intrusives
1	220	28	19	Permian – Mid. Tr Intrusives	4	163	58	212	Permian – Mid. Tr Intrusives
2	192	85	44	Permian – Mid. Tr Intrusives	4	184	78	92	Permian – Mid. Tr Intrusives
2	172	80	85	Permian – Mid. Tr Intrusives	4	163	72	109	Permian – Mid. Tr Intrusives
2	176	74	37	Permian – Mid. Tr Intrusives	4	103	50	33	Permian – Mid. Tr Intrusives
2	222	64	92	Permian – Mid. Tr Intrusives	4	184	78	10	Permian – Mid. Tr Intrusives
2	168	64	1	Permian – Mid. Tr Intrusives	4	195	83	25	Permian – Mid. Tr Intrusives
2	175	49	110	Permian – Mid. Tr Intrusives	4	196	76	13	Permian – Mid. Tr Intrusives
2	26	84	22	Permian – Mid. Tr Intrusives	4	107	57	206	Permian – Mid. Tr Intrusives
2	28	73	15	Permian – Mid. Tr Intrusives	4	210	73	28	Permian – Mid. Tr Intrusives
2	178	72	110	Permian – Mid. Tr Intrusives	4	215	87	93	Permian – Mid. Tr Intrusives
2	188	73	62	Permian – Mid. Tr Intrusives	4	194	77	18	Permian – Mid. Tr Intrusives
2	178	77	18	Permian – Mid. Tr Intrusives	4	201	87	56	Permian – Mid. Tr Intrusives
2	183	67	40	Permian – Mid. Tr Intrusives	4	206	78	7	Permian – Mid. Tr Intrusives
2	191	74	48	Permian – Mid. Tr Intrusives	4	195	86	2	Permian – Mid. Tr Intrusives
2	173	73	24	Permian – Mid. Tr Intrusives	4	191	78	20	Permian – Mid. Tr Intrusives
2	201	88	33	Permian – Mid. Tr Intrusives	4	187	70	19	Permian – Mid. Tr Intrusives
2	172	61	256	Permian – Mid. Tr Intrusives	4	197	76	101	Permian – Mid. Tr Intrusives
2	186	82	63	Permian – Mid. Tr Intrusives	5	100	72	310	Permian – Mid. Tr Intrusives
2	168	71	261	Permian – Mid. Tr Intrusives	5	194	76	9	Permian – Mid. Tr Intrusives
2	157	73	128	Permian – Mid. Tr Intrusives	5	195	72	39	Permian – Mid. Tr Intrusives
2	162	74	66	Permian – Mid. Tr Intrusives	5	204	81	643	Permian – Mid. Tr Intrusives
2	150	71	27	Permian – Mid. Tr Intrusives	5	220	83	46	Permian – Mid. Tr Intrusives
2	151	68	18	Permian – Mid. Tr Intrusives	5	182	80	19	Permian – Mid. Tr Intrusives
2	166	72	70	Permian – Mid. Tr Intrusives	5	30	84	42	Permian – Mid. Tr Intrusives
2	292	61	370	Permian – Mid. Tr Intrusives	5	182	74	87	Permian – Mid. Tr Intrusives
3	208	67	485	Permian – Mid. Tr Intrusives	5	207	88	137	Permian – Mid. Tr Intrusives
3	183	52	56	Permian – Mid. Tr Intrusives	5	204	78	53	Permian – Mid. Tr Intrusives
3	197	87	310	Permian – Mid. Tr Intrusives	5	196	79	4	Permian – Mid. Tr Intrusives
3	187	78	127	Permian – Mid. Tr Intrusives	5	186	88	74	Permian – Mid. Tr Intrusives
3	180	79	102	Permian – Mid. Tr Intrusives	5	184	66	38	Permian – Mid. Tr Intrusives
3	183	77	145	Permian – Mid. Tr Intrusives	5	202	80	186	Permian – Mid. Tr Intrusives
3	186	74	8	Permian – Mid. Tr Intrusives	5	196	83	116	Permian – Mid. Tr Intrusives
3	149	77	150	Permian – Mid. Tr Intrusives	5	203	79	39	Permian – Mid. Tr Intrusives
3	163	71	51	Permian – Mid. Tr Intrusives	5	203	84	14	Permian – Mid. Tr Intrusives
3	172	77	144	Permian – Mid. Tr Intrusives	5	213	87	64	Permian – Mid. Tr Intrusives

5	183	67	9	Permian – Mid. Tr Intrusives	8	165	89	50	Colorado Syenogranites
6	216	89	400	Colorado Syenogranites	8	165	89	390	Colorado Syenogranites
6	195	86	85	Colorado Syenogranites	8	170	68	120	Colorado Syenogranites
6	171	66	20	Colorado Syenogranites	8	355	70	15	Colorado Syenogranites
6	192	77	100	Colorado Syenogranites	8	180	76	100	Colorado Syenogranites
6	180	80	200	Colorado Syenogranites	8	190	84	55	Colorado Syenogranites
6	156	67	63	Colorado Syenogranites	8	190	84	216	Colorado Syenogranites
6	185	81	100	Colorado Syenogranites	8	210	90	86	Colorado Syenogranites
6	195	77	300	Colorado Syenogranites	8	190	75	57	Colorado Syenogranites
6	196	85	130	Colorado Syenogranites	8	210	75	357	Colorado Syenogranites
6	200	89	60	Colorado Syenogranites	8	182	58	30	Colorado Syenogranites
6	185	88	43	Colorado Syenogranites	8	210	89	1000	Colorado Syenogranites
6	175	65	320	Colorado Syenogranites	8	95	70	30	Colorado Syenogranites
6	200	72	500	Colorado Syenogranites	8	206	85	50	Colorado Syenogranites
6	185	77	35	Colorado Syenogranites	8	200	85	320	Colorado Syenogranites
6	205	90	55	Colorado Syenogranites	8	200	77	500	Colorado Syenogranites
6	197	86	290	Colorado Syenogranites	8	227	83	150	Colorado Syenogranites
6	186	86	30	Colorado Syenogranites	8	90	85	700	Colorado Syenogranites
6	200	89	25	Colorado Syenogranites	8	0	68	40	Colorado Syenogranites
6	300	46	65	Colorado Syenogranites	9	250	77	275	Colorado Syenogranites
6	202	80	700	Colorado Syenogranites	9	264	77	28	Colorado Syenogranites
6	0	72	40	Colorado Syenogranites	9	15	64	50	Colorado Syenogranites
6	0	78	100	Colorado Syenogranites	9	25	82	160	Colorado Syenogranites
6	195	78	80	Colorado Syenogranites	9	20	88	195	Colorado Syenogranites
6	185	84	35	Colorado Syenogranites	9	10	84	45	Colorado Syenogranites
6	195	78	40	Colorado Syenogranites	9	85	78	180	Colorado Syenogranites
6	186	85	70	Colorado Syenogranites	10	230	73	26	Piuquenes Monzogranites
6	186	85	10	Colorado Syenogranites	10	200	78	98	Piuquenes Monzogranites
6	18	85	27	Colorado Syenogranites	10	210	72	41	Piuquenes Monzogranites
6	205	85	260	Colorado Syenogranites	10	210	81	28	Piuquenes Monzogranites
6	45	70	75	Colorado Syenogranites	10	290	88	33	Piuquenes Monzogranites
6	160	74	90	Colorado Syenogranites	10	50	90	202	Piuquenes Monzogranites
6	20	74	60	Colorado Syenogranites	10	139	60	81	Piuquenes Monzogranites
6	20	74	105	Colorado Syenogranites	10	45	51	140	Piuquenes Monzogranites
6	20	54	150	Colorado Syenogranites	10	240	80	86	Piuquenes Monzogranites
6	195	80	60	Colorado Syenogranites	10	130	75	210	Piuquenes Monzogranites
7	174	76	35	Colorado Syenogranites	10	308	84	380	Piuquenes Monzogranites
7	358	80	600	Colorado Syenogranites	10	115	82	50	Piuquenes Monzogranites
7	210	60	29	Colorado Syenogranites	10	193	72	25	Piuquenes Monzogranites
7	190	73	33	Colorado Syenogranites	10	160	83	146	Piuquenes Monzogranites
7	199	88	130	Colorado Syenogranites	10	125	83	35	Piuquenes Monzogranites
7	204	86	30	Colorado Syenogranites	10	213	83	285	Piuquenes Monzogranites
7	204	86	38	Colorado Syenogranites	10	32	88	467	Piuquenes Monzogranites
7	201	71	134	Colorado Syenogranites	10	352	77	53	Piuquenes Monzogranites
7	160	83	106	Colorado Syenogranites	10	172	88	24	Piuquenes Monzogranites
7	196	86	346	Colorado Syenogranites	10	175	82	72	Piuquenes Monzogranites
7	14	77	700	Colorado Syenogranites	10	155	86	118	Piuquenes Monzogranites
8	164	75	30	Colorado Syenogranites	10	150	84	113	Piuquenes Monzogranites
8	164	75	30	Colorado Syenogranites	11	55	73	114	Permian – Mid. Tr Intrusives
8	190	81	180	Colorado Syenogranites	11	215	87	68	Permian – Mid. Tr Intrusives
8	174	72	30	Colorado Syenogranites	11	227	89	111	Permian – Mid. Tr Intrusives
8	165	88	47	Colorado Syenogranites	11	62	82	110	Permian – Mid. Tr Intrusives
8	165	88	98	Colorado Syenogranites	11	45	86	60	Permian – Mid. Tr Intrusives
8	231	74	90	Colorado Syenogranites	11	337	80	58	Permian – Mid. Tr Intrusives
8	231	74	18	Colorado Syenogranites	11	60	82	45	Permian – Mid. Tr Intrusives
8	194	87	130	Colorado Syenogranites					
8	193	74	110	Colorado Syenogranites					
8	193	74	60	Colorado Syenogranites					
8	185	74	400	Colorado Syenogranites					
8	165	65	230	Colorado Syenogranites					
8	221	85	130	Colorado Syenogranites					
8	210	85	140	Colorado Syenogranites					

Appendix 4.B. Components and classification of the studied samples as determined through petrographic analysis. Their mineralogy is expressed as volume percentage of the total rock. For each sample, the content in phenocrysts, groundmass, glass, lithic and/or vesicles is detailed. The crystal fragments of tuffs were included in the "phenocrysts" column and their vitreous components in the "glass" column. The primary mineralogy detectable at microscopic scale, is detailed in the "igneous component" column (Plg: plagioclase; Qtz: quartz; Alk fds: alkali feldspar; Cpx: clinopyroxene; Opx: orthopiroxene; Bt: biotite; Amp: amphibole; Ms: muscovite; Op: opaque minerals; Zr: zircon; Ap: apatite and Other: undetermined minerals, which commonly correspond to mafic minerals completely replaced by chlorite. The alteration minerals observed in the samples are also listed, Cly: clays; Ser: sericite; Qz: quartz; Cc: calcite; Chl: chlorite; Ep: epidote; Ce: celadonite; Op: opaque minerals; Srp: serpentine; Lim: limonite; Tit: titanite and Other: other minerals.

Unit	Sample	Petrographic classification	Location		Phenocrystals	Ground mass	Glass	Lithic	Vesicles	Total
			East (m)	North (m)						
Colorado Syenogranites	Dikes									
	GUC-34	Amphibole-bearing andesitic porphyry	387488	6720764	0,19	0,81	0,00	0,00	0,00	1,00
	GUC-35B	Monzonitic quartziferous porphyry	388100	6720671	0,22	0,63	0,00	0,15	0,00	1,00
	GUC-37A	Monzonitic porphyry	387873	6720695	0,30	0,70	0,00	0,00	0,00	1,00
	GUC-37B	Monzonitic porphyry	387873	6720695	0,31	0,69	0,00	0,00	0,00	1,00
	GUC-37C	Silicified porphyritic microdiorite	387873	6720695	0,19	0,81	0,00	0,00	0,00	1,00
	GUC-37D	Silicified porphyritic microdiorite	387873	6720695	0,14	0,86	0,00	0,00	0,00	1,00
Pastos Blancos Formation	Lavas									
	GUC-05	Rhyolite	398992	6702250	0,07	0,93	0,00	0,00	0,00	1,00
	GUC-32	Piroxene-bearing andesite	398939	6701463	0,33	0,40	0,27	0,00	0,00	1,00
	GUC-33	Dacite	387342	6720757	0,03	0,97	0,00	0,00	0,00	1,00
	GUC-38B	Autobreccia	391068	6716828	0,00	0,26	0,44	0,00	0,30	1,00
	GUC-39	Andesite	394452	6714575	0,04	0,96	0,00	0,00	0,00	1,00
	GUC-44C	Andesite	388669	6724800	0,48	0,25	0,27	0,00	0,00	1,00
	GUC-47	Dacite	394690	6721101	0,04	0,96	0,00	0,00	0,00	1,00
	Volcanosedimentary rocks									
	GUC-33B	Lapilli tuff	387342	6720757	0,08	0,00	0,70	0,22	0,00	1,00
	GUC-35A	Lapilli tuff	388100	6720671	0,08	0,00	0,34	0,58	0,00	1,00
	GUC-36	Lithic-bearing vitric tuff	389680	6719524	0,22	0,00	0,40	0,38	0,00	1,00
	GUC-38	Tuffaceous sandstone	391068	6716828	0,07	0,00	0,00	0,93	0,00	1,00
	GUC-40	Vitric tuff	394452	6714575	0,06	0,00	0,76	0,18	0,00	1,00
	GUC-41	Lapilli tuff	396283	6721101	0,05	0,00	0,62	0,33	0,00	1,00
	GUC-42	Vitric tuff	396300	6721183	0,20	0,00	0,67	0,13	0,00	1,00
	GUC-43	Lapilli tuff	387502	6725104	0,19	0,00	0,41	0,40	0,00	1,00
	GUC-44A	Vitric tuff	388669	6724800	0,07	0,00	0,93	<0.01	0,00	1,00
	GUC-44B	Vitric tuff	388669	6724800	0,17	0,00	0,60	0,23	0,00	1,00

	GUC-45	Vitric-bearing crystal tuff	390763	6723287	0,45	0,00	0,42	0,13	0,00	1,00
	GUC-46	Crystal-bearing vitric tuff	394944	6721032	0,45	0,00	0,55	<0.01	0,00	1,00

Unit	Sample	Igneous Components											
		Plg	Qtz	Alk fds	Cpx	Opx	Bt	Amp	Ms	Op	Zr	Ap	Other
Colorado Syenogranites	Dikes												
	GUC-34	0,75	0,00	0,00	0,01	0,00	0,00	0,06	0,00	0,07	0,00	0,00	0,11
	GUC-35B	0,40	0,09	0,24	0,00	0,00	0,00	0,00	0,00	0,05	0,00	0,00	0,07
	GUC-37A	0,48	0,03	0,39	0,00	0,00	0,00	0,00	0,00	0,10	0,00	<0.01	0,00
	GUC-37B	0,52	0,07	0,32	0,00	0,00	0,00	0,00	0,00	0,05	0,00	0,00	0,04
	GUC-37C	0,85	0,00	0,00	0,00	0,00	0,00	0,00	0,00	0,14	<0.01	<0.01	0,01
	GUC-37D	0,39	0,00	0,00	0,00	0,00	0,00	0,05	0,00	0,35	0,00	0,00	0,21
Pastos Blancos Formation	Lavas												
	GUC-05	0,03	0,15	0,74	0,00	0,00	<0.01	0,00	0,00	0,08	<0.01	0,00	<0.01
	GUC-32	0,51	0,00	0,00	0,08	0,10	0,00	0,00	0,00	0,04	0,00	0,00	0,00
	GUC-33	0,48	0,25	0,24	0,00	0,00	0,00	0,00	0,00	0,03	<0.01	0,00	0,00
	GUC-38B	0,20	0,00	0,00	0,00	0,00	0,00	0,00	0,00	0,06	0,00	0,00	0,00
	GUC-39	0,78	0,00	0,00	0,09	0,00	0,00	0,00	0,00	0,03	0,00	0,00	0,10
	GUC-44C	0,61	0,00	0,00	0,00	0,00	0,00	0,00	0,00	0,00	0,00	0,00	0,12
	GUC-47	0,07	0,37	0,37	0,00	0,00	0,00	0,00	0,00	0,07	0,00	0,00	0,12
	Volcanosedimentary rocks												
	GUC-33B	0,05	0,03	0,00	0,00	0,00	0,00	0,00	0,00	0,00	0,00	0,00	0,00
	GUC-35A	0,03	0,02	0,00	0,00	0,00	0,00	0,00	0,00	0,03	0,00	0,00	0,00
	GUC-36	0,17	<0.01	0,00	0,01	0,00	0,00	0,00	0,00	0,02	<0.01	0,00	0,02
	GUC-38	0,02	0,02	0,00	0,00	0,00	0,00	0,00	0,00	0,02	0,00	0,00	0,01
	GUC-40	0,04	<0.01	0,00	0,00	0,00	0,00	0,00	0,00	0,02	0,00	0,00	0,00
	GUC-41	0,04	0,01	0,00	0,00	<0.01	0,00	0,00	0,00	0,00	<0.01	0,00	0,00
	GUC-42	0,00	0,07	0,12	0,00	0,00	0,00	0,00	0,00	<0.01	0,00	0,00	0,01
	GUC-43	0,03	0,06	0,00	0,00	0,00	0,00	0,00	0,00	0,01	0,00	0,00	0,09
	GUC-44A	0,03	0,01	0,00	0,00	0,00	0,00	0,00	0,00	0,03	0,00	0,00	0,00
	GUC-44B	0,13	0,03	0,00	0,00	0,00	0,00	0,00	0,00	0,01	0,00	0,00	0,00
	GUC-45	0,12	0,15	0,14	0,00	0,00	0,02	0,00	0,00	0,02	<0.01	0,00	0,00
	GUC-46	0,38	0,00	0,00	0,00	0,00	0,00	0,03	0,00	0,03	<0.01	<0.01	0,01

Unit	Sample	Alteration Minerals												
		Cly	Ser	Qz	Cc	Chl	Ep	Ce	Op	Srp	Lim	Tit	Other	Total
Colorado Syenogranites	Dikes													
	GUC-34	0,03	<0.01	0,00	0,01	0,10	0,00	0,00	0,00	0,00	0,00	0,15	0,00	0,29
	GUC-35B	0,50	<0.01	0,06	0,02	0,12	0,00	0,00	0,00	0,00	0,00	0,00	0,00	0,70
	GUC-37A	0,55	0,10	0,00	0,04	<0.01	0,00	0,00	0,03	0,00	0,00	<0.01	0,00	0,72
	GUC-37B	0,50	<0.01	0,00	0,01	0,08	0,00	0,00	0,01	0,00	<0.01	0,00	0,00	0,60
	GUC-37C	0,48	<0.01	0,23	0,01	0,00	0,00	0,00	0,10	0,00	0,00	0,00	0,00	0,82
	GUC-37D	0,25	<0.01	0,18	0,02	0,17	0,00	0,00	0,24	0,00	0,00	0,00	0,00	0,86
Pastos Blancos Formation	Lavas													
	GUC-05	0,30	<0.01	0,25	0,00	0,00	0,00	0,00	0,02	0,00	0,00	0,00	0,00	0,57
	GUC-32	0,27	0,12	0,00	0,00	0,07	<0.01	0,00	0,00	0,03	0,00	0,00	0,00	0,49
	GUC-33	0,45	0,00	0,00	0,04	0,00	0,00	0,10	0,00	0,00	0,00	0,00	0,00	0,59
	GUC-38B	<0.01	0,00	0,11	0,06	0,13	0,01	0,00	0,00	0,00	0,00	0,00	0,07	0,38
	GUC-39	<0.01	0,12	0,00	0,00	0,12	<0.01	0,00	0,00	0,00	0,00	0,07	0,00	0,31
	GUC-44C	0,25	0,01	0,00	<0.01	0,31	0,10	0,00	0,00	0,00	0,00	0,05	0,00	0,72
	GUC-47	0,35	<0.01	0,18	0,02	0,00	0,00	0,00	0,00	0,00	0,00	0,00	0,00	0,55
	Volcanosedimentary rocks													
	GUC-33B	0,40	<0.01	0,10	0,00	0,00	0,00	0,03	0,00	0,00	0,00	0,00	0,00	0,53
	GUC-35A	0,26	0,00	0,35	0,01	0,00	0,00	0,00	0,00	0,00	0,03	0,00	0,00	0,65
	GUC-36	0,20	<0.01	<0.01	<0.01	0,10	0,00	0,00	0,00	0,00	0,00	0,00	0,00	0,30
	GUC-38	0,14	<0.01	<0.01	0,04	0,01	0,00	0,02	0,00	0,00	0,00	0,00	0,00	0,21
	GUC-40	0,30	0,03	0,01	0,00	0,00	0,00	0,00	0,00	0,00	0,35	0,00	0,00	0,69
	GUC-41	0,12	<0.01	0,05	0,00	0,00	0,04	0,00	0,10	0,00	0,00	0,00	0,00	0,31
	GUC-42	0,20	0,00	0,10	<0.01	0,00	<0.01	0,00	0,00	0,00	0,12	0,00	0,00	0,42
	GUC-43	0,30	<0.01	0,00	0,01	0,05	0,00	0,00	0,02	0,00	0,00	0,00	0,00	0,38
	GUC-44A	0,35	0,12	0,01	0,00	0,00	<0.01	0,04	0,00	0,00	<0.01	0,00	0,00	0,52
	GUC-44B	0,30	<0.01	0,00	0,00	0,03	0,15	0,00	0,00	0,00	0,00	0,00	0,00	0,48
	GUC-45	0,25	0,02	<0.01	0,01	0,00	0,00	0,00	0,01	0,00	0,00	0,00	0,00	0,29
	GUC-46	0,22	0,07	0,05	0,05	0,04	0,00	0,00	<0.01	0,00	0,02	<0.01	0,00	0,45

Apéndice Capítulo V

Supplementary Material 5.1. Spreadsheets with the geological units from Carboniferous-Triassic that crop out in Chile and Argentina. They include all sets of polygons corresponding to a specific unit, each one with its cartography reference, age, the time(s) interval(s) assigned, geographical region (Andes, North Patagonia or CMPT-LP), composition, total area, and the division of that area according to the proportion of each composition, following the methodology explained in section 3. The units from Chile and Argentina have been ordered according to their latitude and province, respectively.

Ver apéndice digital

Supplementary Material 5.2. Detailed explanation about the methodology used for estimation of composition, age distribution and volume of the Choiyoi Magmatic Province.

Methodology for estimation of composition, age distribution and volume of the Choiyoi Magmatic Province

1. Area calculation

We performed an estimation of the areal distribution of Carboniferous to Triassic plutonic and volcanic rocks exposed in Chile and Argentina, 20°S-45ºS; grouping the outcrops by age and composition. The information has been taken mostly from the geological maps published by the Chilean Geological and Mining Service (1:50,000, 1:100,000, 1:250,000) and the Argentinean Geological Service (1:100,000, 1:250,000). Updated or more detailed geological maps from papers were used in order to complement the geological information. Polygons were drawn for each unit respecting the internal divisions of each one, and facies whose origin was not entirely co-magmatic were discarded (for example: highly reworked volcano-sedimentary facies). The area of each unit was then calculated through ArcGIS 10.1 software (Datum WGS84, Zone 18S, 19S and 20S).

2. Age and composition

The total area obtained for each series of polygons was divided according to its composition into: basaltic, andesitic, dacitic or rhyolitic for volcanic rocks and gabbroic, dioritic, granodioritic, tonalitic or granitic for plutonic ones.

This method entails imprecisions, by inferring percentages from descriptions that may be vague about the predominance of one composition or another. Considering this, it's necessary to establish some criteria that allow us to apply a homogeneous procedure to assign unclear proportions or deal with rocks outside the types considered in this work.

1) Rocks described as basaltic andesite are considered basalts or andesites, depending on which of the two rock types is present in a given unit. If it's associated with both, the area of the unit/facies is divided in equal parts, adding to the total area of both compositions. Rhyodacites are included in dacites and rhyolites.

2) In units that include two compositions without enough information about their proportion, a division in equal parts is considered (50%-50%). The same applies if there are three compositions with unclear proportions (33, 3%-33, 3%-33, 3%), or more than three. This rule also applies when discarding a non co-magmatic fraction from the total area of the unit (*e.g.* sedimentary intercalations, metamorphic rocks, xenoliths, etc.)

3) In the case of rocks appearing in low quantity that are described as “subordinate” or “local” (or another equivalent adjective) within a given unit or facies, a 10% of the total area is assigned to them. If there are several minor compositions and a main one, only the latter is considered (100%), to avoid assigning too much percentage to minor facies to the detriment of the predominant one. As in 2), the same rule is applied to non co-magmatic components.

4) If there are indications that between two compositions one is predominant, the proportion is set on 70%-30%. If there is one main composition and two minor ones, the proportion is 70%-15%-15%. As in 2) and 3), the same rule is applies to non co-magmatic components.

5) Volcanoclastic breccias (constituted mainly of juvenile material) are considered as composed 100% of co-magmatic material. This also happens with volcanic rocks that include sedimentary interbeds described as “scarce“, “very minor”, “thin”, or another adjectives that indicates low quantity. Epiclastic breccias, volcarenites or tuffites, are discarded for being highly reworked.

6) Monzogranites, syenogranites, as well as the scarce monzonites and syenites, are grouped within the granites field. Granodiorites and gabbros also incorporate in their total areas syeno-, monzo- or other rocks subdivisions cropping out in low quantity. Trachyandesites were grouped with andesites and trachydacites with dacites, trachytes with rhyolites-dacites, and shoshonites with basaltic andesites, applying the criteria from 1).

7) Tuffs composition is often not specified, so it’s assumed to be equivalent to the rest of the formation that contains them in that same sector. In the same way, the description of some adjacent map or generalized column of a given formation can be extrapolated, to complete the zones where information is weak.

Table 1 summarize this criteria.

3. Age intervals

In order to visualize the evolution of the magmatic products of the western margin of South America through the 150 Ma prior to the Andean Cycle, five time intervals (350-300 Ma, 300-275 Ma, 275-250 Ma, 250-225 Ma and 225-200 Ma) were arbitrarily defined. Carboniferous–Triassic igneous units, were assigned to one or more of these intervals based on the available ages, extending and refining the procedure presented in Oliveros et al. (2018) for the Triassic–Jurassic magmatism.

Table A.5.1 Summary of the seven criteria to separate units by composition, according to the needs of this work and in case of insufficient information.

N°	***Case***	***Criteria to divide areas***	***Example***
1.	Basaltic andesites and rhyodacites	Grouped in basalts and/or andesites, and rhyolite and/or dacite, depending on which they are associated with.	*Unit with basaltic andesites and andesites: 100% andesites*
2.	Two or three compositions present in one unit without predominance of one or another	%50-%50%, or 33%-33%-33%, respectively	*Unit composed of tonalites, granodiorites and granites: tonalites 33,3%, granodiorites 33,3%, and granites 33% of total area*
3.	Rocks described as “subordinate”, “local” or another equivalent adjective	10% of total area. In case there are several minor facies, they are discarded	*Mainly andesites with local outcrops of dacites: 90% andesites, 10% dacites*
4.	Two or three compositions with predominance of one	70%-30% (two compositions) or 70%-15%-15% (three compositions)	*In the sequence rhyolites are predominant, with dacites and andesites in less amount: 70% rhyolites, 15% dacites, 15% andesites*
5.	Volcanoclastic breccias Epiclastic breccias Volcanic rocks with “scarce” (or equivalent adjective) sedimentary interbeds	100% co–magmatic 0% co–magmatic 100% volcanic (co–magmatic)	*Unit composed of volcanoclastic breccias and ignimbrites with interbedded lutites:* 100% volcanic (co–magmatic)
6.	Monzo -, syeno -	Grouped with granites, Granodiorites or gabbros	*Unit composed of monzogranites and*

	Monzonites and syenites	Grouped with granites	*monzonites: 100% granites*
	Trachydacites, trachyandesites y trachytes	Grouped with dacites, andesites and rhyolites and/or dacites, respectively	*Sequence of dacites, trachydacites and trachytes:* 100% dacites
		Grouped with basalts and/or andesites	
	Shoshonites		
7.	Tuffs without specified composition	Same composition as predominant facies in the same unit or sector	*A sequence of lavas and rhyolitic breccias, sandstones, lutites and tuffs: Tuffs 100% rhyolitic*

The difficulty of assigning the units to the specific intervals depends on the characteristics of their relative or absolute ages. The simplest case occurs when the unit has a single dating, being assigned to a unique interval. If this dating, considering its error, is close to the boundary between two segments, it may overlap in both and be split into two. Now, if the dating overlaps by 75% or more with one of the intervals, the total area is assigned to it. If the unit has more than one dating, the range between these ages (including their errors) is considered, dividing the unit area in case the range does not overlap by more than 75% with one of the intervals. In units with multiple dating, the ages obtained by more reliable methods are considered.

Although in most cases the age obtained for a unit was considered for all its outcrops, there are times when an additional division was feasible. Especially in units of large geographical and temporal extensions, which have a significant amount of dating (e.g. La Tabla Formation), it was possible and pertinent to group age sets that indicate different stages of the same effusive or intrusive event, if these are related to different outcrops. For example, dating at the base and top of a unit.

When dealing with relative ages, the period defined by the stratigraphic information (maximum and minimum ages) and how it overlaps with the defined time intervals was considered, applying the same norm established in the previous cases. A summary of the criteria for age separation is presented in Table 2.

When dividing an area between segments in any of the cases, the particular characteristics of the rocks involved were taken into account. Its geological interpretation, as well as some marked trend in dating in favor of one segment (if there were enough), allowed in some cases to choose one segment over another by assigning 75% of the area to be divided.

4. Volumetric estimation

The volume for the volcanic outcrops of the ChMP was estimated based on thickness data from different localities of the Andean margin. The area covered by this outcrop delimits the volcanic part of the ChMP (ChMP-V) which can be further subdivided into nine zones with specific, and relatively homogeneous, thickness.

The thicknesses assigned for each zone are not necessarily a direct average, and some factors besides the thickness of the sequences are taken into account. They are determined considering intervals of 0.5 km (0.5 km, 1 km, 1.5 km, etc.). Some values define an estimated range (2-3 km) and others, a minimum thickness for incomplete sequences with no clear upper or lower limits (e.g. >1 km). Stratigraphic relationships between units are also considered.

In the southern Frontal Cordillera (zone of 3 km of mean thickness), the Horcajo Fm. overlies the Tambillos Fm (Cortés et al., 1997), and as both reach thicknesses of more than 2-3 km, Choiyoi magmatism could be more than 4 km thick in this area. Also, thicknesses close or over 3 km are found throughout the zone. This is why a mean thickness of 3 km is assigned to this part of Frontal Cordillera, despite some sequences of 0.5-1.2 kms. On the other hand, in the eastern zone of the ChMP-V corresponding to the intracratonic outcrops of the CMPT-LP, rhyolites from Lihué Calel have thicknesses that could exceed 2 km (Linares et al., 1980; Sruoga and Llambías, 1992), but these are not found anywhere else in the zone, and the other two measured sequences do not reach over 1 km. Therefore 1 km is assigned for this zone.

In the northern Frontal Cordillera and Precordillera (zone of 1.5 km of mean thickness) a >0.9 km section of the upper Choiyoi Group overlies the lower andesitic section (Malizia et al., 1999). The latter is well developed in this area, and northern outcrops record andesitic sequences of 0.5-0.8 km thick. Hence the Choiyoi Group in this area probably reaches up to 1.5 km. In the southern part of this zone, the Las Pircas Fm. (1.5 km) overlies the Vega de los Machos Fm. (0.3-3 km) (Rodríguez Fernandez et al., 1996) making up a sequence of probably more than 2-3 km. Considering these cases, the northern outcrops of El Cuerno Fm. (1.8 km) and the Guanaco Sonso sequence in the chilean Frontal Cordillera (0.8-1 km), 1.5 km would be the appropriate mean thickness for this zone.

In the rest of the zones, the mean thickness estimation is more straightforward.

This method involves an extrapolation of the thickness of specific well-preserved sequences to a large zone of volcanism defined by scattered outcrops, therefore some overestimations could take place.

Table A.5.2 Summary of criteria whereby the units can be placed in one or more than one of the 5 age intervals.

Age	***Criteria***	***Example***
Unique dating	If it falls only in one interval (considering error), the area of the unit is completely assigned to this interval. Rule of 75%*	252±3 Ma: error 255–249 Ma → >75% into 275–250 Ma interval → 100% of area assigned to this segment
More than one dating	The span defined by all ages (from the older to the younger) is considered. More reliable dating methods are privileged Rule of 75%* If there are enough dating, the amount of ages in each interval can be evaluated; if a tendency is clear, one segment can be privileged over the other (accumulating all the area) or a proportion of 75%-25% can be set. For large units, it is possible to split dating between different groups of outcrops.	313±2, 297±3 and 294±2 Ma U–Pb. 277±6 Ma biotite K–Ar: K–Ar dating is discarded → the 315–292 Ma range is defined→ no segment accumulates more than 75% of the age range → area divided 50–50% into 350–300 Ma and 300–275 Ma intervals
Relative dating	Age defined by stratigraphy 75% rule*	Loppingian–Middle Triassic (~259-237 Ma) → no segment accumulates more than 75% of the age range → area distributed 50-50% in 275-250 Ma and 250-225 Ma intervals

*If more than 75% of the range defined by one or more dating (considering margin of error) or relative ages, overlaps in one of the segments, 100% of the area of the dated rocks is grouped in that segment.

References

Cortés, J. M., González Bonorino, G., Koukharsky, M. M. L., Pereyra, F. X., Brodtkorb, A., and Ingeoma, S. (1997). Hoja Geológica 3369-09 Uspallata, Provincia de Mendoza.

Linares, E., Llambías, E. J., and Latorre, C. O. (1980). Geología de la provincia de La Pampa, República Argentina, y geocronología de sus rocas metamórficas y eruptivas. Revista de la Asociación Geológica Argentina, 35(1):87-146. Buenos Aires.

Malizia, D., Limarino, C. O., Sosa-Gómez, J., Kokot, R., Nullo, F. E., and Gutiérrez, P. R. (1999). Hoja Geológica 3169-2 Paso del Agua Negra, Provincia de San Juan.

Rodríguez Fernández, L. R., N. Heredia, G. Marín, C. Quesada, A. Robador, D. Ragona and R. Cardó, (1996). Tectonoestratigrafía y estructura de los Andes argentinos entre los 30° 30' y 31° 00' de latitud sur. Actas 13° Congreso Geológico Argentino y 3° Congreso de Exploración de Hidrocarburos, 2: 111 - 124. Buenos Aires.

Sruoga, P., and Llambías, E. J. (1992). Permo-Triassic leucorhyolitic ignimbrites at Sierra de Lihue Calel, La Pampa Province, Argentina. Journal of South American earth sciences, 5(2), 141-152.

Supplementary Material 5.3. Localization of individual data on thickness for units of the Choiyoi magmatic province.

Ver apéndice digital

Supplementary Material 5.4. Geochemical data used in Figure 6 with their references.

Ver apéndice digital